Development of Biomimetic Hydrogels as Cell-Laden Devices for Muscle Regeneration

Róisín Anne Holmes

Submitted in accordance with requirements for the degree of

Doctor of Philosophy

The University of Leeds

School of Mechanical Engineering

December 2017

The candidate confirms that the work submitted is her own and that appropriate credit has been given where reference has been made to the work of others.

This copy has been supplied on the understanding that it is copyright materials and that no quotation from the thesis may be published without proper acknowledgement.

Chapter 2/3 contains data from “Thiol-ene photo-click collagen-PEG hydrogels: impact of water-soluble photoinitiators on cell viability, gelation kinetics and rheological properties. Polymers, 226 (9)” Róisín Holmes, Xuebin B Yang, Aishling Dunne, Larisa Florea, David Wood and Giuseppe Tronci (2017). All of the work contained within this publication is directly attributed to myself with support from the co-authors. Solid state H-1 and C-13 NMR in chapter 2 was a EPSRC funded service provided by Durham University.

Chapter 5 contains data from “Influence of telopeptides on the structural and physical properties of polymeric and monomeric acid-soluble type I collagen.” Róisín Holmes, Steve Kirk, Giuseppe Tronci, Xuebin Yang, David Wood (2017). Materials Science and Engineering: C, 77 (1) 823-827. All of the work contained within this publication is directly attributed to myself with guidance from Steve Kirk. HPLC was a Southern Lights Biomaterials funded service provided by Massey University's Institute of Fundamental Sciences.

Chapter 5 also contains data from “Protease-sensitive atelocollagen hydrogels promote healing in a diabetic wound model”. Giuseppe Tronci, Jie Yin, Roisin A.

Holmes, He Liang, Stephen J. Russell, David J. Wood (2016) Journal of Materials Chemistry B, 4 (45) 7249-7258. This work was directly attributed to Giuseppe Tronci with the exception of Table 1 Chemical, structural and hydrogel properties of 4VBC-functionalised AC networks, the data of which was attributed to myself.

Dedicated to my Dad,

List of Publications and Presentations

Papers

Róisín Holmes, Xuebin B Yang, Aishling Dunne, Larisa Florea, David Wood and Giuseppe Tronci (2017) Thiol-ene photo-click collagen-PEG hydrogels: impact of water-soluble photoinitiators on cell viability, gelation kinetics and rheological properties, *Polymers,* 226 (9)

Róisín Holmes, Steve Kirk, Giuseppe Tronci, Xuebin Yang, David Wood (2017) Influence of telopeptides on the structural and physical properties of polymeric and monomeric acid-soluble type I collagen. *Materials Science and Engineering: C*, 77 (1)

Giuseppe Tronci, Jie Yin, Roisin A. Holmes, He Liang, Stephen J. Russell, David J. Wood (2016) Protease-sensitive atelocollagen hydrogels promote healing in a diabetic wound model. *Journal of Materials Chemistry B*, 4 (45)

Presentations

Róisín Holmes, Xuebin Yang, Giuseppe Tronci. David Wood. Click-Crosslinkable Collagen Hydrogels for Skeletal Muscle Tissue Engineering. Oral presentation at the school of dentistry research day Leeds, UK (2017).

Róisín Holmes, Xuebin Yang, Giuseppe Tronci. David Wood. Click-Crosslinkable Collagen Hydrogels for Skeletal Muscle Tissue Engineering. Poster presentation at TERMIS-EU, Davos, Switzerland (2017).

Róisín Holmes, Xuebin Yang, Giuseppe Tronci. David Wood. Click-cross-linkable Collagen Hydrogels for Cytocompatible 3D Culture In Regenerative Medicine. Poster presentation at TERMIS-Am, San Diego, USA (2016)

Róisín Holmes, Xuebin Yang, Giuseppe Tronci. David Wood. Click-cross-linkable Collagen Hydrogels for Cytocompatible 3D Culture In Regenerative Medicine. Poster presentation at Future Investigators of Regenerative Medicine (FIRM) symposium Platja d'Aro, Spain (2016)

Róisín Holmes, Xuebin Yang, Giuseppe Tronci. David Wood. Investigation of Collagen Hydrogels as Construct Materials for Alveolar Bone Tissue Engineering. Poster presentation at the CDT/DTC Joint Conference, Manchester, UK (2016). Third place poster prize.

Róisín Holmes, Xuebin Yang, Giuseppe Tronci. David Wood. Green Light Initiated Collagen Hydrogels as Cell-Hydrogel Constructs in Regenerative Medicine. Poster presentation at TERMIS-EU, Uppsala, Sweden (2016).

Róisín Holmes, Xuebin Yang, Giuseppe Tronci. David Wood. Collagen Cell-Hydrogel Constructs for Regenerative Medicine. Poster presentation at the School of Dentistry Research Day, Leeds, UK (2016).

Róisín Holmes, Xuebin Yang, Giuseppe Tronci. David Wood. Investigation of Collagen Hydrogels as Construct Materials for Alveolar Bone Tissue Engineering. Poster presentation at the CDT/DTC Joint Conference, Keele, UK (2015)

Acknowledgements

Firstly, I would like to thank my supervisors Professor David Wood, Dr Xuebin Yang and Giuseppe Tronci for their tremendous support and advice over the past three years.

I would like to thank my past and present colleagues in the department of Oral Biology and the institute of Mechanical and Biological Engineering (iMBE) for their understanding, friendship and support over the years with special thanks to Jackie Hudson for the specialist training and support on technical matters. I would like to thank Southern Lights Biomaterials and Massey University (New Zealand) for the industrial research project collaboration with a special mention to Dr Steve Kirk for his help and organisation during my time there. I would also like to thank the Insight Centre for Data Analytics, Dublin City University for allowing me to use their laboratory facilities and their collaboration with the paper.

Finally, I would like to give special acknowledgment to the Doctoral Training Centre for Tissue Engineering and Regenerative Medicine (DTC TERM) for funding my study and providing the opportunity to extend my Chemistry knowledge into the field of Tissue Engineering and Regenerative Medicine. It is also thanks to the funding provided by the DTC TERM that I could attend four international conferences and partake in an industrial placement in New Zealand and collaboration in Ireland.

Abstract

The aim of this thesis was to develop a novel cross-linking strategy to prepare defined collagen-based hydrogel networks to investigate stiffness-induced cell differentiation for skeletal muscle tissue engineering. Volumetric muscle loss (VML) occurs with traumatic injury or aggressive tumour ablation and results in a diminished natural capacity for repair. Whilst autologous muscle transfer offers the gold standard treatment option, the level of success is limited by surgical expertise, availability of healthy tissue, donor site morbidity and a loss of muscle strength and function due to scar tissue formation. As a result, a clear need exists for therapeutic strategies that can enhance the innate ability of skeletal muscle to regenerate following VML.

Thiol-ene photo-click collagen hybrid hydrogels were systematically developed and prepared via step-growth reaction using thiol-functionalised type-I collagen and 8-arm poly(ethylene glycol) norbornene terminated (PEG8NB). Collagen was thiol-functionalised by a ring opening reaction with 2-iminothiolane (2IT), whereby up to 80% functionalisation and 90% triple helical preservation were recorded in addition to improved solubility of the material. Type, i.e. Irgacure 2959 (I2959) or lithium phenyl-2,4,6-trimethylbenzoylphosphinate (LAP), and concentration of photoinitiator were varied to ensure minimal photoinitiator-induced cytotoxicity in line with the *in vitro* study. Gelation kinetics proved to be largely affected by the specific photoinitiator and the concentration, with LAP-containing thiol-ene mixtures leading to 8 times faster gelation times compared to I2959-containing mixtures. Photo-click hydrogels with tunable storage moduli (G': 0.54- 6.4 kPa), elastic modulus (E_c: 1.2- 12.5 kPa), gelation time (τ: 73- 331 s) and swelling ratio (SR: 1500- 3000 wt.%) were prepared. Three of these hydrogels (E_c: 7, 10, 13 kPa) were taken forward for *in vitro* tests with a myoblast cell line due to their similarity to the elasticity of natural muscle. These three hydrogels were shown to support cell attachment, spreading, proliferation and maturation/ differentiation of myoblasts into myotubes. A subcutaneous model was used to analyse the immune response of these new materials at 1, 4 and 7 days after implantation using Mucograft® as the control. Mucograft® was shown to present a lower immune response and reduced inflammation, whereas, the immune response from the hydrogel, promoted angiogenesis, which can be more beneficial for muscle regeneration.

Table of Contents

List of Figures

List of Tables

Abbreviations

2IT	2-iminothiolane
3D	Three-dimensional
4VBC	4-vinyl benzoyl chloride
AF488	Alexa Fluor 488
ANOVA	Analysis of variance
ATR FT-IR	Attenuated total reflectance fourier-transform infrared
C13-NMR	Carbon nuclear magnetic resonance
CD	Circular dichromism
cm	Centimeter
CuCAAC	Cu-catalysed azide–alkyne cycloadditions
DAPI	4’,6-diamidino-2-phenylindole
DMD	Duchenne muscular dystrophy
DMEM	Dulbecco’s Modified Eagle’s Medium
DMSO	Dimethylsulfoxide
DSC	Differential scanning calorimetry
DTNB	50 ,50-dithiobis-(2-nitrobenzoic acid)
DTT	1,4-dithiothreitol
Ec	Young’s modulus (Ec)
ECM	Extracellular matrix
EDC	1-ethyl-3-(3-dimethyl aminopropyl) carbodiimide hydrochloride
EDC	1-ethyl-3-(3-dimethyl aminopropyl) carbodiimide hydrochloride
EDTA	Ethylenediaminetetraacetic acid
ESCs	Embryonic stem cells
EthD-1	Ethidium homodimer-1
EWG	Electron withdrawing group
EY	Eosin Y

F	Functionalisation
FACITs	Fibril-associated collagens with interrupted triple helices
FBGCs	foreign body giant cells
FCS	Foetal calf serum
FDA	Food and Drug Administration
FFMT	Free functional muscle transfer
G	Gel Content
G'	Storage Modulus
G''	Loss Modulus
GelMA	Gelatin-methacrylate
GelNB	Gelatin-norbornene
GMA	Glycidyl methacrylate
H1-NMR	Hydrogen nuclear magnetic resonance
HA	Hyaluronan
HCl	Hydrochloric acid
HEGSH	Hexaethylene glycol (dithiol)
HEPES	4-(2-hydroxyethyl)-1-piperazineethanesulfonic acid
Hyp	Hydroxyproline
I2959	2-Hydroxy-1-[4-(2-hydroxyethoxy) phenyl]-2-methyl-1-propanone
IPSCs	Induced pluripotent stem cells
kPa	Kilopascal
LAP	Lithium phenyl-2,4,6-trimethylbenzoylphosphinate
LCST	Lowest critical solution temperature
Lys	Lysine
MACITs	Membrane-associated collagens with interrupted triple helices
mg	Milligram
mL	Millilitre
mm	Millimeter

mM	Millimolar
MSCs	mesenchymal stem cells
MULTIPLEXINs	Multiple triple-helix domains and interruptions
Mw	Average molecular weight
NAC	N-acetyl-l-cysteine
NaHCO3	Sodium hydrogen carbonate
NaOH	Sodium hydroxide
NBF	Neutral buffered formali
NHS	N-hydroxysuccinimide
NTB	2-nitro-5-thiobenzoic acid
NVP	1-vinyl-2 pyrrolidinone
Pa	Pascal
PBS	Phosphate buffered solution
PCl	Poly(capralactone
PEG	Poly(ethylene glycol)
PEG4NB	4-arm PEG norbornene terminated
PEG4SH	4-arm PEG-thiol
PEG8NB	8-arm PEG norbornene terminated
PEGdA	Poly(ethylene glycol) diacrylate
PNIPAm	Poly (n-isopropylamide)
Pro	Proline
RGD	Arginine-glycine-aspartic acid
rpm	Revolutions per minute
SCs	Satellite cells
SEM	Scanning electron microscope
SEM	Standard error of the mean
SMTE	Skeletal muscle tissue engineering
SPAACs	Strain promoted azide–alkyne cycloadditions

SR	Swelling ratio
TCEP	Tris (2-carboxyethyl) phosphine chloride
TEA	Triethylamine
TEOA	Triethanolamine
TNBS	2,4,6-Trinitrobenzenesulfonic acid
ug	Microgram
UV	Ultraviolet
VML	Volumetric muscle loss

Chapter 1 - Introduction

1.1 Overview of Tissue Engineering

Modern techniques of transplanting tissue and organs from one individual to another have been revolutionary and lifesaving. However, there is a critical gap between the number of patients on the waiting list and the number of donated organs available for such procedures [1]. It is within this context that the field of tissue engineering has emerged. This interdisciplinary field aims to apply the principles of engineering and life sciences towards the development of biological substitutes that restore, maintain, and improve tissue function [2].

Traditional tissue engineering strategies employ a top-down approach to manufacture tissue constructs, whereby cells and biomolecules are seeded onto a scaffold and allowed to diffuse through the material to create the extracellular matrix (ECM) and microarchitecture [3]. In contrast, a bottom-up approach relies on the self-assembly or directed-assembly of a scaffold from smaller cellular components to form the larger construct [4-6].

The aim of this project was to design defined collagen-based hydrogel networks to investigate stiffness-induced cell differentiation

1.1.1 Skeletal Muscle

Skeletal muscle is one of the three major muscle types, the others being cardiac and smooth muscle. It comprises 40-50% of total body mass and is necessary for generating forces for skeletal movement and plays a role in glucose, lipid and energy metabolism [7]. The skeletal muscle itself is located inside the epimysium layer and is composed of bundles of myofibers surrounded by the endomysium, perimysium and an interpenetrating network of blood vessels (Figure 1.1-1) [8]. The myofibers are enormous ribbon-like cells that can contain hundreds of nuclei and can measure several centimetres in length with diameters varying from 15 to 20 mm to more than 100 mm in trained power athletes [9, 10]. In order to generate and sustain mechanical tension and thereby permit movement, the organisation of the myofibers has to be highly structured. The working contractile unit of skeletal muscle is the sarcomere and there can be thousands present

within the muscle cells along the length of a myoblast-fused myofibril [10]. An individual sarcomere contains a matrix of thick filaments of myosin (centre of sarcomere) and thin filaments of actin (periphery).

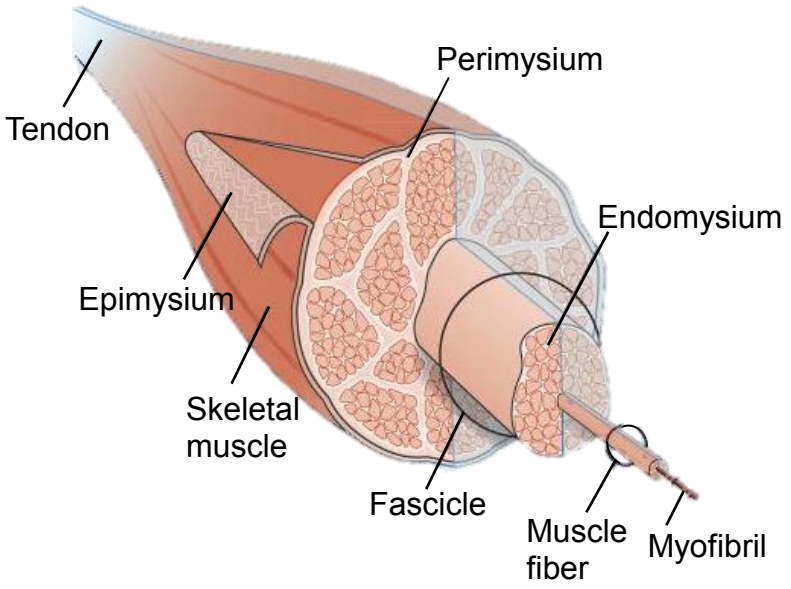

Figure 1.1-1 Schematic of muscle tissue with the ECM categorised as the epimysium, perimysium and endomysium [8].

1.1.1.1 Skeletal Muscle Damage/ Diseases

The most common skeletal muscle injuries are tears, lacerations and contusions which result in physical trauma yet no loss of muscle tissue itself. In sports, muscle injuries account for 10–55% of all sustained injuries [11]. In these cases, muscle has a robust capacity for regeneration even at a mature age, and can undergo a re-building process that involves the formation of new muscle cells, ECM and the re-establishment of vascular networks. When loss is associated with traumatic injury or aggressive tumour ablation, the repair capacity diminishes and if more than 20% of the muscle is lost, the natural repair process fails which results in a loss of function and is termed volumetric muscle loss (VML) [11-13].

Loss of muscle mass occurs in many conditions ranging from denervation, inactivity, microgravity, or systemic diseases such as cancer, sepsis, AIDS, diabetes or dystrophies [10]. Muscular dystrophy refers to a group of inherited disorders characterised by muscle weakness and death of muscle cells leading

to variable degrees of mobility limitation, including confinement to a wheelchair and/ or respiratory failure [14]. The most common of these inherited disorders is Duchenne muscular dystrophy (DMD), which is caused by mutations in the gene encoding dystrophin, an integral part of a complex that links the intracellular cytoskeleton with the ECM in muscle [15, 16].

1.1.1.2 Pathobiology of Muscle Injury and Repair

The healing of injured skeletal muscle can be categorised into three overlapping phases: inflammation, repair, and remodelling [17]. During the initial injury, the blood vessels of the muscle tissue are torn and thus the blood born inflammatory cells such as platelets, gain direct access to the injury site. The platelets are then activated which causes a provisional fibrin clot at the site of injury and the release cytokines, including platelet-derived growth factor (PDGF), transforming growth factor-β (TGF-β), chemokine C-X-C ligand 4, IL-1β and CD47 which contribute to the initial repair process via recruitment of neutrophils, macrophages and fibroblasts [18-21]. Neutrophils are the first cell type to arrive, these destroy any bacteria or remnant cell debris and provide additional signalling for the recruitment of macrophages. Two to three days post-injury, macrophages dominate the cell population. Further leukocyte recruitment to the site of injury allows T lymphocytes to then secrete cytokines and chemokines which modulate macrophage polarisation [17, 22, 23]. These secreted cytokines include epidermal growth factor (EGF), basic fibroblast growth factor (b-FGF), TGF-α, TGF-β and vascular endothelial growth factor (VEGF) which thereafter mediate angiogenesis, myoblast proliferation and the deposition of new ECM and the formulation of granulation tissue within the wound site [20, 23]. These secretions are stimulators for myogenic precursor cell differentiation later in the regeneration process [9, 24]. The final remodelling repair phase is the fusion of newly formed myotubes with existing myofibers and the damaged muscle begins to regain its contractile function [25]. However, in cases of severe volumetric muscle loss, the rate of fibrosis (scar tissue formation) can exceed the rate of myoblast proliferation and myotube formation; and the thick layer of scar tissue prevents fusion with the existing myofibers [25].

Repair technologies, such as autologous muscle flaps, are currently limited in terms of availability of healthy tissue, aesthetics and muscle functionality and could benefit tremendously from advances in tissue engineering. If successful, skeletal muscle tissue engineering will be uniquely equipped for the treatment of

VML with the ultimate goal being the accurate repair and replacement of skeletal muscle defects to restate their pre-existing physical form and function [26].

1.1.1.3 Current Therapies

Trauma to the extremities from motor vehicle accidents or the battlefield have contributed to an increased need for better treatment options for VML, especially for military physicians. While skeletal muscle has an inherent ability to regenerate, the magnitude of these defects limits the natural healing mechanisms.

The current standard of care for large-scale VML injuries is either an autologous muscle flap or free functional muscle transfer (FFMT), both involve a surgeon removing the damaged tissue and grafting healthy muscle from a donor site [11]. Flaps are autologous tissues and bring with them an existing vascular network and mature nerve-muscle junctions [25, 27]. A variant of this treatment method is FFMT, which allows donor tissue to be transplanted by cutting off the arteries, veins, and nerves at the donor site, and sewing them back at the defect site [26]. However, apart from being prone to multiple complications, FFMT requires longer rehabilitation times to account for adequate nerve regeneration and restoration of blood perfusion [25]. While autologous tissue transfers offer the gold standard treatment option, 10% of these surgeries result in complete graft failure due to infection or tissue necrosis [13]. The level of success of these procedures is also limited by surgical expertise, availability of healthy tissue, donor site morbidity and a loss of muscle strength and function due to scar tissue formation [13, 27, 28]. Surgical intervention can also result in alterations of the anatomy and biomechanics for both the recipient and the donor site and pre-injury muscle strength and functionality is difficult to achieve [25].

As a result, a clear need exists for therapeutic strategies that can enhance the innate ability of skeletal muscle to regenerate following VML, especially in those presented by military personnel, where there may be limited donor site availability as a result of extensive trauma [11]. Tissue engineering might offer a solution.

1.1.2 Skeletal Muscle Tissue Engineering

Skeletal muscle tissue engineering (SMTE) aims to replicate the structure and function of skeletal muscle tissue *in vitro* and *in vivo*, in which the ultimate goal

is implantation as a therapeutic device [29]. Various cell-based and material-based approaches have been explored such as delivery of stem cells or progenitor cells and growth factors and using a rationally designed biomaterial. This biomaterial should be capable of providing chemical and physical cues to enhance cell survival, myogenesis and upon implantation, capable to recruit host vasculature and nerves into the defect site [28, 30]. These tissue-engineered muscle constructs could be designed *in vitro* with appropriate structural and mechanical properties to promote rapid muscle repair before implantation [30].

1.1.2.1 Biomaterials for Muscle Regeneration

The design of regenerative devices relies heavily on the use of three-dimensional (3D) scaffolds to provide an appropriate environment, mechanical support and an initial cell anchorage site for the regeneration of tissues. Biomaterials can be made of permanent, biodegradable, naturally occurring, synthetic or hybrid materials. They need to be developed to be compatible with cells in *vitro* and *in vivo* and can be delivered as cellular or acellular matrixes. Cellular would incorporate myoblasts, satellite cells or another myogenic precursor cell, whereas acellular strategies could deliver growth factors to stimulate the recruitment and proliferation of local myogenic progenitor cells to the injury site *in vivo* [13].

From a biomimetic perspective, functional engineered tissue constructs should exhibit native-like structural properties.

This can refer to the densely packed, parallel alignment of myofibrils and myosin/actin filaments [31]. Their ability to organise myoblasts efficiently, to form aligned myotubes *in vitro* would greatly benefit efforts in muscle tissue engineering [32]. Additionally, due to the large tissue defects they would be designed to replace, a vascular system would be necessary to provide clinical application [29].

Biomaterials to encourage myotube parallel arrangement could be achieved by electrospinning synthetic polymers to create uniformly aligned, densely packed fibrous matrices [33]. Additionally, micro-patterning by moulding or printing a gel or polymer surface with nanoscale channels could align myotubes and promote cell fusion [25]. Mechanical and electrical stimulus which imitates *in vivo* activity has also been studied and shown to influence the proliferation and differentiation of cultured myoblasts during myogenesis *in vitro* [34, 35]. Synthetic scaffolds remain the most studied technology in skeletal muscle tissue engineering,

however, a major disadvantage is their low cellular adhesion and proliferation during construct formation compared to natural materials [25].

1.1.2.2 Cells for Muscle Regeneration

In order to translate tissue engineered constructs to ‘off-the-shelf’ available products, it would be crucial to have a large cell bank composed of immunologically transparent cells suitable for any individual, either as myoblasts or myogenic stem cells [36].

Requirements for tissue-specific stem cells are that they proliferate in a self-renewing manner that yields at least one daughter cell retaining its stem cell identity and are capable of differentiating into all the specialised cells in a given tissue [37]. Satellite cells (SCs) reside beneath the basal lamina that surrounds each muscle fibre and are the muscle stem cells that most prominently contribute to physiological skeletal muscle regeneration [38]. Their cell divisions are asymmetric, one daughter is produced which forms another SC and is retained in the niche beneath the basal lamina and the other goes forward as a myogenic cell and fuses with an injured muscle fibre to reconstitute its multinuclear state [39]. These cells are self-renewing so meet the definition of a stem cell. Healthy adult muscle has a slow and infrequent turnover rate compared to skin or blood, with ~ 1-2% of myonuclei replaced weekly, so satellite cells remain mostly quiescent unless activated by exercise or injury [37, 38, 40]. Low numbers are isolated from muscle so the SCs would have to be expanded *in vitro* to obtain sufficient number for a construct before implantation. Current isolation and culturing methods have reported that 30 doublings of SCs can be achieved, with the potential to improve to 50-70 doublings [41, 42]. However, expansion of SCs in culture for a few days results in severe reduction in their ability to produce myofibers upon transplantation *in vivo* [43, 44].

In addition to SCs, other progenitors located outside the basal lamina have been shown to have myogenic potential *in vitro* [15]. Among the most promising new approaches of repair include embryonic stem cells (ES cells) and induced pluripotent cells (iPS cells). ES cells are derived from the inner cell mass of pre-implanted embryos and iPS cells can be derived from many adult human cell types from direct reprogramming by a limited number of genes or by transfection with retroviruses [39, 45]. Other cells linked specifically to muscle differentiation include mesenchymal stem cells (MSCs), CD133+ progenitor cells and blood vessel-associated pericytes and mesoangioblasts [46-49]. Although these cells

may not contribute to physiological muscle regeneration like SCs do, some appear to have advantageous characteristics such as MSCs which are readily available and have immunomodulatory properties [38, 43]. Many studies focus on *in vitro* generation of muscular tissue cell lines such as C2C12 cells which are an established cell line of satellite cells from murine skeletal muscle. These have similar characteristics to those of isolated human skeletal muscle cells, although this cell line approximates myogenesis less closely than primary myoblasts [31, 50]. The process of maturation/ differentiation of these cells involves myoblast anchorage to the substrate, cell spreading, withdrawal from cell cycle and fusion into myotubes.

Important to success of tissue engineering is that the cells are immune acceptable. This comes automatically if the source is autologous, however, if the therapy is to become widely available, the source would have to be non-autologous [36].

1.1.2.3 Cell Microenvironment

A cell's function *in vivo* is orchestrated by complex signals as a result of the surrounding cellular microenvironment. The cues can be in the form of soluble factors, ECM proteins, cell-cell interactions, mechanical or shear forces and the spatial organisation (2D or 3D) of the microenvironment [51].

The process of differentiation describes the acquisition of the phenotype of a cell, most often identified by the expression of specific proteins achieved as a result of differential gene expression, e.g. skeletal muscle cells display highly ordered myosin, actin and other contractile proteins within sarcomeres [39]. Differentiation and merging of myoblast cells *in vitro* can be initiated by reducing serum concentrations in the medium.

Most cells are anchorage dependent and require interaction with the ECM to maintain viability. When adherent, cells are able to exert contractile forces on their environment and sense compliancy that can induce appropriate cellular behaviour. The cues from matrix mechanics are thought to occur by the cells 'pulling' on the scaffold and then generating signals based on this force [52]. On the whole, tissues in the body are viscoelastic which means they possess elastic properties that allow them to return to their original shape after stress is removed, and viscous properties which allow the material to be deformed. When a cell adheres onto a hydrogel, the gel has low resistance to forces and can easily be deformed resulting in a rounded cell. On stiffer materials, cells are less able to

contract the matrix and spread out thus resulting in multiple focal adhesion with the gel [53, 54]. The overall cellular response to mechanical stimuli is defined as mechanotransduction. The stiffness of the ECM is mainly expressed by the elastic modulus (or Young's modulus, E), which is in part regulated by ECM organisation and composition, although tissue elasticity is altered during aging, disease and injury [55].

It is recognised that stem cell behaviour is dependent on tissue stiffness, typically because the cells have to balance the external forces dictated by the mechanical properties of its environment. To do this, cells regulate their cytoskeleton tension, generating internal forces which in turn exert a mechanical force on each cell that is transmitted to the environment by adhesion sites [55]. During the design of a construct material, mechanical properties of the scaffold which resemble native tissue properties are often sought (E_{muscle} ~ 8-16 kPa [56]). The mechanical properties of the natural ECM are of paramount importance in dictating macroscopic tissue functions and regulating cellular behaviour via mechanotransduction signalling because variation in the elasticity of substrates can play an important role in cell morphology and differentiation [57].

1.1.3 Interface Tissue Engineering

Engineering muscle-tendon interfaces has not been extensively studied. However, the muscle-tendon-junction (MTJ) is an important interface in the musculoskeletal system because it acts as the mechanical bridge and transfers considerable forces between muscle and bone [58]. This requires an efficient tendon-to-bone and muscle-to-tendon interface to provide suitable load transfer to the bone with the strength to withstand large forces. Tissue engineering strategies applied to these soft-to-hard interfaces vary in terms of loading environment, mineral distribution and the subsequent healing responses are different (long time for bone) [58]. In terms of the bone-tendon-muscle bridge, tendon and bone scaffolds should be stiff while muscle scaffolds should be compliant and should be able to withstand large forces. This would require three different mechanical profiles, which could be achieved using a gradient biomaterial [59].

1.2 Collagen

The term ‘collagen’ refers to a group of proteins wide-spread in the body which form a triple helix structure of three polypeptide chains consisting of 18 amino acids per turn [60-62]. The polypeptide chains are predominantly made up of the small amino acid, glycine (Gly) which occurs every third position and all collagen members are characterised by the repeating motif of (Gly-X-Y) where X and Y can be any amino acid [63]. The amino acids proline (Pro) and hydroxyproline (Hyp) have high abundance in collagen, so the most common repeating triplet is Gly-Pro-Hyp.

Collagen accounts for over 30% of the total body protein. Tissue-specific, more than 90% of all extracellular proteins in the tendon, cartilage and bone, and more than 50% in the skin, consist of collagen [64, 65]. Collagen type I is fibrillar and is the most abundant structural building block in connective tissues such as bone, tendon and cartilage and provides a prominent role in mechanical strength due to its architectural arrangement [66]. Fibrillar collagen occurs when the triple helical coils assemble into highly orientated aggregates with the characteristic fibril-array structure. When examined under a scanning electron microscope (SEM) the fibrils are defined by a characteristic ‘d spacing’ which is the periodic banding pattern repeating around 69 nm [61]. This type of structure can be commonly identified as a white, fibrous tissue which has a high tensile strength and is relatively inelastic as a result of its architectural arrangement [66, 67]. Other fibril-forming collagens include collagen types II, III, V and XI [61]. Other categories of collagen include network-forming collagens, fibril-associated collagens with interrupted triple helices (FACITs), membrane-associated collagens with interrupted triple helices (MACITs) and multiple triple-helix domains and interruptions (MULTIPLEXINs) [63]. Twenty-nine types of collagen composed of distinct polypetide chains have been identified in vertebrates (Table 1.2-1 (A-B)). Collagen is the major supporting tissue of skeletal muscle and accounts for 1–10% of muscle mass dry weight [8]. Whilst type I and type III predominate in muscle tissue, types IV, V, VI, XI, XII, XIV, XV, and XVIII collagen are also expressed during skeletal muscle development [8]. Type III collagen is prevalent in tissues with some degree of elasticity including the skin and ligaments [68].

Table 1.2-1 (A) Vertebrate collagens I- XVI [61, 63, 69-72]

Type	Category	α Chains	Distribution
I	Fibrillar	α1(I), α2(I)	Dermis, bone, tendon, ligament
II	Fibrillar	α1(II)	Cartilage, vitreous
III	Fibrillar	α1(III)	Skin, blood vessels, intestine
IV	Network	α1(IV), α2(IV), α3(IV), α4(IV), α5(IV), α6(IV)	Basement membranes
V	Fibrillar	α1(V), α2(V), α3(V) α4(V)	Bone, dermis, cornea, placenta
VI	Network	α1(VI), α2(VI), α3(VI), α4(VI), α5(VI), α6(VI)	Bone, cartilage, cornea, dermis
VII	Anchoring Fibrils	α1(VII)	Dermis, bladder
VIII	Network	α1(VIII)	Dermis, brain, heart, kidney
IX	FACIT	α1(IX), α2(IX), α3(IX)	Cartilage, cornea, vitreous
X	Network	α1(X)	Cartilage
XI	Fibrillar	α1(XI), α2(XI), α3(XI)	Cartilage, in vertebral disk
XII	FACIT	α1(XII)	Dermis, tendon
XIII	MACIT	α1(XIII)	Endothelial cells, dermis, eye, heart
XIV	FACIT	α1(XIV)	Bone, dermis, cartilage
XV	MULTIPLEXIN	α1(XV)	Capillaries, testis, kidney, heart
XVI	FACIT	α1(XVI)	Dermis, kidney

Table 1.2-2 (A) Vertebrate collagens XVII- XXIX [61, 63, 69-72]

Type	Category	α Chains	Distribution
XVII	MACIT	α1(XVII)	Hemidesmosomes in epithelia
XVIII	MULTIPLEXIN	α1(XIII)	Basement membrane, liver
XIX	FACIT	α1(XIX)	Basement membrane
XX	FACIT	α1(XX)	Cornea (chick)
XXI	FACIT	α1(XXI)	Stomach, kidney
XXII	FACIT	α1(XXII)	Tissue junctions
XXIII	MACIT	α1(XXIII)	Heart, retina
XXIV	Fibrillar	α1(XIV)	Bone, cornea
XXV	MACIT	α1(XV)	Brain, heart, testis
XXVI	FACIT	α1(XVI)	Testis, ovary
XXVII	Fibrillar	α1(XVII)	Cartilage
XXVIII	FACIT	α1(XVIII)	Dermis, sciatic nerve
XXIX	-	-	Epidermis

1.2.1 Collagen Type I

Collagen type I is a natural polymer and as a scaffold material, it benefits from good biocompatibility, biodegradability, a natural affinity for biomolecules and is a major component in the natural ECM [73]. Its wide applications include sutures, cosmetic surgery, dental composites, bone grafts, wound care and tissue regeneration templates [74]. The constant basic structure of collagen is a triple helix of three left-handed polypeptide chains, usually formed as a heterotrimer by two identical α1(I)- chains and one α2(I)-chain. These can self- aggregate to form collagen fibrils, fibres and fascicles *in vivo* and can be cross-linked by chemical or physical means to form a hydrogel. [75]. The type I triple helix fibres are mostly incorporated with other collagens *in vivo*, for example a composite of

type III and type I collagen is found in muscle and skin and a composite of type V and type I collagen is found in bone and tendon [61, 76].

In terms of using collagen type I as a medical product, clinical observations indicate that 2– 4% of the population possess an allergy to bovine type I collagen, although this can be considered decidedly low,- in comparison, 6% of the population are susceptible to latex allergy [77].

1.2.1.1 Functionalisation

Collagen functionalisation, or cross-linking can be performed to improve its mechanical or biological properties by incorporating new reactive moieties or can be used to produce a film or hydrogel network to meet the demands of *in vitro* or *vivo* applications [75, 78-81]. Cross-linking methods are necessary to stabilise collagen in aqueous solutions *ex vivo* and can be divided into three groups: physical interactions (e.g., ionic cross-linking and hydrogen bonds), chemical reactions (e.g., with glutaraldehyde [82], diisocyanates [83], carbodiimide-activated diacids [78], or photochemical polymerisation [84] or enzyme (e.g., glutaminase) catalysed mechanisms [65, 85].

Collagen can be modified by reaction of its functional groups, more specifically the amino acid unit lysine or post modified hydroxylysine which contains a free-reactive amine group. It has a minor occurrence in the collagen triple helical structure which is dependent on the source of collagen, for example, rat tail type I collagen exhibits an average (hydroxy) lysine, [Lys] content of 3.24×10^{-4} $mol.g^{-1}$ [78]. Functionalisation of this side group can be achieved using a nucleophilic substitution or nucleophilic addition reaction, one example is the reaction with glutaraldehyde which produces an imine bond. Glutaraldehyde efficiently cross-links collagen and produces a hydrogel, however, this method is not appropriate for creating a biological construct because degradation *in vivo* could release glutaraldehyde into the body which is harmful to tissue [85]. To counteract this issue, 1-ethyl-3-(3-dimethyl aminopropyl) carbodiimide hydrochloride (EDC) can be used a zero length cross-linking agent. The efficacy and reaction yield can be improved by incorporating EDC with N-hydroxysuccinimide (NHS). The by-products of NHS/EDC cross-linking are water soluble and therefore could be removed from the hydrogel by repeated washing or dehydration [78].

Functionalisation of the collagen molecule can aid the development of hydrogels with complex and delicate microstructures. To achieve tuneable architecture and stiffness, the hydrogel would present improved tissue-like hierarchical

organisation thus increasing the probability to successfully restore structure, properties and function of the tissue. In addition to altering the stiffness and mechanical properties, functionalisation also provides a passageway to introduce other biochemical moieties such as growth factors.

Retrosynthetic considerations associated with functionalising collagen are representative in terms of solubility, occurrence and availability of functional groups and the preservation of the helical conformation.

1.2.1.2 Telopeptides

Collagen type I is made up of three parts, the triple helix, the N-terminal telopeptide and the C-terminal telopeptide. These terminal telopeptides account for 2% of the molecule and do not possess the repeating Gly-X-Y motif and therefore do not adopt a triple-helical conformation, however, they are involved in the covalent cross-linking of the collagen molecules and are critical for fibril formation [61, 86]. The molecular arrangement into fibrils is stabilised by the formation of covalent cross-links. Initial enzyme-catalysed lysine hydroxylation within the telopeptides allows hydroxylysine-derived aldehydes to form stable ketoimine bonds and a Schiff base reaction occurs between lysine-derived telopeptide aldehydes and adjacent lysine residues, both resulting in formation of cross-links [61, 81]. These intermolecular cross-links stabilise the collagen fibrils and contribute to their physical and mechanical properties.

Telopeptides can be cleaved by treating the collagen with proteolytic enzymes (e.g. pepsin) to produce atelo collagen consisting solely of the triple helical unit. However, since as discussed, the terminal telopeptides play important roles in cross-linking and fibril formation, their removal results in an amorphous arrangement of collagen molecules, although the induced positively charged surface of the atelo collagen results in a significant increase in solubility [77].

Despite its widespread acceptance as a safe and multifunctional material, the status of collagen as an animal-derived biomaterial has always raised concerns regarding its potential to evoke an immune response [77].

There is little variation in the amino acid sequences of the triple helical region between mammalian species, whereas a far greater degree of variability is found in the amino acid sequence of the telopeptides. So pepsin-solubilised atelo collagen was created to provide a potential immunological benefit compared to traditional acid-soluble collagen.

Antigenic determinants of collagen have been classified into one of three categories [61]:

1. Helical - recognition by antibodies dependent on 3D conformation
2. Central - recognition based solely on amino acid sequence and not 3D conformation
3. Terminal - located in the non-helical C- and N- telopeptides

However, the location of the major antigenic sites on the collagen molecule varies depending on the donor/ recipient species pairing. When calf collagen is transferred to a rabbit, the major antigenic site is from the terminal telopeptides and in comparison, when calf collagen is transferred to a rat, the major antigenic site is helical [77, 87]. No study has been made on the major antigenic sites when bovine collagen is transferred to humans.

In general, macromolecular features of a protein not common to the host species are more likely to encourage an immune response than shared features and the cleavage of the terminal telopeptides could provide collagen with a non-immunogenic status, although this could also be grossly overstated and more research should be produced on the area [77].

1.3 Collagen Hydrogels

Hydrogels are three-dimensional cross-linked networks composed of hydrophilic components held together by covalent bonds or via physical intra- or intermolecular attractions such as hydrogen bonds. Along with their ability to encapsulate biological factors, cells and drugs due to their high water affinity, they represent a promising material for tissue engineering [88]. They also can possess properties such as controllable degradability and the ability to be processed or formulated into injectable constructs [89].

Collagen is a popular option for a natural hydrogel because it is the major structural component of the ECM of most tissues, although other naturally derived polymers including agarose, alginate, chitosan, fibrin, gelatin and hyaluronic acid have been developed [73]. Natural polymers have excellent biocompatibility and biodegradability and excellent affinity for biomolecules due to their natural cell recognition sites. As a scaffold material, a collagen hydrogel would exhibit excellent biocompatibility and would benefit from the ability to degrade naturally in the body by enzymes such as metalloproteases, collagenase and serine proteases or as a result of hydrolysis [74]. Challenges to

consider when using collagen hydrogels include the high costs of manufacturing due to the time-consuming process for isolation and purification of collagen from its source and the conservative techniques necessary for cross-linking to avoid denaturation of the collagen which would eliminate its cell-recognition benefits.

Classical collagen hydrogels self-assemble under mild conditions with a physiological stimulus such as changing the pH to 7 and raising the temperature to 37 ^{o}C. The properties of these hydrogels are highly dependent on a large number of fabrication parameters such as collagen tissue source, solubilisation method, pH and temperature, solution components, ionic strength and collagen concentration which can cause a degree of variability [90]. Self-assembled collagen hydrogels have a degree of control over their mechanical properties in terms of the initial collagen concentration. Increasing the concentration from 0.3-2 wt.% (3- 20 mg/mL) has been shown to have a comparable increase in the elastic modulus from ~30 Pa to ~1800 Pa [91]. The highest concentration is limited by collagen's poor solubility in weakly acidic solutions and therefore, alone, these hydrogels have limited scope to mimic 3D tissues. Whilst the highest concentration (20 mg/ mL) has an elastic modulus similar to neuronal tissues (0.1- 1 kPa [57]), the high fibre structure was reported to be too dense to permit cell migration and sufficient viability [90, 91].

Although collagen hydrogels demonstrate great potential as a candidate for a construct material, they suffer from inferior mechanical properties and are not appropriate for load bearing application. However, it has been shown that mechanical stiffness can be altered by changing cross-link density, cross-linker type or from incorporation/ hybridisation with synthetic or other natural materials [79, 92, 93].

A combination of natural and synthetic hydrogels, also known as a hybrid hydrogel, has been used to improve the biological and mechanical properties of each material [94]. Synthetic polymers possess tuned mechanical properties and can be batch produced, so in combination with collagen, they could benefit from each other in terms of viability for cells, degradability, hydrophilicity, stiffness and viscoelasticity. Although the disadvantage of hybrid scaffolds is that during degradation, it could liberate small residual polymer fragments which would elicit inflammation and a host response.

1.3.1 Click Chemistry

'Click Chemistry' is a term introduced by Sharpless in 2001 to describe reactions that are fast, high yielding, selective, insensitive to ambient oxygen and water, possess readily available starting materials, generate inoffensive by-products, use mild reaction conditions and require simple product isolation [95]. This class of biocompatible reactions is an appealing approach for the preparation of hydrogels for tissue engineering.

Since the initial recognition of the copper catalysed azide-alkyne cycloaddition as click chemistry, a number of reactions have now been classified including the Diels-Alder cycloaddition, Michael-addition, photo-initiated thiol-ene, nucleophilic ring-opening such as epoxides and aziridines and non-aldol carbonyl chemistry reactions which include the formation of ureas, oximes and hydrazones [95-97]. Two important classes of click reactions are Cu-catalysed azide–alkyne cycloadditions (CuAAC) and thiol-X conjugation. Since first reports of CuAAC reactions by Sharpless *et al*, they have been viewed as ideal for chemical synthesis, drug discovery, bioconjugation, and biochemistry due to their fast reaction rate, high efficiency, excellent regiospecificity (one product formed exclusively) and biorthogonality (can occur inside living systems). However, concerns about the toxicity of the copper catalyst and the need for additional purification have restricted the use of these conjugation reactions in biomaterials applications [97]. As a consequence, there has been a strong interest in the development of metal-free click reactions that proceed in aqueous media at room temperature without the need for a catalyst. The Bertozzi group introduced strain promoted azide–alkyne cycloadditions (SPAACs) using cylooctynes as an alternative to CuAAC. The superiority of SPAAC in comparison with other click reactions is that it proceeds efficiently even in a mild physiological environment without the need of a catalyst or UV-light exposure.

Click chemistry has been incorporated into natural polymers. Guaresti *et al* successfully synthesised a chemically cross-linked chitosan–based hydrogel based on the Diels- Alder click reaction. The Diels-Alder reaction required mild heating and gelation occurred after 2 hours at 65 ^{o}C with no side reactions. Whilst this reaction does not require any harmful catalyst, it does require heat, so would not be appropriate to apply to collagen or for cell encapsulation [98]. Fu *et al* reported an injectable hyaluronic acid (HA)-based hydrogel cross-linked with azide-modified poly(ethylene glycol) (PEG) via SPAAC with gelation times 5- 50 minutes [99]. The disadvantage of applying this reaction to collagen is that it would require modification with bulky azide or cycloocytyne groups, neither of

these groups are present in nature and so could disrupt the natural triple helical conformation and prove difficult to synthesise. Desai *et al* reported alginate hydrogels formed by norbornene- tetrazine functionalisation, this reaction required no heating or catalyst which allowed easy incorporation of cells with high post-encapsulation viability although reaction times were ~ 2 hours [100]. While these reactions were all incorporated with natural polymers to form hydrogels, the reaction times were very slow and could not hold application as an injectable device and their classification as click reactions should even be questioned. A second major class of click chemistries are the Michael-addition, thiol-ene and thiol–yne reactions which have appeared as promising strategies for the preparation of hydrogels due to their high reactivity, superb selectivity, and mild reaction conditions.

Table 1.3-1 Click chemistry strategies to form hydrogels [101].

Click Reaction	Functional Groups	Advantages	Disadvantages
CuAAC	Alkyne, azide	Bioorthogonality	Toxic copper catalyst
SPAAC	Cyclooctyne, azide	No catalyst, biorthogonality	Difficult synthesis of cylooctyne precursors
Diels-Alder	Double bond, 1,3 diene	No catalyst, accelerated by water, thermosreversible	Slow gelation, requires heat
Thiol-ene	Thiol, double bond incapable of homopolymerisation	Spatiotemporal control, fast gelation	Potential toxicity from the photoinitiator and radicals
Thiol Michael-addition	Thiol, electron-deficient double bond	Reaction can take place at pH 7 with no additional catalyst	Cross-reactivity of thiols, easy oxidation

1.3.1.1 Thiol Michael-Addition

Michael-type additions have been studied since the 1940s although only recently classified as click chemistry [102]. Thiol Michael-addition involves the addition of a thiol (Michael donor) across a double bond in an acrylate, acrylamide, vinyl sulfone or maleimide (Michael acceptor) with or without the help of a base catalyst. The Michael acceptors require an electron deficient carbon-carbon double bond and generally possess an adjacent electron withdrawing group (EWG) [103]. The base, such as triethylamine, abstracts a proton from the thiol generating the thiolate anion, RS^-, and the conjugate acid, although adjustment of pH, and thiol group with low pK_a can generate the nucleophilic thiolate anions without the need of a base catalyst. This nucleophilic thiolate anion can then attack the electrophilic carbon on the electron-deficient double bond generating the intermediate carbon-centred anion. This then abstracts the proton from the conjugate acid, yielding the thiol Michael-addition product and the regeneration of the base catalyst [103]. After initiation, this propagation is very rapid and proceeds without interference from other proton sources (e.g. water) (

Figure 1.3-1).

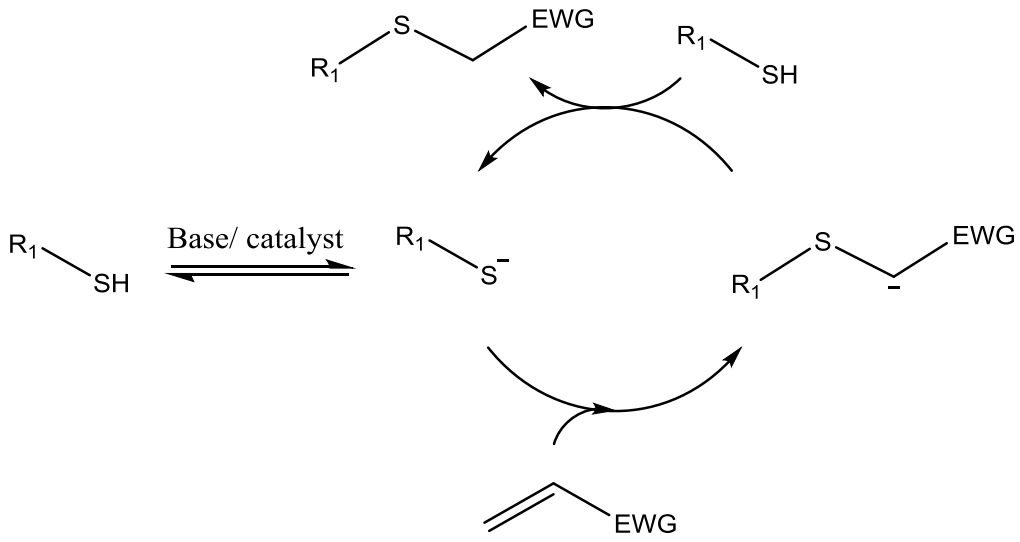

Figure 1.3-1 The step-growth base-catalysed thiol Michael addition reaction pathway. Addition of a thiolate anion across the electron-deficient double bond.

Michael-addition reactions are highly efficient, although the rate is dependent on several factors including the solvent polarity, pH, base catalyst strength, pK_a of the thiol group and the corresponding thiolate species, steric bulk of the thiol

group and how susceptible the carbon double bond is for nucleophilic attack, due to the nature of the EWG [103].

Incorporation of this approach to produce hydrogels based on natural polymers has been popular due to its tolerance to a wide variety of functional groups, and easy access to thiol and ene functionalised reagents. Li *et al* reported hybrid collagen-hyaluronic acid hydrogels prepared via Michael addition reaction of maleilated collagen and thiol modified hyaluronan. The reaction mixture was neutralised to pH 7 using beta-glycerophosphate disodium salt as the only base, although long reaction times ~8-24 hours were a disadvantage [104]. Ravichandran *et al* reported collagen functionalised with a methacrylate group and a Michael-addition reaction with thiol-terminated multi-arm polyethylene glycol (PEG). This method also reported very long gelation times ~3-4 hours [80]. These reactions are not abiding by the click chemistry requirement of fast reaction times and in comparison, papers which only include synthetic polymers in the Michael-addition reaction reported gelation times in seconds/ minutes [105-107].

1.3.1.2 Thiol-Radical Reaction

Schlaad *et al* first identified the thiol-radical reaction as click chemistry which was shown to include both the thiol-ene (double bond) and thiol-yne (triple bond) reaction [108]. A major advantage of these reactions is their ability to photoinitiate, referred to as photo-click chemistry [97]. The thiol-ene polymerisation proceeds via a radical step-growth mechanism in which an ene group orthogonally forms a covalent bond with a single thiol group, whilst conventional polymerisation forms a network by a chain-growth mechanism. The addition involves the propagation of a thiyl radical to a carbon-carbon double bond, followed by chain transfer to another thiol functional group and eventual termination (Figure 1.3-2). Light-initiation holds advantages for small molecule synthesis, surface and polymer modification, collagen modification and cell-encapsulation [103]. To initiate the reaction, an appropriate combination of light source and photoinitiator should be used and the rate is significantly improved when there is an overlap between the wavelength of the light source and the absorption spectra of the photoinitiator, thus allowing the generation of sufficient radicals. In addition to photoinitiator and light source, the relative polymerisation rates of the thiol-ene systems are fastest for norbornene and vinyl ether moieties because the overall conversion is directly related to the electron density on the ene, with electron-rich enes reacting faster than electron-poor enes, norbornene

> vinyl ether > alkene vinyl ester > n-vinyl amides > allyl ether > acrylate [103]. Using double bonds which are incapable of homopolymerisation ensures the only reaction occurring is the step-growth thiol-ene reaction, and the carbon-centred radical is always transferred to a thiol moiety rather than propagation of the carbon-centred radical through the double bond [109].

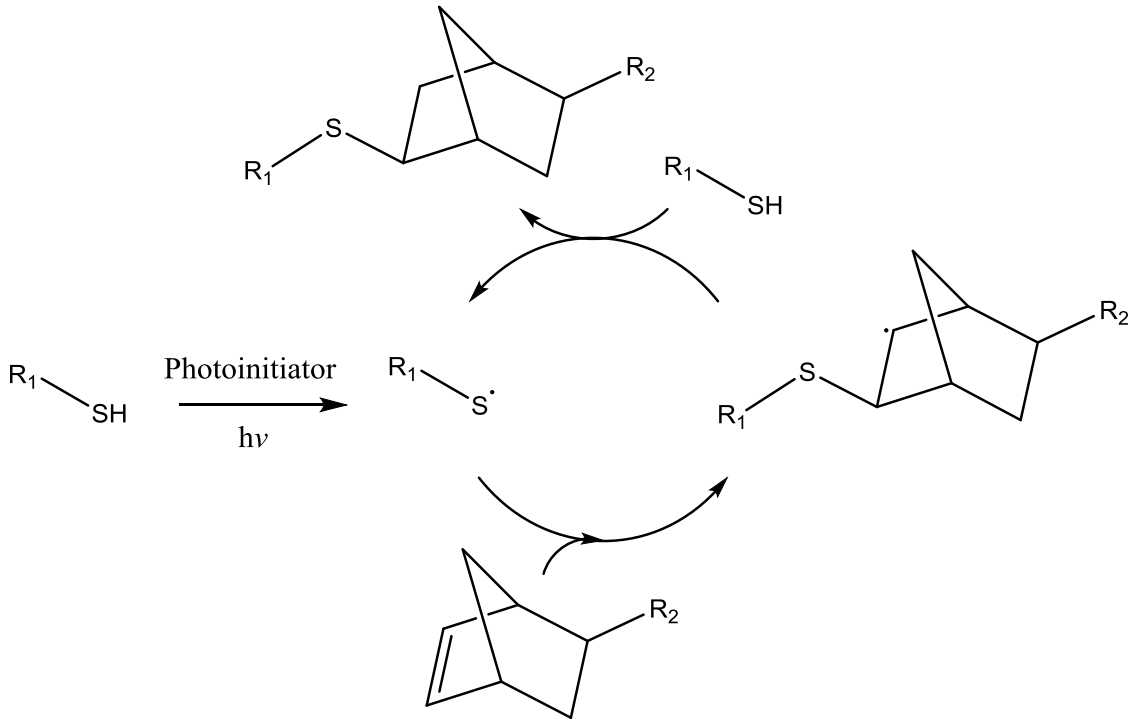

Figure 1.3-2 The step-growth thiol-ene reaction pathway. Addition of a thiyl radical across norbornene followed by chain-transfer from a carbon-centred radical to a thiol group.

One additional advantage of the thiol-ene reaction compared to tradition radical chain-growth reactions is its ability to overcome oxygen inhibition and thus be performed in a broader range of atmospheric conditions (Figure 1.3-3). This is unlike traditional chain-growth polymerisation which often requires an innate nitrogen environment to prevent oxygen inhibition of the radical propagation step.

The thiol-ene reaction has been incorporated into the preparation of synthetic and natural hybrid hydrogels. Lin *et al* reported that hydrogels could be formed in less than 3 min from norbornene-functionalised 4-arm PEG (PEG4NB) with a dithiol peptide, in which both the mechanical and biochemical properties of hydrogels could be controlled by thiol/ene ratio, PEG molecular weight and architecture, polymer concentration, or peptide sequences [110].

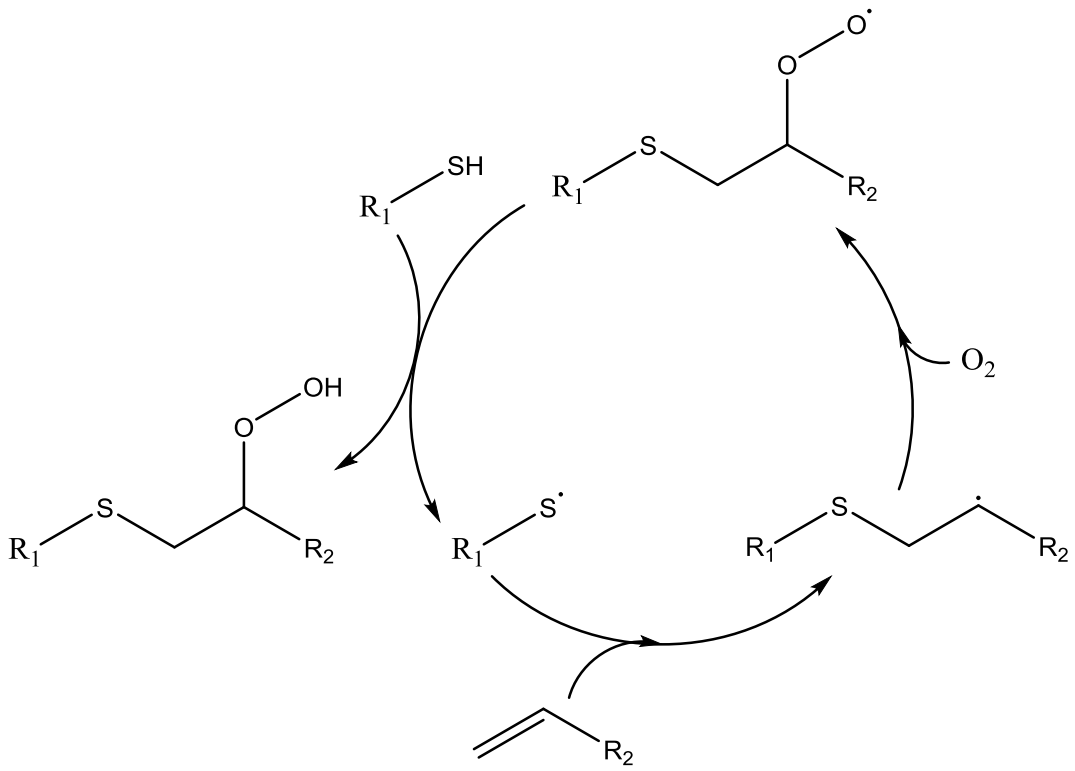

Figure 1.3-3 Schematic to show the oxygen inhibition of a radical thiol-ene reaction. Oxygen reacts with polymerising radicals to form inactive peroxy radicals; however, for thiol-ene reactions, the peroxy radical abstracts a hydrogen from the thiol to form an active thiyl radical that restarts the polymerisation with little change in the reaction rate.

Mũnoz *et al* reported gelatin-PEG hybrid hydrogels prepared with norbornene-functionalised gelatin capable of *in situ* photo-encapsulation of human mesenchymal stem cells (hMSCs) [111]. Gelatin is formed by the hydrolysis of collagen and as such does not possess the triple helical conformation and is not limited to reaction temperatures below 37 ^{o}C or poor solubility. The method to produce gelatin functionalised with norbornene by Mũnoz *et al* required a pH 8 solution, carbic anhydride (20% (w/v)) and reaction temperature of 50 °C which could not be transferred to collagen.

Thiol-ene click chemistry was incorporated into collagen by Russo *et al*. This used a thiol-functionalised collagen solid surface and allyl α-D-glucopyranoside with 1 hr exposure to UV light [112]. The issue with this reaction is that it is a *pseudo*-click reaction although it was not reported to be in the paper. Allyl ethers, unlike vinyl ethers can react by homopolymerisation so both a chain-growth and

a step-growth reaction would be taking place, although granted that allyl ether homopolymerisation is slow due to the electron rich ene group.

1.3.2 Injectable Hydrogels

An interesting feature of hydrogels is their ability to be mixed with, and encapsulate cells and molecules prior to gel formation, thus providing a potential avenue to deliver cells and bioactive factors in a minimally invasive manner. An injectable hydrogel would also be extremely effective at filling irregular spaces and could configure the exact shape of a defect. Therefore, it should be capable of undergoing gelation *in situ* after injection and in order to do so, the gelation kinetics require the polymer solution to gel and solidify within a clinically acceptable timescale. The typical methods to induce gelation, include thermal and photochemical polymerisation, enzymatic and ionic cross-linking and click chemistry. The majority of these cross-linking techniques require the use of a catalyst to proceed which could be toxic to tissues and would therefore be inappropriate for *in situ* gelation. To counteract this issue, thiol click chemistry, e.g. Michael-type addition reactions could be used as a method of non-toxic *in situ* gelation via reaction between a thiol and acrylate, so long as the reaction did not require the use of a catalyst and the reaction conditions could be tailored to allow a fast rate of reaction and gelation time < minutes [113]. Xu *et al* reported an interesting study incorporating the design of an injectable biodegradable biomimetic scaffold based on thiolated collagen and the block copolymer oligo(acryloyl carbonate)-b-poly(ethylene glycol)-b-(oligo(acryloyl carbonate) (OAC-PEG-OAC) by means of a Michael-type addition reaction. This reported a gel point ranging from 0.4 to 8.1 min and mechanical properties which could be tuned by degree of collagen thiolation, the solution pH and polymer concentration [114].

An attractive solution could involve the introduction of a temperature or pH sensitive moiety onto the polymer backbone in order to induce polymer gelation *in vivo* [115]. Although, to successfully shape and fill the irregular defect, it is necessary that the hydrogel possesses good mechanical strength, a predefined shape or the ability to physically bind to adjacent tissues.

Injectable hydrogels based on native collagen could promote a matrix for improved cell attachment and tissue growth by providing the functionality of the ECM. In conjunction as a hybrid hydrogel with collagen, the thermoresponsive polymer Poly(N-isopropylacrylamide) (PNIPAM) could produce an injectable

scaffold because it undergoes a conformational change at its lowest critical solution temperature (LCST) (32 ^{o}C) at which point it becomes insoluble in water and forms a gel. This is a similar temperature to the body, although *in vitro* the presence of ions in such as magnesium sulphate in cell culture media reduces the LCST of the polymer due to competitive hydrogen bonding between water, the anions and the PNIPAM, thereby shifting the LCST to a lower temperature [116]. The cells could be suspended in the aqueous hybrid polymer solution below the LCST and then transferred into moulds or injected *in vivo.*

Additional advantages of injectable hydrogels include reduced patient discomfort and lower risk of infection from surgery due to the minimally invasive procedure. Disadvantages of injectable biomaterials are their current poor mechanical strength rendering them too weak for load-bearing applications, the lack of control over the pre-polymerised solution, the high degree of viscosity, their undefined porosity and low stability due to swelling and subsequent dissolution of the polymers, - although gel strength and stability has the capacity to be improved by increasing cross-link density or incorporation of inorganic molecules [54].

1.3.3 Cell Encapsulation

Previously, *in situ* cell encapsulation has focussed on collagen hydrogels self-assembled by physical entanglements. The stiffness of these type of hydrogels can be controlled by increasing the concentration of collagen in the solution. However, it is not feasible to dissolve higher than 2 wt.% (20 mg/mL) of collagen in a weakly acidic solution. Cross *et al* reported that collagen hydrogels at concentrations 3, 8, 10, 15, and 20 mg/ml produce hydrogels with stiffness 30 Pa to ~1800 Pa [117]. These physically entangled hydrogels are prepared by neutralising the collagen solution and have long gelation times (20- 60 minutes) [117, 118]. Therefore they are not appropriate for use as an injectable device and are limited to mimic weak ECM materials.

Chemically cross-linked hydrogels can be used to mimic stiffer ECM materials, although as discussed, it is important that any reagents, photoinitiators or reaction conditions be designed in a cytocompatible manner if cell encapsulation is to be possible. The thiol-ene photo-click reaction is not oxygen-inhibited and requires a lower radical concentration to initiate the reaction than the chain-growth mechanism which has been shown to yield high initial radical concentrations. This would not be ideal for the encapsulation of cells and proteins

prone to radical-mediated damage since free-radicals can cause damage to cell membranes, nucleic acids, and proteins, which can lead to cell death [111, 119]. If the gelation method requires light exposure, the light source and exposure times should be tailored to reduce cell cytotoxicity.

Additionally, to remain viable, encapsulated cells require a constant supply of oxygen, nutrients and means to remove metabolic waste products. *In vivo* this is achieved through vasculature and it is understood that cells situated 100 – 200 µm from an oxygen supply will not survive [120]. A major barrier in the development of functional tissue-engineered constructs is vascularisation and this is an important feature that should be incorporated into scaffold design by way of channels or appropriate pore size [5, 121]. Porosity can warrant apt oxygen and mass transfer, however, the pore size has to be large enough for cells to migrate into the matrix, although not so large that it hinders cell attachment.

Microchannnels which resemble the vascular system of human tissues have been reported using methods such as lithography, micromoulding and bioprinting [5]. Microfluidic channels in a 3D hydrogel could provide constructs to mimic and flourish similar to natural tissues. Micromoulding is a simple approach to construct a patterned cell-encapsulated hydrogel, cells are first suspended in a gel and then moulded on a patterned wafer to generate microchannels of different shapes and sizes to allow nutrients and oxygen to easily diffuse [94]. Hydrogels capable of being cross-linked by exposure to light hold potential for photopatterning. This method is fast and highly reproducible and has been used to fabricate hydrogel constructs with predesigned microchannels for vascularisation or perfusion so long as the hydrogel has sufficient mechanical properties to support a shape *in vitro* [120].

Although it should be noted that an organised array of microchannels, does not represent the complexity and irregularity of the vascular system present in the natural tissue.

1.3.4 Stiffness

Hydrogel mechanical properties are determined by the type of polymer used, concentration, cross-linker type, cross-link density and the physiological conditions. Tronci *et al* demonstrated that mechanical stiffness of collagen hydrogels could be varied by incorporating various vinyl-containing chemical moieties onto the backbone of the polymer followed by photopolymerisation.

These methods have achieved collagen hydrogels with higher stiffness than previously procured from functionalised collagen hydrogels (> 28 kPa) [79]. Plastic compression of collagen hydrogels *in vitro* is a rapid and reproducible technique for the production of scaffolds. Compressive stress is applied to the collagen hydrogel so the excess water is removed and the fibre structure becomes denser, resulting in the enhanced stiffness of the hydrogel, however issues include cell viability and proliferation on these densely fibrillar networks [122].

Work by Wong *et al* demonstrated that the use of polymeric collagen with acid-soluble collagen could be used to alter the mechanical properties of collagen hydrogels. Polymeric collagen, often found in older, dense tissues of the tendon is physiologically cross-linked and is therefore a strong and stable material. Collagen-based research predominantly focuses on acid-soluble ("monomeric") collagen which possess weaker mechanical properties than mature, polymeric collagen. A stiffer collagen hydrogel was reported by Wong *et al* by blending acid-soluble collagen with the polymeric suspension [123].

Natural hydrogels exhibit better biocompatibility and cell affinity than synthetic hydrogels, although they possess poor control over the mechanical properties, water content and degradation rate. Hybrid hydrogels made of natural and synthetic polymers seem to be an obvious solution to capitalise on the advantages of both [120]. These hybrid hydrogels can consist of a polymeric network loaded with inorganic nanoparticles, which are dispersed between the polymer chains or obtained from the dispersion of at least two types of polymers interconnected via chemical or physical means. Incorporation of hard inorganic particles or dendrimers which have been physically trapped in the hydrogel network has been shown to improve the mechanical properties and bioactivity of collagen hydrogels [124-126].

Synthetic polymers are attractive candidates for tissue engineering constructs because they can be easily synthesised in large quantities with controlled molecular weights, molecular architectures, and depending on the polymerisation method, functional groups can be introduced by means of co-polymerisation or modification of the reactive end-group [124].

PEG hydrogels are among the most widely used synthetic materials in 3D cell culture due to their good biocompatibility, varied molecular weights and their wide range of functional end-groups and although non-degradable, they have been incorporated with MMP-sensitive peptides to make them physiologically degradable [127]. PEG hydrogels have adjustable mechanical properties and

allow easy control of the scaffold architecture and have also been approved by the Food and Drug Administration (FDA) for various clinical applications [120, 128].

1.4 Photoinitiators

Photopolymerisation reactions are driven by chemicals that produce free-radicals when exposed to specific wavelengths of light. A variety of photoinitiators are available capable of dissociation into a high-energy radical state after excitation from a light source [129]. 2-Hydroxy-1-[4-(2-hydroxyethoxy) phenyl]-2-methyl-1-propanone (Irgacure™ 2959 (I2959)) and Lithium phenyl-2,4,6-trimethylbenzoylphosphinate (LAP) are two water-soluble type I photoinitiators which dissociate into two radicals following photon absorption. They are both capable of producing radicals when exposed to ultraviolet (UV) light (365 nm). I2959 is a commonly used photoinitiator for encapsulation of cells within hydrogels due to its well-established cytocompatibility at low concentrations [93, 129]. However, one major drawback is low water-solubility which causes difficulties in applications where a higher concentration is required (> 0.5% (w/v)). Another drawback is that the absorbance of I2959 peaks at ~280 nm, this means it can suffer from competing absorbance when used in conjunction with collagen due to the aromatic amino acids absorbing at ~265 nm [130].

Visible-light photoredox processes take place under mild conditions with typical irradiation sources such as LED torchers or lamps in conjunction with a type II initiator system such as the organic dye, eosin Y [131, 132]. A type II photoinitiator often requires a co-initiator to generate a sufficient number of radicals, and an increased oxidative efficiency is recorded when eosin Y (as the photocatalyst) is used in conjunction with triethanolamine (TEOA) [133-135]. Eosin Y presents a characteristic peak in the UV/Vis spectrum ~ 512 nm (green light) and upon excitation, eosin Y (EY) has increased redox potential. The radical cation, EY+• generated can undergo electron transfer with TEOA producing TEOA+• and regenerates ground state EY. In the absence of TEOA, the lifetime of EY+• is ~345 μs, while in the presence of 1.5×10^{-3} M TEOA the lifetime of EY+• is shortened to ~22.9 μs [135]. This process can be used as an oxidising agent for organic reactions such as the reduction of nitrobenzene, although its potential use as a visible light initiator for photopolymerisation has been reported [131, 133]. Visible-light systems hold advantages over traditional

UV-photoinitiators. The cytocompatible visible-light would eliminate any potential cellular toxicity imparted by UV radiation, which would also reduce the risk of peptide denaturation during UV exposure [130]. In addition, costs are reduced when the light source is from a LED compared to a UV lamp.

1.5 Immune Response

The final challenge for tissue engineering is presented in moving a bench-top concept into a living system [36]. Before the use of autologous or autogenic cells can be challenged, it has to be ensured that the construct is immune acceptable.

Innate and active immune responses are the two components of this highly complex system of host defence. The non-specific innate immune response is antigen-independent and activated immediately (~seconds) to provide effective initial defence. In comparison the delayed active immune response (~days) is antigen-dependent and recognises and reacts to different substances with a degree of specificity and more effectively combats the foreign material [17, 136]. All materials implanted into a mammalian recipient are subject to response by the host's innate immune system [137]. The cascade of overlapping events that take place include blood-material interactions and the deposition of a protein film on the biomaterial, provisional matrix formation, acute inflammation, chronic inflammation, granulation tissue formation, foreign body reaction and fibrosis and capsule development [138].

The major biomaterial-associated factors that could influence the host response include the chemical composition of the material, hydrophobicity/ hydrophilicity, elastic modulus, crystallinity, degradation profile, degradation product toxicity and surface topography [18, 139-141]. The patient characteristics are also of considerable importance to the immune response and a degree of variability can be observed dependent on age, sex, general health, physical mobility and general lifestyle features of the patient [141].

Surgical implantation is invariably associated with damaged tissue or cells at the surgical site which induces an acute inflammatory response mediated by neutrophils. Within seconds after implantation, circulating leukocytes and plasma proteins, such as fibrinogen, complement cascade (C5), albumin and IgG adsorb to the surface of the biomaterials forming a provisional matrix which provides a substrate with which inflammatory cells can interact [142]. The adsorption/ desorption of the plasma proteins is dependent on the physical and functional

nature of the biomaterial surface and the protein-affinity can determine the subsequent degree to which the material elicits a foreign body giant cell response [140]. Acute inflammation follows the deposition of the provisional protein matrix and consists of the emigration of neutrophils to the implant site. The chronic inflammation phase is typically characterised by the presence of macrophages which become activated and secrete cytokines to recruit leukocytes and other cell types involved in the foreign body reaction to the site of the implant. Within 2 to 4 weeks, unresolved inflammation, marked by macrophage fusion into large multinucleated foreign body giant cells (FBGCs) surround the implant in a thick layer of fibrotic scar tissue which holds implications in terms of the material's longevity [143, 144]. Although some inflammation may be desirable to mediate the healing process, a persistent inflammatory response around the implanted device prevents its functional interaction with the surrounding tissue, and will eventually lead to device failure [145]. The foreign body response with an outcome of tissue encapsulation is an undesirable outcome for tissue engineering strategies which seek to promote functional recovery.

Several mechanisms have evolved to put the brakes on the inflammation. Alternatively activated macrophages express more IL-10 than classically activated macrophages (macrophages stimulated for tissue remodelling vs macrophages stimulated to kill microbes) which inhibits the production of various inflammatory cytokines. Growth factor and cytokine delivery have been shown to have wide ranging effects upon the success of implantable constructs *in vivo* [143].

1.5.1 Immune Modulation

Current strategies to mediate the foreign body reaction focus on reducing protein adsorption, initial cell adhesion, inflammatory cytokine secretion and FBGC fusion. The biological response of the host focuses on surface interactions between the biomaterials and the biological system. Current strategies in the design of immunomodulating biomaterials include altering the surface chemistry, roughness or geometry of the material to determine the degree to which the serum proteins adsorb onto it and cell adhesion [144]. The adsorbed provisional protein layer provides binding sites for protein-specific receptors on monocytes and macrophages which can thus dictate compatibility of the material that is placed in the body [137, 143]. Synthetic coatings such as poly(lactic coglycolic acid) (PLGA) or PEG, have been used to render an implant biocompatible due to their ability to prevent protein adsorption and thus inhibiting recognition by the

immune cells [137]. Additionally, imprinting of a parallel pattern on the surface of the polymer has been shown to affect macrophage adhesion *in vivo* independent of the biomaterial surface chemistry [144]. Although adherence to roughened materials will trigger a more rapid production of reactive oxygen species compared to smooth materials and an exacerbated inflammatory response [146].

Another approach for modulating the immune response is incorporation of bioactive cues such as adhesion sites, growth factors, anti-inflammatory mediators or drugs to mediate material-host tissue interaction, for example, coatings that release or generate nitric oxide (NO) reduce thrombogenesis and inflammation [143, 144].

The immune response has the potential to cause extensive damage; however, recent approaches have attempted to modulate tissue response in a manner to promote wound healing and improve implant integration. Although chronic inflammation and foreign body reactions have to be avoided since they can lead to device failure [143]. Whether a material should elicit an immune responses to initiate the repair/ regeneration processes or remain 'invisible' to the host presents a biocompatibility paradigm [141].

1.5.2 What Makes a Good Scaffold?

Biomaterials are central to many strategies for regenerative medicine. Defined as a substance that has been engineered to take a form which is used to direct the course of any therapeutic or diagnostic procedure, they provide mechanical stability and an initial site for cell adhesion and migration [147].

Biocompatibility refers to the ability of a material to perform with an appropriate host response in a specific situation, with the definition changing over the years to follow the transition of biomaterials science from a subject that was almost solely concerned with implantable medical devices, such as hip replacements to biomaterials used in tissue engineering.

For tissue engineered constructs, an increasing number of applications require that the material should specifically react with the tissues rather than be ignored by them [141]. Implantation of muscle constructs *in vivo* which provide a foreign body reaction can result in angiogenesis and the in-growth of blood vessels than enable cell viability in the long-term [35]. Inflammation can also result in spontaneous healing through initiation of the natural healing process which promotes the activation of resident stem cells [141]. Clearly chronic inflammation should be avoided since there is no point in designing a complex system for

guiding tissue regeneration if it is ultimately destroyed by the influx of inflammatory cells.

1.6 Aims and Objectives

The aim of this project was to design defined collagen-based hydrogel networks to investigate stiffness-induced cell differentiation. The following objectives were identified in order to achieve this goal:

1. Functionalise collagen with either thiols or vinyl groups using facile, cell-friendly method whilst keeping the triple helical conformation intact to accomplish hydrogels.
2. Examine novel synthetic strategies for cross-linking collagen to prepare defined covalent networks with reliable, varied molecular architecture and substrate stiffness.
3. Chemical, physical and mechanical characterisation of hydrogels
4. *In vitro* tests with myoblast cell line to examine differentiation and proliferation
5. *In vivo* subcutaneous model on best performing hydrogel to analyse the immune response.

Chapter 2 - Functionalisation of Collagen Type I and Photoinitiator Comparison

2.1 Introduction

The aim of this chapter was to extract and characterise type I collagen before functionalisation to provide reactive moieties to prepare hydrogels by photopolymerisation, physical cues (e.g. temperature) or click chemistry. These reactions were developed to abide by synthetic considerations such as low reaction temperatures (below 37 ^{o}C) to prevent collagen denaturation and the use of non-hazardous solvents and/ or chemicals. An analysis of water-soluble photoinitiators was also performed as a prerequisite before the development of a novel cross-linking strategy in chapter 3.

Collagen is a naturally occurring polymer and the most abundant structural protein in the extracellular matrix (ECM) [148]. Twenty-nine different types of collagen have been identified, characterised by their triple helical conformation with the largest subgroup comprising of fibril-forming type I collagen [63, 149]. The advantages of using collagen as a scaffold material include good biocompatibility, permeability, availability, natural affinity for biomolecules and good biodegradability [4, 148, 150]. Although drawbacks include poor mechanical performance, potential antigenicity and batch to batch variability. As a biomaterial, collagen can be used intact, spun into fibres or as a swollen hydrogel with a wide range of applications including sutures, tissue replacement and skin regeneration templates [74, 151].

2.1.1 Collagen Functionalisation

Intra- and intermolecular cross-linking takes place *in vivo* to impart desired mechanical stability on collagen fibrils [152]. This enzyme-mediated cross-linking does not occur *in vitro* and consequently, reconstituted forms of collagen suffer from poor mechanical performance [153]. Collagen functionalisation, or cross-linking can be performed to improve its mechanical or biological properties by incorporating new reactive moieties or can be used to produce a film or hydrogel network to meet the demands of *in vitro* or *vivo* applications [75, 78-81]. Several

chemical techniques have been developed to functionalise collagen which rely on the modification of the amine and carboxyl groups within the molecules to produce new covalent bonds [154]. Glutaraldehyde was the most employed method to cross-link collagen involving the formation of an imine group from the lysine or post-modified hydroxylysine amino acid, although issues arose due to toxicity [155].

Epoxy compounds possess a highly strained three-membered ring which is susceptible to a nucleophilic attack predominantly with the amine groups of (hydroxy) lysine residues, whose cumulative occurrence counts for ~3.24 x 10^{-4} $mol \cdot g^{-1}$ ([Lys]) of collagen [78, 156-158]. Nucleophilic substitution reactions also occur with acyl chlorides or alkyl halides where the electronegative halogen group provides a carbon susceptible to nucleophilic attack by the amine in conjunction with a base e.g. triethylamine [75, 159].

Another method for functionalisation is a dehydration reaction between the hydroxy (lysine) amine and a chemical (or conversely, carboxy-containing Asp or Glu) with an available carboxylic acid group. Carbodiimide 1-ethyl-3-(3-dimethyl aminopropyl) carbodiimide (EDC) reagent can be used as a zero-length cross-linker in this reaction incorporated with N-hydroxysuccinimide (NHS) to activate the carboxylic acid group and thereby increase its reactivity for attack by the amino group [159]. The by-products of NHS/EDC cross-linking are water soluble and therefore can easily be removed by washing [85].

An advantage of chemical cross-linking is that the mechanical performance of the resulting hydrogel can be systematically adjusted via variation in cross-linker type and cross-link density, so that controlled tissue-specific ECM analogues can be successfully obtained [73, 75, 79]. Limitations include reagent toxicity, side reactions and lack of triple helical preservation in resulting cross-linked systems, the latter being key to ensure high affinity for cells and mechanical stability in physiological conditions. Modification considerations should dictate low reaction temperatures and the use of non-hazardous solvents and/or chemicals [160].

‘Click’ chemistry is a method which invokes high reactivity, selectivity and uses mild reaction conditions; two examples being the Michael-type thiol addition reaction, which requires an electron deficient double bond and a catalyst and the thiol-ene radical addition, which requires the use of an electron rich vinyl group incapable of homopolymerisation and a photoinitiator [101].

To produce a collagen hydrogel by incorporating thiol click chemistry, it would first be necessary to functionalise collagen to contain an available thiol or vinyl group.

2.1.2 Photoinitiators

The preparation of hydrogels by photopolymerisation holds interest due to its potential use for injectable devices, 3D printing or for *in situ* cell encapsulation. However, various parts of this process are potentially toxic to cells, including exposure to certain wavelengths, free radicals and the photoinitiators themselves [132, 161].

Irgacure-2959 (I2959), lithium phenyl-2,4,6-trimethylbenzoylphosphinate (LAP) and eosin Y are an examples of water-soluble photoinitiators that require different wavelengths of light to react (Figure 2.1-1). I2959 and LAP are type I photoinitiators that release radicals upon exposure to wavelength 365 nm (UV) and 405 nm (violet/blue light) respectively [11]. Eosin Y is a dye which acts as a type II photoinitiator when used in conjunction with a co-initiator e.g. triethanolamine (TEOA) and exposed to visible light, 516 nm (green light). The photochemistry of eosin Y is well investigated: upon excitation, eosin Y becomes more reducing and more oxidising compared to in its ground state [162].

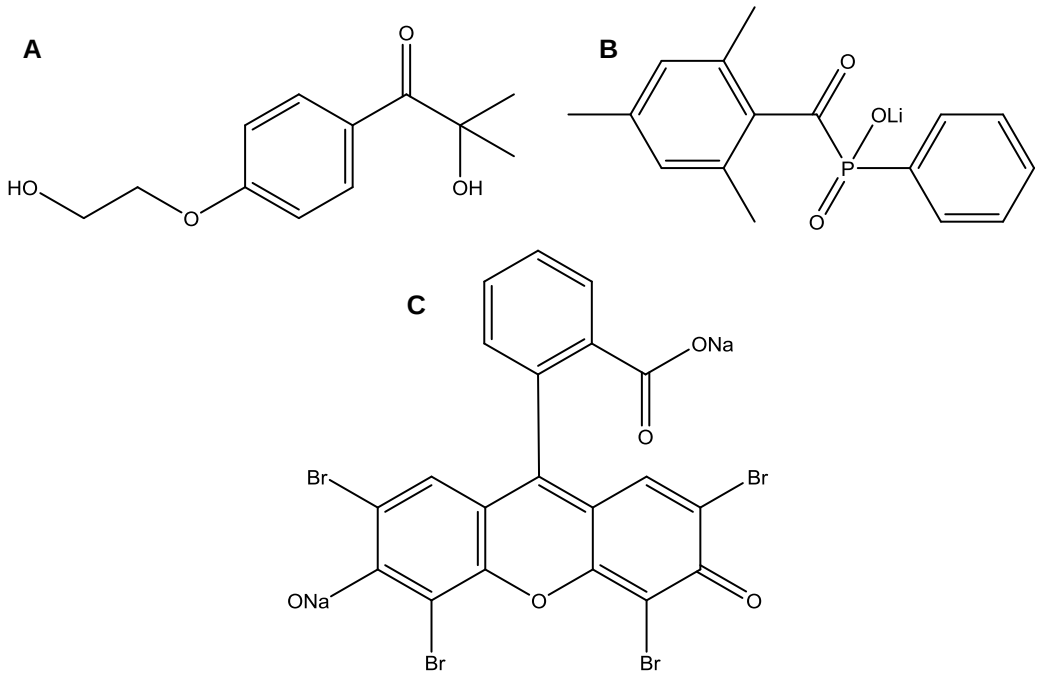

Figure 2.1-1 Chemical structures of the initiators (a) I2959, (b) LAP and (c) eosin Y

2.2 Materials and Methods

2.2.1 Materials

Rat tails were acquired from the University of Leeds' animal house. Acetic acid (17.4 M), glycidyl methacrylate, 4-vinylbenzoyl chloride, 2,4,6-trinitrobenzenesulfonic acid, poly(n-isopropylacrylamide), carboxylic acid terminated (Mn 10,000) and dulbecco's phosphate buffered saline were purchased from Sigma-Aldrich. N-(3-Dimethylaminopropyl)-N′-ethylcarbodiimide hydrochloride, 98 +% and tris(2-carboxyethyl)phosphine hydrochloride, 98% were purchased from Alfa Aesar. 1,3-Phenylenediacetic acid was purchased from VWR International. Triethanolamine, 99+%, eosin Y disodium salt, diethyl ether, anhydrous 99 +%, 2-iminothiolane hydrochloride, 98% and n-acetyl-L-cysteine, 98% were purchased from Fischer Scientific Ltd. 5-norbornene-2-carboxylic acid, 98%, mix , poly(ethylene glycol) divinyl ether (Mn 250), poly(ethylene glycol) diacrylate (Mn 700) and 2-mercaptoethanol were purchased from Sigma. Dithiothreitol was purchased from Life Technologies. 2-Hydroxy-1-(4-(2-hydroxyethoxy)phenyl)-2-methylpropan-1-one (I2959) was purchased from Fluorochem Limited. Lithium phenyl-2,4,6-trimethylbenzoylphosphinate was purchased from Tokyo chemicals industry. ATPlite™ Luminescence Assay System, 1000 Assay Kit was purchase from Perkin Elmer. LIVE/DEAD Viability/Cytotoxicity Kit for mammalian cells and n-hydroxysuccinimide were purchased from Thermo Fischer Scientific. Acrylate PEG succinimidyl carboxymethyl ester (Mw 2000, 3000) was purchased from JenKem Technology USA.

2.2.2 Collagen Type I

Type I collagen was isolated in-house via acidic treatment of rat-tail tendons. Briefly, rat-tails were defrosted in ethanol before the skin was removed using a scalpel. The tails were allowed to dry before the exposed tendons (approx. four per tail) were removed, placed in acetic acid (17.4 mM) and stirred for 48 hours. The solution was centrifuged (11,000 rpm, 40 min) and the pellet removed to leave the soluble collagen type I dissolved in the acetic acid. The solution was freeze-dried to produce white, acid-soluble collagen type I.

2.2.3 Collagen Functionalisation

Collagen can be functionalised using the long, unhindered amine group (NH_2) on (hydroxy) lysine [Lys]. This has an occurrence of 3.24 x 10^{-4} mol.g^{-1} collagen type I. A TNBS assay was used to quantify the functionalisation of the collagen and an Ellman's assay was used to show the presence of thiol groups. ^{1}H NMR and ATP FT-IR were not used due to overlapping peaks from the amino acids already present in collagen.

2.2.3.1 Dehydration Reaction

N-(3-Dimethylaminopropyl)-N′-ethylcarbodiimide hydrochloride (EDC)/ N-hydroxysuccinimide (NHS) can be used together to perform a dehydration reaction between an amine group and a carboxylic acid group (COOH) in aqueous conditions.

2.2.3.1.1 Collagen-NAC

Collagen was dissolved in HCl (10 mM, 0.8 wt.%). N-acetyl-l-cysteine (NAC)) (5-50 M excess [Lys]) was stirred with EDC (1:3 M NAC: EDC), NHS (1:1 M NHS: EDC) in phosphate buffer at 0 ^{o}C for 30 minutes. 2-mercapto ethanol (2ME) (1:1 M NHS: 2ME) was added and stirred for 10 minutes to deactivate the NHS/EDC not reacted with NAC so it would not cross-link the amine and carboxylic groups on the collagen. The deactivation step allowed confidence that the only reaction taking place was between the activated NAC and the amine group. The activated NAC solution was added to the collagen mixture and stirred for 24 hours. The solution was precipitated into ethanol (20 x excess), stirred for a further 24 hours then centrifuged (11,000 rpm, 40 min) and the pellet air dried (Figure 2.2-1).

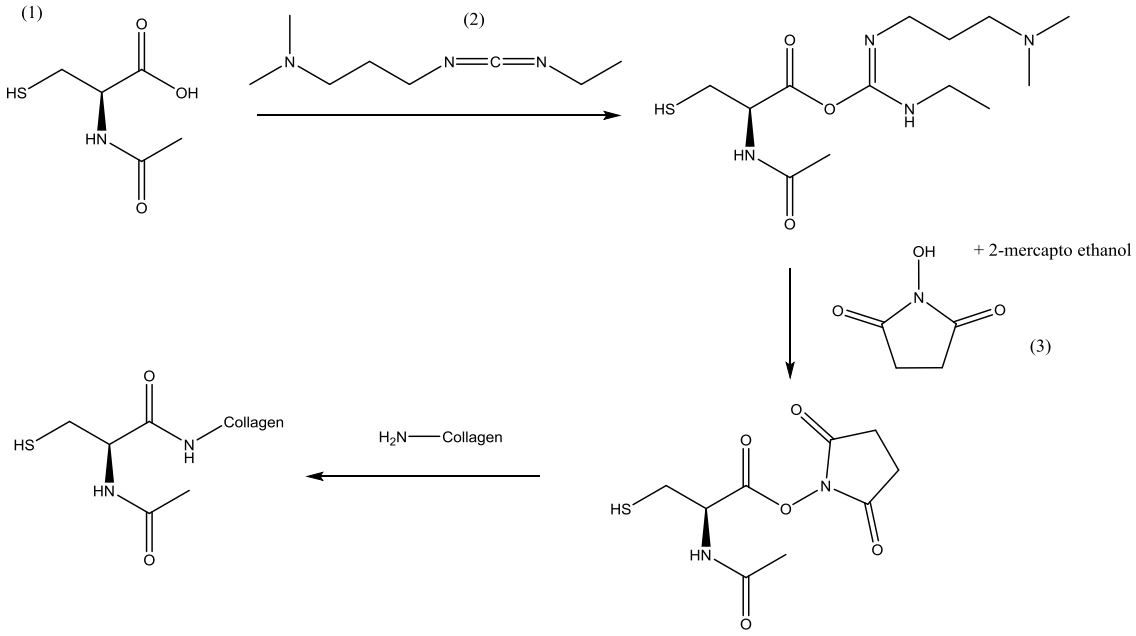

Figure 2.2-1 Activation of n-acetyl-l-cysteine (1) with EDC (2) and NHS (3) to produce a semi-stable NHS-ester followed by a substitution reaction with lysine.

2.2.3.1.2 Collagen-Norbornene

A dehydration reaction was performed to attach a norbornene group to the collagen back bone. Collagen was dissolved in HCl (10 mM, 0.8 wt.%). 5-norbornene-2-carboxylic acid (10 M excess [Lys]) was stirred with NHS (1:3 M norbornene: NHS), EDC (1:1 M NHS: EDC) in dimethyl sulfoxide (DMSO) (10 wt.% with respect to norbornene g) at 0 ^{o}C for 30 minutes. 2ME (1:1 M NHS: 2ME) was added to deactivate the non-activated EDC and stirred for 15 minutes. Collagen and DMSO solutions were combined and stirred for 24 hours. The solution was precipitated into ethanol (20 x excess), stirred for 24 hours then centrifuged (11,000 rpm, 40 min) and air dried (Figure 2.2-2).

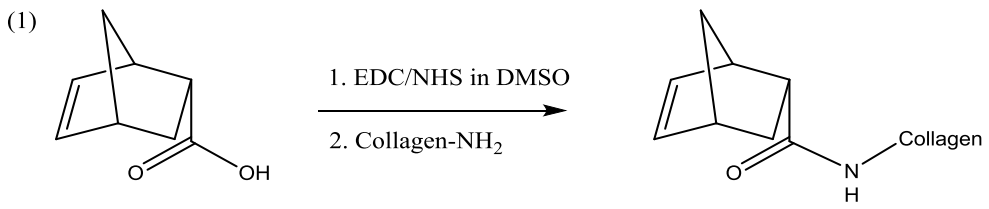

Figure 2.2-2 norbornene-2-carboxylic acid (1) dehydration substitution reaction with collagen (EDC/NHS).

2.2.3.1.3 Collagen-PNIPAM

A dehydration reaction was performed to attach thermoresponsive PNIPAM to the collagen backbone. Collagen was dissolved in hydrochloric acid (10 mM, 0.8 wt.%). Poly(n-isopropylamide) (PNIPAm) carboxylic acid terminated (10,000 $g.mol^{-1}$) (x 4 M excess [Lys]), EDC (1:3 [COOH]) and NHS (1:1 [EDC]) were stirred in PBS at 0 ^{o}C for 30 minutes. 2-mercapto ethanol (1:1 [EDC]) was added and stirred for a further 10 minutes. Both mixtures were combined and stirred overnight. The solution was precipitated into ethanol (20 x excess), stirred for a further 24 hours then centrifuged (11,000 rpm, 40 min) and the pellet air dried (Figure 2.2-3).

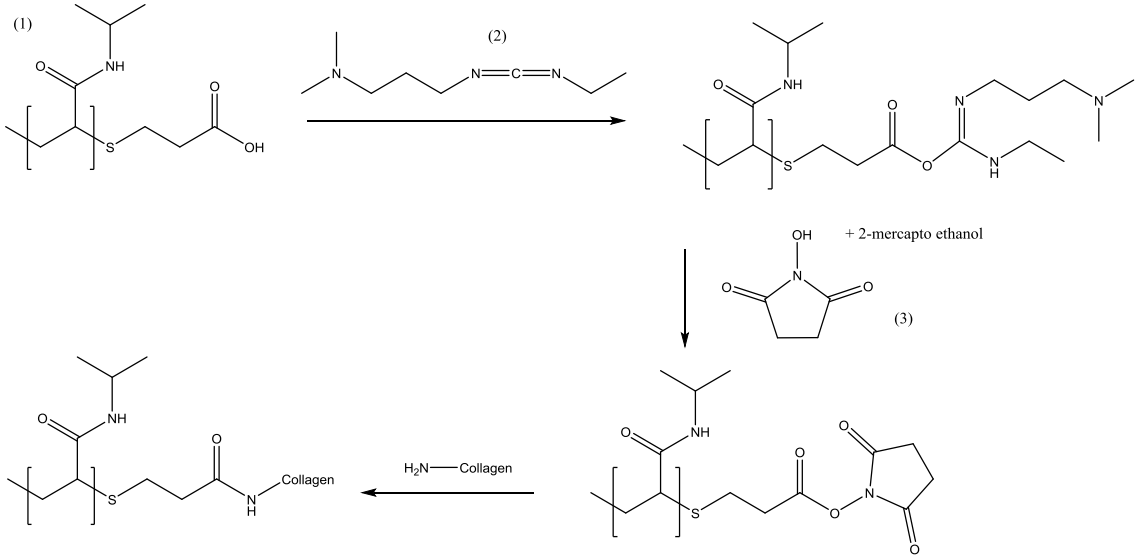

Figure 2.2-3 Activation of poly(N-isopropylacrylamide), carboxylic acid terminated (1) with EDC (2) and NHS (3) to produce a semi-stable NHS-ester followed by a substitution reaction with lysine.

2.2.3.2 Nucleophilic Addition/ Substitution Reaction

2.2.3.2.1 Collagen-2IT

Collagen type I was stirred in acetic acid (17.4 mM, 1 wt.%) until dissolution. The pH of the solution was adjusted to pH 7.4 and then 2-iminothiolane (Traut's reagent, 2IT) (10-30 M excess [Lys]) was added with 1,4-dithiothreitol (DTT) (1:1 [2IT]) to reduce disulphide bonds formed within the collagen-2IT and the solution was stirred for 24 hours .The solution was precipitated into ethanol (20 x excess),

stirred for a further 24 hours then centrifuged (11,000 rpm, 40 min) and the pellet air dried (Figure 2.2-4).

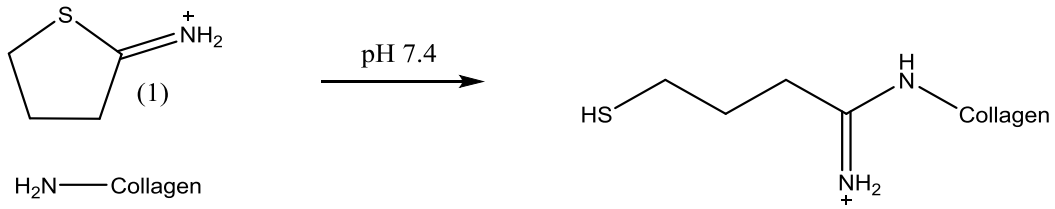

Figure 2.2-4 Ring-opening nucleophilic addition reaction of Traut's reagent (1) and lysine at pH 7.4.

2.2.3.2.2 Collagen-PEG-Acrylate

Collagen type I was dissolved in acetic acid (17.4 mM, 0.8 wt.%) the pH was adjusted to pH 7.0. NHS-PEG-acrylate was added (0.5-1 M excess to [Lys]) and left to react overnight. The solution was precipitated into ethanol (20 x excess), stirred for a further 24 hours then centrifuged (11,000 rpm, 40 min) and the pellet air dried (Figure 2.2-5).

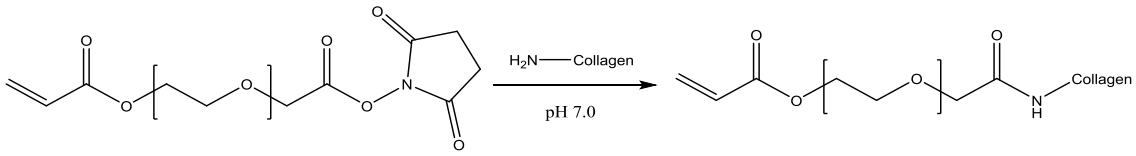

Figure 2.2-5 Nucleophilic substitution reaction between lysine and NHS ester.

2.2.3.2.3 Collagen-GMA/ Collagen-4VBC

Two vinyl moieties: Glycidyl methacrylate (GMA) and 4-vinylbenzyl chloride (4VBC) were attached to the collagen backbone by a substitution reaction. Collagen type I was dissolved in HCl (10 mM, 0.25 wt.%) and then the pH adjusted to 7.4. Tween20 (1%) was added to the solution followed by GMA or 4VBC (10-50 molar excess) and trimethylamine (1:1 to vinyl) and the solution was stirred for 24 hours. The solution was precipitated into ethanol (20 x excess),

stirred for a further 24 hours then centrifuged (11,000 rpm, 40 min) and the pellet air dried (Figure 2.2-6).

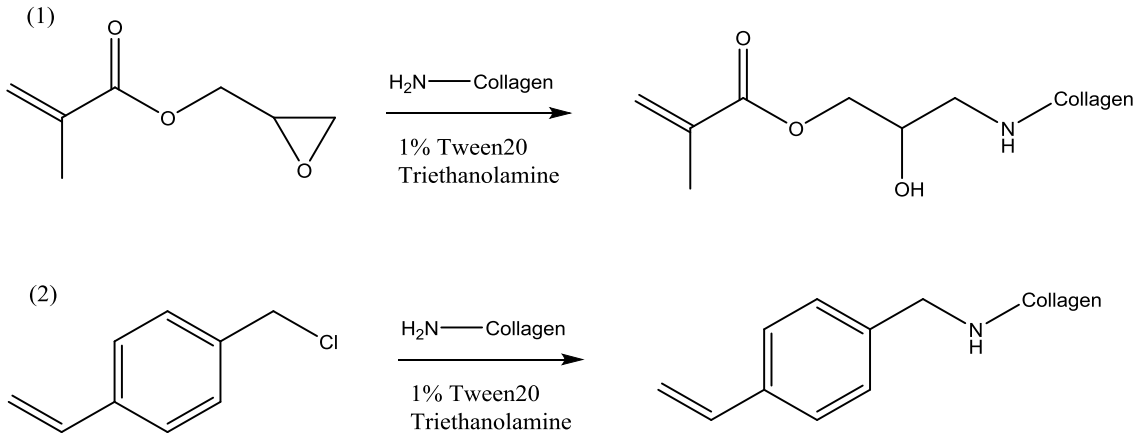

Figure 2.2-6 Nucleophilic addition reaction of GMA (1) and nucleophilic substitution reaction of 4VBC (2) with lysine.

2.2.4 Photoinitiators

Three commercially available, water-soluble photoinitiators were studied to examine their effectiveness with collagen for photopolymerisation: Irgacure 2959 (I2959) (365 nm), lithium phenyl-2,4,6-trimethyl-benzoylphosphinate (LAP) (365 nm) and eosin Y (EY)/ triethanaloamine (TEOA) (516 nm). Interpenetrating network hydrogels were prepared using collagen type I dissolved in acetic acid (17.4 mM, 0.8 wt.%), polyethylene glycol diacrylate (PEGdA) (Mn 700) (10% (w/v)) and eosin Y (0.1 mM)/ TEOA (0.75% (w/v) followed by exposure to green light.

2.2.4.1 *In Vitro* Cytotoxicity Assay

G292 cells (1 x 10^4 cells in 100 µL) cultured in 96-well plates were exposed to increasing concentrations of I2959, LAP and eosin Y/TEOA (0.01, 0.05, 0.1, 0.5% (w/v)). ATPlite assay was used to assess cell viability after 24 hours in culture. The absorbance of the experimental groups was normalised with respect to the corresponding tissue culture plastic control group to provide relative survival [129, 132].

2.2.5 Characterisation

2.2.5.1 Trinitrobenzenesulfonic (2,4,6) acid (TNBS) Colorimetric Assay

This assay was performed to determine the content of free-available amine groups and thereby the degree of functionalisation. Functionalised collagen (0.011 g) and a reference sample (0.001 g) were placed in a vial. Sodium hydrogen carbonate ($NaHCO_3$) (4%, 1 mL) and TNBS (0.5%, 1 mL) were added. Hydrochloric acid (HCl) (6 N, 3 mL) was added to the reference sample. This was stirred at 40 ^oC for 3 hours. HCl (6 N, 3 mL) was then added to non-reference sample and stirred at 60 ^oC for 1 hour to complete the reaction. Dilution in water (5 mL) was followed by extraction in diethyl ether (3 x 15 mL). An aliquot (5 mL) was removed and diluted in water (15 mL). Absorbance was measured at 346 nm.

The degree of collagen functionalisation, *F*, was determined by TNBS colorimetric assay, according to the following equations:

Equation 2.2.1

$$\frac{mol\ (Lys)}{g\ (collagen)} = \frac{2.Abs\ (346\ nm).0.02\ L}{1.46\ x\ 10^4(M^{-1}cm^{-1}).b.x}$$

Where: *Abs (346 nm)* is the absorbance value at 346 nm, *0.02* is the volume of sample solution (in litres*), 1.46 x 10*^{4} is the molar absorption coefficient for 2,4,6-trinitrophenyl lysine (in $M^{-1}{\cdot}cm^{-1}$), *b* is the cell path length (1 cm) and *x* is the sample weight.

Equation 2.2.2

$$F = 1 - \frac{mol(Lys)_{functionalized\ collagen}}{mol(Lys)_{native\ collagen}}$$

Where: *mol(Lys)* $_{native\ collagen}$ and *mol(Lys)*$_{functionalised\ collagen}$ represent the total molar content of free amino groups in native and functionalised collagen, respectively. The nomenclature (Lys) is hereby used to recognise the amine contribution of lysines and post-modified hydroxylysines.

2.2.5.2 Circular Dichroism (CD)

This technique was used to evaluate the secondary structure of collagen. CD spectra of functionalised samples were acquired with a ChirascanCD spectrometer (Applied Photophysics Ltd) using solutions in acetic acid (0.2 $mg.ml^{-1}$, 17.4 mM). Sample solutions were collected in quartz cells of 1.0 mm path length, whereby CD spectra were obtained with 4.3 nm band width and 20 nm min-1 scanning speed. A spectrum of the acetic acid (17.4 mM) control solution was subtracted from each sample spectrum. To present the data in terms of ellipticity (θ), the data is normalised by scaling to molar concentrations and Mean Residue Weight (MRW) for the peptide bond (90 Da) [163].

Equation 2.2.3

$$\theta_{mrw,\lambda} = \frac{MRW\ x\ \theta_{\lambda}}{10\ x\ d\ x\ c}$$

Where θ_{λ} is observed ellipticity (degrees) at wavelength λ, d is path length (1 cm) and c is the concentration (0.2 $mg.ml^{-1}$).

The ratio of the magnitude of the positive to negative peaks (RPN) was used as an indication of the triple helix architecture and for functionalised samples and quantification of the triple helix preservation was calculated by normalisation of RPN values with respect to the RPN value of native collagen.

Temperature ramp measurements at 221 nm fixed wavelength were conducted from 20 to 60 °C with 20 °C/hour heating rate, so that denaturation temperature (T_d) was determined as the mid-point of thermal transition.

2.2.5.3 Attenuated Total Reflectance Fourier-transform Infrared (ATR FT-IR) Spectroscopy

ATR FT-IR was carried out on dry samples using a Perkin-Elmer Spectrum BX spotlight spectrophotometer with diamond ATR attachment. Scans were conducted from 4000 to 600 cm^{-1}. Data attained from ATR FT-IR was dismissed for functionalised collagen as a result of hidden peaks from the amino acids on collagen.

2.2.5.4 Nuclear Magnetic Resonance Spectrometry (NMR)

Solid state NMR was performed on dry samples using Varian VNMRS & Bruker Advance III HD. Carbon-13 and H-1 spectra were recorded. This service was provided by the solid-state NMR Service at Durham University as part of a EPSRC service.

2.2.5.5 Ultraviolet/ Visible (UV/VIS) Spectrometry

UV/Vis spectroscopy was carried out on solutions (1 µL) using a Thermo Scientific NanoDrop Lite spectrophotometer or (1.5 mL) in a quartz vial to use JENWAY 6305 spectrophotometer.

2.2.5.6 ATPlite Assay

A vial of lyophilised ATP standard solution (9.6 µmole) was reconstituted in ATP buffer solution (5 mL). The media from cells cultured in a 96 cell well plate was removed. Mammalian cell lysis solution (50 µL) was added and the plate was shook for five minutes in an orbital shaker at 700 rpm. ATP solution (50 µL) was added and shook for a further 5 minutes. An aliquot (50 µL) was removed and added to an optiplate. This was dark adapted for 10 minutes inside the machine before the luminescence was measured using a Perkin Elmer TopCount [129].

2.2.6 Statistics

Data has been expressed as mean ± standard error of the mean (SEM) unless n > 20, when it is expressed as mean ± standard deviation. Statistical analysis was performed using MiniTab software. Levene's test was used to test for variance in data, t-test for comparison of two different groups, one-way ANOVA followed by post-hoc Tukey test on data when Levene's test showed $p \geq 0.05$ and equal variances could be assumed and a Welch's ANOVA followed by a post-hoc Games-Howell on data when Levene's test $p \leq 0.05$ and equal variances could not be assumed. Statistical significance was determined by $p \leq 0.05$.

2.3 Results and Discussion

Sample nomenclature used in this work is as follows: functionalised collagen is coded as "collagen-X", where "X" identifies the functional reactive group used.

GMA - glycidyl methacrylate (vinyl group), 4VBC -.4-vinylbenzyl chloride (vinyl group), NAC - n-acetyl-l cysteine (thiol group) and 2IT - 2-iminothiolane (thiol group).

2.3.1 Collagen Type I

Soluble collagen type I was extracted from rat tail tendons. TNBS assay showed an occurrence of (hydroxy) lysine (NH_2) of 3.24 x 10^{-4} mol.g^{-1} due to 100% attachment of TNBS onto the amine groups. CD was used to analyse the triple helical conformation of the collagen (Figure 2.3-1). The unique supercoiled polyproline type II secondary structure of the protein backbone exhibits distinct CD transitions, including a positive peak at 221 nm and a negative peak at 198 nm which is characteristic of the triple helix conformation [163-165]. The magnitude ratio of the positive peak to the negative peak (RPN) can be used as an indication of the triple helical structure. This was calculated as 470414: (-)3739571 =0.126 (literature RPN 0.117 [79]) for collagen type I. Normalisation of corresponding RPN value of functionalised collagen with respect to the RPN value of native collagen can be used as an indication of the preservation of the triple helix [166].

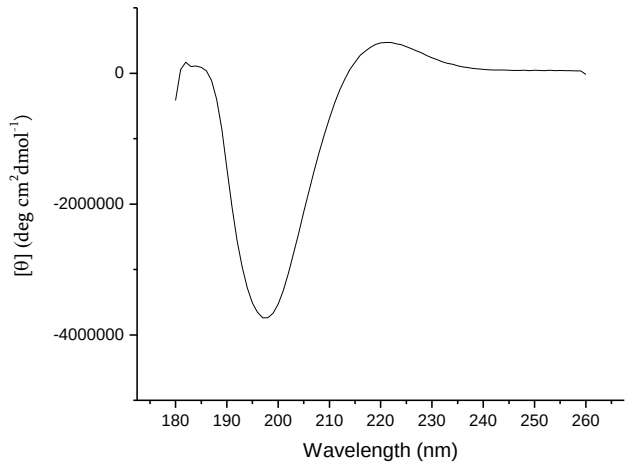

Figure 2.3-1 CD spectra of collagen type I.

Changes in the positive peak at 221 nm are indicative of changes to the triple helix structure, so this wavelength was monitored in a CD melting curve experiment to show the thermal denaturation with increasing temperature (Figure 2.3-2). The denaturation temperature was measured at the temperature of half the initial ellipticity, this was recorded to be 36.5°C with a literature value of RT collagen type I T_d – 37 ^oC [167].

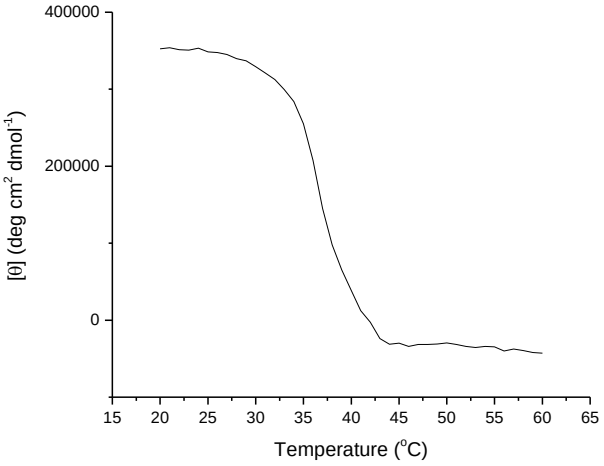

Figure 2.3-2 Temperature-ramp CD spectra of collagen type I.

NMR spectroscopy is a technique used for determining the structure of organic compounds. Solid-state proton and carbon-13 nuclear resonance spectroscopy was performed on collagen type I (Figure 2.3-3). The formation of the collagen triple-helix conformation requires the presence of the repeating Gly-X-Y motif, with the most common repeating sequence being Gly-Pro-Hyp. Therefore most of the peaks arising from NMR on collagen will be due to these major amino acid residues, glycine (33%), proline (12%) and hydroxyproline (9%) [168]. ^{1}H NMR was shown to only provide moderate information on the collagen structure because of many overlaps of the resonances (Figure 2.3-3 B) [169] Figure 2.3-3 (A) shows a broad peak in the carbonyl carbon chemical shift region (~170 ppm) which is indicative of the peptide bonds in collagen. The peaks in the 30-80 ppm aliphatic region are mainly due to the major amino acid residues, Gly, Pro and Hyp. The peaks recorded were 70.97, 59.62, 54.56, 49.65, 47.84, 43.07, 38.66, 32.95, 30.28 and 25.29 ppm. In the literature, Gly Cα is stated to display two peaks of relative intensity at 43.37 and 42.60 ppm [169]. The most intensive peak in the ^{13}C NMR was at 43.07 ppm. Due to the information from the literature, this peak could be indicative of Gly Cα, although sufficient distinction was difficult due to spectral resolution. In the aliphatic region of the spectrum, the only other peak which could be easily resolved was the Hyp peak due to the hydroxyl group attached to the carbon increasing its electronegativity. From the literature, Hyp peaks are shown to resonate at 38.9 and 71.1 ppm, so this could be assigned as the highest peak in the aliphatic region of 70.97 [170]. The other peaks in the aliphatic region are not straightforwardly assigned due to each amino acid producing several ^{13}C peaks at overlapping chemical shifts.

A

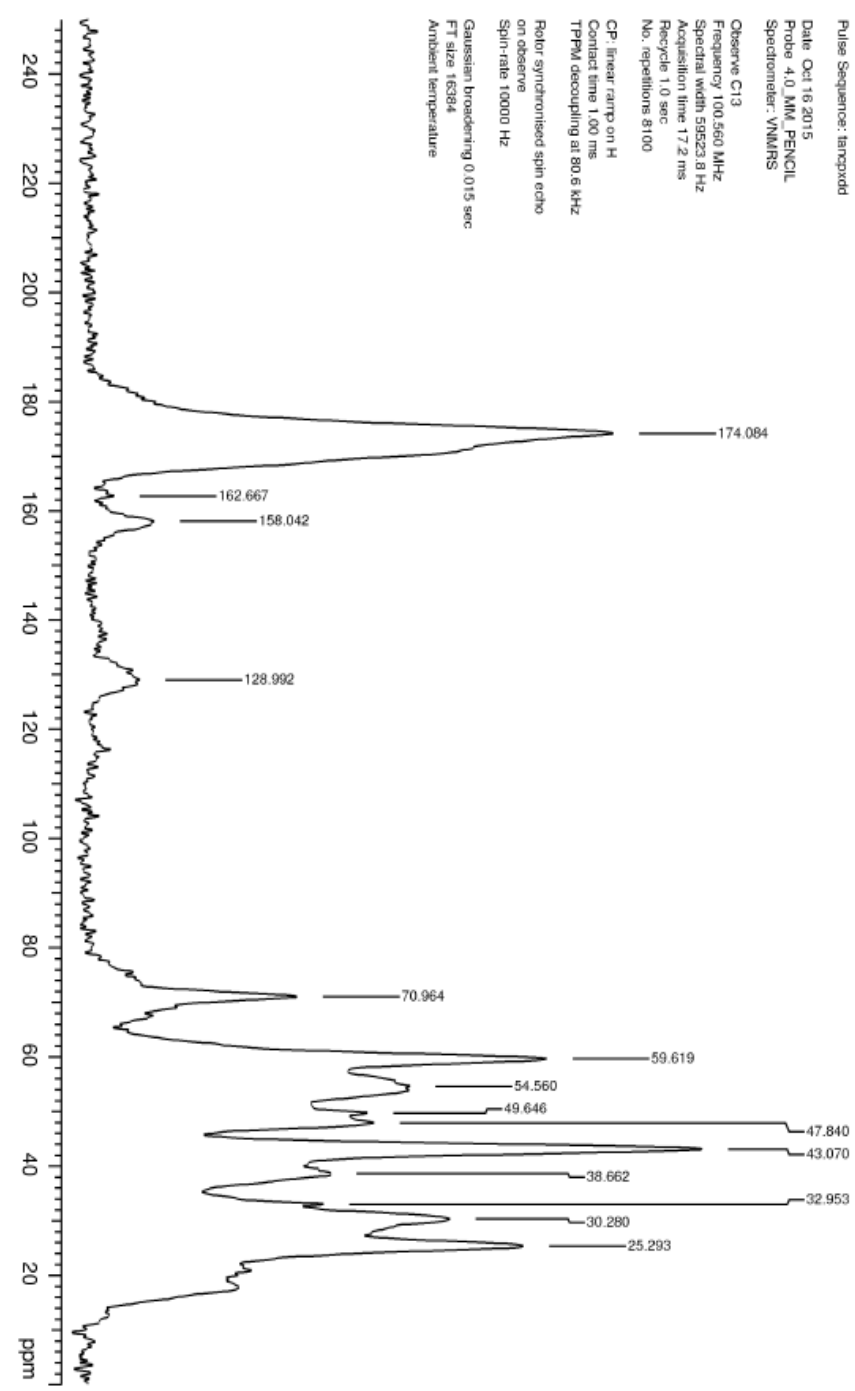
14305827
Rat tail type 1 collagen
File: 17cfjw_20151016_01
Pulse Sequence: tanqpxdd
Date Oct 16 2015
Probe 4.0_MM_PENCIL
Spectrometer: VNMRS
Observe C13
Frequency 100.560 MHz
Spectral width 59523.8 Hz
Acquisition time 17.2 ms
Recycle 1.0 sec
No. repetitions 8100
CP: linear ramp on H
Contact time 1.00 ms
TPPM decoupling at 80.6 kHz
Rotor synchronised spin echo
on observe
Spin-rate 10000 Hz
Gaussian broadening 0.015 sec
FT size 16384
Ambient temperature
174.084
162.667
158.042
128.992
70.964
59.619
54.560
49.646
47.840
43.070
38.662
32.953
30.280
25.293
240
220
200
180
160
140
120
100
80
60
40
20
ppm

B

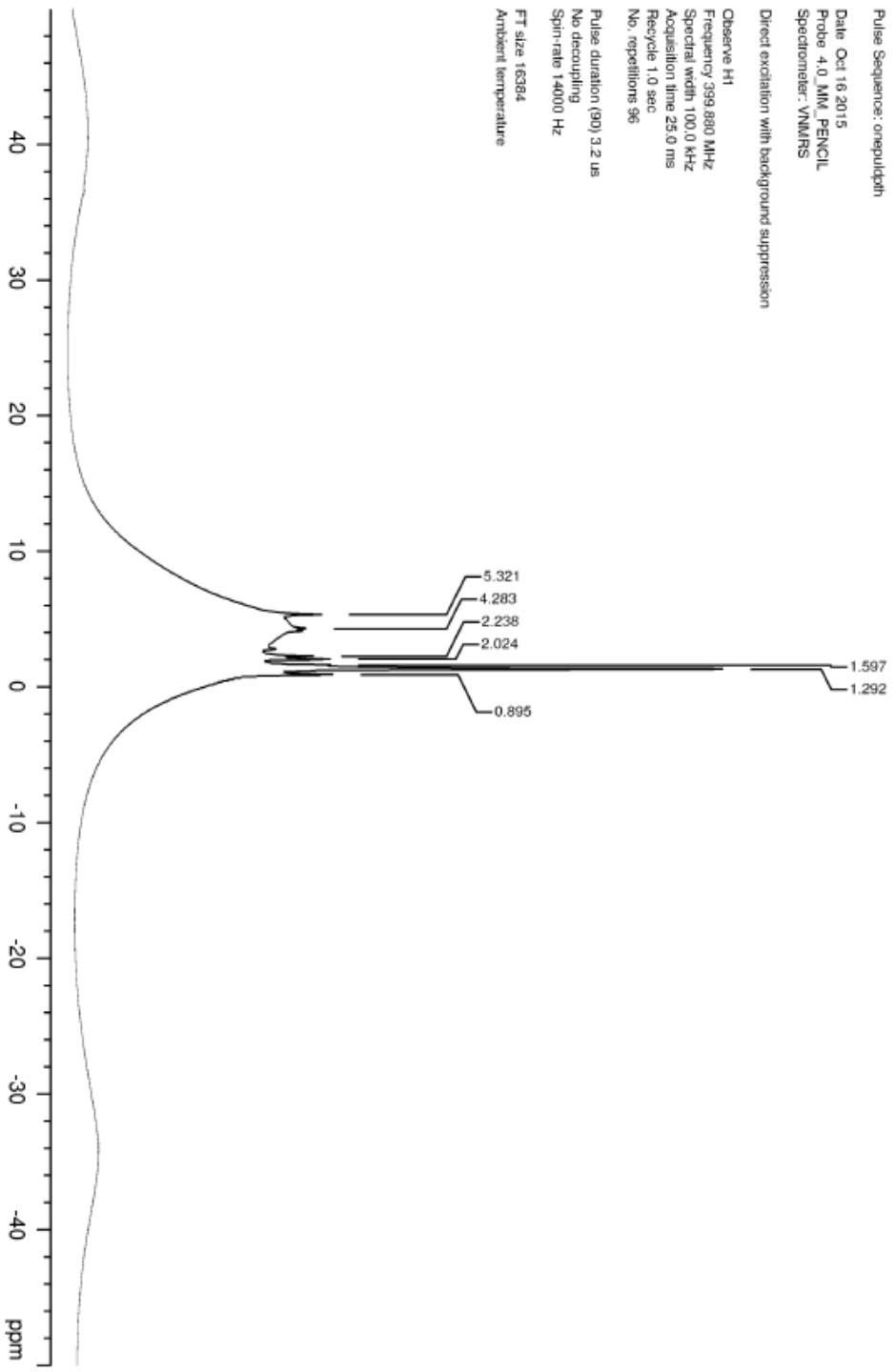

Figure 2.3-3 Solid-state nuclear resonance spectroscopy of collagen type I (A) ^{13}C NMR spectrum (B) ^{1}H NMR spectrum.

FTIR spectra of collagen displayed no distinction between the amino acids. Although the amide bonds are observed in terms of carbonyl, C=O peak (1650 cm^{-1}), C-N stretch (1240 cm^{-1}) and N-H stretch (1550 cm^{-1}). Additionally, a broad peak was observed at ~ 3300 cm^{-1} indicative of -OH (3320 cm^{-1}) and NH stretching 3020 cm^{-1} [78, 171].

2.3.2 Collagen Functionalisation

2.3.2.1 Collagen-GMA/ Collagen-4VBC

Collagen was initially functionalised with vinyl-bearing moieties GMA (flexible) and 4VBC (rigid) following protocols by Tronci *et al*, to produce water-stable biomimetic systems with good preservation of the triple helical network [75, 79]. As discussed in section 3.2.2.2, hydrogel networks were subsequently obtained following UV irradiation of the vinyl-functionalised collagen. The degree of functionalisation was calculated by a TNBS assay whereby a lowered molar content of free, non-reacted (hydroxy) lysine groups was observed (< 3.24 x 10^{-4} $g{\cdot}mol^{-1}$ [Lys]). It was shown by Tronci *et al* that the degree of collagen functionalisation could be controlled based on the monomer type and the molar excess of monomer with respect to [Lys]. To obtain similar degrees of functionality, 50x excess of GMA and 30x excess of 4VBC were used to prepare collgen-GMA (F~40%) and collagen-4VBC (F~44%), similar to the literature values [79]. As discussed in section 4.2.3.2, the collagen-4VBC material was taken forward using a rat calvarial defect model to study it's *in vivo* stability.

2.3.2.2 Collagen-PNIPAm

Poly(N-isopropylacrylamide) (PNIPAm) is a temperature responsive polymer which forms a hydrogel when heated above 32 ^{o}C. By grafting this polymer onto the collagen backbone, it could provide a facile means to encapsulate cells in a physical hydrogel at 37 ^{o}C without the need of an additional harmful base or photoinitiator. Three collagen-PNIPAM papers were identified. Nistor *et al* reported a co-monomer NIPAM mixture being polymerised over a collagen support, so no functionalisation with the collagen molecule [172]. Barnes *et al* reported hybrid collagen and poly(N-isoproylacrylamide-co-styrene-graft-NVP) (NSN) hydrogels, although this was an interpenetrating hydrogel network of both solutions heated to 37 ^{o}C [173]. Fitzpatrick *et al* reported collagen functionalised

with PNIPAM using EDC/NHS chemistry to graft PNIPAM amine-terminated onto the collagen backbone (COOH groups from Asp and Glu) [174]. The problem with this published method (Fitzpatrick) is that when the COOH groups are activated on Asp and Glu, they are also susceptible to nucleophilic substitution reaction by the amine group on (hydroxy) lysine (in addition to the amine-terminated PNIPAM). To solve the issue of the unwanted side reactions, in the current study, a similar reaction was attempted whereby carboxylic acid-terminated PNIPAM (Mw 10,000) was activated using EDC/NHS rather than Asp or Glu and grafted to collagen by reaction with the (hydroxy) lysine groups. As stated in previous work by Tronci *et al*, the degree of functionalisation is affected by both monomer type and the molar excess of monomer, however, due to the expense of the PNIPAM-carboxylic acid terminated chemical, an excess of only 2x or 4x was used. TNBS assay showed functionalisation up to 53.3% and this new material was dissolved in acetic acid (1 wt.%, 17.4 mM). However, when this new collagen-PNIPAM solution was warmed in the incubator to 37 ^{o}C, gelation was not achieved, instead the solution turned cloudy and the viscosity increased. The characteristic thermoresponsive collapsed structure over 32 ^{o}C of PNIPAM was observed (cloudy solution), however, no physical hydrogel was formed. This was attributed to the overall concentration of the PNIPAM in the solution being too low to contribute to the thermal-gelling. Even at a functionalisation of 53.3% of the 3.24 x 10^{-4} mol.g^{-1} (hydroxy) lysine groups, PNIPAM would still contribute a low w/v (%) of the overall collagen-PNIPAM solution (1 wt.%). Yan *et al* reported a PNIPAM hydrogel (20 wt.%) with elastic modulus (G') in the Pa range, however, collagen is limited by its solubility to achieve concentrations this high [175]. Ohya *et al* reported the synthesis of PNIPAM-gelatin via a two-step process ending in graft copolymerisation of NIPAM. The advantage of using gelatin was that the final concentrations they used of the PNIPAM-gelatin for testing were 5 and 20 w/v (%) thereby allowing the PNIPAM to surpass its critical gelation concentration [176]. Therefore it was acknowledged that grafting PNIPAM onto the backbone of gelatin would be more preferential than grafting onto collagen due to the higher concentration that could be achieved in a solution.

2.3.2.3 Collagen-PEG-Acrylate

Acrylate PEG succinimidyl carboxymethyl ester was purchased to provide a friendly, facile means to functionalise collagen. The PEG molecule possessed an acrylate and an NHS group which could be used in a nucleophilic substitution

reaction with hydroxy (lysine). This chemical was very expensive although the NHS functionality made it very reactive, an excess of 0.5x provided a degree of functionalisation 43.9% and an excess of 1x degree of functionalisation was 79.1%.

Unfortunately this acrylate-PEG functionalised collagen had very poor solubility in weakly acidic solutions of acetic and hydrochloric acid and would not dissolve even when the experiment was repeated several times. Despite the reaction taking place in the dark, it was presumed that one step during the process had caused some of the vinyl groups to react, thus providing a non-soluble network [75].

2.3.2.4 Thiol Click Chemistry

Cysteine is a naturally occurring amino acid which contains an available thiol group. This amino acid is not present in collagen type I however, it was used as biomimetic inspiration when deciding means to functionalise collagen to provide an available thiol group. N-acetyl-l-cysteine (NAC) was identified as a derivative of cysteine wherein an acetyl group is attached to the nitrogen atom (providing a COOH group). This compound is non-toxic and is sold as a dietary supplement. A dehydration reaction with NAC and EDC/NHS was devised to successfully thiolate collagen (collagen-NAC). NAC like most thiols (RSH), can be oxidised by a large variety of radicals and also serve as a nucleophile (electron pair donor) to produce both a thiolate anion RS^- and thiyl radical ($RS^•$) and can be potentially used for thiol click chemistry [177]. The pK_a of NAC is 9.51 and is relatively high compared to cysteine, pKa 8.18 [177].

Additionally, a base-free reaction with Traut's reagent (2IT) was examined as another means to thiolate collagen. Whilst NAC was a more biomimetic approach to thiolate collagen, it involved EDC/ NHS activation whereas 2IT would react with (hydroxy) lysine using a ring-opening reaction at pH 7.4 without the need of an additional, harmful base. This ring opening reaction also maintains the charge properties similar to the original amino group.

The functionalisation of the primary amine groups of collagen was confirmed using a TNBS assay and represented as the degree of functionalisation. The degree of triple helix preservation (%) of the collagen after functionalisation was determined using CD with normalisation against the RPN value of native collagen (Figure 2.3-4).

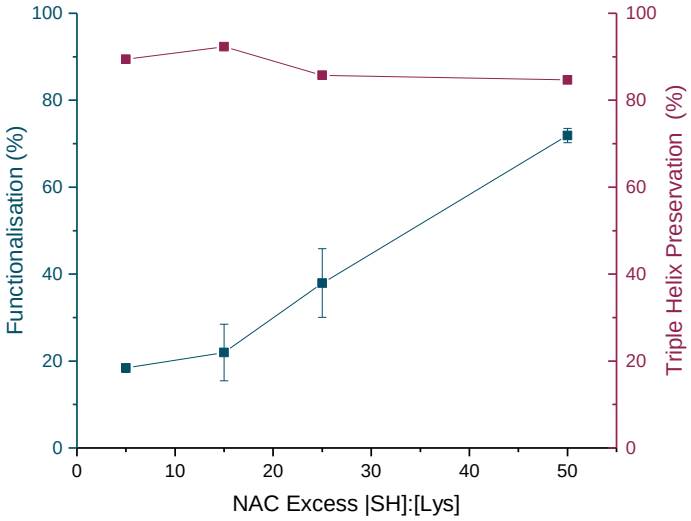

Figure 2.3-4 Degree of functionalisation and triple helix preservation in collagen products reacted with NAC at varied [NAC]:[Lys] molar ratios. Data presented as means ± SEM.

Increasing the excess of NAC in the reactant mixture with respect to the available primary amine [Lys] showed a comparable increase in the degree of functionalisation of the collagen. Using 5 times excess presented 18% functionalisation whereas 50 times excess presented 72% functionalisation. Triple helical preservation showed a decrease from 90→85% with increasing degree of functionalisation of the collagen. The collagen-NAC (50x excess) was used for most experiments due to its high degree of functionality (72%) and triple helical preservation (85%). It was found that this new material was only soluble in acetic acid (17.4 mM) and would not dissolve in hydrochloric acid (10 mM) or PBS.

In comparison, when collagen was functionalised with 2IT, a 5 times excess presented a 55% functionalisation, whereas 20 times excess presented 80% functionalisation (Figure 2.3-5). The degree of triple helical preservation was relatively unaffected by the increased conversion of amine to thiol groups (preservation >89 %); this is beneficial to preserve the material's stiffness and natural high affinity for cells [178]. Up to 72% functionalisation (15x excess), triple helical preservation remained above 95%. The preservation decreased to 89% above 80% lysine functionalisation. For this reason, future experiments used a 15 times excess (72% functionalisation) to keep triple helical preservation above 95%. This high degree of triple helical preservation is likely due to the small amount of steric hindrance from the small, five-atom spacer 2IT.

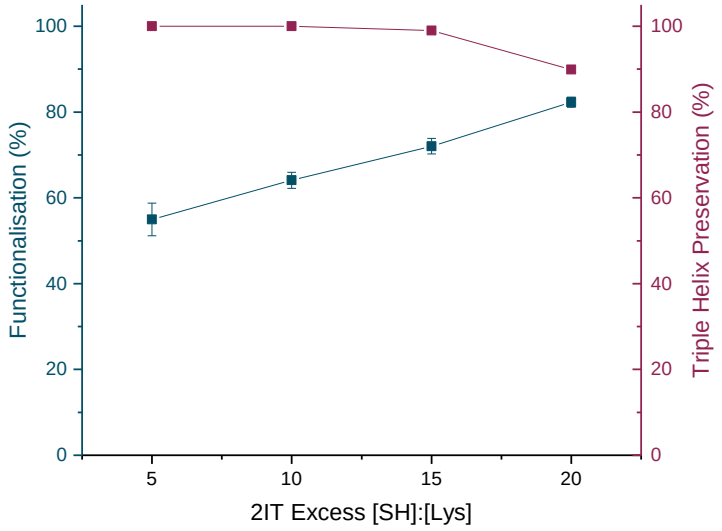

Figure 2.3-5 Degree of functionalisation and triple helix preservation in collagen products reacted with 2IT at varied [2IT]:[Lys] molar ratios. Data presented as means ± SEM.

The benefit of the additional 2IT thiol group was the improved solubility of the functionalised collagen. Collagen-2IT was soluble in PBS (0.01M). This improved solubility was likely due to the 2IT providing charge properties similar to the original amino group and due to the added hydrophilicity. Improved solubility of functionalised collagen was also reported by Tronci *et al*, whereby the photo-active collagen-GMA material was soluble in PBS [75].

The preparation of any thiol-containing precursor meant the presence of disulphide bonds needed to be considered. When the collagen-2IT functionalisation experiment was being designed, it was noted that when the collagen solution (1 wt.%) and 2IT were mixed overnight at pH 7.4, a weak gel was formed (Figure 2.3-6). This meant that disulphide bonds were formed between the thiol-containing 2IT after it was attached to the collagen. This mixture was often too gel-like to stir to add a reducing agent. Instead the synthesis method was altered to include an equimolar ratio of dithiothreitol (DTT) to reduce disulfide bonds. After the 24 hour reaction, the solution had the same collagen-like viscosity and there was no gel formation like previously. This altered synthesis route meant there were no concerns over the formation of disulphide bonds in the synthesis method. It also meant that in later experiments, it was apparent whether disulphide bonds were formed because of the gel-like structure the solution would take at 1 wt.% concentration (Figure 2.3-6).

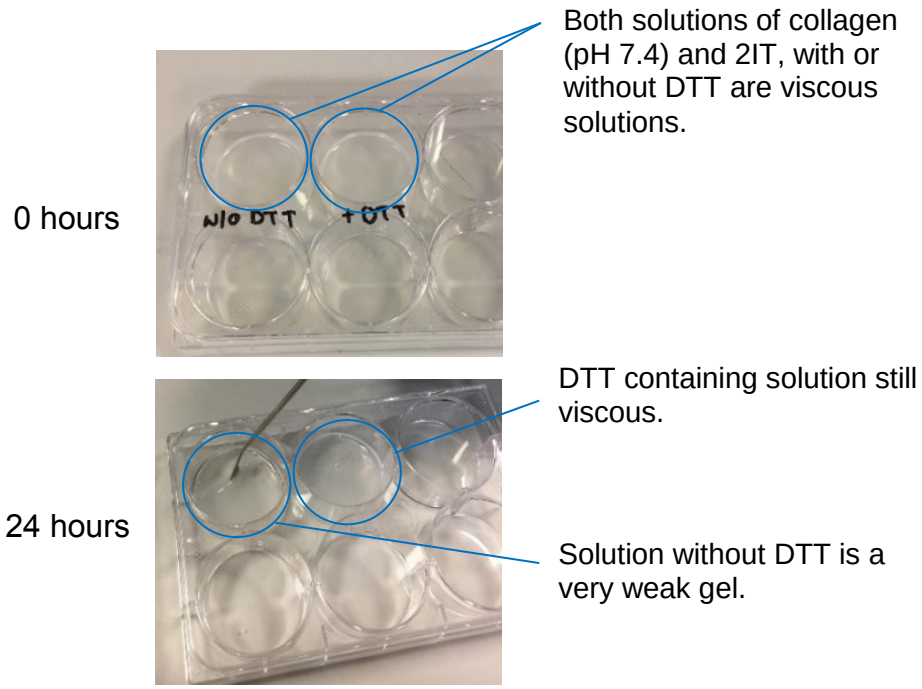

Figure 2.3-6 Synthesis of collagen-2IT to demonstrate what the presence of disulphide bonds looks like in a 1 wt.% solution.

Work by Zhang *et al* reported incorporation of sulphydryl groups by immersing collagen scaffolds in 100 µL of 2IT (2.5 mg ml^{-1}) dissolved in PBS with ethylenediaminetetraacetic acid (EDTA) (4 mM) (used to prevent oxidation of the sulphydryl groups) for 12 hours [179]. This paper provided no quanitification of the degree of functionalisation, however this method was employed by the same research group in a later paper which used a ninhydrin assay to quanitfy the amine groups and reported a 1% conversion [180]. This method of immersing pre-formed scaffolds meant that the improved solubility (PBS, 0.01 M) from functionalisation of collagen with 2IT was not reported [181].

Kommareddy *et al* reported the synthesis of gelatin functionalised with 2IT. Gelatin was dissolved in deionised water (pH 7.4) and 2IT (2x excess) was added for 15 hours similar to the design in the current study. Disulphide bond formation was desirable in this work to stabilise the nanoparticles so no EDTA/ DTT was added [182].

A temperature ramp was used to compare whether the thiol-functionalisation of collagen-NAC and collagen-2IT affected the degradation temperature (T_d) of the collagen (Figure 2.3-7). This was taken at half the initial ellipticity and recorded: collagen 36.5 ^oC, collagen-NAC 38.5 ^oC and collagen-2IT 39.5^oC.

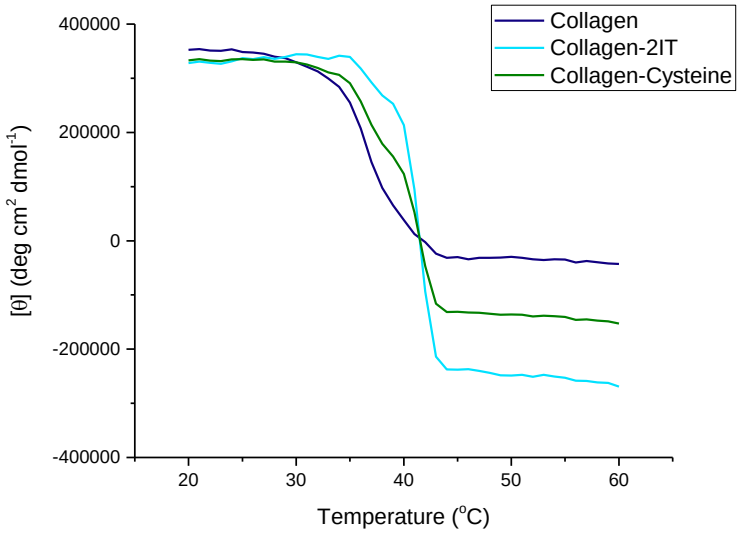

Figure 2.3-7 Temperature-ramp CD spectra of collagen type I, collagen-2IT and collagen-NAC.

For all samples, the 221 nm-molar ellipticity was observed to decrease with increasing temperature reflecting heating-related triple helix denaturation and all were shown to display comparable T_d ~ 35-39 °C. The higher T_d for the thiol functionalised collagen could be due to triple helix-stabilising hydrogen bonds or hydrophilic interactions [75].

A literature search has shown no evidence to date of any previous preparation of thiol-functionalised collagen using NAC and whilst collagen functionalised with 2IT has been reported, no identical synthetic method was found nor any that reported similar high degrees of functionality to the work in the current study. Xu *et al* reported another means to thiolate collagen which involved a 2-step reaction. The first step involved a reaction with succinic anhydride to yield carboxylated collagen. This was then further reacted with 2-mercaptoethylamine hydrochloride to produce the thiolated collagen and whilst this recorded high functionalisation (F ~92%), it could be strongly argued that the methods reported using NAC and 2IT were preferable due to their facile means and the use of non-harmful chemicals [183].

2.3.2.5 Collagen-Norbornene

Thiol-ene reactions require a double bond incapable of homopolymerisation. It thus followed that once thiol-functionalised collagen had been prepared, it was desirable to make collagen functionalised with a double bond incapable of homopolymerisation. Vinyl ethers are incapable of homopolymerisation,

however, none could be found with a reactive chemical group such as COOH or C-X. Norbornene is also incapable of homopolymerisation and 5-norborbornene-2-carboyxlic acid (norbornene-COOH) was selected. This chemical was not water-soluble even when tween20 was added to improve the miscibility, so the EDC/NHS activation step was performed in DMSO before being added to a collagen solution. High degrees of functionalisation were recorded (F ~60%), however this collagen suffered from poor solubility and fell outside of the modification considerations set during the start of this work which dictated that no hazardous solvents and/or chemicals should be used in the modification of collagen. Mũnoz *et al*, reported gelatin functionalised with norbornene using carbic anhydride. This materials decomposes on contact with water and is stated to be dangerous. Briefly, GelNB was prepared via reacting gelatin with carbic anhydride in aqueous buffer solutions at 50 °C. The reaction time and the buffer pH were adjusted to obtain GelNB, F~ 36% [184]. This reaction mechanism would have posed difficulties for collagen because it is desirable to keep collagen at pH 7.4 for the natural triple helices and collagen should not be heated above 37 ^{o}C because the triple helices will denature [184].

2.3.3 Photoinitiators

Once the functionalisation of collagen had been explored, the next step was to analyse water soluble photoinitiators in terms of their light excitation (wavelength), molar absorptivity and their cytocompatibility at varied concentrations. It was noted that direct toxicity of a photoinitiator can be caused by either the light source or the chemical photoinitiator [130].

I2959 is a commonly used water-soluble (< 1 wt.%) photoinitiator (365 nm) and is considered to be cytocompatible at low concentrations. LAP is less well-researched than I2959, however it benefits from higher water-solubility than I2959 (< 5 wt.%) and can be used at 365 (UV) or 405 nm (violet light). During this work, it was desirable to develop a novel hydrogel synthetic route which could enable cell encapsulation. UV light is a well-established genetic mutagen at lower wavelengths although the higher 365 nm can be used to mitigate some of the mutagenic effects for low exposure times [130].

A visible light photoinitiated reaction would be more desirable and an extensive review of the literature led to the selection of the dye, eosin Y as a type II photoinitiator capable of releasing radicals after exposure to visible/green light when used with a hydrogen-donating co-initiator e.g. triethanolamine (TEOA)

[130, 131, 133, 185, 186]. Further work by Shih *et al* demonstrated that the reaction still worked using only eosin Y when hydrogen-donation could be generated from sulfhydryl groups (thus creating thiyl radicals) [131]. A cytocompatible visible light photoinitiator would eliminate any potential cellular toxicity imparted by UV radiation, especially when long exposure times are necessary (> 5 min) [130].

Shih *et al* reported PEGdA hydrogels formed using eosin Y (0.1 mM), TEOA (0.75 % (w/v)) and co-monomer, 1-vinyl-2 pyrrolidinone (NVP) (0.1 % (w/v)) together with the PEGdA precursor and visible light irradiation [187]. NVP was used as a co-monomer (vinyl group), however, if this chemical was used in a thiol click reaction, it would result in step and chain-growth photopolymerisation reaction rather than just step-growth (as preferable). In a similar reaction, Hao *et al* stated that using 1% (w/v) NVP compared to 0% increased the final gel stiffness, likely due to additional cross-links from the chain-growth polymerisation. Additionally, they also stated that whilst the inclusion of NVP did not affect cell viability, although it did affect cell spreading and osteogenic differentiation [185]. It was decided that the type II eosin Y visible light photoinitiator would only be incorporated into collagen polymerisation reactions if the use of NVP could be avoided. This was because if this visible light polymerisation method was incorporated into click chemistry, it could cause a pseudo-step growth reaction due to addition homopolymerisation from the NVP which would alter the results.

Precursor solutions were prepared using eosin Y (0.1, 0.5, 1 mM) and TEOA (0.5, 0.75, 1% (w/v) dissolved in acetic acid (17.4 mM). The first problem encountered was that the collagen would not dissolve in these solutions. This was due to TEOA. This material is primarily used as a surfactant and acts as a pH-buffer which made the collagen insoluble. It was discovered that if the eosin Y/ TEOA solutions were concentrated 100-fold, they could be mixed into a pre-dissolved collagen solution (acetic acid, 17.4 mM). This had to be added whilst the collagen solution was being vortexed to ensure fast mixing of the eosin Y/ TEOA concentrate. The visible light type II photoinitiator was first attempted with a collagen-PEGdA solution to examine which concentration of the eosin Y/TEOA would work since collagen solutions often require more photoinitiator due to viscosity, poor solubility or competing absorbance. Due to potential cell cytotoxicity, the ideal reaction conditions were to use the lowest concentration of eosin Y, and due to issues with pH-buffering and solubility issues, the lowest concentration of TEOA as possible. The optimal combination was found to be

eosin Y (0.007 % (w/v)) and TEOA (0.75% (w/v)) in terms of solubility and would polymerise the collagen-PEGdA solution to form a hydrogel within 60 seconds after exposure to green light without the need to incorporate NVP. Bahney *et al* reported that TEOA had a toxic effect at a concentration of 1.5 % (v/v), so it was beneficial in the current study that only half of that amount was needed [130]. It was also discovered that the presence of TEOA was fundamental to co-initiate the eosin Y with visible (green) light in a collagen/ PEGdA solution. This was because the reaction worked by the excitation of the eosin Y dye molecules into a triplet state (green light, 516 nm) and initial abstraction of a hydrogen atom from amine-bearing co-initiators (TEOA). This subsequently abstracts a hydrogen from the acrylate group, thus forming carbonyl radicals which propagate and polymerise the PEGdA [185, 188].

The rate of a photopolymerisation reaction is directly proportional to the initiator concentration, light intensity, the molar extinction coefficient and photoinitiator efficiency [188]. UV-Vis spectra of all three photoinitiators and collagen were compiled into one graph (Figure 2.3-8).

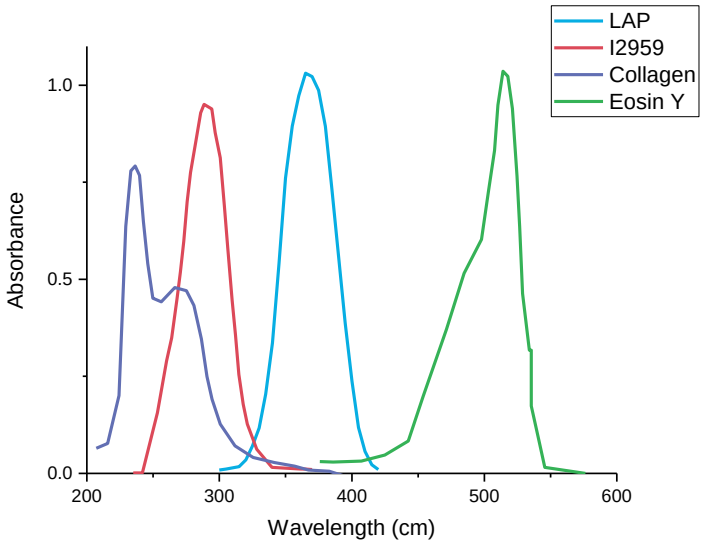

Figure 2.3-8 UV/Vis spectrum showing the absorbance of collagen, I2959, LAP and Eosin Y.

The maximum absorption wavelength of LAP was found to be 380 nm, with a high absorbance still recorded at 365 nm (molar extinction coefficient (ε): 218 $M^{-1}{\cdot}cm^{-1}$) [132]. In comparison, I2959 had a peak maximum at 285 nm, where it also displayed competing absorbance against the peak from the aromatic amino acids in collagen, whilst displaying minimal absorbance at 365 nm (ε: 4 $M^{-1}{\cdot}cm^{-1}$) [132]. Eosin Y displayed no competing absorbance with collagen and showed

high molar absorbance at its peak 516 nm (green light) (ε > 100,000 M^{-1} cm^{-1}) [187]. The weak absorbance profile of I2959 and its competing absorbance with the collagen severely limits its utility for photopolymerisation reactions performed at 365 nm, nevertheless it is commonly used at this wavelength to reduce cytotoxicity to cells and for general lab safety [189]. The competing absorbance and low molar extinction coefficient (365 nm) also means a higher concentration of this photoinitiator can be required to generate sufficient number of radical to initiate a reaction, although this again is inhibited due to the poor solubility of I2959 in aqueous solutions.

Photoinitiator toxicity was evaluated using an ATPLite assay on G292 cells cultured with an increased concentration of either LAP, I2959 or eosin Y/TEOA for 24 hours (0.005, 0.01, 0.05, 0.1, 0.5% (w/v)). TEOA was added to the solutions at the same ratio it would occur with the relative eosin Y concentration due to its necessary contribution as a co-initiator.

The relative survival of the cells was calculated by normalising the absorbance readings of the samples against the control, which was G292 cells grown on tissue culture plastic with five repeats (Figure 2.3-9).

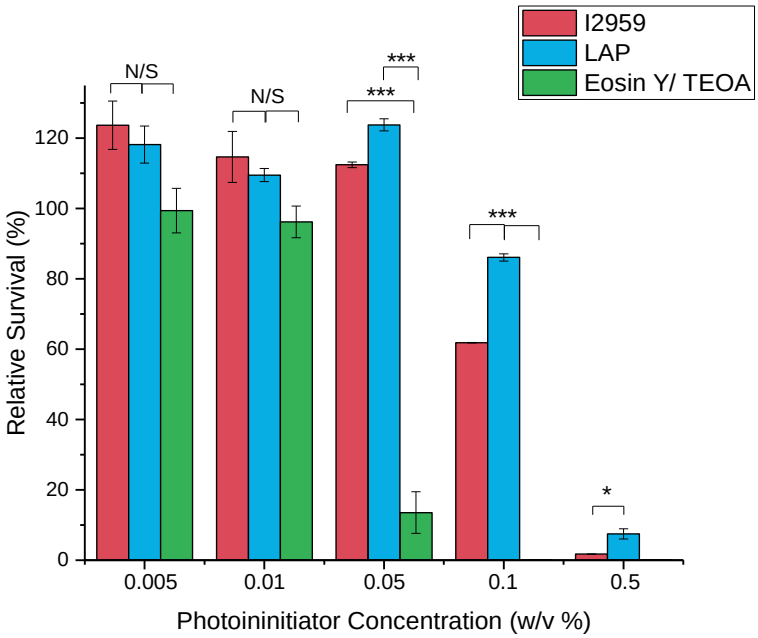

Figure 2.3-9 Relative survival of G292 cells cultured in cell culture medium supplemented with increasing photoinitiator. Cell survival was quantified using an ATPlite viability assay. Data are presented as means ± SEM. * p < 0.05; *** p < 0.001, N/S no significance (n= 5).

Minimal initiator induced cytotoxic response is key to enable gelation *in situ* in biological environments in the presence of cells. The results showed that there was no detected cell toxicity after culturing the cells for 24 hours in photoinitiator concentrations below 0.01% (w/v) for LAP, I2959 and eosin Y/TEOA. Photopolymerisation reactions are driven by chemicals that produce free radicals when exposed to specific wavelengths of light. Type I photoinitiators (I2959 and LAP) commonly use concentrations above 0.1% to ensure efficient generation of radicals for the reaction to occur; although it has been reported that when incorporated with peptides, I2959 does not initiate photopolymerisation reactions as effectively at concentrations below 0.3% [129, 130, 190]. The relative survival of comparable photoinitiator concentrations was: LAP 0.1% (w/v): 86% survival, LAP 0.5% (w/v): 7.5% survival, I2959 0.1% (w/v): 62% survival and I2959 0.5% (w/v): 1.7% survival. The type II photoinitiator eosin Y used in conjunction with TEOA has been shown to initiate reactions at lower photoinitiator concentrations which is beneficial because at comparable concentrations to I2959 and LAP, it is cytotoxic: EY/TEOA 0.5% (w/v): 0.04% survival, EY/TEOA 0.1% (w/v): 0.1% survival, EY/TEOA 0.05% (w/v): 13.5% survival, EY/TEOA 0.01% (w/v): 96.2% survival and EY/TEOA 0.005% (w/v): 99.4% survival. The concentration of eosin Y used in the visible light reactions was 0.007% (w/v) which lies between 96.2 and 99.4% (no relative toxicity). The relative survival of cells in eosin Y/TEOA outperformed LAP and I2959 and it was known that cells would have better survival rate when exposed to visible light compared to UV (365 nm). However, there were many disadvantages of using eosin Y/TEOA with visible/ green light exposure.

One disadvantage was the visible-light eosin Y hydrogels would remain orange in colour even after long incubation periods (>48 hours) in PBS, indicating that the dye would not leach out of the hydrogel (Figure 2.3-10).

Figure 2.3-10 Visible-light initiated collagen-PEGdA hydrogel (d - 1 cm) after 48 hours incubation in PBS.

This was unexpected because it was thought unlikely that the eosin Y dye (Mw – 691.85 $g \cdot mol^{-1}$) would be physically 'trapped' within the swollen hydrogel, however, the long-lasting orange colour was also noted by Shih *et al*. They offered the explanation that a termination step between radical-bearing eosin Y and the carbonyl radicals could cross-link the dye to the PEGdA [187]. Additionally, a second possibility could be a strong binding affinity between eosin Y and the PEG hydrogel leading to difficulty leaching the dye out. The orange-coloured visible light induced hydrogels are problematic for cell imaging since the strongly green-light absorbing dye interferes with traditional LIVE markers and Alexa flour 488 (green). Another issue with visible/ green light photoinitiation was that most photo-curing rheometers available to study the gelation kinetics have inbuilt UV lamps and the 3D printers available in the university also used UV curing with no option for visible light/ green lamps.

Nevertheless, as indicated in the eosin Y/TEOA – collagen development, the main issue was the difficulty incorporating this solution with collagen due to the pH buffering TEOA. This had been overcome in this work by vortexing the collagen solution before adding the eosin Y/TEOA concentrate as proof of principle for this visible-light mediated polymerisation method. However, this vortexed solution required immediate exposure to light otherwise the TEOA would result in clumping of the collagen. This meant that the solution could not be stored and in terms of application, cell encapsulation or 3D printing would face unnecessary difficulties.

Accordingly, the decision was made to put aside visible-light photoinitiation using eosin Y/TEOA due to TEOA solubility/ dye trapping/ visible light issues and focus on the type I photoinitiators, LAP and I2959 until the novel synthetic method had been designed and tested. Shih *et al*, reported that mechanistically, eosin Y could be used without TEOA. After excitation by a visible light source, the eosin radical could abstract a hydrogen from thiol-containing cross-linkers (such as bis-cysteine-containing peptide) to create thiyl radicals instead of from a co-initiator such as TEOA. These thiyl radicals could then react with a PEG multi-arm norbornene terminated macromer. Using eosin Y (0.1 mM) as the only initiator, Shih *et al* reported a gel point of ~100 seconds and shear modulus ~100 Pa, both indicative of poor photoinitiator efficacy and inefficient deprotonation of the thiol group. This would impede incorporation of a solely eosin Y visible-light mediated method into the synthesis of collagen hydrogels in the current study. However, Shih reported that when tyrosine was added (1 mM), it improved the efficiency of the bis-cysteine- peptide deprotonation to produce a hydrogel with

gel point ~22 seconds and shear modulus ~1000 Pa with the same system [186]. This interesting result implies that chemicals that increase the deprotonation efficiency of either collagen-NAC or collagen-2IT could be explored to re-examine visible light once a synthetic method to produce click chemistry hydrogels had been designed.

2.4 Conclusion

Collagen type I was successfully extracted, characterised and functionalisation was examined as a preliminary step to hydrogel formation and to tailor the mechanical properties of resultant hydrogels.

The installation of functional groups at the side chain was examined with focus on preservation of the triple helix structure and the use of no hazardous solvent/ chemicals. Collagen-PNIPAM was prepared as a thermoresponsive collagen precursor material, however, it was discovered that the overall concentration of PNIPAM was too low to result in a physical gel because of the low [Lys] available. Two thiol modified collagen precursor materials were prepared with the aim to use them for a thiol click chemistry reaction to produce a hydrogel. Collagen-NAC benefitted from its biomimetic design, and no occurrence of collagen functionalised with NAC could be found in the literature, so this remained novel. Collagen-2IT benefitted from better solubility than collagen-NAC and was soluble in PBS. Collagen-2IT also required a lower excess of 2IT compared to NAC to achieve the same degree of functionalisation, 72% (15x vs 50x excess respectively). Collagen-2IT also benefited from higher degree of triple helical preservation, likely due to the small, flexible 2IT moiety. The photoinitiators I2959, LAP and eosin Y/TEOA were examined in terms of their absorption and toxicity. I2959 was shown to have a significantly reduced absorption at 365 nm and it was shown that it could be compromised when used in combination with collagen which also absorbs light in the UV range. The relative survival of cells in increasing concentrations of these photoinitiators were examined. Eosin Y/ TEOA displayed excellent cell compatibility (~100% cell survival) and a high extinction coefficient at 516 nm. However, as a visible-light photoinitiator with collagen, it would have to be used without TEOA due to solubility. Future work could examine chemicals that could improve the efficiency of thiol deprotonation for visible light polymerisation. However until a collgen click chemistry reaction is designed, LAP and I2959 will be used as water-soluble photoinitiators.

Chapter 3 - Collagen Hydrogels and Click-Chemistry

3.1 Introduction

The aim of this chapter was to develop a novel cross-linking strategy for the preparation of collagen hydrogels, ideally to be used for cell encapsulation or as an injectable device. This should lead to physical and mechanical characterisation before selecting three hydrogels with properties similar to the natural muscle (~8-16 kPa) to take forward for *in vitro* studies.

The design of regenerative devices relies heavily on the use of three-dimensional (3D) scaffolds to provide the appropriate environment, mechanical support and an initial cell anchorage site for the regeneration of tissues and organs [191]. As a biomaterial, hydrogels provide a 3D hydrated framework with tissue-like elasticity for culturing cells. They also possess the ability to encapsulate cells and molecules prior to gelation, thus affording a minimally invasive avenue to deliver cells and bioactive factors [51, 192, 193]. Collagen type I is a natural polymer and is the most abundant structural building block in connective tissues such as bone, tendon and cartilage [74, 194].

As a scaffold material, collagen is inherently biocompatible and bioactive, and is a major component of the natural extracellular matrix (ECM), however its use as a biomaterial may be limited due to batch-to-batch variability, potential antigenicity, time-consuming isolation process and difficulty in tuning features such as stiffness, degradation and bioactivity [73]. Self-assembled collagen hydrogels are mechanical dictated by the collagen concentration. It is difficult to produce pure collagen hydrogels with a stiffness above 1 kPa without extensive chemical cross-linking which can fundamentally alter the triple helical conformation or degradability of the collagen fibrils. Chemical cross-linking can often be performed via covalent modification of lysine and hydroxylysine residues and amino termini, cumulatively counting for ~ 3×10^{-4} $mol \cdot g^{-1}$ of collagen [78, 156-158, 195]. An advantage of chemical cross-linking is that mechanical performance and degradation can be controlled via variation in cross-linker type, cross-link density or hybridisation with synthetic materials, regardless of environmental conditions, such as pH or temperature, resulting in tissue-specific ECM analogues [73, 79, 196]. Limitations include reagent toxicity,

side reactions and lack of preservation of the triple helical conformation of collagen.

3.1.1 Click Chemistry

'Click' chemistry is a term introduced by Sharpless in 2001 which has the definition: "*A click reaction must be of wide scope, giving consistently high yields with a variety of starting materials. It must be easy to perform, be insensitive to oxygen or water, and use only readily available reagents. Reaction work-up and product isolation must be simple, without requiring chromatographic purification*" [197].

So 'click' chemistry refers to cross-linking methods which invoke high reactivity, use mild reaction conditions and small amounts of photoinitiator/ catalyst and generate no harmful by-products [101, 198]. As such, click chemistry is an appealing approach for the formation of collagen hydrogels.

Among click reactions, thiol-click chemistry has been shown to be a powerful tool for the efficient formation of thioether linkages (i.e., C–S–C) [199]. Examples of two thiol-click reactions include: Michael-addition, which requires an electron-deficient carbon-carbon double bond (vinyl) and a base; and the thiol-ene and thiol-yne reaction, which proceed via a radical mediated, step-growth mechanism between a thiol and a vinyl group that can be initiated using a light source and a photoinitiator (Figure 3.1-1) [103, 200].

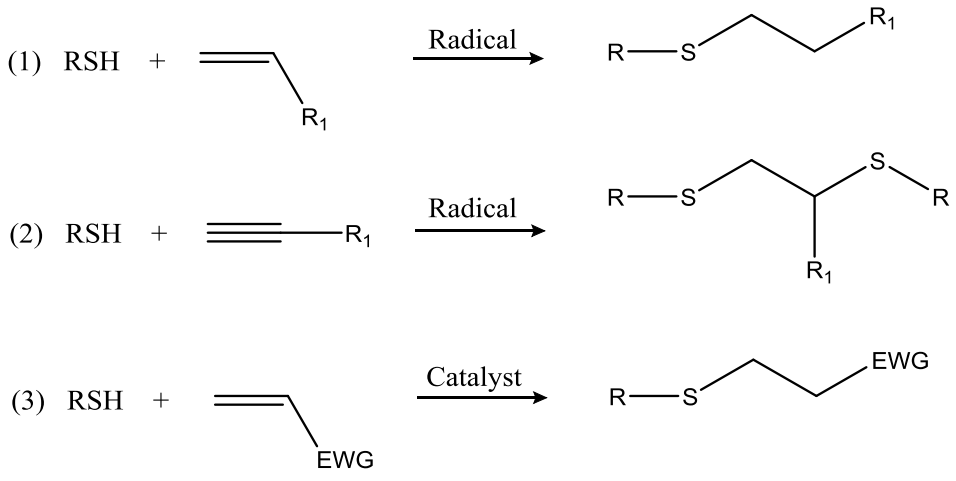

Figure 3.1-1 Click Chemistry additions to carbon-carbon multiple bonds. (1) thiol-ene, (2) thiol-yne and (3) Michael-addition. EWG – electron withdrawing group.

The thiol-ene reaction requires the use of a double bond incapable of homo-polymerisation to ensure the only reaction taking place is the thiol-ene click reaction, such is the case for vinyl ether or norbornene-based mono-/macromers [201].

Although thiol-ene and Michael-addition hydrogels have been reported, none had been prepared using collagen as the precursor material, thus providing the opening for a novel cross-linking strategy for the preparation of collagen hydrogels [110, 111, 186, 201, 202]. Note that a collagen hydrogel incorporating Michael-addition was released in 2016 [80].

3.1.2 Cell Encapsulation/ Injectable Hydrogels

As a result of the reaction selectivity and oxygen insensitivity, an interesting feature of thiol-click mixtures is their potential to be mixed with cells and molecules prior to gel formation, thus providing a potential avenue to deliver cells and bioactive factors in a minimally invasive manner.

Injectable hydrogels are extremely effective at filling irregular spaces and configure the exact shape of a defect. In order to do so, the gelation kinetics require the polymer solution to gel and solidify within a clinically acceptable timescale *in vivo* [115]. Although to successfully fill the irregular defect, it is necessary that the hydrogel possesses good mechanical strength, a predefined shape or the ability to physically bind to adjacent tissues.

The typical methods to induce cross-linking gelation, include thermal and photochemical polymerisation, enzymatic and ionic cross-linking and click chemistry. The majority of these cross-linking techniques require the use of a catalyst or photoinitiator to proceed which could be toxic to tissues and would therefore be inappropriate for *in situ* gelation. Although, as mentioned, a feature of click chemistry is that it uses a lower amount of photoinitiator/ catalyst compared to traditional reactions. Additionally, traditional homopolymerisation which is a chain-growth reaction, has been shown to yield high initial radical concentrations which can cause radical-mediated cell damage which would be an inappropriate method for cell-encapsulation [184].

To achieve collagen gelation *in situ*, a major hurdle for the thiol-click reactions is the necessary use of a non-toxic and water-soluble photoinitiator/ catalyst [54, 203].

Upon light exposure, photoinitiators generate free radicals that may cause cellular damage at varied extent, depending on the gelation kinetics of the reacting mixture [204]. Additionally, most of the commercially-available photoinitiators are intended for use in organic solvents or dental resins and are therefore mostly insoluble in aqueous solutions of collagen.

3.2 Methods

3.2.1 Materials

2-Hydroxy-1-(4-(2-hydroxyethoxy)phenyl)-2-methylpropan-1-one (I2959) was purchased from Fluorochem Limited. Lithium phenyl-2,4,6-trimethylbenzoylphosphinate (LAP) was purchased from Tokyo chemicals industry. 8-arm PEG Norbornene (PEG-NB) (Mw: 20,000 $g.mol^{-1}$) was purchased from JenKem Technology USA. Collagenase Clostridium histolyticum, 4-arm PEG Norbornene (Mw: 10,000 $g.mol^{-1}$), Glycidyl methacrylate, 4-vinylbenzyl chloride, dulbecco's phosphate buffered saline, poly(ethylene glycol) diacrylate (mn 700), tris (2-carboxyethyl) phosphine chloride, hexaethyleneglycol dithiol and 4-(2-hydroxyethyl)-1-piperazineethanesulfonic acid (HEPES) were purchased from Sigma Aldrich. Photocol was purchased from Advanced BioMatrix. Ellman's reagent was purchased from Cambridge Bioscience.

3.2.2 Gelation Methods

Collagen hydrogels can be prepared by many methods. In this research, hydrogels formed by ionic or physical means are not examined because stronger gels were preferential (> 5 kPa) for application as tissue engineered constructs [83].

3.2.2.1 General Design Considerations

A variety of parameters must be considered when designing materials for use as cell-hydrogel constructs, including cytocompatibility of the chemical reagents, all the base polymers and chemistries must maintain and support cell viability during hydrogel fabrication, modification, and culture. The mechanism for forming materials in the presence of cells should not result in significant cell death, DNA

damage, or expression of cell stress markers. Furthermore, the resulting material must have an appropriate pore size (roughly > 10 nm) to allow for nutrient, waste, and soluble factor (e.g. growth factors) diffusion within the matrix, as well as potential diffusion of biochemical reagents. For cell imaging, a material that is optically clear or does not interfere with light transmission is beneficial [205].

3.2.2.2 Chain-Growth Photopolymerization

The initiator, 2-hydroxy-1-[4-(2-hydroxyethoxy) phenyl]-2-methyl-1-propanone (I2959) (1%) was dissolved in either PBS (0.01 M) or acetic acid (17.4 mM) depending on whether the photopolymerisation was with functionalised collagen-GMA or collagen-4VBC respectively. The solution was stirred at 37 ^{o}C for 2 hours until the photoinitiator was completely dissolved and the solution was colourless. The solution was cooled to room temperature and then the functionalised collagen (0.8 wt.%) was added and stirred for 2 days. The solution was aliquoted into cell well plates and exposed to UV light (365 nm) for 30 minutes on both sides.

3.2.2.2.1 PhotoCol®

Advanced BioMatrix PhotoCol® was sold as a kit including lyphophlilised methacrylated collagen, neutralisation solution and I2959. Methacrylated collagen type I (0.1 g) and acetic acid (12.5 cm^3, 20 mM, 8 mg/ mL) were stirred until dissolution at 8-10 ^{o}C. Neutralisation solution (1 mL) and I2959-methanol solution (0.135 mL, 0.1%) were chilled in an ice bath. These solutions were combined and stirred thoroughly, keeping temperature below 10 ^{o}C. The solution was incubated at 37 ^{o}C for 30 minutes until gel formation before exposing to UV light (365 nm) for 30 minutes.

3.2.2.3 Click Chemistry

3.2.2.3.1 Thiol-Ene Free-Radical Addition

Collagen-SH (1 wt.%) was dissolved in PBS (0.01 M) containing either LAP or I2959 (0.1% (w/v) or 0.5% (w/v)). The results from chapter 2 showed there was relative cell survival at both these concentrations. PEG-NB (2 -4 % (w/v)) was added to the collagen solution. Exposure to UV light (Spectroline, 365 nm)

resulted in complete gelation by a thiol-ene step-growth reaction mechanism (Figure 3.2-1).

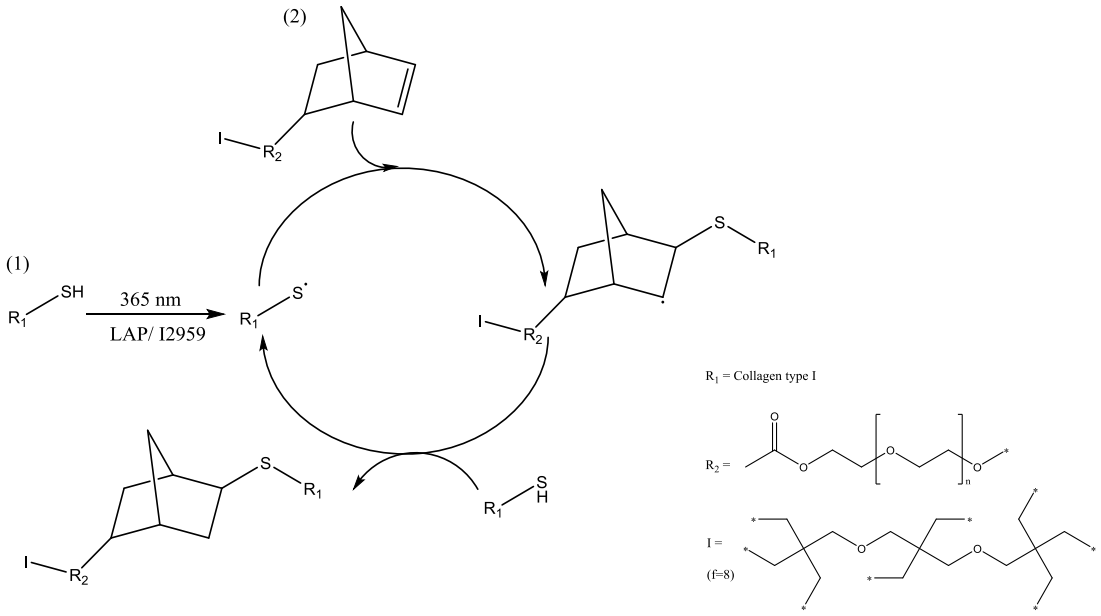

Figure 3.2-1 Illustration of the thiol-ene photo-click reaction mechanism between collagen-2IT (1) and PEG-NB (2).

The thiol-ene click reaction was also attempted with: collagen-NAC (40% functionalised) and collagen-4VBC (44% functionalised) (1:1); collagen-NAC and collagen-GMA (40% functionalised) (1:1); collagen-NAC (40% functionalised) and collagen norbornene (70% functionalised) (1:1.75) and collagen-2IT (72% functionalised) and collagen-norbornene (70% functionalised) (1:1).

3.2.2.3.2 Thiol Michael-Addition

Collagen-GMA dissolved in PBS (0.8 wt.%). Hexa(ethylene glycol) dithiol (1:0.5 M (GMA:SH)) was added followed by tris (2-carboxyethyl) phosphine chloride (TCEP) (1:1 M SH:TCEP) and the solution stirred for 10 minutes. TEA (1:1 M SH: TEA) was then added.

Collagen-NAC was combined with collagen-GMA (1:1 40% functionalised) in acetic acid (17.4 mM, 0.8 wt%) and the pH was adjusted to either 9.5 or 10.5 using sodium hydroxide (NaOH, 5M) and gently shook for 24 hours. The pKa of n-acetyl-l-cysteine was 9.51 [177].

3.2.3 Physical Characterisation

3.2.3.1 Swelling Test

This was performed to quantify the water-uptake of the hydrogel. A dehydrated sample (2 – 5 mg) was placed in distilled water (1 mL) under mild shaking. The SR was calculated according to the following equation:

Equation 3.2-1

$$SR = \frac{M_{s-}\, M_d}{M_d}\ x\ 100$$

Where M_s is swollen weight and M_d is dried weight. Swollen samples were paper blotted prior to measurement of M_s.

3.2.3.2 Gel Content

In addition to the swelling ratio, the gel content was determined to investigate the overall portion of the covalent hydrogel network insoluble in 10 mM HCl solution. Dried hydrogel networks of known mass (M_d) were equilibrated in 10 mM HCl solution for 24 hours. Resulting hydrogels were air dried and weighed (M_{d1}). The gel content (G) was calculated using:

Equation 3.2-2

$$G = \frac{M_{d1}}{M_d}\ x\ 100$$

3.2.3.3 Degradation Test

Dried hydrogels (M_d) were placed in HEPES-buffered saline (pH 7.4) with 0, 0.2 or 2 mg/ml collagenase and incubated at 37 ^{o}C for 1, 3, 5 and 7 days. At the given time point, they were removed, dried and the new weight recorded (M_{d1}). Every 2 days, the collagenase solution was removed and fresh collagenase solution was added to prevent loss of enzyme activity [206].

Equation 3.2-3

$$Mass\ Loss\ (\%) = \frac{M_d - M_{d1}}{M_d}\ x\ 100$$

3.2.3.4 Ellman's Assay

This was used to quantify the number of available thiol groups. Ellman's agent (4 mg/mL) dissolved in sodium phosphate buffered solution (pH 8, 0.1 M) was added to the collagen sample (1.4 mg) and shook for 15 minutes. Absorbance was then measured at 412 nm using a UV/Vis spectrophotometer.

Equation 3.2-4

$$c = \frac{A}{b\varepsilon}$$

Where, *c* is the concentration of thiol, *A* is the absorbance, *b* is the path length and *ε* is the molar extinction coefficient 14150 $M.cm^{-1}$.

3.2.4 Mechanical Characterisation

3.2.4.1 Compression Test

Compression testing was used to calculate Young's (elastic) modulus (E_c). Water-equilibrated hydrogel discs (Ø: 12 mm) were compressed at room temperature with a compression rate of 3 $mm{\cdot}min^{-1}$ (Instron ElectroPuls E3000). A 250 N load cell was operated up to complete sample compression. Stress-strain lines were recorded and the compression modulus quantified as the slope of the plot linear region up to 20% strain.

Equation 3.2-5

$$\sigma_c = \frac{F}{A}$$

Where σ_c is stress (Nm^{-2} or Pa), *F* is force (N), and *A* is the cross sectional area of the sample (m^2).

Equation 3.2-6

$$\epsilon = \frac{\Delta l}{l_0}$$

Where ε is strain, l_0 is the original length (m) and Δl is the difference between l and l_0 (m).

Equation 3.2-7

$$E_c = \frac{\sigma_c}{\epsilon}$$

Where E_c is compressive strength, or Young's modulus (Nm^{-2} or Pa).

3.2.4.2 UV-Curing Rheometer

Rheology curing measurements were performed on the thiol-ene reactant mixtures. The measurements were carried out on an Anton Paar MCR 301 rheometer using a CP50-2 tool with a diameter of 49.97 mm and a cone angle of 1.996°. UV light (365 nm) curing was initiated after 60 seconds with a light intensity of 4450 $\mu W \cdot cm^{-2}$ at 25 °C. The gelation time (τ) was quantified as the temporal interval between UV activation and complete chemical gel, where complete gelation was measured at the maximum recorded value of storage modulus (G'_{max}). The gel point was taken at the time in which the storage (G') and loss modulus (G'') equate. Amplitude sweep tests were performed on photo-cured hydrogels using the PP15 parallel plate tool at an angular frequency of 100 rad s^{-1} and a normal force of 1 N.

3.2.5 Structural Properties

3.2.5.1 Scanning Electron Microscopy (SEM)

Hydrated gels were investigated by cool-stage via SEM (JEOL SM-35). Whereas freeze-dried samples were mounted onto 26 mm stubs and placed inside the specimen chamber of a Hitachi S-3400N VP-SEM. SEM images were captured via backscattered electron detection at 5 kV and 12 – 13 mm working distance.

3.2.6 Statistics

Data has been expressed as mean ± standard error of the mean (SEM) unless n > 20, when it is expressed as mean ± standard deviation. Statistical analysis was performed using MiniTab software. Levene's test was used to test for

variance in data, t-test for comparison of two different groups, one-way ANOVA followed by post-hoc Tukey test on data when Levene's test showed $p \geq 0.05$ and equal variances could be assumed and a Welch's ANOVA followed by a post-hoc Games-Howell on data when Levene's test $p \leq 0.05$ and equal variances could not be assumed. Statistical significance was determined by $p \leq 0.05$.

3.3 Results and Discussion

Sample nomenclature used in this work is as follows: functionalised collagen is coded as "collagen-X", where "X" identifies the functional reactive group used. GMA - glycidyl methacrylate (vinyl group), 4VBC -.4-vinylbenzyl chloride (vinyl group), NAC - n-acetyl-l cysteine (thiol group) and 2IT - 2-iminothiolane (thiol group). Thiol-ene hydrogels are coded as "CollPEGX", where "Coll" and "PEG" refer to 2IT-functionalised collagen and 8-arm norbornene terminated PEG, respectively, and "X" identifies the PEG content (2-4.5% (w/v)) in the thiol-ene mixture.

3.3.1 Chain-Growth Hydrogels

Collagen hydrogels were prepared using collagen-GMA and collagen-4VBC (Table 3.3-1). Collgen-GMA (50 x excess, 40% functionalised) was found to have a swelling ratio of 1220 ± 126 wt.%, similar to the literature value, 1363 ± 70 wt.% [79]. Collagen-4VBC (30 x excess, 44% functionalised) was found to have a high swelling ratio of 2064 ± 72 wt.% with a literature value of 1996 ± 182 wt.% [79].

Table 3.3-1 Chemical, mechanical and physical properties of collagen functionalised with 4VBC and GMA. Degree of functionalisation, F, compressive modulus, E_c, swelling ratio, SR and gel content, G. Represented as means ± SEM.

Sample ID	F (%)	E_c (kPa)	SR (wt.%)	G (wt.%)
Collagen-GMA (50 x)	40 ± 6	n.a	1220 ± 126	94 ± 4
Collagen-4VBC (30 x)	45 ± 4	60.1 ± 11.3	2064 ± 72	97 ± 4

Collagen-4VBC and collagen-GMA hydrogels were repeated many times using the excess of 50 x and 30 x so that their degree of functionality would be kept similar and any difference in the mechanical or physical properties would be due to the linker.

In the literature, collagen-4VBC (25 x, 50 x excess) was stated to have a very high compressive modulus (E_c: 150 ± 54– 168 ± 40 kPa) in lieu of its high swelling ratio and collagen-GMA (25 x, 50 x excess) (E_c: 30 ± 7– 50 ±18 kPa) [79]. Mechanical properties generally are supposed to decrease in hydrogels with increased swelling ratio, however collagen-4VBC has a higher compressive modulus and swelling ratio compared to collagen-GMA. This difference between the methacrylate GMA moiety and the aromatic 4VBC moiety was put down to molecular organisation and secondary interactions, such as π-π stacking, altering the stiffness of the aromatic collagen backbone [79]. These stiff hydrogels would be more suitable for bone tissue engineering rather than muscle tissue engineering due to their similarity to the pre-calcified collagen matrix.

During this research, there has been a significant degree of variability in the collagen-4VBC hydrogels, which was put down to either the batch of collagen, the cross-linker or the highly concentrated solution of I2959 (1 % (w/v)) which could cause issues with solubility due to the high viscosity. There is also a degree of user-induced variability since the synthesis steps need to be done very precisely to minimise variations. On occasions other than those reported in Table 3.3-1, after synthesising collagen-4VBC properties have been reported as E_c ~14.3 ± 5.1 kPa and SR – 600 ± 58 wt.%.

To counteract these issues, it would be beneficial to have a cross-linking method which requires less photoinitiator, since I2959 (1% (w/v)) is very toxic to cells, and a functionalised collagen precursor material with increased solubility or hybridisation with a synthetic material to overcome issues that may arise from batch variability of the collagen. Most importantly, a simple preparation method would greatly reduce user-induced variability.

3.3.2 Systematic Development of Click Chemistry Hydrogels

Click chemistry reactions are intrinsically insensitive to ambient oxygen or water and need a lower concentration of free-radicals/ catalyst to initiate the reaction compared to traditional chain-growth polymerisation which has been shown to yield high initial radical concentrations [110, 184]. This is highly appealing for cell-hydrogel devices since it reduces the toxicity of the pre-polymer solution and

reduces radical-mediated cell damage [184]. The reduced toxicity was reported by Mũnoz *et al*, which stated that the cell viability in step-growth gelatin-norbornene (GelNB)-DTT hydrogels (~97% of counted cells stained green) was significantly higher than in chain-growth gelatin-methacrylate (GelMA) hydrogels (~85% of counted cells stained green) both using LAP (1 mM) [184].

This initial increased viability of the step-growth hydrogels was only 11–12% higher than that in the chain-growth GelMA hydrogels, however, Mũnoz stated that this difference might affect long-term cell proliferation, spreading, cell–cell interactions, matrix deposition, and differentiation. Additional review of the literature provided further evidence of step-growth vs chain growth hydrogels and the increased cytocompatibility for *in situ* encapsulation [110, 207].

Click chemistry had not been incorporated into collagen, so offered a novel method for cross-linking. When systematically developing these novel hydrogels, it was important to reiterate that for a cell-hydrogel construct to be used for *in vitro* encapsulation or as an *in situ* injectable device [208]:

- All the reagents should be cell-friendly/ bioinert.
- The precursor materials should be water- soluble for dissolution in PBS or basal media.
- A low concentration of photoinitiator/ catalyst should be used to ensure good cell viability and cytocompatible hydrogel formation.
- Fast gelation times to ensure minimal cell-damage particularly if a UV light source is required.
- Facile, accurate means to provide tunable mechanical/ physical properties to represent ECM of different tissues.

Michael-addition (base-mediated) and the thiol-ene reaction (radical-mediated) were the two thiol click chemistry reactions that were taken forward in this work for the formation of novel collagen hydrogels. No harmful metal catalyst was required for the reaction, unlike the Cu-catalysed azide/alkyne cycloaddition (CuAAC) or atom-transfer radical polymerisation (ATRP) click chemistry reactions. Additionally, these two reactions are not thermodynamically controlled, unlike the Diels-Alder click reaction which requires heat to proceed [41].

Thiol Michael-type addition requires the use of a thiol group, a nucleophile catalyst such as triethylamine (TEA) and an electron deficient double bond such as a methacrylate or a vinyl sulfone, which both possess an electron withdrawing group (EWG) adjacent to the double bond [209].

Thiol-ene free-radical chemistry requires the use of thiol group, a photoinitiator and a light source and a non-sterically hindered terminal double bond which can be electron rich or electron deficient. The double bonds utilised in the thiol-ene reaction should be non-homopolymerisable, e.g. allyl ether, vinyl ether, norbornene to prepare a true step-growth radical reaction. The thiol–ene step growth mechanism is based on the addition of a thiol to a vinyl (ene) functional group with the thiol radical propagation shown below [210]:

Equation 3.3-1 The thiol radical propagation. The consumption of the thiol radical (1) and the production of the thiol radical (2)

$$\boldsymbol{RS\cdot + R'CH = CH_2 \overset{k_1}{\rightarrow} R'C\cdot H - CH_2SR} \qquad (\mathbf{1})$$

$$R'C\cdot H - CH_2SR + RSH \overset{k_2}{\rightarrow} R'CH_2 - CH_2\,SR + RS\cdot \qquad (2)$$

Methacrylate-thiol-ene and PEGdA-thiol-ene systems have been reported extensively in the literature [211]. However, this is not a true thiol-ene reaction and will be hereby referred to as a pseudo thiol-ene reaction, because additional kinetic parameters are incorporated into the rate equation for the consumption of the double bond [210]:

Equation 3.3-2 Rate equation if the double bond is capable of homopolymerisation and a pseudo thiol-ene reaction occurs

$$\frac{d[C=C]}{dt} = -k_{SR}[C=C][S\cdot] - k_{CR}[C=C][C\cdot]$$

k_{SR} and k_{CR} are thiol radical propagation, and carbon radical propagation kinetic parameters.[210]

As previously stated collagen-GMA and collagen-4VBC had already been synthesised. GMA contains an electron deficient double bond which would be appropriate for Michael-addition reaction, so the first thiol click reaction was attempted using collagen-GMA and hexaethylene glycol (dithiol) (HEGSH) (Figure 3.3-1).

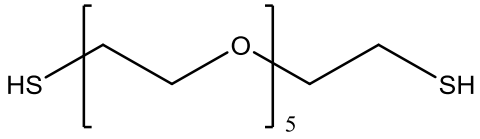

Figure 3.3-1 hexa(ethylene glycol) dithiol.

Collagen-GMA and HEGSH were combined (1:1 ene: SH) with triethylamine (TEA) (1:1 TEA: SH). This reaction did not work even when an excess of thiol (1:10 ene: SH) was used to counteract the difficulties of using a bi-functional group to make a hydrogel. Another theory was that disulphide bonds were being formed rather than the thiol Michael-addition reaction. To prevent this, TCEP was used to prevent disulphide bridges (1:1 SH). However no gelation took place. Further experiments were performed varying the excess of ene: SH, TEA: SH and SH:TCEP and varying the pH of the solution (pH 7.5, 8, 8.5, 9, 9.5, 10) prior to addition of TEA with no success.

During this period, collagen-NAC was prepared as a different thiol precursor group. The focus shifted to a click reaction between collagen functionalised with a thiol and collagen functionalised with a double bond or a high molecular weight PEG precursor material, whereby similar degrees of functionalisation were achieved.

Michael-addition reaction was attempted using collagen-NAC with either collagen-GMA or PEGdA and using NaOH to initially prepare the alkaline solution before the base was added (TEA). From a review of the literature, it was known that NAC had a pK_{aSH} 9.5, in comparison pK_{aSH} for cysteine is 8.3 [177, 212]. For this reason, the pH of the solution was always changed to 10 before the reaction to create the thiolate anion. However, there was no gelation. There was concern that disulphide bonds might have formed due to oxidation of the NAC group (reduced availability of S^- for reaction), so a reducing agent was added. Collagen-NAC was again combined with collagen-GMA in acetic acid (0.8 wt.%,17.4 mM), this time, TCEP (1:1 M SH:TCEP) was added equimolar to the thiol groups and stirred for 10 minutes to reduce disulphide bond formation, the pH then buffered to 10 and TEA (1:1 M SH:TEA) was added and the solution was shook gently for 24 hours. No gelation occurred using PEGdA or collagen-GMA using this method.

To analyse whether the n-acetyl-l-cysteines are joined together between their side chains via disulphide bonds (–S–S–), an Ellman's assay was performed on the collagen-NAC samples to quantify the degree of available thiol groups (SH) with increasing excess of NAC (Table 3.3-2).

Table 3.3-2 Table to show available free thiols (%) calculated from Ellman's assay and the degree of functionalisation calculated from a TNBS assay. Means ± SEM (n=3).

Sample ID	Ellman's (%)	TNBS (%)
NAC (10 x)	6.4 ± 1.2	18.4 ± 1.0
NAC (15 x)	8.9 ± 0.7	22.0 ± 6.5
NAC (25 x)	14.6 ± 1.1	37.9 ± 7.9
NAC (50 x)	13.0 ± 1.7	71.9 ± 1.6

These results for the available thiol groups show that the thiol concentration calculated from Ellman's assay was lower than the thiol concentration known to be present due to the TNBS assay. This experiment was repeated with one collagen-NAC solution treated with TCEP for 10 minutes to reduce disulphide bonds.

Table 3.3-3 Ellman's assay performed using TCEP for 10 minutes to reduce disulphide bonds. Means ± SEM (n=3).

Sample ID	Ellman's (%)
NAC (15 x) untreated	8.2 ± 1.4
NAC (15 x) TCEP	7.3 ± 0.2

The concentration of thiol recorded was not significantly different for the two groups.

The predominant reagent for protein thiol quantification in Ellman's reagent is 50, 50-dithiobis-(2-nitrobenzoic acid) (DTNB) which reacts with thiolate anions in a thiol–disulfide exchange reaction, generating the chromogenic product 2-nitro-5-thiobenzoic acid (NTB) [213]. The limitations of this reaction are discussed in many papers, work by Hansen *et al* and Dingova *et al* convey that because only the thiolate form of the thiol in question reacts with DTNB, the rate of the reaction is highly dependent on the pH and the pKa of the thiol group. This means that a reaction pH of at least 7.0 is required. However, at this pH the thiolate anion can also participate in unwanted side reactions such as alkylation and oxidation reactions. Ellman's assay also suffers from limited sensitivity with a detection limit of approximately 3 nmol in a typical 1-ml cuvette. Accordingly, it is unsuited

for quantification of samples containing low concentrations of thiols such as dilute protein solutions [213]. Unfortunate when attempting to use the Ellman's assay with a collagen solution.

So despite the fact that Ellman's assay is cheap and fast, it has limitations when used for biological samples [214]. Hansen *et al* suggested a preferential 4,4-dithiodipyridine (4-DPS) (pH 2.5-6) followed by HPLC detection which is particularly useful for the sensitive detection of thiols. They state that 4-DPS has a great advantage over DTNB due to its hydrophobic nature and somewhat small size [213].

The barriers associated with the thiol/ disulfide exchange reactions pose potential pitfalls to determine the concentration on free-available thiols. In addressing these challenges, it is important to ensure that the methods selected to quantify the redox status of thiols and di-sulphides are the same as the system under investigation [215]. One of the requirements for the hydrogel precursor material in this work was that it should be water-soluble for dissolution in PBS or basal media (pH 7.4). The newly suggested 4-DPS method to quantify thiols is not appropriate at this pH. Due to the balanced thiol/ disulphide exchange, it would be necessary that any method to quantify the thiols should be the same as the system to which it will be used (pH 7.4), otherwise the concentration of free-thiols recorded wold not be accurate. From here on, TNBS assay was used as the sole quantifiable measure of thiolation.

A practical examination of the presence of disulphide bonds was perfomed using a swelling test. Collagen hydrogels were formed by neutralisation of collagen-NAC (10, 15, 25 and 50 x excess) and a swelling test performed with non-functionalised collagen and chemically cross-linked collagen (EDC/NHS) as the controls. In principle, water acts as plasticiser in biopolymers so that specifically lowered storage moduli should be expected in materials displaying increased swelling ratio [83]. To relate this to collagen-NAC, the presence of disulphide bonds should provide an increased storage modulus compared to non-functionalised collagen hydrogels, and therefore present a lower swelling ratio.

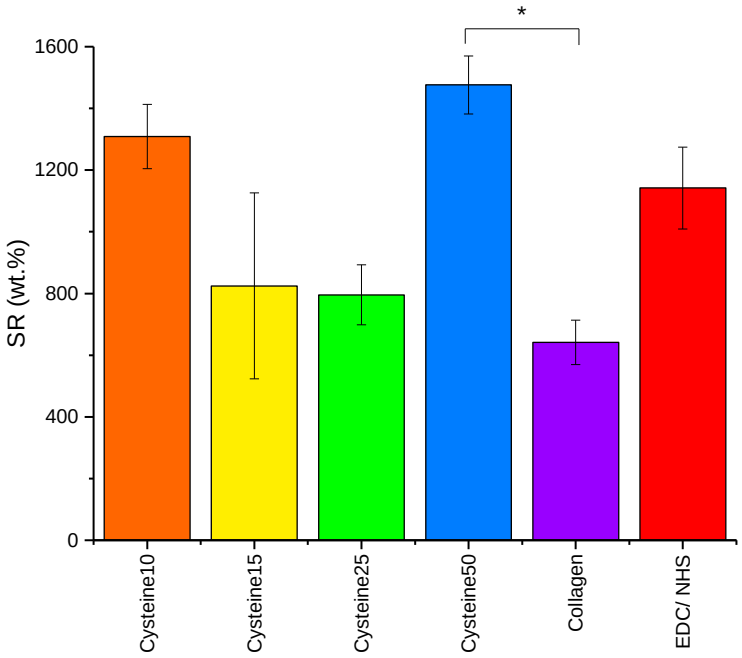

Figure 3.3-2 Swelling ratio of functionalised collagen-NAC and collagen hydrogels using TEOA and EDC/NHS collagen as the control n=4.

Figure 3.3-2 showed that collagen-NAC and collagen hydrogels formed by neutralisation and the collagen hydrogels formed from EDC/NHS chemical cross-linking all possess similar swelling ratio. The results are all non-significant to each other except for collagen-NAC (50 x excess) and collagen which were statistically different. This implied that there were additional interactions going on to produce hydrogels with higher swelling ratio, although this cannot be explained by the presence of disulphide bonds which should provide an increased storage modulus and a lower swelling ratio. Instead, this higher swelling ratio is more likely due to the increased functionalisation of the collagen-NAC (50 x excess) providing a hydrogel with increased hydrophilicity (NAC thiol group) and therein, a higher swelling ratio. ^{1}H NMR and FT-IR showed too much noise from the large collagen biopolymer to recognise a -SH or a S-S bond.

The reaction kinetics and yield of the thioether product for the thiol Michael-addition have been shown to depend on multiple factors such as the thiol pK_a, the steric accessibility of the thiol, the nature of the electron withdrawing group coupled to the double bond and strength and concentration of the base catalyst [216]. The rate-limiting step of the thiol-Michael addition reaction pathway is the nucleophilic attack of the thiolate anion to the double bond and the reaction as shown to proceed faster the more electron deficient the double bonds is (Figure 3.3-3) [105, 216].

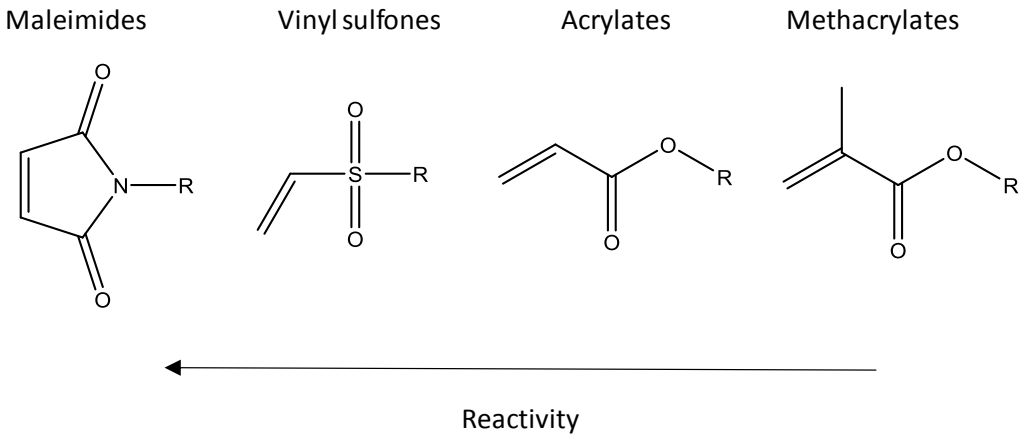

Figure 3.3-3 Commonly used electron-deficient vinyl groups for thiol-Michael Addition Reactions displaying increasing reactivity.

At the time, the electron deficient double bond and the structure and pK_a of the thiol group were considered the most important factors impacting the reaction rate. Concern was had over the high pK_a of the collagen-NAC and it was thought that the additional alkyl group gained from functionalisation of NAC with collagen, may have further increased the pK_a of the thiol hydrogen. This was thought to be the reason why the Michael addition reaction was not working and it was rejected for the thiol-ene free-radical addition. There was also concern that the considerations set out for cell-hydrogel *in situ* encapsulation were not being followed. The TEA base was not cell friendly and neither was the pH 10 environment and the collagen-NAC was only soluble in weak acetic acid solutions and not PBS. This reaction was supposed to be simple, robust, and highly effective reaction under facile reaction conditions, however it was abandoned because the reaction would not work.

Further review into the literature showed emphasis on how employing a strong nucleophile as a catalyst instead of the base, such as an imidazole, can limit the dependence of the reaction on the pK_a of the thiol [216]. Although it is noted that whilst imidazole is water soluble, it is a dangerous chemical so not appropriate for use with cells, however, had this been discovered sooner, it could have been used in this reaction.

A paper by Ravichandran *et al* reported the successful Michael-addition reaction with collagen functionalised with methacrylic anyhydride and a multi-arm PEG thiol terminated group at pH 8 almost two years after it had dismissed in this work [80]. Although it was noted that the lower pH 8 meant they had a thiol group with

a lower pKa_{SH}. The paper also used a multi-arm PEG thiol (4 arm and 8 arm), whereas the only attempt with a thiol functionalised PEG in this work was with HEGSH which was bifunctional - the multi-arm thiol groups may have aided the synthesis [80].

The thiol-ene free-radical addition performed by UV polymerisation was preferential in terms of biomaterial design, however, it would be difficult to divulge whether a thiol photo-click reaction was taking place unless a double bond incapable of homopolymerisation was used such as norbornene or vinyl ether. A large stock of functionalised collagen-GMA and collagen-4VBC had been made during the start of the research (both react by chain-growth homopolymerisation) which was why the Michael-addition was the first click chemistry reaction to be attempted.

Collagen-norbornene had been synthesised as a collagen precursor material incapable of homopolymerisation. A thiol-ene reaction was attempted using this product, collagen-NAC, I2959 and a UV light source. The main issue of this reaction was the poor solubility of collagen-norbornene. The addition of the conjugated side group had decreased its solubility in weak acetic acid. This was not ideal because the focus was on preparing a bioinert prepolymer solution, preferably soluble in PBS or basal media for cell encapsulation *in situ*.

PEG is a FDA approved material and is considered bioinert when the molecular weight is above 3000 $gmol^{-1}$. Extensive toxicity studies were performed by Working *et al* which confirm this. Intravenous injections of saline or 10% PEG-3350 in 0.85% NaCl at doses of 10, 30, or 90 mg/kg/day were given to nine beagle dogs for up to 178 days. No changes were observed in appetite or body weight and there were no clinical signs of toxicity [217].

Other benefits of PEG is that it's water-soluble and has end groups which are easily chemically modified. For example, it was found that multi-arm PEG norbornene terminated compounds were commercially available from select companies. It would have been more ideal if biodegradable synthetic polymers such as poly(capralactone) (PCL) were available with chemically modified end groups. However, the process by which these polymers are formed (cationic or anionic polymerisation) make end group termination limited if impossible.

A water-soluble, high molecular weight multi-arm PEG norbornene had been identified and ordered. Before this product arrived, it was noted that interest still lay in identifying whether a reaction with collagen-NAC and a vinyl group

(capable of homopolymerisation) would proceed via pseudo step-growth reaction or by solely a chain-growth reaction of the vinyl group. To briefly investigate this, hydrogels were prepared using both a collagen solution and a collagen-NAC solution with PEGdA. The collagen solution would be a chain-growth reaction of the PEGdA and the collagen-NAC solution could be a pseudo step-growth reaction, with the reaction first dominated by the chain-growth homopolymerisation and then the step-growth thiol-ene reaction, as was previously reported by Cramer *et al* [210].

Table 3.3-4 Sample ID, mechanism and PEG concentration to determine whether solely a chain growth mechanism is occurring. Presented as means ± SEM (n=3).

Sample ID	PEGdA (w/v)	E_c (kPa)	SR (wt.%)	G (wt.%)
Collagen(0.9)	0.1	569 ± 84	466 ± 14	97 ± 1
Collagen-NAC (0.9)	0.1	489 ± 36	429 ± 27	96 ± 1
Collagen(0.88)	0.12	546 ± 71	451 ± 16	96 ± 1
Collagen-NAC (0.88)	0.12	450 ± 8	399 ± 22	93 ± 6
Collagen (0.85)	0.15	945 ± 89	358 ± 24	90 ± 0
Collagen-NAC (0.85)	0.15	625 ± 37	430 ± 17	88 ± 5

Mechanical and physical testing of the chain and pseudo step hydrogels showed no statistical significance in the results using a Welch's ANOVA followed by a post-hoc Games-Howell .

Xu *et al* reported hydrogels prepared from a thiol-ene reaction using PEGdA and gel-PEG-Cys (gelatin), similar to this current study. It was stated that since gel-PEG-Cys could react with PEGdA via the thiol-acrylate reaction and compete with the acrylate-acrylate reaction, increasing gel-PEG-Cys concentration would increase the probability of thiol–acrylate reaction while decreasing the probability of the acrylate- acrylate reaction. Since the thiol-acrylate cross-linker involves larger macromolecules that are more flexible than acrylate-acrylate cross-linker, hydrogels containing more gel-PEG-Cys would be expected to have less chain

rigidity and higher mass swelling and increasing the PEGdA concentration resulted in a lower mass swelling ratio [211]. Gel-PEG-Cys (G) and PEGdA (P). In line with the results by Xu *et al* they did gain significant difference between the swelling ratio of the two hydrogels: G5P5 G10P5 where the difference is the increased gel-PEG-cys (G) concentration. Although there was no significant difference between the swelling ratio of the hydrogels: G10P5 G10P7.5 G10P10 where the only difference is an increasing PEG (P) concentration similar to the results reported in this work. It is doubtful that this is a thiol-ene reaction and instead perhaps, similar to the previous experiment in this work (Figure 3.3-2), the difference between G5P5 and G10P5 is due to the polar interactions and increased hydrophilicity of Gel-PEG-cys [211]. It is in the author's opinion that the only reaction taking place in the aforementioned collPEG results (Table 3.3-4), and the results by Xu *et al* was predominantly an acrylate-acrylate reaction and not a pseudo step-growth reaction.

During this work, concerns were raised about collagen-NAC and how it did not follow rule 2 of the requirements for cell encapsulation *in situ* "*the precursor materials should be water- soluble for dissolution in PBS or basal media*". Collagen-NAC was only soluble in weak acetic acid, however a new thiol-collagen precursor was made using 2-imidothiolane (Traut's reagent, 2IT). This reaction used no harmful catalyst or base and produced collagen-2IT which has added benefits compared to collagen-NAC as discussed in chapter 2, but best of all, it was soluble in PBS (0.01 M).

Collagen-2IT with multi-arm PEG-NB was first attempted using 4-arm PEG norbornene terminated (PEG4NB) and LAP photoinitiator. By this point it was established that LAP was the preferable photoinitiator when used with collagen at 365 nm due to its high absorbance at this wavelength and the lower degree of cytotoxicity. This reaction was successful however, when attempted with PEG divinyl ether, it would not work, predicted due to its bi-functional structure-there are more available norbornene groups to incorporate into the reaction and form a hydrogel if there are 4 arms. This result is reflected in work by Mũnoz *et al,* which reported a comparison of step-growth (GelNB) and chain growth hydrogels (GelMa). Both functionalisation of norbornene and methacrylate were ~ 45%. The chain-growth GelMA hydrogel yielded a higher shear modulus (~0.9 kPa) than that in step-growth GelNB-DTT gelation (~0.4 kPa) [184]. When compared with GelMA hydrogels, the lower moduli of GelNB-DTT hydrogels at equivalent gelatin content could be a result of the short DTT linker and/or the orthogonal cross-links formed after the step-growth gelation. When 4-arm PEG-thiol

(PEG4SH) was used as the hydrogel cross-linker, the equilibrium shear modulus of the GelNB PEG4SH hydrogel was increased to roughly 5 kPa from 0.4 kPa with DTT. The results from Mũnoz *et al* therefore imply that a small, bifunctional cross-linker is not ideal when used with the thiol-ene reaction, which could explain why PEG4NB resulted in gelation and PEG divinyl ether did not. It was more desirable to have stronger hydrogels, so based on this paper and the previous work with bifunctional groups not working, reagents such as divinyl ether reagent were no longer used, additional there was no attempt to use a bifunctional norbornene reagent [184].

Further work went into comparing PEG4NB and PEG8NB. PEG8NB was predicted to form better hydrogels due the increased number of norbornene groups available to react. The concentration of the collagen-2IT solution and the concentration of PEG4NB and PEG8NB were varied until a satisfactory arrangement was made. DTT was also included and not included to establish whether it was necessary to break down disulphide bonds. Hydrogels were prepared using PEG8NB and collagen-2IT with either no DTT or equimolar (1:1 SH) DTT. These hydrogels were tested using compressive tests and a swelling ratio.

Table 3.3-5 Table to show Young's modulus and swelling ratio of click chemistry hydrogels using collagen-2IT and PEG8NB (3%) to examine whether DTT should be added. Expressed as mean ± SEM (n=6).

Sample ID	E_c (kPa)	SR (wt.%)
Coll-PEG8NB	5.9 ± 0.6	4224 ± 254
Coll-PEG8NB DTT	2.9 ± 0.2	1742 ± 119

The difference between the compressive moduli ($p < 0.01$) and swelling ratio ($p<0.005$) of the two samples were statistically significant. It would appear that the DTT has reacted with the PEG8NB preferentially over the collagen-2IT, no doubt due to steric hindrance of the collagen. This was not expected, it was thought that DTT would break down any disulphide bonds present and an increase in Young's modulus would be observed. The small DTT cross-linker reacts preferentially despite its bi-functional nature which disagrees with previous work which used PEG divinyl ether and PEGdA to no success.

What was taken from this experiment was that DTT was not necessary for the reaction to proceed using collagen-2IT to break down any disulphide bonds, and

since the hydrogel solutions were designed with the idea of cell-encapsulation in mind, it was preferable not to include unnecessary chemicals.

Thiol-norbornene reactions should also limit disulfide bond formation compared to thiol Michael-addition reactions due to the radical-mediated disulphide cleavage [186]. Additionally, as discussed in chapter 2, a high presence of disulphide bonds in a collagen-2IT (1 wt.%) solution would be very apparent because a very weak hydrogel would be formed (Figure 3.3-4) prior to addition of PEG-NB or gelation.

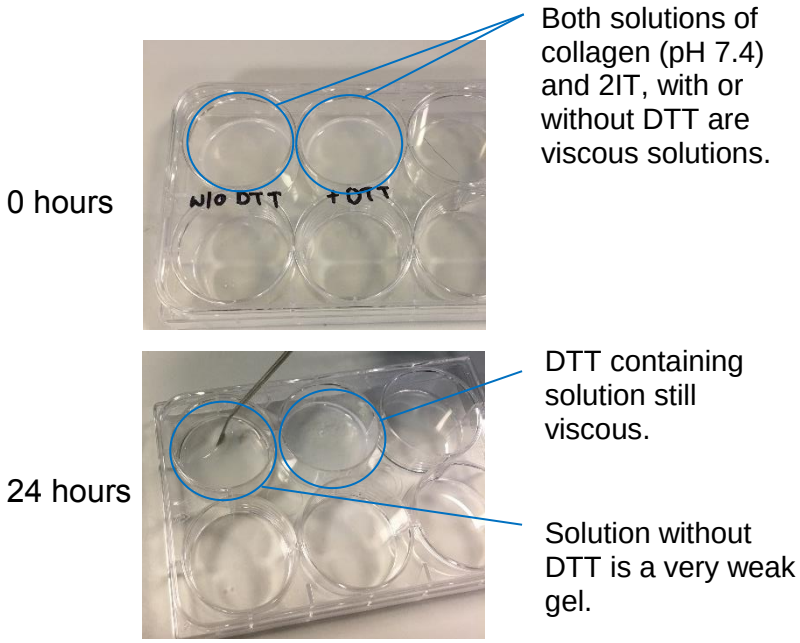

Figure 3.3-4 Synthesis of collagen-2IT to demonstrate what the presence of disulphide bonds looks like in a 1 wt.% solution.

Table 3.3-6 A-C shows the molar ratio of SH: NB at each collagen-2IT concentration and with increasing volumes of PEG8NB and PEG4NB. The concentration of the collagen-2IT solution and the concentration of PEG4NB and PEG8NB were varied until a satisfactory arrangement was made.

Table 3.3-6 (A) A table to show the concentration of collagen-2IT (1 mL, 0.8 and 0.9 wt.%, 80% functionalisation) and the molar ratio of SH: NB achieved with an excess of either PEG4NB (20,000 g.mol^{-1}) or PEG8NB (20,000 g.mol^{-1}).

Collagen-2IT (wt.%)	Molar ratio (SH: NB 1: x)	PEG4NB (% (w/v))	PEG8NB (% (w/v))
0.8	2.5	2.6	1.3
0.8	3	3.1	1.6
0.8	3.5	3.6	1.8
0.8	4	4.1	2.1
0.8	4.5	4.7	2.3
0.8	5	5.2	2.6
0.8	5.5	5.7	2.8
0.8	6	6.2	3.1
0.8	6.5	6.7	3.4
0.8	7	7.3	3.6
0.9	2.5	2.9	1.5
0.9	3	3.5	1.8
0.9	3.5	4.1	2.0
0.9	4	4.7	2.3
0.9	4.5	5.2	2.6
0.9	5	5.8	2.9
0.9	5.5	6.4	3.2
0.9	6	7.0	3.5
0.9	6.5	7.6	3.8
0.9	7	8.1	4.1

Table 3.3-7 (B) A table to show the concentration of collagen-2IT (1 mL, 1 and 1.1 wt.%, 80% functionalisation) and the molar ratio of SH: NB achieved with an excess of either PEG4NB (20,000 g.mol^{-1}) or PEG8NB (20,000 g.mol^{-1}).

Collagen-2IT (wt.%)	Molar ratio (SH: NB 1: x)	PEG4NB (% (w/v))	PEG8NB (% (w/v))
1	2.5	3.2	1.6
1	3	3.9	1.9
1	3.5	4.5	2.3
1	4	5.2	2.6
1	4.5	5.8	2.9
1	5	6.5	3.2
1	5.5	7.1	3.6
1	6	7.8	3.9
1	6.5	8.4	4.2
1	7	9.1	4.6
1.1	2.5	3.6	1.8
1.1	3	4.3	2.1
1.1	3.5	5	2.5
1.1	4	5.7	2.9
1.1	4.5	6.4	3.2
1.1	5	7.1	3.6
1.1	5.5	7.8	3.9
1.1	6	8.6	4.3
1.1	6.5	9.3	4.6
1.1	7	10	5

Table 3.3-8 (C) A table to show the concentration of collagen-2IT (1 mL, 1.2 wt.%, 80% functionalisation) and the molar ratio of SH: NB achieved with an excess of either PEG4NB (20,000 g.mol^{-1}) or PEG8NB (20,000 g.mol^{-1}).

Collagen-2IT (wt.%)	Molar ratio (SH: NB 1: x)	PEG4NB (% (w/v))	PEG8NB (% (w/v))
1.2	2.5	3.9	1.9
1.2	3	4.7	2.3
1.2	3.5	5.4	2.7
1.2	4	6.2	3.1
1.2	4.5	7	3.5
1.2	5	7.8	3.9
1.2	5.5	8.6	4.3
1.2	6	9.3	4.7
1.2	6.5	10.1	5.1
1.2	7	10.9	5.5

It was found that a molar ratio of at least 1:3 SH: NB was needed for stable hydrogels to be formed. This is likely due to the large size of the PEG-NB cross-linkers and small number of available thiol groups, collagen-2IT (0.01 g) 80 Abs% functionalised, ~2.6 x 10^{-6} moles SH (2IT)). If this was used at 1 wt.% (1 mL) the thiol groups available would be ~ 2.6 x 10^{-6} moles.mL^{-1}. This is very low and an excess would be needed to ensure the reaction can proceed. Cramer *et al* stated that using a 1:1 stoichiometric ratio of thiol and acrylate lead to incomplete conversion of the thiol monomer, instead a 1:4 stoichiometric mixture of thiol to acrylate functional groups lead to roughly equivalent conversion of both functional groups [218]. Note that this is for pseudo click reaction.

One way of achieving a tunable cross-link density in step-growth hydrogels is by adjusting the concentration of the cross-linker. Mũnoz *et al* reported a varied concentration of bi-functional thiol cross-linker (DTT) to 10, 15, or 20 mM thiol, so [SH]: [GelNB] 1:2, 1: 3, or 1: 4 because [GelNB] was fixed at 5 wt%. [184] Interestingly, Mũnoz *et al* reported that the highest storage modulus was achieved at 1:3 ratio SH: NB. A statistically reduced storage modulus was then

reported for 1: 4. This was likely caused by insufficient orthogonal hydrogel cross-linking due to an excess amount of thiol groups. It is worth noting that the exact stoichiometric ratio of thiol is only known from TNBS assay, Ellman's assay, as discussed has limitations [184].

Collagen-2IT (1.2 wt.%) was slightly more difficult to dissolve in PBS (0.01 M) than at the lower concentrations of 0.8 wt.% or 1 wt.%. For this work, it was important that the functionalised collagen be capable of dissolving in a cell-friendly solvent in order to be applicable to cell-encapsulation or injectable devices. For this reason, lower concentrations than 1.2 wt.% were explored further. From the table, it was clear that to achieve the same molar ratio SH: NB, PEG4NB required double the concentration of PEG8NB. This is because it has four norbornene groups compared to eight. This could mean that at higher concentrations, less of the PEG4NB is held together in a covalent-bound network. This was demonstrated using a gel content test (Table 3.3-9).

Table 3.3-9 Table to show gel content depending on whether PEG4NB or PEG8NB was used. Represented as means ± SEM (n =4).

Sample ID	PEG-NB (%)	G (wt.%)
CollPEG8NB	3.5	85 ± 4
CollPEG4NB	3.5	58 ± 7
CollPEG8NB	4	85 ± 1
CollPEG4NB	4	78 ± 7
CollPEG8NB	4.5	93 ± 3
CollPEG4NB	4.5	73 ± 3

The gel content was lower for PEG4NB than it was PEG8NB suggesting less material held together as a covalent bond. The PEG4NB 3.5% hydrogel had a significantly lower gel content, 58 wt.% than the PEG8NB 3.5% hydrogel, 85 wt.%. This was due to the higher SH: NB excess ratio for PEG4NB compared to PEG8NB denotating that some of the large PEG4NB (10,000 $g.mol^{-1}$) molecules could freely escape from the hydrogel network (Figure 3.3-5).

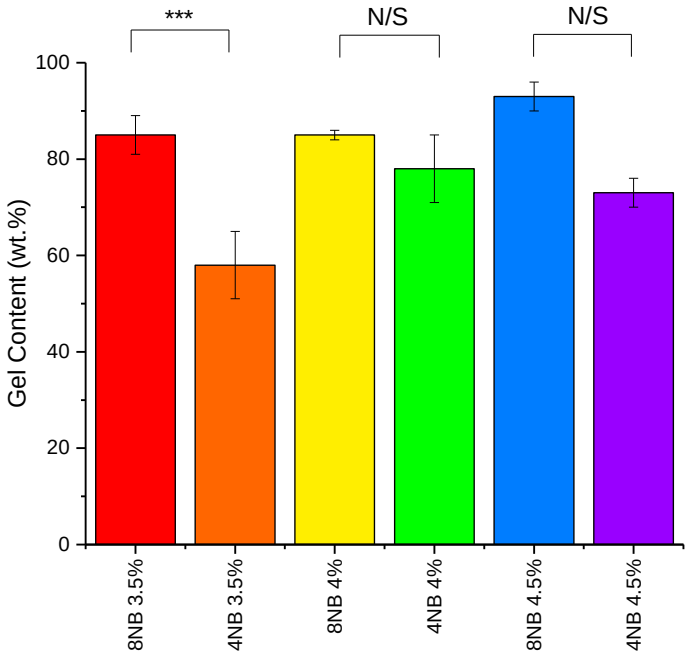

Figure 3.3-5 Graphical representation of gel content depending on whether PEG4NB or PEG8NB was used. Represented as means ± SEM n =4 ***p<0.005.

A significant difference was only displayed in the 3.5% hydrogels, it was decided that a test to compare the modulus of two weak PEG8NB and PEG4NB hydrogels should be performed.

PEG8NB was shown to produce stronger hydrogels at 3.5% compared to PEG4NB although not significantly different due to the sample size (n=4) (Figure 3.3-6).

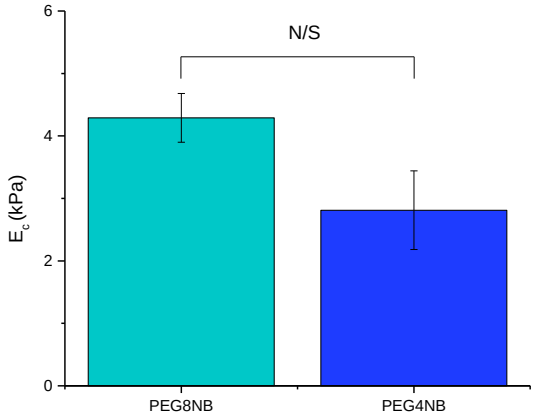

Figure 3.3-6 Compressive modulus of PEG8NB and PEG4NB (3.5%) and collagen-2IT (1 wt.%) n=4.

The architecture of the two hydrogels can also be observed in Figure 3.3-7 with no difference discernible between using 4-arm and 8-arm PEG norbornene terminated.

However, due to the high excess SH:NB, the lower gel content values and the lower recorded compressive modulus, proceeding experiments used PEG8NB. This meant that the excess of SH:NB should not exceed 1:8.

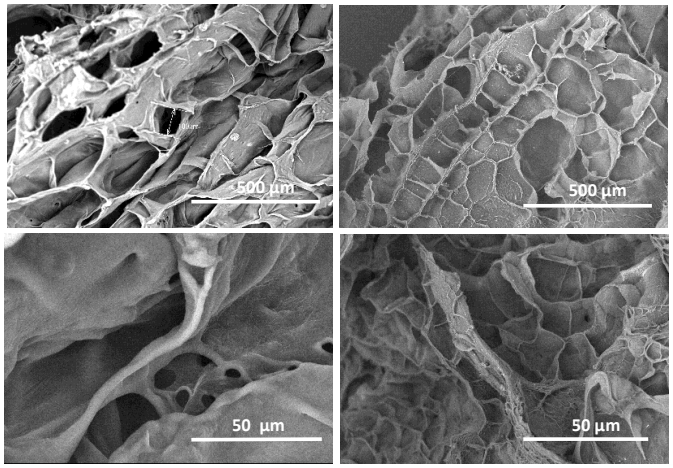

Figure 3.3-7 SEM images hydrated hydrogels. LHS PEG4NB RHS PEG8NB (3.5%). 100 x 1000 x images.

In regard to the concentration of collagen-2IT to use, Mũnoz *et al* reported that the properties of GelNB hydrogels were tuned by using different weight concentrations of GelNB in the precursor solution or thiol-containing linkers with different functionality (DTT or PEG-tetra-thiol) [184]. To relate this to collagen-2IT the concentration of collagen could be altered or the norbornene-containing linkers, PEG4NB and PEG8NB. Mũnoz *et al* reported that increasing the GelNB content in the precursor solution from 4, 5, or 6 wt.% resulted in a shear modulus of approximately 0.2, 0.4, or 0.8 kPa respectively [184]. However, due to gelatin's denatured state, it is possible to dissolve it at a higher concentration than collagen, so while an increase of 1 wt.% of the GelNB had a comparable increase in the shear modulus by 200 Pa, it would not be possible to increase the concentration of collagen by the same amount. It was also more desirable to have varied hydrogels with increasing modulus in the kPa region rather than 100s Pa, so the concentration of the PEG-NB linker was varied rather than the concentration of collagen-2IT.

3.3.3 Thiol-Ene Photo-Click Collagen-PEG Hydrogels

Six different collagen-PEG hydrogels were prepared with varied PEG8NB content to allow a level of control over the mechanical and physical properties as previously deduced from the work by Mũnoz *et al*. This level of control was also reported by Singh *et al* which showed that varying the concentration of PEG4NB in the thiol-ene reaction, achieved shear moduli ranging from 520–1150 Pa [219].

Figure 3.3-8 Photo-curing of thiol-ene hydrogels using a UV-rheometer.

Confirmation of thiol-ene hydrogel formation was obtained via UV-rheology curing time sweep measurements during which storage (G') and loss (G'') moduli were recorded (Figure 3.3-8). Comparable to the liquid state, the collagen-PEG mixture was initially found to be predominantly viscous. The UV light was turned on 60 seconds after the start of the time sweep, which promptly induced the formation of a covalent network, and is clearly indicated by the detection of a gel point (the time at which the storage and loss moduli equate) seven seconds after the photo-activation (Figure 3.3-9) [220].

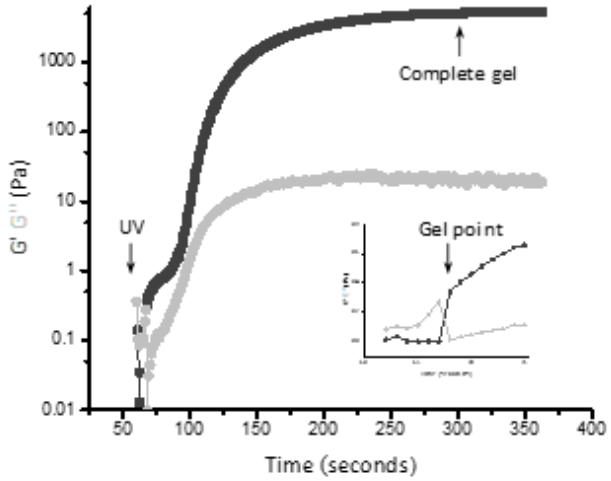

Figure 3.3-9 Typical gelation kinetics profile of thiol-ene mixture CollPEG4 (LAP 0.5% (w/v)). UV light was activated 60 seconds after the start of the time sweep measurement, resulting in complete gelation after nearly 300 seconds. The inner image presents a zoomed-in plot of the initial stage of gel formation, indicating a gel point after just 7 seconds of UV activation.

The storage modulus was found to increase with time and UV exposure until a plateau was reached within 300 s, indicating no further elastic properties (complete chemical gel).

Figure 3.3-10 depicts that G' and G'' were independent of the strain amplitude.

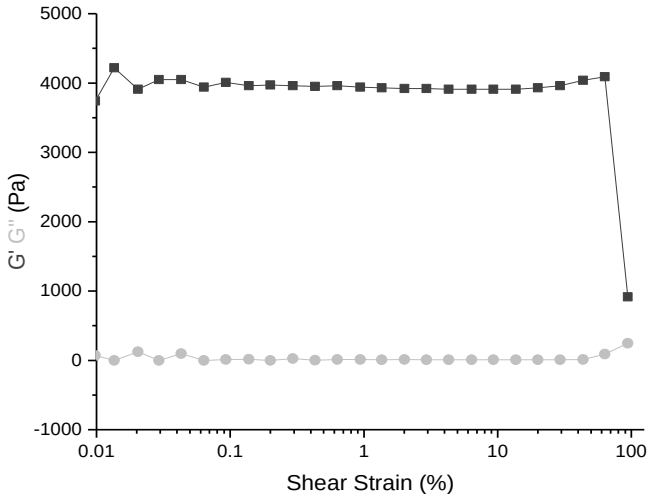

Figure 3.3-10 Amplitude sweep of collPEG4 click chemistry hydrogel.

This viscoelastic (LVE) region (G'> G'') is consistent with a solid-like material, so therefore the cross-link structure remains intact during deformation. At the

highest shear strain ~ 100% the hydrogel exhibits nonlinear viscoelastic behaviour and G' decreased by 0.25 orders of magnitude although the transition of G'< G'' never occurs, so therefore no transition is experienced from solid (gel) to liquid (viscous fluid) [221].

A photoinitiator comparison of LAP and I2959 at two different concentrations was characterised by the gelation kinetics of the collagen-PEG thiol-ene mixture. The results from Table 3.3-10 showed a significant difference in gelation time ($p \leq 0.005$) depending on choice of photoinitiator, whether LAP or I2959 was used in the pre-polymer thiol-ene solution. The I2959-based hydrogel-forming solutions took approximately 8 times as long to reach gel completion compared to LAP-containing thiol-ene solutions, regardless of photoinitiator concentration. Fairbanks *et al* reported similar results when comparing the polymerisation of PEGdA using either LAP or I2959. Their results stated that the gelation was one order of magnitude (10 times difference) lower for LAP than with I2959 with 365 nm illumination at comparable photoinitiator concentrations [132].

Table 3.3-10 Effect of photoinitiator type and concentration on both gelation kinetics and storage modulus obtained of thiol-ene mixture CollPEG3.5 as investigated via time and amplitude sweeps, respectively. Data presented as means ± SEM (n= 5).

Photoinitiator	G' (Pa)	Ƭ (s)
I2959 (0.1%)	190 ± 22	1496 ± 43
I2959 (0.5%)	3029 ± 100	1683 ± 33
LAP (0.1%)	232 ± 39	279 ± 11
LAP (0.5%)	3360 ± 91	187 ± 6

The slower gelation rate displayed by hydrogel-forming thiol-ene mixtures prepared with I2959 compared to LAP could be due to competing absorbance at 365 nm with collagen and the specific wavelength used (365 nm), LAP absorbs more light at this wavelength than I2959 leading to a higher initiation rate as discussed previously in section 2.3.3.

Interestingly, in one graph Fairbanks *et al* normalised their results to take into account the light absorption differences which exist between LAP and I2959 and it showed that LAP-photoinitiated polymerisation still gels at earlier times than I2959-photoinitiated. This outcome indicates that the faster gelation times with

LAP as the photoinitiator was not due only to the higher molar absorptivity of LAP, but also due to a higher initiation efficiency or quantum yield [132].

Other than the gelation time, the choice of photoinitiator had no comparable effect on the storage modulus. At 0.5% (w/v), LAP and I2959 presented an average storage modulus of 3360 Pa and 3029 Pa; whilst at 0.1% (w/v) photoinitiator, LAP and I2959 presented a storage modulus of 232 Pa and 190 Pa. Despite the photoinitiator-induced variation in gelation kinetics, this data suggests comparable cross-link density among previously-mentioned hydrogel formulations, as expected, considering the selectivity and oxygen-insensitivity of the thiol-ene click reaction.

The photoinitiator concentration had a large effect on both the storage modulus and the gelation kinetics. During section 2.3.3 of this work, the toxicity of photoinitiator supplemented media at increasing concentrations was examined using cell viability assays after 24 hours. It was established that photoinitiator concentrations below 0.05% (w/v) were not toxic. However, type I photoinitiator concentrations this low would not succeed in complete gelation when incorporated with collagen due to issues of competing absorbance, viscosity and issues with solubility, instead ≥0.1% (w/v) are required. When the photoinitiator concentration in cell culture media was increased from 0.1 → 0.5% (w/v), it resulted in cell survival LAP: 86 → 8 Abs.% and I2959: 62 → 2 Abs.%. It is important to note that these results are from photoinitiator supplemented media and the cell survival would be lower when used in conjunction with the hydrogel precursor since the radicals released themselves are highly reactive and often cytotoxic [132]. Due to these cell survival results at 0.1 and 0.5 % (w/v) and the knowledge that this figure would be lower when the cells are exposed to the radicals from the thiol-ene reaction; to use this novel photo-click collagen-PEG precursor material for cell encapsulation, a photoinitiator concentration of 0.1% (w/v) or lower would be needed. Unfortunately, the results showed that decreasing the photoinitiator concentration from 0.5% to 0.1% (w/v) in the thiol-ene mixture resulted in a 15-fold decrease in the storage modulus, for both photoinitiators. Compared to 0.5% (w/v), the photoinitiator efficiency at 0.1% (w/v) appears to be too low to efficiently release enough radicals to complete the click chemistry a reaction, thus resulting in fewer thiol-norbornene cross-links and a hydrogel with reduced storage modulus. Concentrations of 0.5% (w/v) would be too cytotoxic, so the application of cell-hydrogel encapsulation or *in situ* injectable devices had to be abandoned. It was clear that despite the optimal water-soluble photoinitiator (LAP) and the click chemistry cross-linking system,

which uses less photoinitiator than traditional chain-growth polymerisation, the concentration of photoinitiator needed to gain desirable mechanical properties was still too high for cell encapsulation, although at least it was no longer necessary to prepare hydrogels with photoinitiator 1% (w/v).

As a result of the enhanced gelation kinetics and hydrogel storage modulus, the remaining rheological studies were carried out on thiol-ene solutions containing LAP 0.5% (w/v), aiming to induce further control on gelation kinetics, as well as hydrogel mechanical and physical properties. It is noted than a LAP 1% (w/v) solution was also attempted but no significant increase in storage modulus was observed so it could be concluded that 0.5% (w/v) released a sufficient quantity of free-radicals to complete the thiol-ene reaction.

Six thiol-ene photo-click samples were prepared which displayed a significantly increased storage and loss modulus with the increased concentration of PEG-NB in the thiol-ene solution reported in Table 3.3-11 ($p < 0.05$).

Table 3.3-11 Mechanical and physical properties of six click chemistry gels using LAP (0.5%) Data presented as means ± SEM (n= 5).

Sample ID	G' (Pa)	G'' (Pa)	Ƭ (s)	Tan δ (× 10^{-3})
CollPEG2	540 ± 23	5.1 ± 1.0	73 ± 3	5.3 ± 0.2
CollPEG2.5	1150 ± 46	5.8 ± 0.1	110 ± 6	6.3 ± 0.1
CollPEG3	2040 ± 50	8.6 ± 0.3	133 ± 6	5.7 ± 0.1
CollPEG3.5	3360 ± 91	11.1 ± 0.6	187 ± 6	5.0 ± 0.1
CollPEG4	4810 ± 41	13.2 ± 0.8	301 ± 13	3.5 ± 0.1
CollPEG4.5	6360 ± 72	15.6 ± 0.7	331 ± 14	2.2 ± 0.1

The photo-click gels displayed a G' in the range of 500 – 6400 Pa depending on the thiol-ene formulation, thus indicating a significant degree of tunability in the mechanical properties of the hydrogels. Tan δ is a representation of the ratio of the viscous (loss) and elastic (storage) moduli (G"/G'). This parameter identified how tacky/sticky the hydrogel was [222]. Interestingly, Tan δ was observed to

decrease with increasing PEG content, ultimately leading to increased hydrogel stiffness and reduced tackiness of the resulting hydrogel. This data provides further evidence that PEG is integrated in a covalent network rather than acting as secondary plasticising phase, as also supported by respective gelation kinetics profiles (Figure 3.3-11).

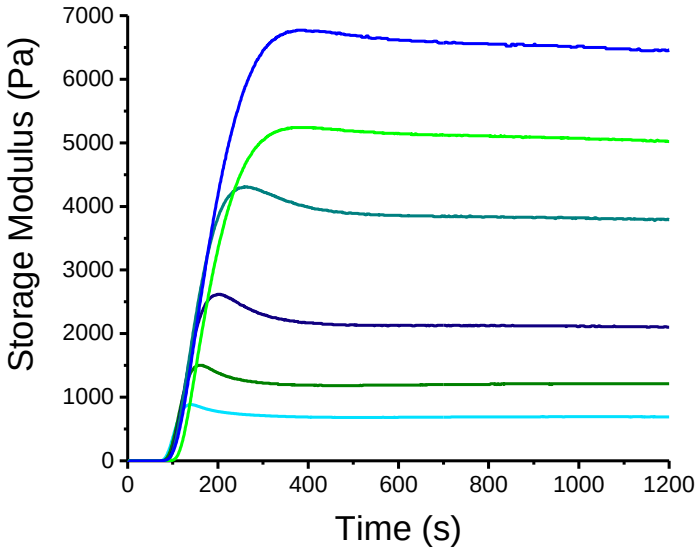

Figure 3.3-11 Curing time sweep measurements of thiol-ene collagen mixtures prepared with 0.5% (w/v) LAP and varied PEG content.

Shear modulus (G) is represented as:

Equation 3.3-3

$$G = G' + iG''$$

A significant increase was observed in the shear modulus ($p \leq 0.005$) with increasing concentration of the cross-linker PEG8NB (0.5%), for the six click chemistry hydrogels prepared (Figure 3.3-12).

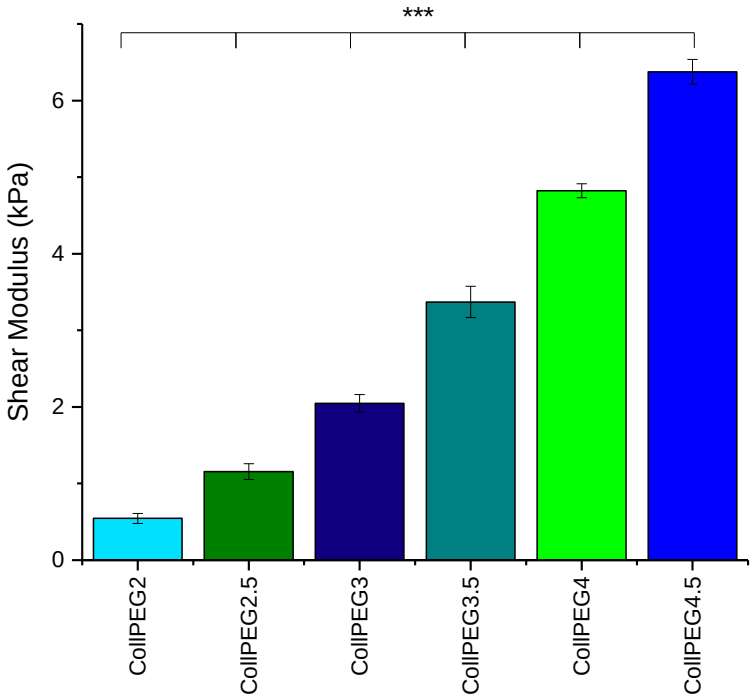

Figure 3.3-12 Shear Modulus of 6 click chemistry gels. Represented as mean ± SEM . *** p < 0.005

With the constant [collagen-2IT] at 1 wt.%, the molar ratios of [SH]: [NB] for the six photo-click hydrogels are as follows ~ 1: 3, 1: 3.75, 1: 4.5, 1: 5.25, 1: 6, 1: 6.75.

Even though it was possible to characterise the degree of substitution on collagen-2IT on a reduction in free amine group content (TNBS assay), the exact molecular weights of collagen and hence the molar concentrations of norbornene groups were difficult to define. However, based on the shear modulus (Figure 3.3-12) the 1: 6.75 value gave rise to click chemistry collagen hydrogels with the highest shear moduli indicating that the stoichiometric ratio of thiol-to-ene at this R value could be close to one [184].

Figure 3.3-13 depicts the gelation kinetics for the six photo-click hydrogels prepared. The gel point was defined as the point where the storage and loss modulus equate. This occurred 5-14 s after UV light exposure for all the photo-click hydrogels. The general pattern showed that the gel point decreases with the increasing PEG-NB content in the hydrogels, likely due to the higher excess of norbornene compared to the thiol group allowing the reaction to occur faster. Figure 3.3 13 B shows the time to complete gelation (□), taken at G'_{max} and showed a general increase with the increasing PEG-NB content in the hydrogels, likely due to the higher cross-link density (73- 300 s).

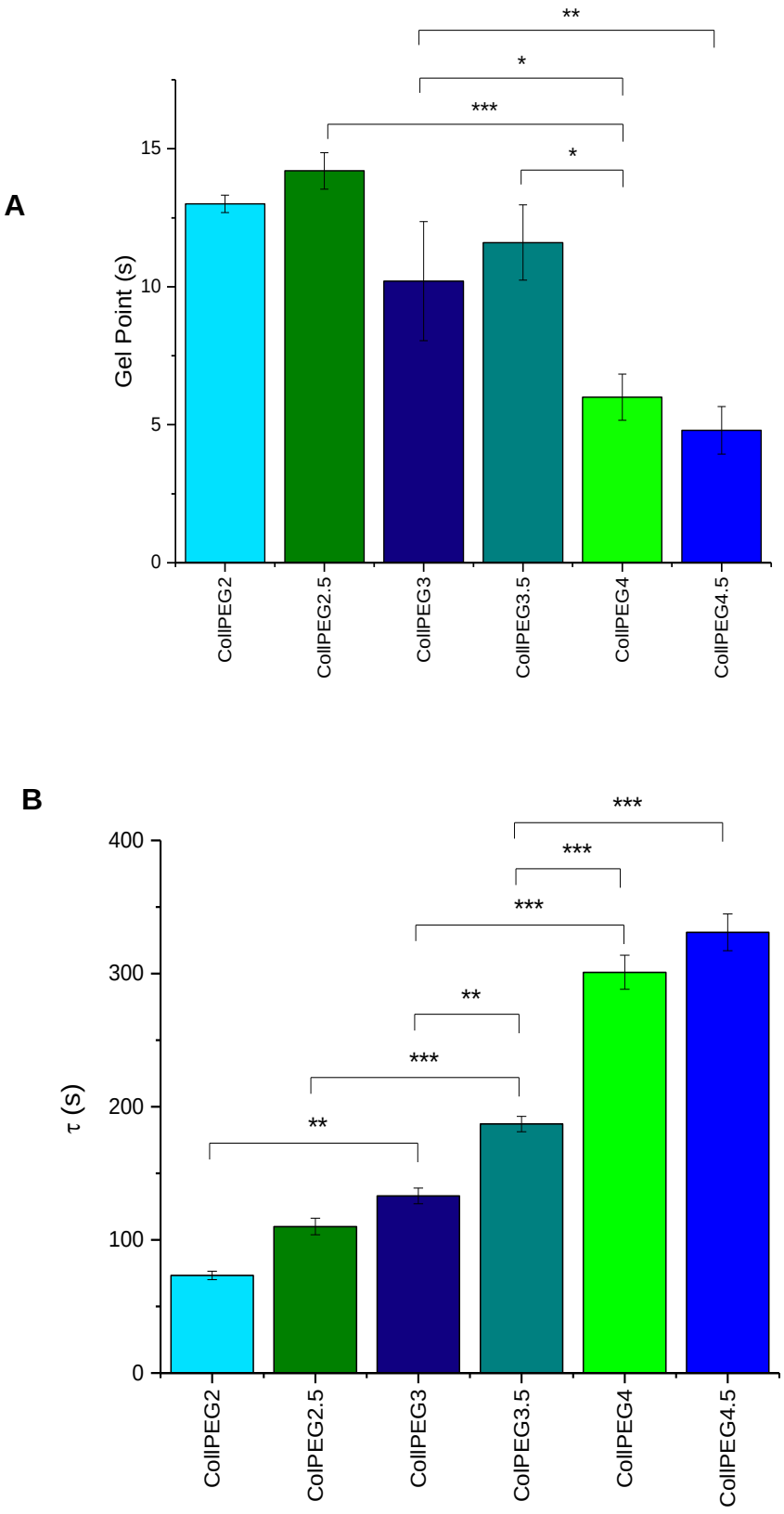

Figure 3.3-13 Graphs depicting the time to the gel point A) and the time to complete gelation, Ʈ((B) for the six click chemistry gels. Depicted as means ± SEM n= 5. * p < 0.05, ** p < 0.01 *** p < 0.005.

In comparison, Mũnoz *et al* reported the gel point of GelNB and DTT hydrogels ~ 12 s and complete gelation ~ 300 seconds of light exposure [184]. Interestingly, the UV light source used by Mũnoz *et al* was 365 nm, 10 mW cm^{-2} whereas the UV light source used in these photocuring experiments was 365 nm, 4450 $\mu W \cdot cm^{-2}$ (4.45 $mW \cdot cm^{-2}$). Which was half the light intensity and low enough to look directly at it (briefly) (Figure 3.3-14).

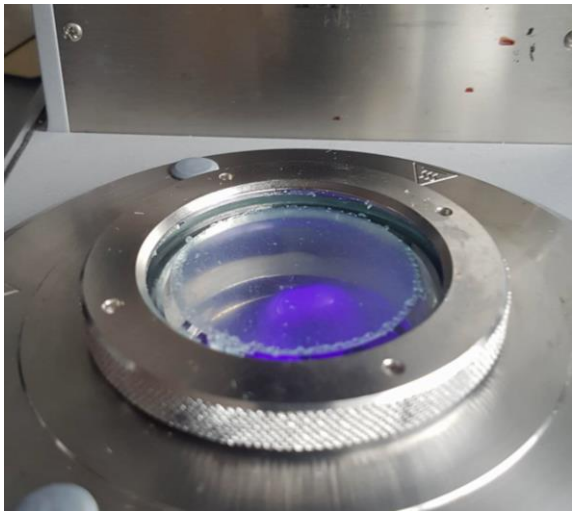

Figure 3.3-14 Photo-curing 4 cm rheometry plate with low intensity UV light source, 365 nm, 4.45 $mW \cdot cm^{-2}$

The gel points for the thiol-ene experiments by Mũnoz were comparable to the results of these photo-click hydrogels despite a lower intensity of light being used. A paper by Lin *et al* used PEG4NB and cysteine modified peptide with PEGdA as the control using UV light 365 nm, 5 mW/cm^2 (more comparable to the UV light used for this experiment), and recorded a gel point of 7 s for the thiol-ene reaction and 125 s for the chain-growth PEGdA reaction [110]. These figures by Lin *et al* emphasise the success of the thiol-ene reaction in comparison to traditional chain-growth reactions in terms of gelation kinetics.

It was noted that the light intensity used by Mũnoz *et al*, Lin *et al* and in this current study for the photocuring experiments was still very low. In comparison, cordless dental LED lights are used in the 420-480 nm range and use an intensity of 1000 – 5000 $mW.cm^{-2}$. From the UV-Vis absorption profile of LAP shown in chapter 2, LAP would be capable of releasing radicals when exposed to 420 nm light. Since dental lamps use a light intensity 1000x higher than the one used in this photo-curing experiment, further work could go into repeating it at a different

wavelength to analyse how fast the gelation kinetics could become with these higher dental intensities that are currently used safely in the clinic.

The rate of production of primary free radicals (R_i) from the photo-sensitised free-radical initiators can be expressed by [132]:

Equation 3.3-4

$$R_i = \frac{2\phi\varepsilon f I C_i}{N_a h\upsilon}$$

Where R_i is the rate of photoinitiated polymerisation, ϕ is the quantum yield for initiation, ε is the extinction coefficient, f is the photoinitiator efficiency, I is the incident light intensity(mW.cm^{-2}), N_A is Avogadro's number, h is Plank's constant and v is the frequency of initiating light.

The quantum yield for initiation of the photoinitiator efficiency could not be found in the literature for LAP. However, from the above equation it is possible to deduce that:

Equation 3.3-5

$$R_i = kI$$

CollPEG3.5 took 187 seconds to reach complete gelation with 4.45 mW·cm^{-2}. If k =R_i/I, for this pre-polymer solution and R_i = 1/(t – complete gelation), k = 0.0012 s^{-1}m·W^{-1}·cm^2. Using the equation and the k value, a lamp intensity of 10 mW cm^{-2}, could result in a far lower complete gelation time ~83 seconds, comparable to Mũnoz *et al*.

Viscosity experiments were performed using rheology for the six photo-click thiol-ene solutions prior to UV light exposure (Figure 3.3-15).

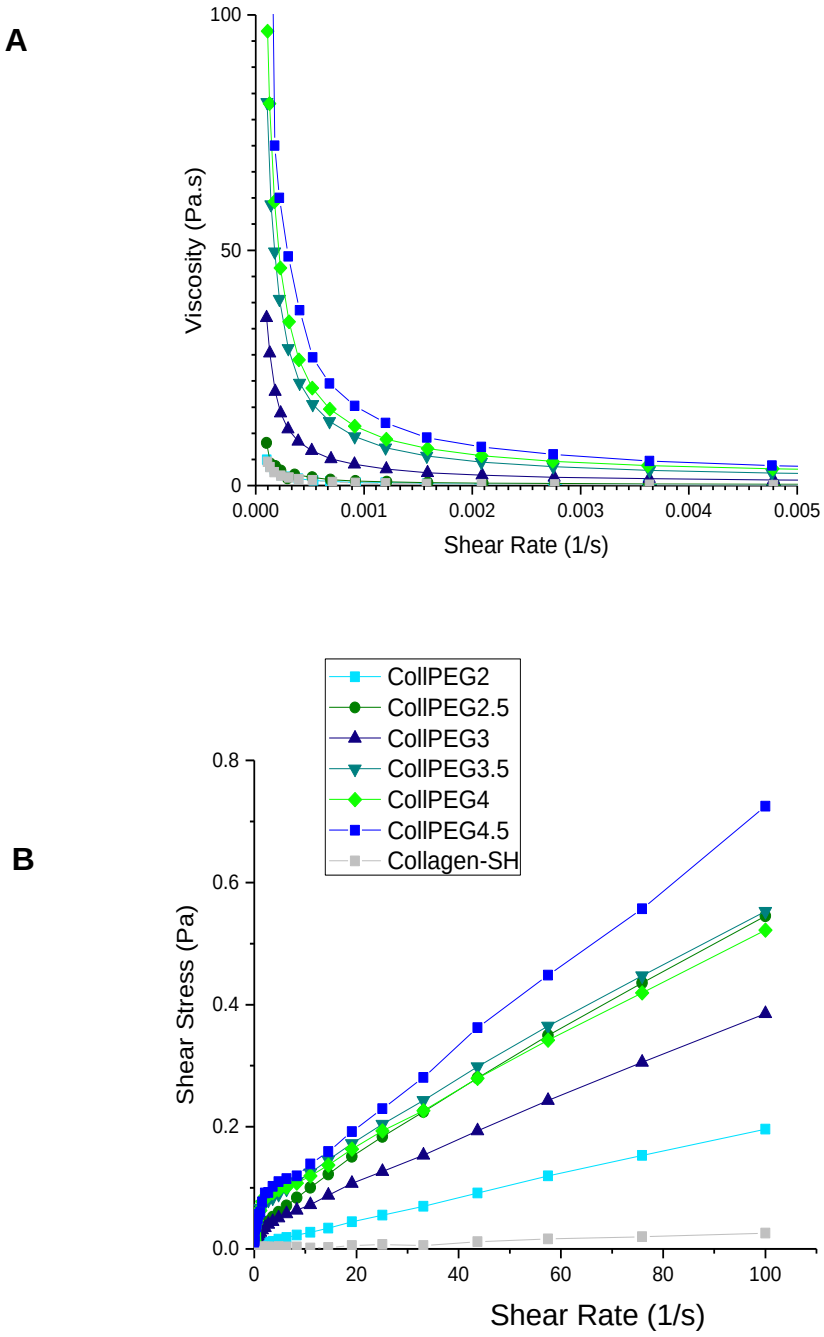

Figure 3.3-15 Shear rate against viscosity represented with linear scale (A) and log10 scale (B) and shear stress against shear rate (C) for the six thiol-ene solutions and collagen-2IT (1 wt.%).

Viscosity experiments are important if the gels are to be used as for *in situ* gelation although the flow of these complex materials cannot be characterised by a single value of viscosity, instead viscosity changes with changing conditions such as shear stress. In order, to do a direct comparison, viscosity can be

compared at zero-shear. As expected, the viscosity increases with increased concentration of PEG8NB, due to its high molecular weight (**Error! Not a valid bookmark self-reference.**).

Table 3.3-12 Viscosity of samples at zero-shear rate. Represented as means ± SEM (n=3).

Sample ID	Zero-Shear Viscosity (Pa.s)
Coll-SH (1 wt.%)	4.8 ± 0.6
CollPEG2	5.5 ± 0.6
CollPEG2.5	9.0 ± 5.3
CollPEG3	36 ± 16
CollPEG3.5	81 ± 12
CollPEG4	97 ± 24
CollPEG4.5	104 ± 21

Compression testing was used to calculate the elastic moduli of the six click chemistry hydrogels by plotting stress-strain curves (Figure 3.3-16).

The linear region of the stress-strain curve is known as the elastic region. In this region, once the stress acting on the material is removed, the material can return back to its original shape. Statistically significant results are observed in the elastic moduli of the hydrogels: collPEG3, collPEG3.5, collPEG4 and collPEG4.5. The weakest hydrogels showed no significant difference between collPEG2 and collPEG2.5. This could be due to the Instron and the load cell denotation reduced sensitivity with very weak hydrogels ~1 kPa.

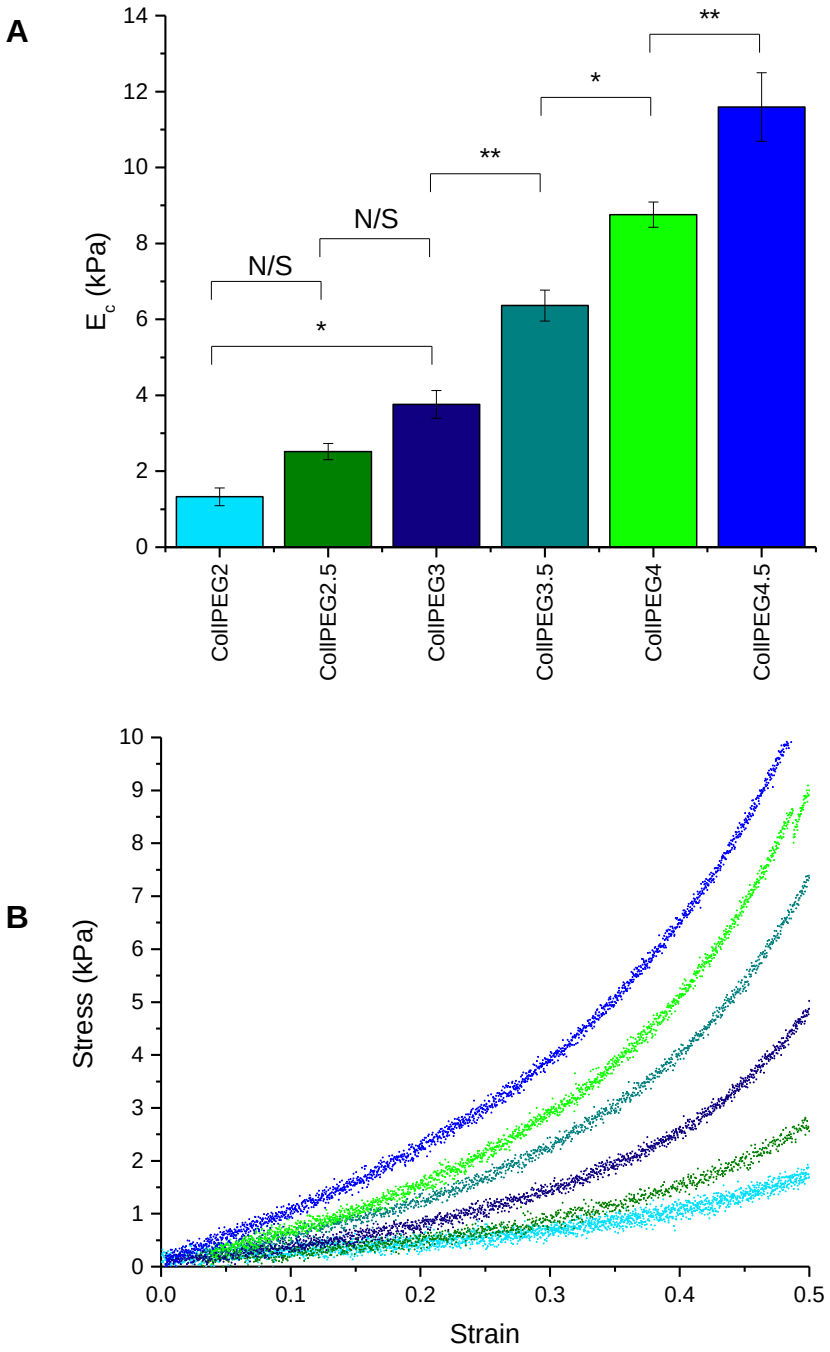

Figure 3.3-16 (A) Compressive moduli of the six click chemistry hydrogels. Represented as means ± SEM n= 7. (B) Stress-strain curve of the six click chemistry hydrogels. Young's modulus (E_c) calculated by the gradient up to 20% strain.

Swelling and gel content were quantified to gain insight into the network architecture of the six photo-click collagen-PEG hydrogels (Table 3.3-13). Other than the swelling ratio providing information on the cross-link density, the gel content was used to assess the portion of extractable material not involved in the formation of the thiol-ene photo-click covalent network [79]. As observed from

the resultsTable 3.3-13 Swelling ratio and gel content of the click chemistry gels. Data represented as mean ± SEM (n=4)., high gel content (G > 90 wt.%) was found for all the thiol-ene photo-click gels investigated, suggesting all the material was held together as a covalent network.

Table 3.3-13 Swelling ratio and gel content of the click chemistry gels. Data represented as mean ± SEM (n=4).

Sample ID	SR (wt.%)	G (wt.%)
CollPEG2	1530 ± 130	90 ± 1
CollPEG2.5	2130 ± 150	86 ± 3
CollPEG3	2340 ± 240	97 ± 1
CollPEG3.5	2640 ± 220	90 ± 2
CollPEG4	2840 ± 71	91 ± 1
CollPEG4.5	3010 ± 127	90 ± 1

This observation provided further confirmation that the presented synthetic thiol-ene approach successfully enabled the rapid formation of defined covalently cross-linked collagen-based networks.

A paper by Xu *et al*, performed a Michael-addition reaction using thiolated collagen, with a gel content of 77 wt.% recorded [114]. This is a lower G value than the one obtained in this study using thiolated collagen and a thiol-ene photo-click reaction, suggesting a higher yield of network formation than the Michael-type approach.

Other than the gel content, the swelling ratio increased from 1530 wt.% to 3010 wt.% from collPEG2 to collPEG4.5, despite the increased storage modulus of these samples, although due to the small n=4, the swelling ratios of the six photo-click hydrogels are not statistically significant (Figure 3.3-17). This increase in swelling ratio could be due to the increased content of hydrophilic PEG incorporated into the hydrogel and the extended cross-linker chain length between the collagen chains. The swelling ratio for these hydrogels was very high and in comparison, collagen hydrogels formed using EDC (20 x excess) report a swelling ratio of 1595 wt.% [223].

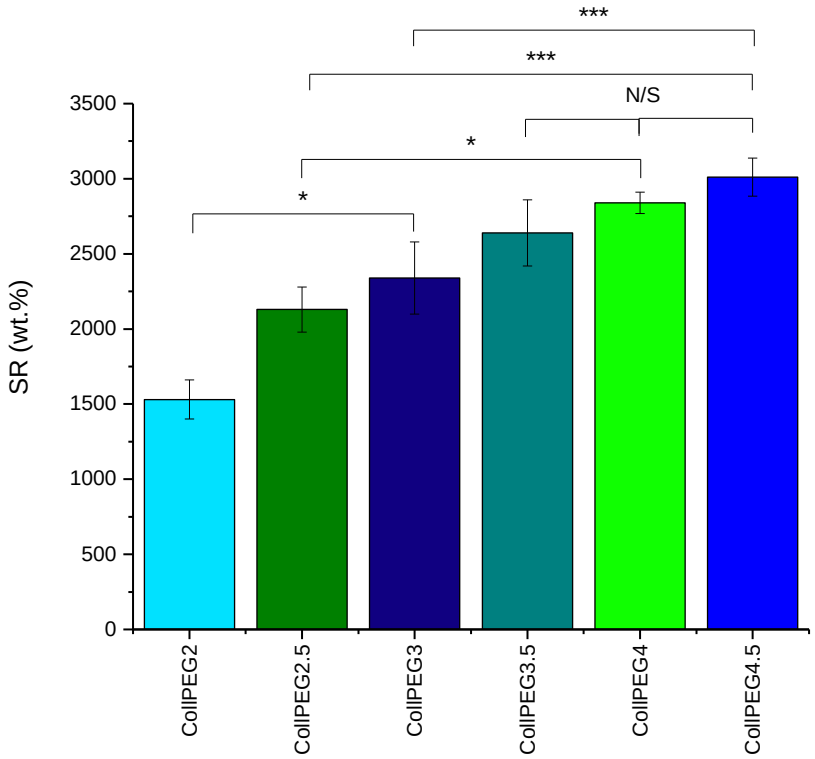

Figure 3.3-17 Swelling ratios of the six photo-click hydrogels. Represented as means ± SEM n=4.

Swelling ratio is an important feature for the design of regenerative devices since a high swelling ratio is expected to promote increased diffusion of nutrients and cellular waste into and out of the collagen hydrogel [224].

To further analyse the swelling behaviour of the photo-click hydrogels, a swelling kinetic experiment was used to assess the amount of time needed for the gels to reach equilibrium with water (Figure 3.3-18). The stiffer hydrogels, CollPEG4.5, CollPEG4 and CollPEG3.5, were found to reach equilibrium after 10 minutes' incubation in distilled water, whereas the weakest gel, CollPEG2, needed 360 minutes to reach equilibrium with water. These results further confirm the relationship between PEG content in the thiol-ene reacting mixture, and previously-observed swelling ratio of the resulting hydrogels.

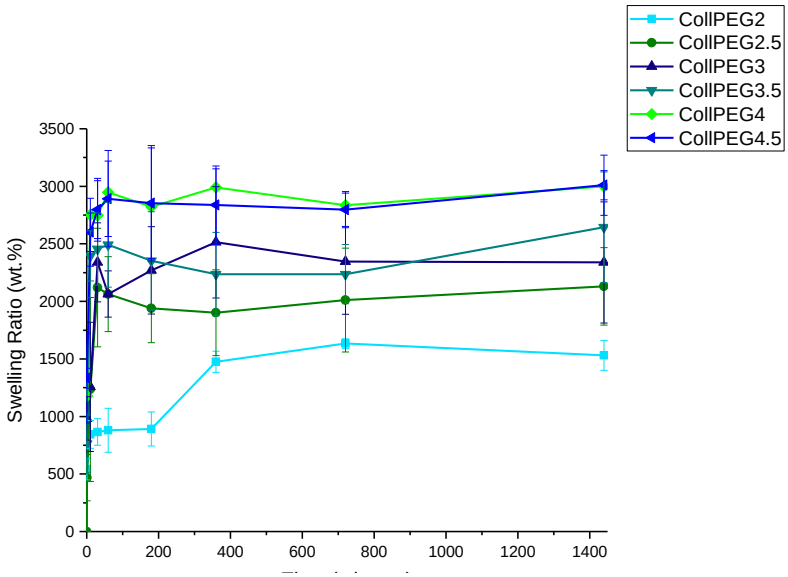

Figure 3.3-18 Swelling kinetics profile of thiol-ene collagen hydrogels prepared with 0.5% (w/v) LAP and varied PEG content.

SEM images were taken in the wet state to analyse the morphology of the photo-click gels in near-physiological conditions (Figure 3.3-19).

Pore sizes in the range of 10 – 30 µm were observed. Pores may likely be formed in the hydrogels following stirring and casting of the thiol-ene mixture. Pore size is an important feature in regenerative devices to allow sufficient material surface for cell seeding and cell diffusion. Additionally, pores should be large enough to promote vascularisation [225]. Work by Chiu *et al* stated that when using PEG hydrogels, cell and vessel invasion was limited to the external surface of the gels with smaller pore size (25 -50 µm), whereas hydrogels with larger pores (50 – 150 µm) permitted mature vascularised tissue formation throughout the entire material volume [226].

The mesh size of molecular porosity of the hydrogel is correlated to the swelling behaviour of the hydrogel and mechanical properties since lower swelling and higher elastic modulus indicates a smaller mesh size.

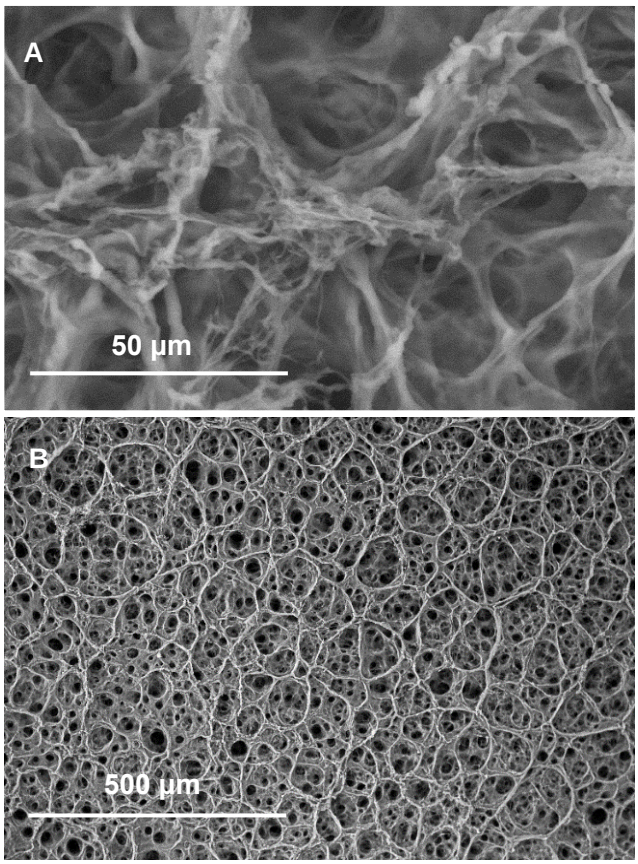

Figure 3.3-19 Cool-stage SEM images of hydrated sample CollPEG4. Magnifications: A: 1000×; B: 100x

3.3.4 Hydrogels for Muscle Tissue Engineering

Three collagen-PEG hydrogels were chosen based on their mechanical properties to use as the scaffold materials for skeletal muscle tissue engineering, with the aim to establish whether substrate stiffness has a comparable effect on the maturation/ differentiation of myoblasts into myotubes and whether hydrogel mechanical properties influence cellular mechanotransduction.

Engler *et al* used AFM to calculate the Young's modulus of mouse muscle 12 ± 4 kPa (n=3) [56]. This agreed with Collinworths *et al* which calculated an elastic moduli 11.5 ± 1.3 kPa for myoblasts and 45.3 ± 4.0 kPa for myofibers [227]. Striated muscle elasticity is given as E_{muscle} ~ 8–17 kPa [57].

The three strongest hydrogels based on their Young's modulus (E_c) were collPEG3.5, collPEG4 and collPEG4.5 (6.7, 9.5 and 12.5 kPa respectively) to examine whether the hydrogel mechanical properties influence cellular mechanotransduction.

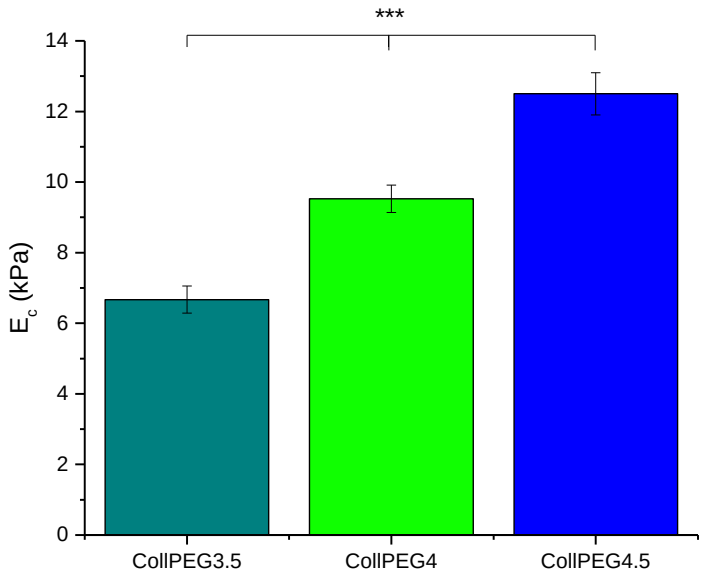

Figure 3.3-20 Compressive modulus, E_c of the three photo-click hydrogels n=7.

Hydrogel mechanical properties are typically reported as either their shear modulus (G) or their elastic modulus (E), two values that are related to each other as a function of the material's Poisson's ratio (*v*).

Equation 3.3-6

$$E = 2G(1 + \nu)$$

Most hydrogels are assumed to have a Poisson's ratio of around 0.45–0.5, meaning that E ≈ 3G [67]. Although a paper by Castro *et al* and Knapp *et al*, which look into Poisson's ratio of collagen hydrogels, state that biological hydrogels tend to adopt a Poisson's ratio between 0.20 and 0.30 for the solid part so E ≈2.5 [228, 229].

However, the shear modulus (G) for these three hydrogels were reported as 3.4, 4.8 and 6.4 kPa, so E ~ 2G.

Due to the high degree of statistical significance ($p<0.005$), the results from the rheology were highly believable. The results from the elastic modulus were also statistically significant and highly reproducible (Table 3.3-14). So it was believable that E= 2G rather than 2.5G/ 3G and v= -0.015. Although, negative Poisson values correspond to auxetic materials which these hydrogels are not.

Table 3.3-14 Table to show reproducibility of the photo-click hydrogels. Expressed as means ± SEM (n=7).

Sample ID	E_c (2016) (kPa)	E_c (2017) (kPa)
CollPEG3.5	6.4 ± 0.4	6.7 ± 0.4
CollPEG4	8.8 ± 0.3	9.5 ± 0.4
CollPEG4.5	11.6 ± 0.9	12.5 ± 0.6

A paper by Parma *et al* reported collagen-mimetic peptide-modifiable hydrogels with characterisation using rheology and compression testing. The equilibrium storage moduli of all hydrogels ~8 kPa up to strains of 1%. These hydrogels were further characterised using confined compression testing. All hydrogel formulations had similar compressive moduli of ~2.5 kPa and therefore, E=0.3G [230].

A paper by Kocen *et al* looked into the viscoelastic behaviour of polysaccharide gellan gum hydrogels with increasing content of bioactive glass (BAG) using rheology compression testing and dynamic mechanical analysis (DMA) [231].

The sample for 0 wt.% BAG was stated to have a compressive modulus (E) of 6.6 kPa and shear modulus from rheology (G*) of ~ 5 kPa. E= 1.3G and again, E = 2.5G/ 3G does not apply for this hydrogel.

Kocen *et al* stated that although all three techniques, rheology, compression and DMA (not performed in this work) describe the mechanical properties of the hydrogel composites, they do not provide the same material property and cannot be directly connected because types of deformation are different. For example, unlike compression deformation, pure shear does not lead to volume changes, so it is not sensitive to variations in the Poisson ratio and bulk properties.

However, it is logical to expect that the stiffest material should have the highest modulus value for both methods which is the case for the materials reported in this work. CollPEG4.5 was the stiffest material which was reflected in it having the highest modulus for both rheological and compression testing.

It was important to examine the degradation of the material. Degradation *in vitro* using bacterial collagenase can correlate with *in vivo* degradation although differences in the cleavage mechanism mean the *in vitro* analysis should only be used as preliminary results for determining degradative behaviour [232].

The mass loss was determined at 1, 3, 5 and 7 days using collagenase 0.2 and 2 mg/mL and HPBS as the control (Figure 3.3-21). The solutions were replenished every 48 hours during the degradation experiments to prevent reduced collagenase activity. PEG hydrogels are inherently biocompatible and non-degradable, so in theory, as a hydrogel they could be rendered biodegradable by incorporating collagenase-sensitive material into the backbone.

The results showed no mass loss over 7 days with the hydrogels incubated in HPBS at 37 ^{o}C. At 0.2 mg/mL, collPEG3.5 had mass loss of 10.8% at day 3 and 33.8% at day 7, compared to 2 mg/mL where there was 42.7% mass loss at day 3 and 50.5% at day 7. These results were substantially different for the two stiffer, more highly cross-linked hydrogels: collPEG4 and collPEG4.5. At 0.2 mg/mL, both collPEG4 and collPEG4.5 had a mass loss of 0% at day 3 and at day 7, collPEG4 had mass loss of 6.1% and collPEG4.5 a mass loss of 3.7%. At 2 mg/mL, collPEG4 had mass loss of 10.1% at day 3 and 10.4% at day 7 and collPEG4.5 had mass loss of 6.2% at day 3 and 8.2% at day 7.

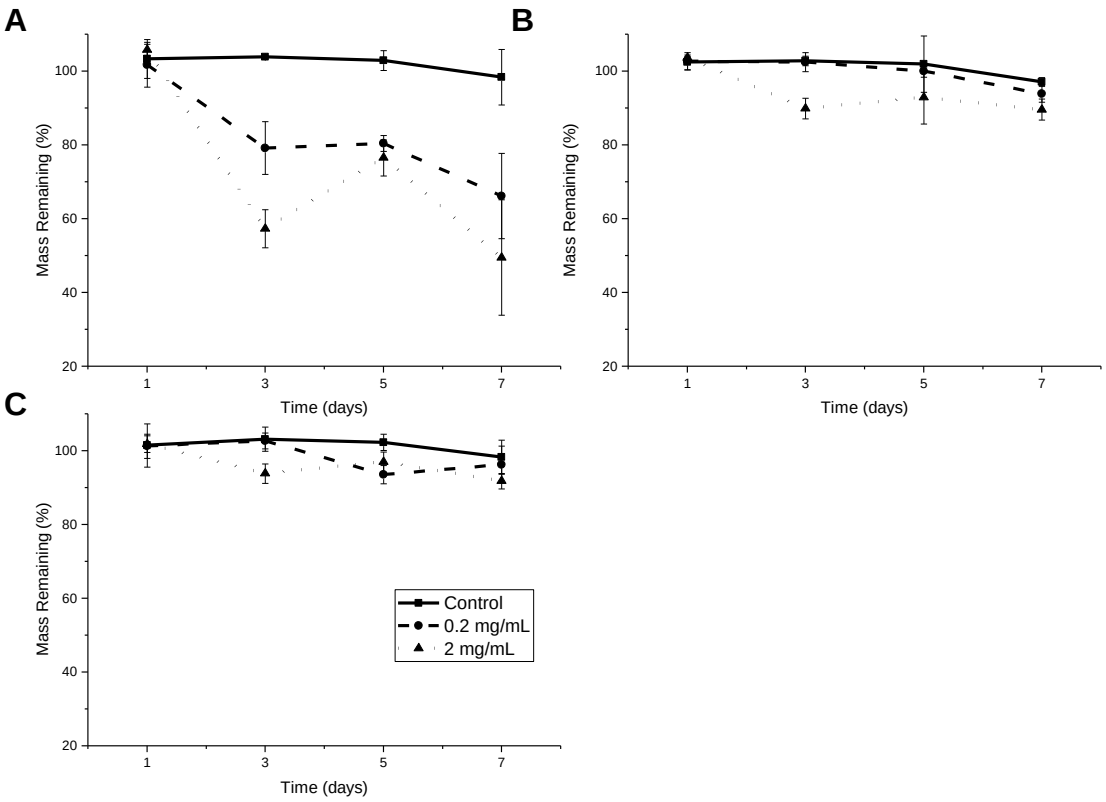

Figure 3.3-21 Degradation Graphs of collPEG3.5 (A), collPEG4 (B) and collPEG4.5 (C). Represented as means ± SEM n=3.

Alberti *et al* used collagenase to analyse the degradation of de-cellularised tendon with and without chemical cross-linking using glutaraldehyde. It was shown that cross-linking reduced degradation, highly cross-linked showed 1.9% mass loss, moderate cross-linking showed 2.1% mass loss, compared to non-cross-linked samples which showed 33.5% mass loss using collagenase (1 mg/mL) over 100 hours (4 days) [232].

The mass loss in this work appeared to be higher than for Alberti *et al*. This could be due to the higher weight of Alberti's samples providing reduced margin of error when re-weighing the samples. It could also be due to the bacterial collagenase. Clostridium histolyticum collagenase, which was used in this experiment, has been shown to cleave collagen into several small fragments and hence provide difficulty when weighing (Figure 3.3-22).

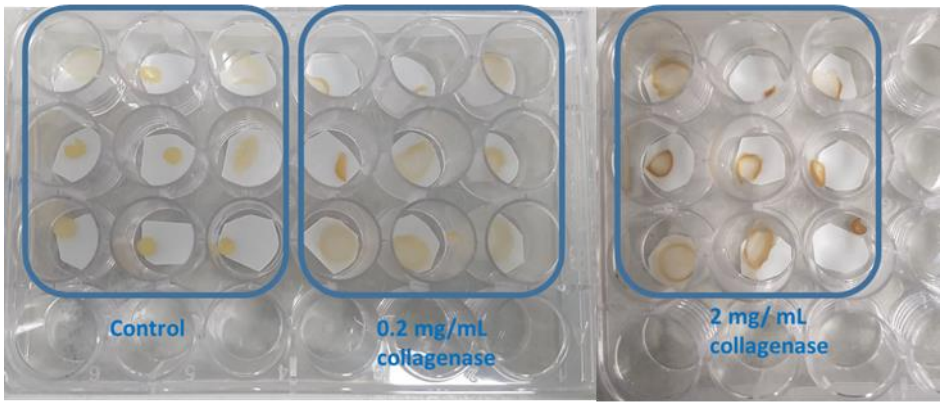

Figure 3.3-22 Photos of the three hydrogels at day 3. CollPEG3.5 observed at the top, more degraded with 2 mg/ mL of collagenase.

The results do confirm that increasing cross-linking does reduce degradation with collagenase. Although a paper by Helling *et al* stated that a cross-linking method/ high resistance to collagenase degradation may be associated with elevated foreign body response, although resistance to enzymatic degradation should not be used alone as means to assess the efficacy and safety [233].

Collagenase, in addition to being produced by some bacteria, is made by the body as part of its normal immune response and assists in destroying extracellular structures. So whilst the concentration of collagenase chosen for this work was 0.2 mg/mL and 2 mg/ mL, this would be very different when used in an animal model *in vivo* and would also depend on whether the animal had been previously exposed to the material and developed an active immune response.

In vitro tests for degradation have to be performed as preliminary results because the degradation behaviour should correlate with *in vivo* degradation behaviour. However, the percentage mass loss results would have no comparison *in vivo*. The best way to investigate degradation appeared in a paper by Duan *et al*, which used a fluorescent dendritic star molecule. They implanted PLGA/d-p48 nanofibrous membranes subcutaneously which could be observed using animal fluorescent imaging system at different time points after implantation, thus providing live imaging analysis [234].

This paper solved the issues faced by incorporating fluorescent molecules for *in vivo* imaging: macromolecule diffusion, fluorescent molecule toxicity, scaffold incorporation and using a molecule which can be traced by a non-invasive manner for a long time period [234].

An experiment was performed prior to cell culture experiments to ensure that the cells would experience the same mechanical properties at day 7 compared to day 1. Compression testing was performed after 1, 3, 5 and 7 days incubation in PBS. The elastic moduli were shown to have no statistical significance between the results (Figure 3.3-23).

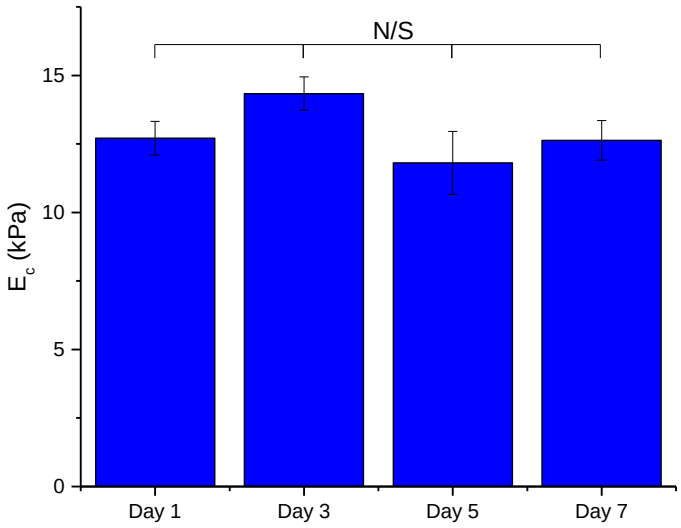

Figure 3.3-23 Compressive testing of collPEG4.5 after being left in PBS for 1, 3, 5 and 7 days. Represented as means ± SEM (n= 7).

These newly synthesised photo-click hydrogels demonstrated excellent shape memory. After dehydration, they were shown to equilibrate with water and return to their original shape and volume (Figure 3.3-24). Compared to the collagen-4VBC hydrogels which after dehydration, do not regain their initial volume and

remain as flat disks. In terms of clinical application, the hydrogels could be implanted in a sterile, dehydrated state and then expand and to fit a defect.

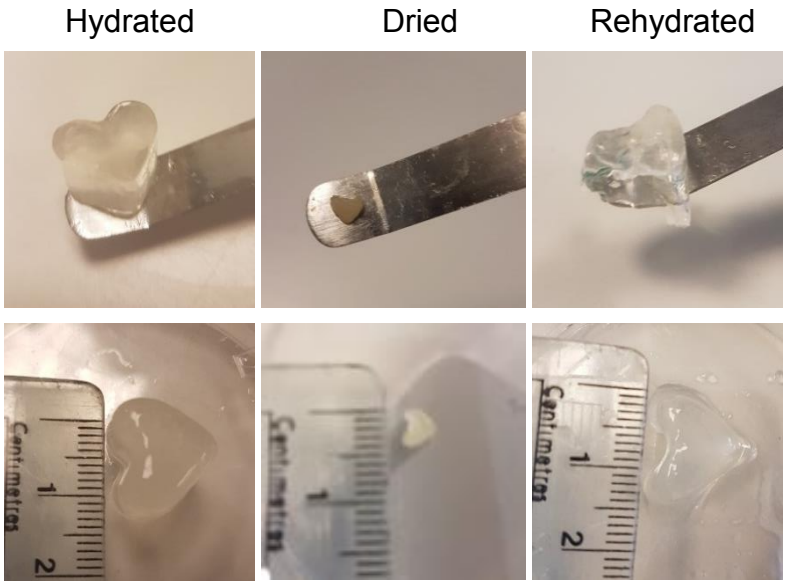

Figure 3.3-24 Pictures demonstrating the shape-memory of the photo-click hydrogels.

The photo-click hydrogels also report a very high swelling ratio of up to 3000 wt.%. Another application could be as a wound dressing for wound healing if delivered as a dehydrated film. As a hydrogel, it benefits from the ability to incorporate small molecules such as growth factors, which in a wound healing application, could be further investigated to prevent fibrosis and scarring.

3.3.4.1 Photocol© Hydrogels

Three kits of methacrylated type I collagen were selected to prepare photopolymerised collagen hydrogels as a commercial control for the cell culture experiments. The PhotoCol® kit was selected to provide collagen gels with varied stiffness based on collagen concentration and cross-linking. The results from Table 3.3-15 were taken from the Biomatrix website showed varied stiffness (using rheology) when different concentrations were used, with and without cross-linking

Table 3.3-15 Gel stiffness of PhotoCol® at varying concentrations with and without UV cross-linking. Taken from: advancedbiomatrix.com/photocol/photocolmethacrylated-type-i-collagen-kit-for-crosslinkable-hydrogels-5201-1ea/

Concentration (mg/ mL)	UV Cross-Linking	Shear Modulus (Pa)
6	Yes	2020
6	No	3880
8	Yes	3320
8	No	6025

The protocol involved preparing collagen hydrogels by fibrillogenesis, - neutralising the collagen solution below 10 ^{o}C before warming it up to 37 ^{o}C, which is when the shear modulus of the non-cross-linked hydrogels was measured using the rheometer. After heating up to 37 ^{o}C, the hydrogels were then exposed to UV light (365 nm) for 5 minutes before the cross-linked modulus was measured.

After receiving the kits, the first issue encountered was that the protocol said to use I2959 (0.1% (w/v)), as should be clear by now, this is far too low for a collagen solution. The second problem was that they said the hydrogel could be photo cross-linked when it was already a hydrogel (from the self-assembled neutralisation and fibrinogenesis step), rather than as a solution. Collagen is a huge molecule and with 40% of the total lysine residues of the collagen molecule methacrylated, when held apart as a self-assembled gel, it would make it more difficult for these methacrylate groups to form a network.

However, the protocol was followed and made very weak hydrogels. These did not become more stiff after exposure to UV light as predicted, likely due to the material not being in the liquid state and due to the low photoinitiator concentration stated to use in the protocol and provided in the kit.

Two other issues with this product was that no error or ‘n’ number was stated on the shear modulus (Table 3.3-15). Additionally, the shear modulus of 8 mg/mL solutions (0.8 wt.%) was 3320 Pa. As stated previously, a paper by Cross *et al* produced collagen hydrogels at 3, 8, 10, 15, and 20 mg/ml with a range of elastic modulus 30 Pa to ~1800 Pa. Since elastic modulus is meant to be ~ 2.5G/ 3G,

the figures for PhotoCol® look far off. In fact, when looking at the other products from Advanced Biomatrix, FibriCol® stated that:

"The varied gel stiffness (rheology) of type I collagen - FibriCol® collagen was tested to determine the stiffness (Young's modulus) of 3D gels at various concentrations (8, 4, 2, 1 mg/ml). At 8 mg/ml, ~950 Pa and at 4 mg/ml ~600 Pa"

Firstly, they have confused shear modulus with Young's modulus, and secondly, the result using 8 mg/mL was 3x lower than that of PhotoCol®. The addition of methacryate groups of ~40% of the lysines would not contribute to the stiffness increasing by that amount.

The PhotoCol® hydrogels were not held together as a polymer network and could not be used as the control material for the cell culture experiments. However, since three photo-click hydrogels collPEG3.5, collPEG4 and collPEG4.5 had already been chosen, it was decided that these could be compared to each other with tissue culture plastic as the control rather than using another hydrogel with similar mechanical properties (supposedly PhotoCol®).

3.4 Conclusions

This chapter examined various ways to incorporate click chemistry into the preparation of collagen hydrogels and a thiol-ene photo-click reaction was systematically designed.

This method was developed to ensure that all the reagents were cell-friendly/ bioinert, the precursor materials were water-soluble, a low concentration of photoinitiator/ catalyst was used with resulting fast gelation times and facile, accurate means to provide tunable mechanical/ physical properties.

From this work, it was decided that the best precursor materials for the thiol-ene reaction was collagen-2IT and PEG8NB and the gelation kinetics and storage modulus were examined using water soluble photoinitiators LAP and I2959 at concentrations of 0.1% and 0.5% (w/v). The rheological experiments showed that decreasing photoinitiator concentrations had a detrimental (15 fold) effect on storage modulus. The I2959 photoinitiator was shown to be the least preferable photoinitiator when used at 365 nm, leading to longer gelation times compared to LAP. Further work using LAP 0.5% (w/v) showed that photo-click collagen-PEG hydrogels could be successfully prepared with tunable physical and mechanical properties by altering the PEG content and thereby the number of thiol-ene cross-links. CollPEG2 to collPEG4.5 presented G= 0.54 – 6.4 kPa and

E_c= 1.2 – 12.5 kPa, with SR= 1500- 3100 wt.%. Such soft and highly swollen systems offer widespread application for constructs for muscle regeneration and wound healing devices. The three hydrogels with mechanical properties closest to natural muscle E_c ~ 8-17 kPa were chosen to take forward in the cell culture experiments, collPEG3.5, collPEG4 and collPEG4.5.

Chapter 4 – Cell Work and Animal Models

4.1 Introduction

There were three main aims to this chapter. The first was to determine the effect of hydrogel stiffness on cell attachment, spreading, proliferation and maturation/ differentiation of C2C12 mouse myoblast cells. The second was to analyse the immune response of this new material compared to a commercially available material for soft tissue repair. The third was to compare the stiff hydrogel, collagen-4VBC (30x excess) with a control sample, BioGide® as a purely biomaterial-based approach for bone formation in a critical sized bone defect model. This could be used as the basis to analyse the potential use of collagen-4VBC (30x excess) in a gradient hydrogel for interface tissue engineering.

Skeletal muscle tissue engineering (SMTE) aims to replicate the structure and function of skeletal muscle tissue *in vitro* and *in vivo*, with the aim for implantation as a therapeutic device [29]. Skeletal muscle is a highly organised composite structure comprising of bundles of myofibrils, myofibers, blood vessels and nerves highly orientated in a parallel alignment [31]. Myofibrils are the elongated contractile threads capable of actuating muscle contraction through the relative movement of two interlocking macrostructures, the thin actin filaments and thick myosin filaments [29]. Myofibers are formed when the undifferentiated muscle cells, myoblasts fuse together to form multinucleated myotubes characterised by their centralised nuclei [25].

In their niche, cells are presented with an array of complex biophysical and biochemical signals from the surrounding extracellular matrix (ECM). The Young's modulus, E, often referred to as elasticity or stiffness is an intrinsic ECM characteristic [235]. Matrix stiffness has been shown to have a profound effect on cell spreading, morphology and differentiation [57, 236-238]. Mesenchymal stem cells (MSCs) show lineage-specific differentiation when cultured on substrates matching the stiffness corresponding to native tissue; soft tissue-like matrices (~ 2kPa) tend to induce differentiation into neural cells, whereas, matrices with stiffness closest to muscle (~10 kPa) form myocytes and when cultured on stiff substrates similar to that of pre-calcified bone (~ 40 kPa) become osteoblasts [237]. So soft matrices cause neurogenic differentiation, stiffer

matrices cause myogenic differentiation and rigid matrices cause osteogenic differentiation.

Engler *et al* cultured C2C12 myoblast cells on hydrogel matrices with stiffness' 1, 8, 11 and 18 kPa. This work showed a narrowness for the optimum substrate stiffness, with a lower percentage of striation on 1 and 18 kPa matrices compared to cells on the intermediate matrix stiffness of 8 and 11 kPa [56]. Myoblast maturation/ differentiation of the photo-click hydrogels will be examined in the current study to examine the narrow variation in substrate stiffness.

4.1.1 Muscle Cells

The cells primarily responsible for muscle regeneration are satellite cells (SCs), which are a specific type of stem/ precursor cell found beneath the surrounding basal lamina and outside the myofiber plasma membrane [239]. They can be activated in response to muscle injury, which causes their proliferation, fusion and differentiation into multinucleated myotubes and then muscle fibres [29]. Other cell populations such as mesenchymal stem cells (MSCs) can contribute to restoration of muscle functionality, additionally, myoblasts, induced pluripotent cells (IPSCs) or embryonic stem cells (ESCs) could be used [25].

The cell line C2C12 is a subclone, originally obtained by Yaffe and Saxel (1977). C2C12 cells consists of a pure population of murine myoblasts that proliferate and differentiate rapidly in culture, forming contractile myotubes and synthesising characteristic muscle proteins [240].

The C2C12 cell line was used in this project because they are already widely used for studies of muscle biology and regeneration and have similar properties to isolated human skeletal muscle cells [50]. Myogenic differentiation on tissue culture plastic is well established in terms of sequence of events and protein expression [236].

In this work, the clinical application would involve cells administered in muscle tissue on a scaffold. For this however, the cells would have to be from an autologous or allogeneic setting, be accessible in large numbers, grow homogenous *in vitro* without loss of differentiation potential, reach the sites of muscle regeneration and be able to differentiate *in situ* and give rise to normal physiology [43]. Fishman *et al* conducted a review on the appropriate cell type for skeletal muscle tissue engineering conforming to the aforementioned factors. SCs were considered to be the obvious candidate, however, they cannot migrate extensively within muscle and would require local injection into skeletal muscle

at a distance of a few mm from each other, additionally, only low numbers can be isolated from autologous muscle and expanding *in vitro* decreases regenerative potential [43, 241, 242].

4.1.2 Myotube Alignment

Skeletal muscle consists of long bundles of parallel myotubes that are formed by differentiation and fusion of myoblast cells. However, when cultured *in vitro*, myoblasts and myotubes lose their innate organisation and instead adopt a random distribution [243]. It is an important requirement of engineering functional skeletal muscle to possess an *in vitro* system capable of mimicking the aligned actin /myosin filaments of physiological muscle architecture to guarantee the generation of longitudinal force after contraction.

The alignment can be achieved by electrospinning, microchannels, unidirectional freeze-drying of hydrogels (collagen matrices with nearly axially oriented pores reported by Madaghiele et al [244]), electrical stimulation or mechanical force [245].

4.1.3 Muscle Regeneration

Skeletal muscle regeneration after tissue damage can be summarily divided into several overlapping phases: the inflammation and activation of stem cells, differentiation and fusion of satellite cells and deposition of a provisional ECM and finally maturation of the newly formed myofibers and remodelling of the tissue [4].

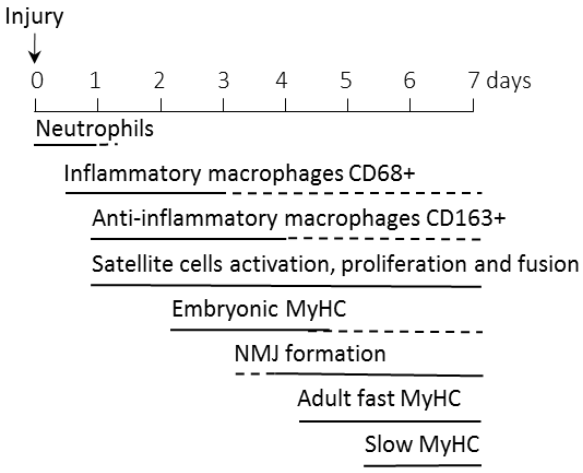

Figure 4.1-1 Major events in muscle regeneration.

The inflammation phase involves muscle necrosis, invasion of neutrophils (~2 hr after injury) which secrete chemotactic signals that recruit macrophages. Pro-inflammatory macrophages (M1) are responsible for phagocytosis and the activation of satellite cells (characterised by the expression of the CD68 surface marker (rats) and lacking the CD163 [246]) and anti-inflammatory macrophages (M2) contribute to the proliferation and differentiation of these cells to myoblasts and myotubes [25]. During this repair phase, fibrosis can occur as well as invasion of nerves and blood vessels. The final remodelling repair phase is the fusion of newly formed myotubes with existing myofibers, and the damaged muscle begins to regain its contractile function [25]. However, in cases of severe volumetric muscle loss, the rate of fibrosis (scar tissue formation) can exceed the rate of myoblast proliferation and myotube formation and this thick layer of scar tissue can prevent the fusion with the myofibers [25]. Thus macrophages have a central regulatory role in the muscle response to injury, not only by removing necrotic tissue but also by promoting muscle regeneration [246].

4.1.3.1 Bone Regeneration

Muscle influences fracture or defect healing due to its proximity to bone and abundant vascularity. This can provide an important source of osteogenic growth factors and stem cells to stimulate bone healing [247, 248]. Injury to either tissue compromises physical function because both are necessary for load-bearing and movement.

In the case of bone, a defect that will not heal without intervention is termed a “critical size defect” [249]. Mulliken *et al* reported a 4 mm critical size calvarial defect in Charles River rats [250]. Currently, the gold standard treatment is an autogenous bone graft which involves the harvest of ‘donor’ bone from a non-load-bearing site [251, 252]. However, this leads to donor site morbidity and can lead to immune or inflammatory response of the host tissue after implantation. Ideally, a purely biomaterial-based approach would be desirable in terms of production costs, safety, approval process and availability. Nevertheless, it remains a challenge to achieve complete regeneration of a bone defect or fracture [251].

4.2 Methods

4.2.1 Materials

C2C12 mouse C3H muscle myoblasts were purchased from Sigma Aldrich. ATPlite luminescence assay kit was purchased from PerkinElmer. LIVE/DEAD Viability/Cytotoxicity Kit was purchased from Life Technologies. Oregon Green 488 Phalloidin was purchased from Fischer Scientific Ltd. 4',6-diamidino-2-phenylindole (DAPI) and Horse Serum were purchased from Sigma. Myosin 4 Antibody Alexa Fluor 488 (MF20), eBioscience TM and Insulin-Transferrin-Selenium were purchased from Thermo Fischer Scientific. Antibody CD68 Alexa Fluor 488 was purchased from Bio-Rad. SD rats (male) were purchased from Charles River. Vicryl and Ethilon sutures were purchased from Miller Medical. Dental Implant Trephine Bur, Drill TPHB-B4 was purchased from amazon. Micro Drill Circular Saw and Mandril were purchased from Fine Science. Bio-Gide® and Mucograft® were purchased from Geistlich Biomaterials.

4.2.2 Cell Work

Three hydrogels: collPEG3.5, collPEG4 and collPEG4.5 with elastic moduli (E) 7, 10 and 13 kPa were selected for biological testing. The hydrogels were gamma sterilised in the dry state to prepare for cell culture and were either treated or untreated for cell attachment and spreading experiments. Treated hydrogels were swollen in DMEM: FCS (50:50) overnight and untreated were not. Treated hydrogels were given the nomenclature collPEG3.5 + FCS, collPEG4 + FCS or collPEG4.5 + FCS.

Photocol® was purchased as a commercial, photopolymerisable collagen hydrogel with similar elastic moduli to the three photo-click hydrogels, however, this product was found not to work. Instead the three hydrogels were compared against each other and tissue culture plastic control.

Cells were grown in cell culture media (Dulbecco's Modified Eagle Medium (DMEM), foetal calf serum (FCS) (10%), Penicillin Streptomycin (PenStrep) and incubated at 37 ^{o}C and 5% CO_2.

4.2.2.1 Cytotoxicity Studies

Three types of cytotoxicity test are stated in ISO 10993-5: extract, direct contact and indirect contact tests [253].

4.2.2.1.1 Extract Cytotoxicity

Dried hydrogel samples (0.001 g) were incubated cell culture media (1 mL) for 72 hours. After incubation, the sample extract was recovered by centrifugation and the incubated cell culture media was applied to 50% confluent C2C12 cells cultured on a polystyrene 96-well plate. Dimethyl sulfoxide (DMSO) (50:50 DMEM) was used as the negative control, whilst cell culture media was used as the positive control. Five repeats were used. After 48 hours, cell viability was assessed using an ATPLite luminescence assay.

4.2.2.1.2 Direct Contact Cytotoxicity

Collagen hydrogels (100 µL) were prepared in 96-well plates. These were air dried and sterilised via gamma radiation. The sterilised hydrogels were then swollen in cell culture media in the 96-well plate, returning to their original size. C2C12 mouse myoblasts (1×10^4 cells) were added to each hydrogel. DMSO (50:50 DMEM) was used as the media for the negative control and cells were grown on tissue culture plastic as the positive control. Measurements were also taken for hydrogels without cells, cell culture media without cells and a blank. Five repeats were used. After 1, 3 and 5 days, cell viability was assessed using an ATPLite luminescence assay. Due to the ability of cells to migrate and due to their ease of attachment onto treated tissue culture plastic, prior to the ATP assay, the hydrogels had to be transferred to a fresh well plate to ensure the cell viability was not from the cells that had migrated/ initially attached to the tissue culture plastic

4.2.2.1.3 ATPLite Assay

A vial of lyophilised ATP standard solution (9.6 µmole) was reconstituted in ATP buffer solution (5 mL). The media from cells cultured in a 96-well plate was removed. Mammalian cell lysis solution (50 µL) was added into each well and the plate was shook for 10 minutes in an orbital shaker at 700 rpm. ATP solution (50 µL) was added and shook for a further 10 minutes. An aliquot (50 µL) was removed and added to an optiplate. This was dark adapted for 10 minutes before the luminescence was measured using a Perkin Elmer TopCount [129].

To find the relationship between luminescence and cell count, C2C12 cells were seeded at increasing known density on tissue culture plastic. These were left for 3 hours for cell attachment before an ATPLite assay was performed to produce a standard curve, the gradient of which provided the relationship between luminescence and cell number. All graphs were plotted using cell number.

4.2.2.2 Cell Attachment

C2C12 cells cultured in a T175 flask were stained with a calcein AM (LIVE). The cells were trypsinised and then re-suspended in cell culture media. A low density of cells (1 x 10^5 cells per mL) were seeded onto the treated and untreated hydrogels: collPEG3.5, collPEG4 and collPEG4.5 (the samples of each group were triplicated: n=3). After 3 hours, three photos were taken from each well (3 technical repeats) using fluorescent inverted microscopy and cells were counted using image-J.

4.2.2.3 Cell Spreading

C2C12 cells were cultured on treated and untreated hydrogels: collPEG3.5, collPEG4 and collPEG4.5 (the samples of each group were triplicated: n=3). After 24 hours, three photos were taken from each well (3 technical repeats) using fluorescent inverted microscopy and cell surface area was calculated using image-J.

To calculate the area: Image – type – 8 bit. Image – adjust – threshold. Analyse – analyse particles – outline thresholds.

4.2.2.4 Cell Proliferation

C2C12 cell proliferation was assessed by measuring the cell count in each well at days 3 and 5 using an ATPLite assay. These readings were normalised to the reading of cells at day 0 and divided by the total number of days.

4.2.2.5 Cell Maturation/ Differentiation

C2C12 cells were seeded onto the tissue culture plastic or the three hydrogels (50% confluency) and continually cultured to 70% confluency (2- 3 days) to allow the cells to adjust to their environment using normal cell culture media. From the previous results it was noted that the hydrogels showed lower cell attachment

compared to tissue culture plastic. To overcome this, the hydrogels had to be seeded at a higher initial cell density than the tissue culture plastic. To induce myotube formation, the media was then changed to a myogenic differentiation media (DMEM, 1% PenStrep, 1% FCS and 1% insulin-transferrin-selenium (ITS)). This media was replaced every day and the samples of each group were triplicated: n=3.

4.2.2.5.1 Maturation/ Differentiation Evaluation

Maturation/ differentiation evaluation was performed staining C2C12 nuclei and F-actin at the two end points (3 and 7 days). From the fluorescent images acquired at low magnification, it was possible to quantify the differentiation grade, calculating fusion index and myotube area. Fusion index was calculated by dividing the total number of nuclei in myotubes (≥ 2 nuceli) by the total number of nuclei counted. Clear, distinguishable myotubes were grouped in two categories: those with two to four nuclei and those with five or more nuclei. The percentage of myotubes in each category was calculated as myotube (%) [254-256]. For samples stained for myosin and DAPI, percentage differentiation was calculated as the number of cells stained positive for myosin heavy chain over the total number of cells [257].

4.2.2.6 Cell Staining

Nikon A1R confocal microscope was used to image the cells. A triangular- and line-based image quantification method was designed to reduce bias and achieve reproducibility of the results.

4.2.2.6.1 LIVE/DEAD Stain

Cells were washed three times prior to the assay with PBS. The LIVE/DEAD components of calcein AM (green fluorescence live cells ex/em ~495 nm/~515 nm) and ethidium homodimer-1 (EthD-1) (red fluorescence dead cells ex/em ~495 nm/~635 nm) were diluted with PBS to make calcein AM (2 µM) and EthD-1 (4 µM) respectively. 50 µL of each working solution were added to tissue culture plastic control, 200 µL was added to hydrogels to make up for diffusion/ 3D environment. Incubate at room temperature for 30 minutes, washed three times with PBS followed by imaging.

4.2.2.6.2 Oregon Green 488 Phalloidin Staining

Phalloidin selectively stains F-actin (green fluorescence). The stock solution was prepared by adding methanol (1.5 mL) to oregon green 488 phalloidin (300 units) and freeze in vials (50 µL). The cells were washed three times in PBS and fixed with 10% neutral buffered formalin (NBF) for 15 minutes. The cells were washed three times in PBS and permeabilised with 0.1% Triton X-100 for 15 minutes. The cells were washed three times in PBS then a vial of Oregon green 488 phalloidin stock (50 µL) was diluted in 450 µL PBS as the working solution, which was used for the incubation of cells for 2 hours and counterstained with DAPI.

4.2.2.6.3 DAPI Stain

De-ionised water (2 mL) was added to DAPI (5mg/ mL) to create the stock which can be stored (≤ 6 months). DAPI stock was further diluted in PBS and the DAPI solution (300 nm, 100- 400 µL) was added to cover the permeabilised cells and incubated at room temperature for 1-5 minutes. Washed with PBS (x3) and imaged.

4.2.2.6.4 Myosin 4 Antibody, Alexa Fluor 488 (MF20)

The cells were washed three times in PBS and fixed with 10% neutral buffered formalin (NBF) for 15 minutes. The cells were washed three times in PBS and permeabilised with 0.1% Triton X-100 for 15 minutes. The cells were washed three times with PBS and incubated in horse serum (1%) in PBS for 15 minutes. Cells were washed three times in PBS and incubated in myosin 4 antibody (5 µg/mL) for 4 hours at room temperature and counterstained with DAPI [258].

4.2.3 Animal Model

A subcutaneous model was used to analyse the immune response the new photo-click hydrogel. A calvarial bone defect model was used to examine a purely biomaterial-based approach for bone regeneration.

4.2.3.1 Local Innate Immune Response

The collPEG4.5 hydrogel and Mucograft® samples (1 cm diameter) were implanted subcutaneously in six Sprague Dawley (SD) male rats (300-350 g). At time points 1, 4 and 7 days, the samples were dissected out and fixed with 10% NBF for 24 hours for histological analysis.

A pilot study had previously been performed to ensure the hydrogel was still present after 14 days *in vivo*. For the formal *in vivo* study, two rats were used per

time point. The rat was placed in a trifluorane chamber and anaesthetised (level 5 trifluorane and 2.5% oxygen) ~ 2 minutes. After induction, the animal was transferred onto a heated mat and anaesthesia was maintained (level 2.5 trifluorane and 2.5% oxygen) delivered via a nose cone. Anaesthesia was assessed by lack of reflex to toe pinch. The upper and lower sections of the back were shaved and two full thickness skin incisions were made per section, the subcutaneous tissues were then blundly dissected using artery forcepts to create spaces/ pockets and four PBS swollen collPEG4.5 hydrogels were implanted within these pockets (away from the incision). The wounds were closed using 5-0 ethilion sutures. Four Geistlich Mucograft® samples were used as the control per time point. The wound was cleaned with sterile injection water and the triflourane switched off and the oxygen left on until the rats were fully recovered. Vertegesic (0.03 mg/mL, 300 µL) injection was given to the rat.

At the chosen time points, the rats were schedule 1 killed using a carbon dioxide chamber for 6 minutes followed by cervical dislocation. The samples and the surrounding tissue were then dissected out and fixed in 10% NBF.

4.2.3.2 Critical Size Calvarial Defect Model

The rat was placed in a trifluorane chamber and anaesthetised (level 5 trifluorane and 2.5% oxygen) ~ 2 minutes. After induction, the animal was transferred onto a heated mat set to 37 ^{o}C and anaesthesia was maintained (level 2.5 trifluorane and 2.5% oxygen) delivered via a nose cone. Anaesthesia was assessed by lack of reflex to toe pinch. The rat was shaved from the bridge of the snout between the eyes to the caudal end of the skull/calvarium using electric clippers. After shaving, an alcohol swab was used over the shaved area. Using the scalpel, an incision (~1.5 cm) was made down to the periosteum over the scalp from the nasal bone to just caudal to the middle sagittal crest or bregma. The periosteum was divided and gently pushed laterally using tissue forceps. The calvarium was scored with the surgical drill and trephine before applying a gentle pressure to prevent dural or brain injury until the defect nears the appropriate thickness (~1-2 mm). The trephine and calvarium were irrigated with sterile injection water to prevent thermal injury. The trephinated portion of bone was able to be displaced.

The 4VBC (1.2 wt.%) hydrogel swollen in PBS (4 mm diameter) was placed into the left defect, whilst the control, Bio-Gide® (swollen in PBS 4 mm diameter) was placed in the right-hand defect. Vicryl was used to suture together the periosteum and ethilion was used to suture the skin together. The wound was cleaned with

water and the triflourane switched off and the oxygen left on. Vertegesic (0.03 mg/mL) (300 µL) injection was given to the rat. When the rat came around, it was transferred to a clean cage.

At the time point of 2 or 6 weeks, sch 1 of rats using a carbon dioxide chamber for 6 minutes followed by cervical dislocation. The rats were dissected in the fume hood. A scalpel was used to cut down the centre of the head and the skin was pushed back. The scalpel was then used to cut a rectangular shape out of the soft tissues with the two defect sites inside. A circular saw was then used to cut into the bone following the rectangular shape traced by the scalpel. The rectangle containing the bone and the two defect sites was removed (Figure 4.2-1). This was then cut it half to separate the control Bio-Gide® defect site and the 4VBC defect site which were stored in 10% NBF for 24 hours before histological assessment.

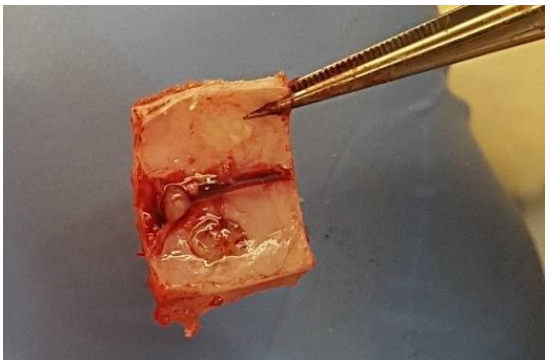

Figure 4.2-1 Cranial section with two defect sites. Bio-Gide® defect site at the top, 4VBC defect site at the bottom

4.2.3.3 MicroCT

Bone samples were scanned for structural analysis by SkyScan-1072 high-resolution desk-top micro-CT system (source voltage, 60 kV, source current, 135 mA; exposure, 2702 ms, rotation step, 0.750 deg, frame averaging, 3, image pixel size 26.9 µm) (n=3). The scans were oriented so that the bone was upright and analysed with ImageJ software. Import – image sequence. Stacks – Reslice. Spacing 26.9 µm. Crop circle 4 mm in diameter. Edit – clear outside. Measure area. This area had to be multiplied by the spacing (26.9 µm) to find the bone volume of one stack. This method of analysis using Image J was chosen because it was the most repeatable (n=3).

4.2.3.4 Plastic-embedding

Specimens were infiltrated with Osteo-Bed Resin with 2 changes over 12 hours. The infiltrated specimen was placed in an air-tight container and allowed to sit overnight at room temperature under a fume hood prior to raising the temperature for polymerisation to allow for a secondary infiltration of the embedding solution. Polymerisation for 24 hours at a temperature between 31.5–34.5 °C. The Osteobed kit proved to be very problematic due to its sensitivity to oxygen, the need to be in a fume hood and to be kept at a temperature between 31.5–34.5 °C for the polymerisation reaction (the lab had no nitrogen inlet). This had to be attempted many times before the samples were sufficiently embedded and even when this was achieved, the resin appeared grainy (Figure 4.3-32 B).

4.2.3.5 De-mineralisation

X-ray images of the bone samples were taken using a Omnicure 51500 Dental X-ray machine and analysed using corestream CS7600 prior to demineralisation. The bone samples were then placed in formic acid (10%) and stirred gently for 4 days. Images were re-taken to ensure complete de-mineralisation (n=3).

This demineralised bone was then cut in half (Figure 4.2-2) before it was dehydrated, fixed and mounted onto slides and stained for H&E, Goldner's Trichrome and Sanderson's rapid bone stain.

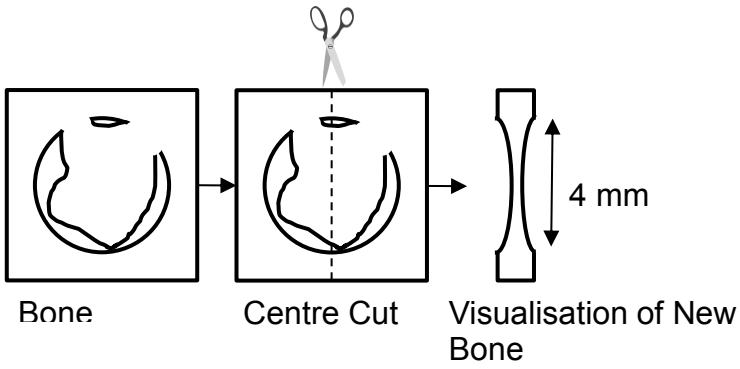

Figure 4.2-2 Demineralised bone sample was cut in half prior to dehydration and placed on side when embedding to allow visualisation of the new bone formed in the defect.

4.2.3.6 Histology

Specimens were fixed in 10% NBF for at least 24 hours before samples were dehydrated, paraffin embedded, sectioned using a microtome (4 µm) and

mounted onto glass slides. The specimens were deparaffinised with xylene (10 minutes), followed by exposure to a series of gradient ethanol solutions (100%–70%) (5 minutes in each). Bone sections (n=3) were embedded with Osteo-bed resin and cut with an accutom (100 μm) embedded bone samples which were de-plasticised overnight using Osteo-Bed Bone Embedding Solvent at 37–45 °C.

4.2.3.6.1 Von Kossa Stain

This technique was used to demonstrate deposits of calcium or calcium salt so it is not specific for the calcium ion itself. Calcium salts appeared black or brown-black, nuclei appeared red and cytoplasm appeared pink.

Samples were brought to water and incubated in 1% silver nitrate solution under UV light (up to 60 minutes) then rinsed in several changes of distilled water. Incubated in 5% sodium thiosulfate (5 minutes) followed by thorough rinsing in distilled water. These were then counterstained with nuclear fast red (5 minutes) and rinsed in distilled water. Dehydrated to xylene and mounted with Permount mounting medium.

4.2.3.6.2 Hematoxylin and Eosin (H&E) Stain

This technique was used to demonstrate full cellular detail. Muscle appeared deep pink, acidophilic cytoplasm appeared red, basophilic cytoplasm appeared purple and nuclei appeared purple/ blue.

Samples were brought to water and incubated in hematoxylin (3 minutes) followed by rinsing in a water bath. These were incubated in Scot’s tap water (30 seconds) before being stained with eosin (3 minutes). Samples were washed thoroughly in a water bath before being dehydrated to xylene and mounted with Permount mounting medium.

4.2.3.6.3 Goldner’s Masson Trichrome

This technique was used to demonstrate new bone and osteoid formation. Cytoplasm appeared brick red, connective tissue appeared green and nuclei appeared dark brown to black.

Samples were brought to water and then incubated in Weigert’s hematoxylin solution (10 miinutes). These were then washed thoroughly in a water bath and rinsed with distilled water. Stained with fuchsin solution (Biebrich scarlet-acid) (15 minutes), followed by thorough rinsing with distilled water before being submerged in Phosphotungstic acid (10 minutes) until the red colour from

collagen disappears. Incubated with hematoxylin green (1 minute), quickly rinsed, dehydrated to xylene and mounted with Permount mounting medium.

4.2.3.6.4 Sanderson's Rapid Bone Stain

This technique was used to demonstrate new bone formation. Osteiod appeared blue, nuclei appeared blue, soft tissues appeared blue and mineralised bone appeared pink.

Samples were brought to water and the Sanderson's rapid bone stain solution was heated to 50-60 ^{o}C. The samples were incubated in the stain (2 minutes) before excess was wiped off and samples were counterstained in fuchshin solution (10 seconds). Samples were dehydrated to xylene and mounted with Permount mounting medium.

4.2.3.6.5 Weigert Van Gieson's Stain

This technique was used to demonstrate muscle. Collagen appeared bright red, muscle appeared yellow/ orange and nuclei appeared dark blue.

Samples were brought to water and incubated in Weigerts solution (25 minutes) followed by rinsing in distilled water. Samples were then submerged in acetic acid (10%) and then rinsed in water. Samples were then stained with a solution of Weigert's hematoxylin – solution A and Weigert's hematoxylin -solution B (50:50) (10 minutes) followed by thorough rinsing in water. Samples were then stained with Van Gieson's picrofuchsin solution (5 minutes) before being quickly rinsed in water (2 s) and excess stain dabbed away. Samples were dehydrated to xylene and mounted.

4.2.3.7 Immunohistochemistry

CD68 recognises the rat ED1 antigen which is expressed on most macrophages populations. Slides were brought to water and blocking solution was prepared. This was made of goat serum (0.5 mL), bovine serum albumin (BSA) (0.1 mL) and PBS (9.4 mL). Blocking solution (200 µL) was added to each slide and incubated for 30 minutes in a humidity chamber. The blocking solution remained on the negative control, the positive controls were coated in CD68 AF488 in PBS at different concentrations (1/5, 1/10, 1/25) (200 µL) and incubated overnight and counterstained with To-Pro-3.

4.2.4 Statistics

Data has been expressed as mean ± standard error of the mean (SEM) unless n > 20, when it is expressed as mean ± standard deviation (SD). Statistical analysis was performed using MiniTab software. Levene's test was used to test for variance in data, t-test for comparison of two different groups, one-way ANOVA followed by post-hoc Tukey test on data when Levene's test showed $p \geq 0.05$ and equal variances could be assumed and a Welch's ANOVA followed by a post-hoc Games-Howell on data when Levene's test $p \leq 0.05$ and equal variances could not be assumed. Statistical significance was determined by $p \leq 0.05$.

4.3 Results and Discussion

Sample nomenclature used in this work is as follows: thiol-ene hydrogels are coded as "CollPEGX", where "Coll" and "PEG" refer to 2IT-functionalised collagen and 8-arm norbornene terminated PEG, respectively, and "X" identifies the PEG content (2-4.5% (w/v)) in the thiol-ene mixture. 4VBC hydrogels refer to collagen functionalised with 4-vinylbenzyl chloride (vinyl group).

4.3.1 Cell Attachment, Spreading, Proliferation and Maturation/ Differentiation on Hydrogels with Varied Elastic Moduli

4.3.1.1 C2C12 Cell Viability

To confirm the biocompatibility of the hydrogels, an extract and a direct cytotoxicity test was performed using C2C12 murine myoblast cells.

ATP assays are fast and sensitive means to measure cell viability and work on the basis that when cells lose membrane integrity and die, they no longer synthesise ATP [259]. To find the relationship between luminescence from an ATP assay and the number of cells, cells of known densities were seeded in a 96 cell-well plate and after attachment (3 hours), an ATPlite assay was performed. Based on this data, a standard curve was plotted with cell count against luminescence, thus quantifying the relationship between luminescence and number of cells (Figure 4.3-1).

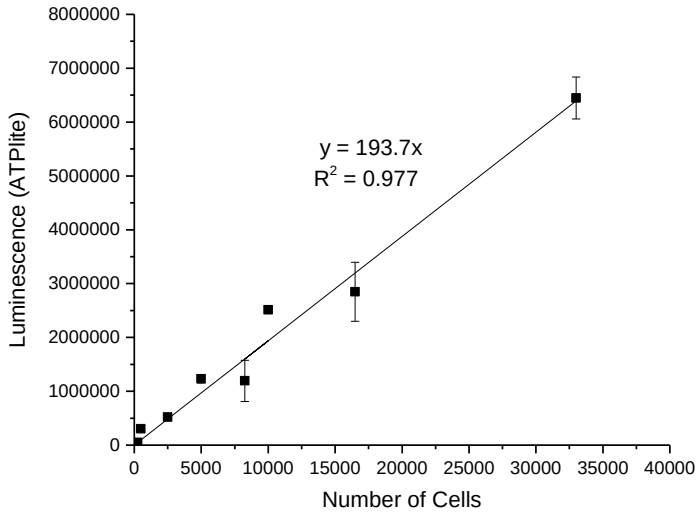

Figure 4.3-1 Relationship between luminescence reading from ATPlite assay kit and cell count (n=5).

An extract cytotoxicity test is suitable for detecting the toxicity of soluble substances of medical devices and can be used to provide an initial first impression of the cytotoxicity which is said to be consistent with the results of animal toxicity tests [253].

The graph (Figure 4.3-2) shows that there was no significant difference between the number of cells grown from the extract of the hydrogels compared to the positive control (cell culture media) after two days and there were no cells present in the negative control. This was an important test to do with the hydrogels because even though the materials were all chosen based on their bioinert status, the photoinitiator used was still at a high enough concentration to cause cell death.

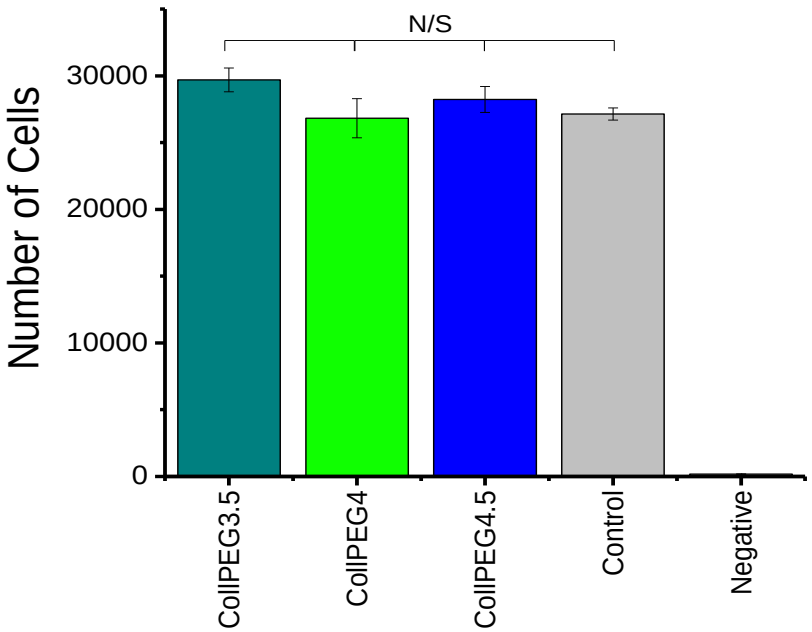

Figure 4.3-2 Extract cytotoxicity test. Data represented as means ± SEM (n=5). N/S: no significant difference

In comparison to the extract, the direct cytotoxicity test was used to examine the direct cytotoxicity of the hydrogels on cells *in vitro* which reflects the biological safety of the tested materials.

Figure 4.3-3 shows the results, whereby the number of cells on hydrogels, cells on hydrogels DMSO: DMEM (50:50) (negative control), hydrogels in media, cells alone (positive control), media alone and a blank were measured using an ATP assay. It was shown that the number of cells on the hydrogel at each time point was generally lower than the tissue culture plastic control. However, this is predicted to be due to initial cell attachment; tissue culture plastic has been specially plasma treated for increased cell attachment, so it has to be assumed that cells will preferentially bind do it.

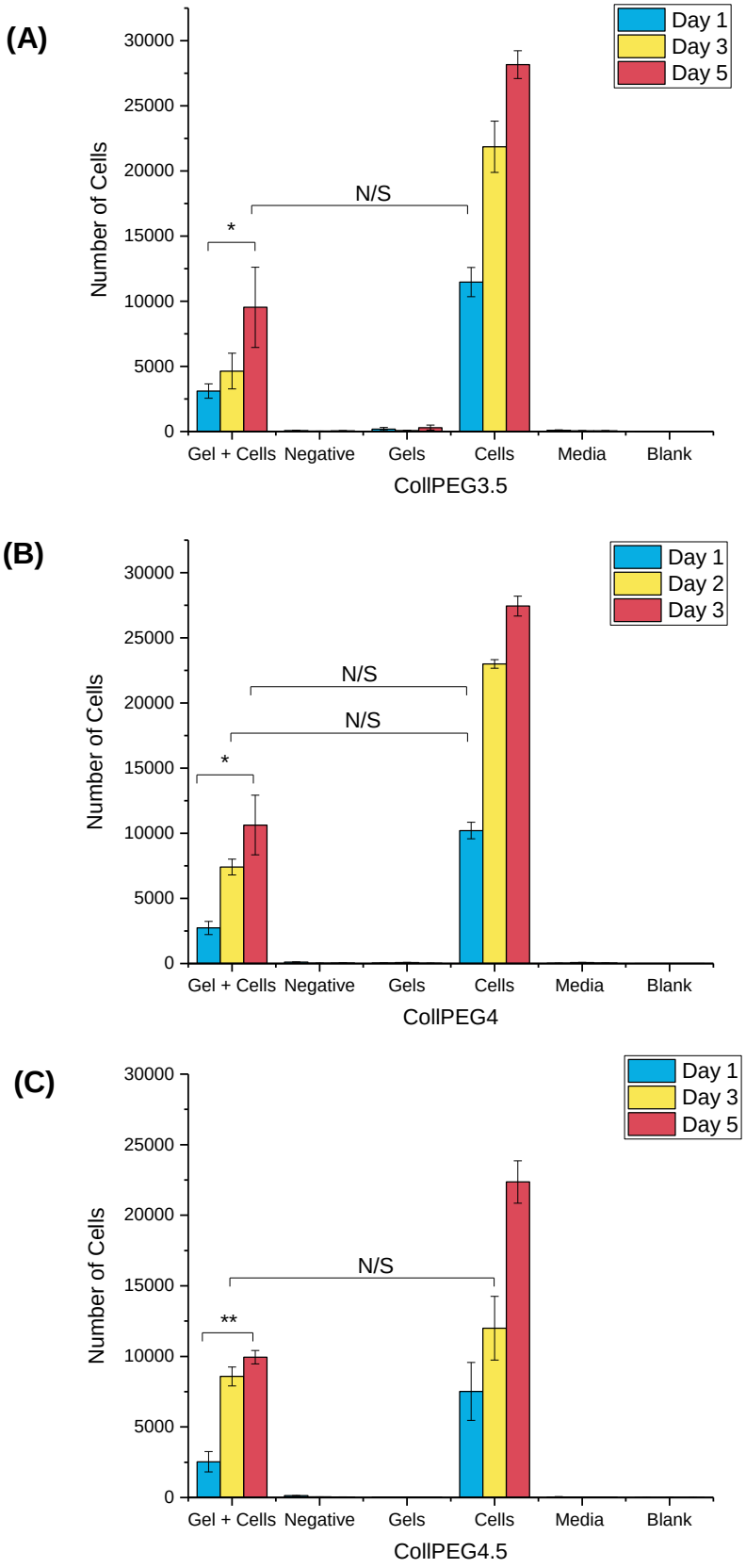

Figure 4.3-3 Direct cytotoxicity graphs for the three hydrogels. CollPEG3.5 (A), collPEG4 (B) and collPEG4.5 (C). Data represented as means ± SEM (n =5). *p<0.05, **p<0.01, N/S: no significance.

Figure 4.3-3 A shows that after 1, 3 and 5 days of culture, the number of cells on the CollPEG3.5 hydrogel was significantly lower than that of cells alone group (positive control) at the same time points ($p \leq 0.05$). There was no significant increase in the number of cells on the hydrogel between days 3 and day 1 ($p \geq 0.05$), although the trend showed an increased cell number at day 3. The total number of cells on the hydrogels had significantly increased after 5 days of culture compared to after 1 day of culture in the same group ($p \leq 0.05$). There were no cells detected in the media alone, blank, hydrogel alone, and the negative control group. These results were also reflected in Figure 4.3-3 B for the total number of cells on the CollPEG4 hydrogel.

Figure 4.3-3 C shows that the total number of cells on the collPEG4.5 hydrogels had significantly increased after 5 days of culture compared to after 1 day of culture ($p \leq 0.01$). There was again no significant increase between days 3 and day 1 although the trend showed an increased cell number at day 3 and there were no cells detected in the media alone, blank, hydrogel alone, and the negative control group.

A significantly higher number of cells on day 5 compared to day 1 has been reported for all three hydrogels. Hassan *at el* reported that comparable cellular activity on day 7 compared to day 1 is indicative of no cytotoxic effect of the material, so due to the significantly higher cellular activity on day 5 compared to day 1, we can confirm that there was no direct cytotoxic effect as a result of the materials [260]. The overall trend shows the cell number increasing from day 1 to day 3 and 5. This shows that the cells are proliferating on the hydrogels and if the materials were cytotoxic, we would expect a negative trend.

During this work, we aimed to compare all three hydrogels in order to evaluate their efficacy as a cell-laden hydrogel device for muscle tissue engineering and the dependency on substrate stiffness. A comparison of the cytotoxicity of the three hydrogels at 1, 3 and 5 days is shown below (Figure 4.3-4).

There was no significant difference between the number of viable cells on the three hydrogels at either of the three of the time points. There was however a significantly higher number of viable cells on the tissue culture plastic, however, as discussed this is due to the enhanced attachment of cells on tissue culture plastic due it its treatment.

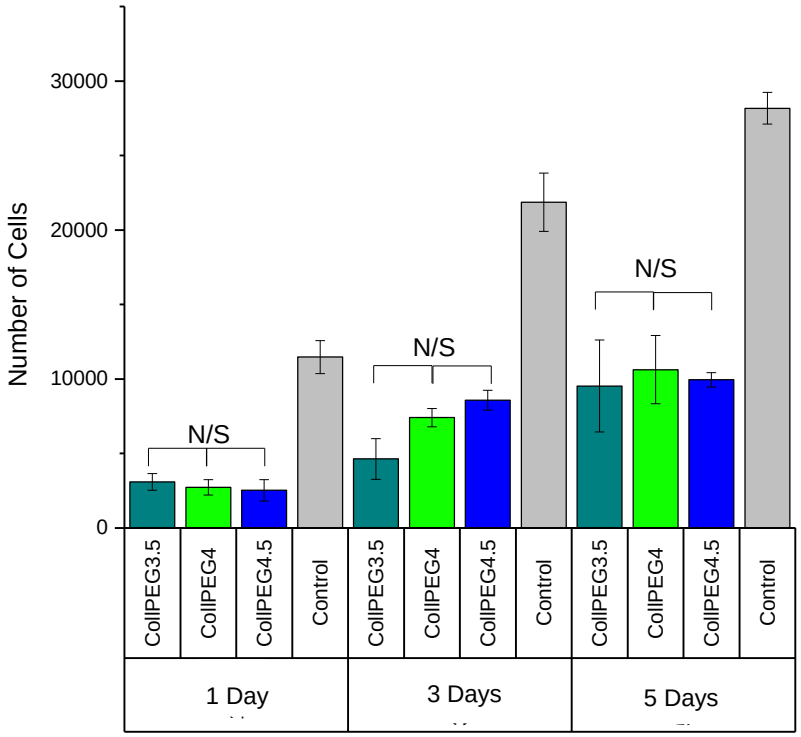

Figure 4.3-4 Direct cytotoxicity of the three hydrogels compared to tissue culture plastic control. Data represented as means ± SEM (n=5). N/S no significance.

4.3.1.2 Cell Seeding/ Spreading/ Proliferation

Cell adhesion, spreading and proliferation were initially studied as a prerequisite for cell maturation/ differentiation. Most cells are anchorage-dependent so it was desirable to examine whether the different stiffness' (7, 10 and 13 kPa) would be discernible to the cells and affect the cellular adhesion, spreading or proliferation.

Scaffolds should be designed in a way that facilitates cell attachment so part of the study was to examine whether incubation in a FCS rich media (DMEM supplemented with 50% FCS) for 24 hours would significantly impact the ability of the hydrogels to encourage adhesion and spreading of the cells. A serum-containing media should result in the formation of a surface layer ('coating') of adsorbed proteins. This subsequently mediates interactions with cells because among the deposited serum proteins contains the RGD amino acid sequence which is recognised by cell-surface integrin receptors [261]. Therefore, overnight incubation in FCS rich media prior to cell seeding could encourage cell adhesion on the three hydrogels. Although it was noted that the C2C12 cells were cultured in 10% supplemented FCS media, so when this media is seeded onto the

hydrogel, the protein coating may be sufficient to attach the same number of cells compared to hydrogels incubated overnight in 50% supplemented FCS media.

Figure 4.3-5 shows the number of cells attached the three hydrogels (FCS treated and non-treated) and the tissue culture plastic control, 3 hours after seeding represented as number of cells per mm^2. There was very little spreading after 3 hours and cells appeared rounded and the C2C12 cells were calculated to have a diameter of 21.1 ± 0.5 µm (n=10).

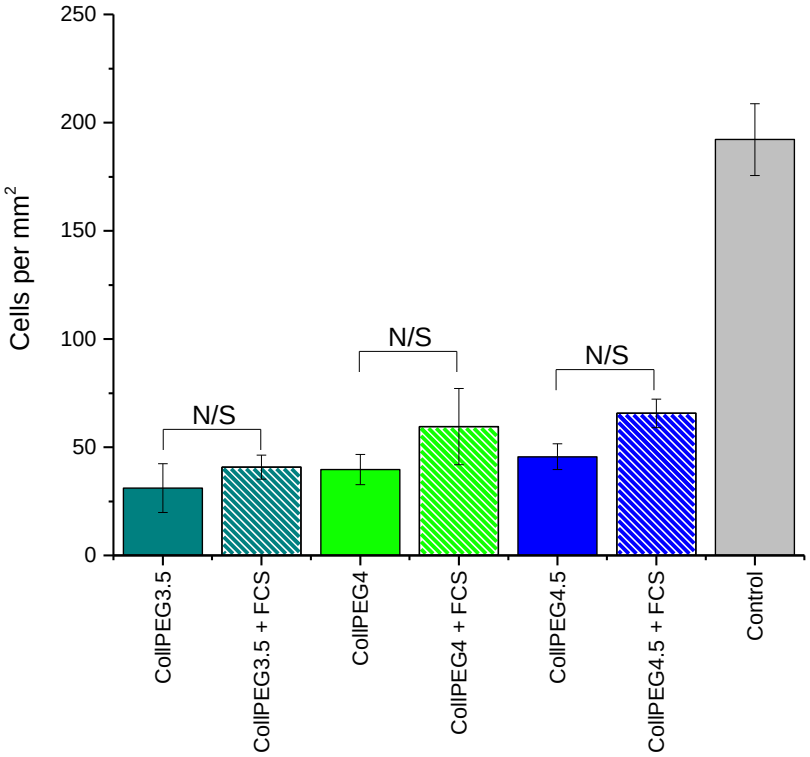

Figure 4.3-5 Cell attachment onto scaffolds after 3 hours. Data represented as means ± SEM (n= 3). N/S no significance.

There was no statistical difference in the number of cells attached onto hydrogels after 24 hours incubation in FCS rich media compared to the non-treated hydrogels ($p \geq 0.05$). However, statistical significance might have been observed with a higher n number because the overall trend showed a higher cell attachment on the FCS treated hydrogels. CollPEG3.5 31 vs 41 cells per mm^2, collPEG4 40 vs 50 cells per mm^2 and collPEG4.5 46 vs 66 cells per mm^2 for untreated and FCS treated hydrogels respectively.

The tissue culture plastic control showed a statistically higher number of cells attached to it compared to all three of the hydrogels, FCS treated or non-treated. As mentioned, tissue culture plastic is plasma treated to improve cell attachment

by incorporating more oxygen onto the cell culture surface, rendering it more hydrophilic. The hydrogels have not been plasma treated so it is expected that tissue culture plastic outperforms the hydrogels. The cells which have not attached onto the hydrogels would have attached (preferentially) to the surrounding plastic. It was noted that tissue culture plastic has an elastic modulus of ~3 GPa, rendering it supraphysiological compared to soft tissues like muscle yet the cells attached preferentially to it [42].

To examine the influence of hydrogel stiffness on cell adhesion, a line graph was plotted (Figure 4.3-6). As stated, there was no statistical significant difference between the results, however there was a general increasing trend in the number of cells attached on the hydrogels collPEG3.5 → collPEG4.5 (7 → 13 kPa) and significance may have been observed with a higher sample size.

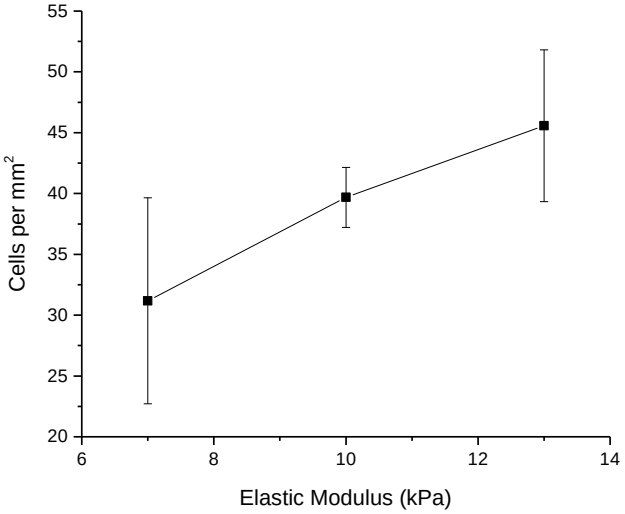

Figure 4.3-6 Line graph to show the trend between elastic modulus and cell attachment. Data represented as means ± SEM (n=3).

After 24 hours, most of the cells no longer appeared rounded, indicative that they had started to spread and the surface area was measured using image J.

Figure 4.3-7 shows the effect of different substrates on the surface area of C2C12 cells after 24 hours. Unlike the cell seeding experiment where the tissue culture plastic outperformed the three hydrogels, the results showed that the choice of substrate had no significant effect on C2C12 cell spreading, although the highest mean cell spreading area was reported using tissue culture plastic. There was also no significant difference in cell spreading between the FCS treated and non-treated hydrogels similar to the cell adhesion experiment. For this reason, the hydrogels were no longer incubated in 50% FCS for 24 hours

prior to cell seeding. This is preferable because this representation would never be used in a clinical setting.

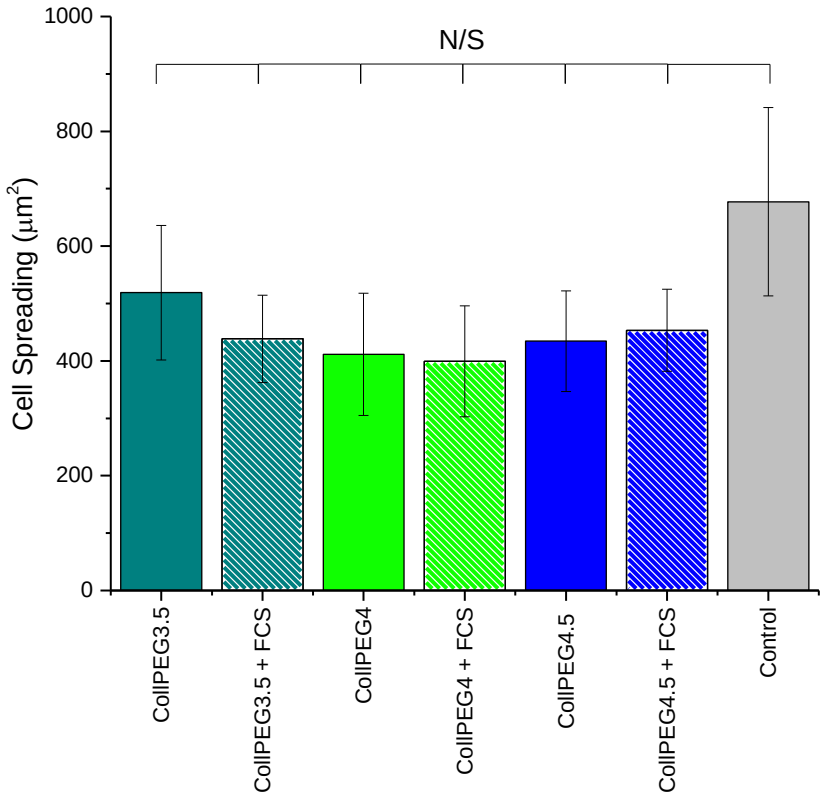

Figure 4.3-7 Cell spreading after 24 hours. Data represented as means ± SEM (n=3). N/S no significance.

In order for cells to sense substrate elasticity, they pull against the matrix, which will in turn cause cellular mechanical transduction signals based on the force required to deform the matrix. Changes in substrate rigidity have been shown to effect cell spreading and fibroblasts have been shown to exhibit an increased spreading on stiffer substrates [262]. However, the results from this work showed that C2C12 cells were not influenced by substrate rigidity and there was no significant difference in the cell area after 24 hours between the three hydrogels or the control, although the highest mean cell spreading was recorded with the tissue culture plastic control, 677 ± 164 µm^2 despite its supraphysiological nature.

Engler *et al* reported that myoblasts (C2C12 cells) spread and elongate more on increasingly stiff substrates after just 4 hours using hydrogels with stiffness 2, 3, 4 and 8 kPa and glass as the control [56]. However, by 24 hours, the results showed that the spreading on the stiffest hydrogels and glass were statistically

similar in terms of cell area, which indicates that with time, spreading became less dependent on substrate elasticity [56]. However, Engler *et al* did report that the highest mean cell area was on the supraphysiological glass control. Both these observations are reflective of the results from this work.

Cell proliferation on each of the materials was examined and the results showed no statistical significance between each of the three hydrogels or the control (Figure 4.3-8).

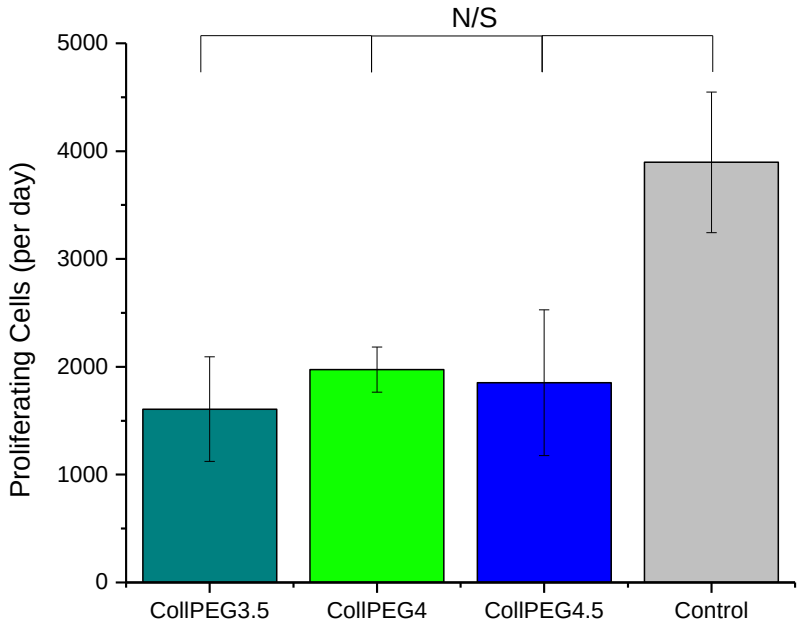

Figure 4.3-8 C2C12 proliferation. Data represented as means ± SEM (n=3).

However, the tissue culture plastic control showed a larger number of mean proliferating cells and it was predicted that statistical significance could have been achieved with a higher sample size despite its supraphysiological stiffness. This prediction was based on work by Skardal *et al*. The paper examined substrate elasticity on cell proliferation using surfaces of 2, 5, 15, and 50 kPa and tissue culture plastic as the control and found a significantly higher degree of cell proliferation on tissue culture plastic [263].

Tissue culture plastic has been shown to be preferential in terms of adhesion, spreading and proliferation for these experiments, however, it was noted that this is due to factors other than just the substrate stiffness (control plastic is supraphysiological at ~ 3 MPa), such as plasma treatment, chemical composition or surface topography which have been researched and evolved in culture plastic over decades [263]. The adhesion, spreading and proliferation of the cells on the

3D hydrogels should be more representative of *in vivo* conditions because traditional 2D culture using tissue culture plastic does not replicate *in vivo* elastic moduli.

4.3.1.3 C2C12 Maturation/ Differentiation

The three hydrogels were shown to support the growth of C2C12 cells, likely due to the hydrophilic materials they are prepared from: thiol-functionalised collagen and PEG (Figure 4.3-9).

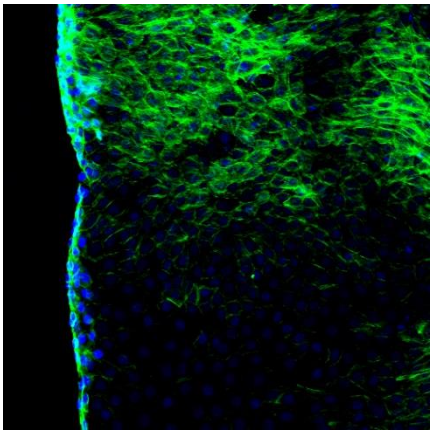

Figure 4.3-9 Confocal microscopy f-actin staining (green) and nuclear staining (blue) showing the edge of collPEG3.5 hydrogel at day 1.

Maturation/ differentiation of C2C12 cells is the process the myoblasts take from a proliferating state to fusing to form myotubes. This was induced by switching to a low serum media to starve the cells. The myoblast maturation/ differentiation at 90% confluency (d0) proved to produce myotubes at too high occurrence to accurately determine the fusion index and myotube formation. Figure 4.3-10 shows cells after 3 and 7 days. The actin filaments appear to have been remodelled to form the myotubes by day 3, with no clear comparison between day 3 myotubes and day 7 at this high confluency.

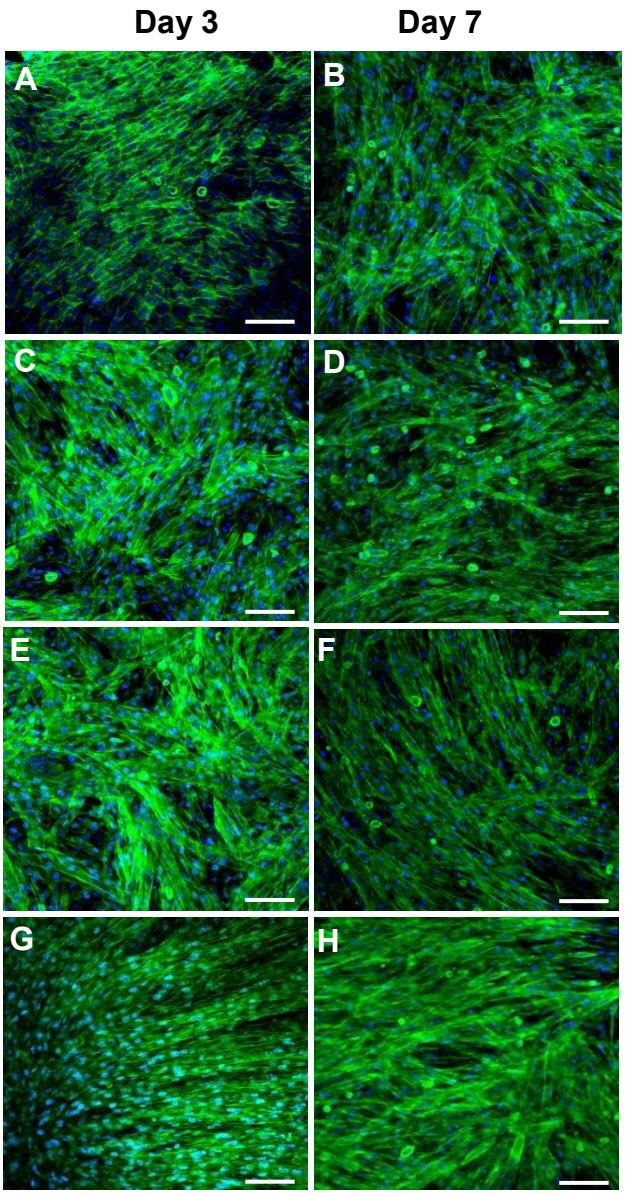

Figure 4.3-10 Immunofluorescent images showed C2C12 maturation and myogenic differentiation on hydrogels. F-actin (green) nuclear counterstain (blue). Imaged at d3 and d7 after differentiation when d0 = 90% confluency. CollPEG3.5 (A) and (B), collPEG4 (C) and (D), collPEG4.5 (E) and (F) and control (G) and (H). Scale bars represent 100 µm.

Ricotti *et al* used C2C12 cells grown to 90% confluency on a polyelectrolyte film and tissue culture plastic (control) with day 3 and 7 time points and f-actin staining (Oregon 488 phalloidin) similar to this work [255]. The images from the tissue culture plastic control at day 3 and 7 are shown (taken from the paper by Ricotti *et al*) (Figure 4.3-11).

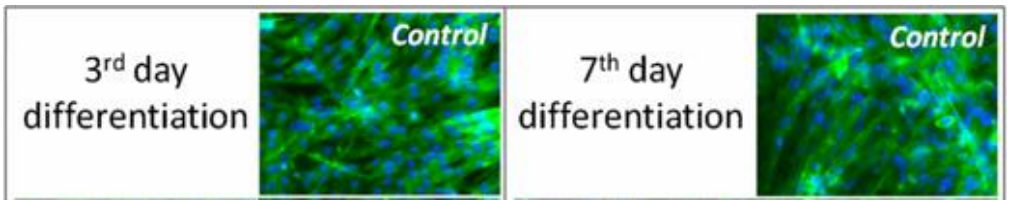

Figure 4.3-11 Nuclei and F-actin staining of C2C12 cells after 3 and 7 days of differentiation. Taken from Ricotti *et al* Figure 3 [255].

The fusion index was determined by dividing the total number of nuclei in myotubes (≥ 2 nuclei) by the total number of counted nuclei. For this work, Ricotti *et al* reported a fusion index of 0.2 at day 3 and 0.27 at day 7 with no statistical significance between each time point. Despite the high confluency, it is apparent that more than 20% of the cells are in myotubes (≥ 2 nuclei) on day 3 (Figure 4.3-11). The experiment was performed in triplicate with the error of the 0.2 fusion index reported as ~ 0.05. The small error means that despite the image at day 3, the fusion index was never reported near 1.0 and implies a level of bias in the way the total number of nuclei in myotubes was calculated and whether the high confluency (~90%) made it too difficult to be accurate and to produce reproducible graphs.

A paper by Velica *et al*, describes an un-biased means to quantify C2C12 myogenic differentiation. In this paper, it was stated that growth media should be swapped for differentiation media at d0 when cells are 70% confluent. This then provides a sharp increase in fusion index and myotube density after 3 days in differentiation media [264]. The paper was designed to prevent bias, so for the sake of reproducibility, the experiments in this work took 70% confluency as d0 (Figure 4.3-12).

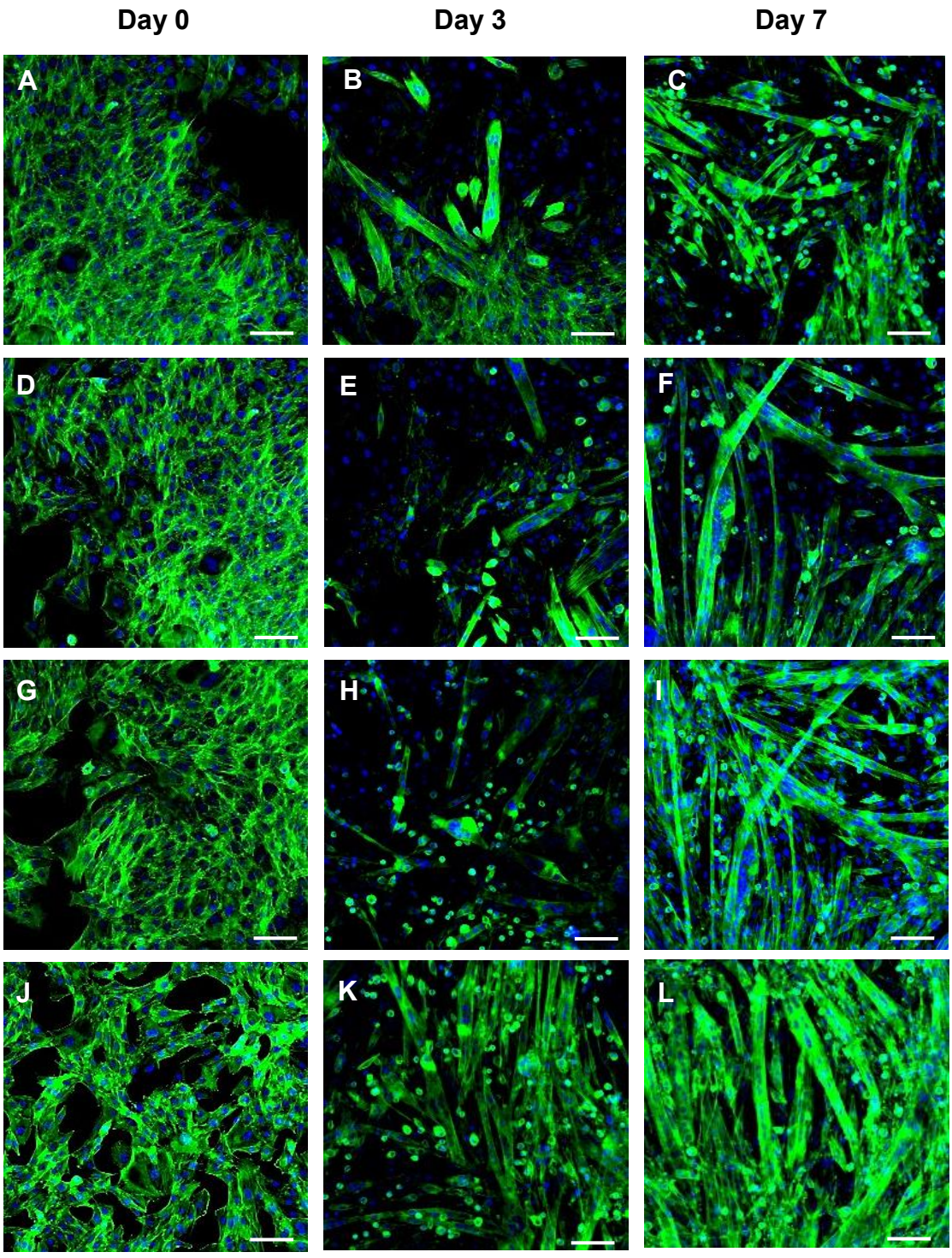

Figure 4.3-12 Immunofluorescent images showed C2C12 maturation and myogenic differentiation. F-actin (green) and nuclear counterstain stain (blue). Images taken at day 0, 3 and 7 of differentiation. CollPEG3.5 (A), (B) and (C), collPEG4 (D), (E) and (F), collPEG4.5 (G), (H) and (I) and control (J), (K) and (L). Scale bars represent 100 µm.

The first phase of myogenic maturation/ differentiation is characterised by actin filament remodelling. This change in the cell morphology can be visualised in the images from day 0 compared to day 3 and 7 as the nuclei begin to fuse together (Figure 4.3-12 A, B, C). It was noted that the myoblast cells appeared more 'clumpy' on the hydrogels at day 0 compared to the tissue culture plastic control likely due to the surface topography. However, once the cells began to fuse together this observation was no longer true and myotube formation was observed from day 3 in a random alignment.

Fusion index was calculated (Figure 4.3-13), however, no statistical significance was observed between the fusion index of the three hydrogels or the tissue culture plastic control at day 3 or 7 of maturation/ differentiation.

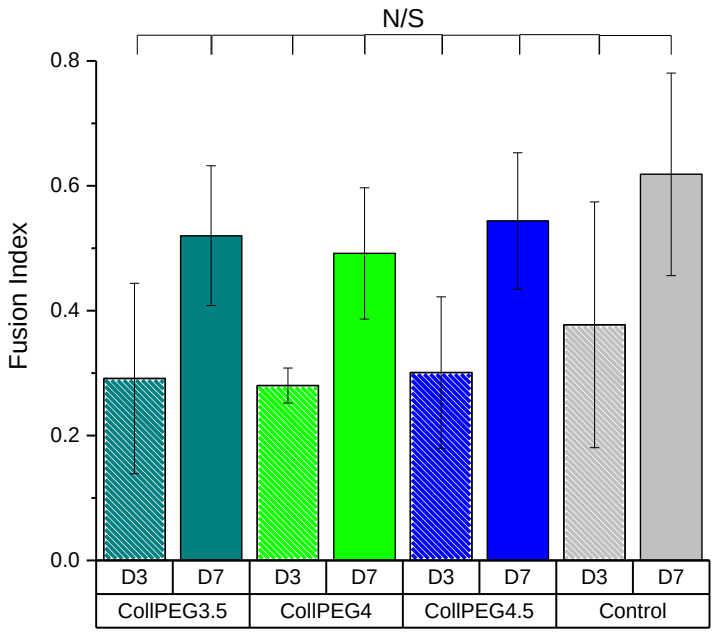

Figure 4.3-13 Fusion index as a measure of the number of fused nuclei in myotubes (≤ 2) to total number of nuclei. Data represented as means ± SEM (n=3). N/S, no statistical significance.

,

The control displayed the higher mean fusion index at day 3 and day 7, 0.38 and 0.62 respectively, it is possible that with a higher sample number, the control could promote a statistically high degree of myotube formation than the three hydrogels.

Ding *et al* used an experimental group of satellite cells (SCs) cultured on an elastic chitosan/beta-glycerophosphate/ collagen hydrogel (12 kPa) and a control group of SCs cultured on standard tissue culture polystyrene plates to investigate the influence of a substrate with elastic modulus similar to murine muscle tissue [239]. Similar to this work, d0 was determined at 70% confluency

and differentiation was analysed at day 5 with a fusion index of 0.89 for the hydrogel and 0.60 for the tissue culture plastic control. At day 7 in this work, a fusion index of 0.62 was reported for the control which is comparable to the work by Ding *et al*, but the hydrogel with similar stiffness, CollPEG4.5 (13 kPa) had a lower fusion index (although not statistically lower) of 0.54 at day 7 [239]. The importance of matrix elasticity in the efficiency of myogenic differentiation is stated in the literature, and although not reflected in this work, it is reported in the work by Ding *et al*. The different results could be due to the different cell type used, Ding *et al* used SCs whereas in this work C2C12 cells were used.

Figure 4.3-14 shows a comparison of the size of the myotubes from the f-actin images. Myotube (%) was calculated in terms of small (2-4 nuclei) or large (≥ 5 nuclei) myotubes with 30-100 myotubes analysed for each sample.

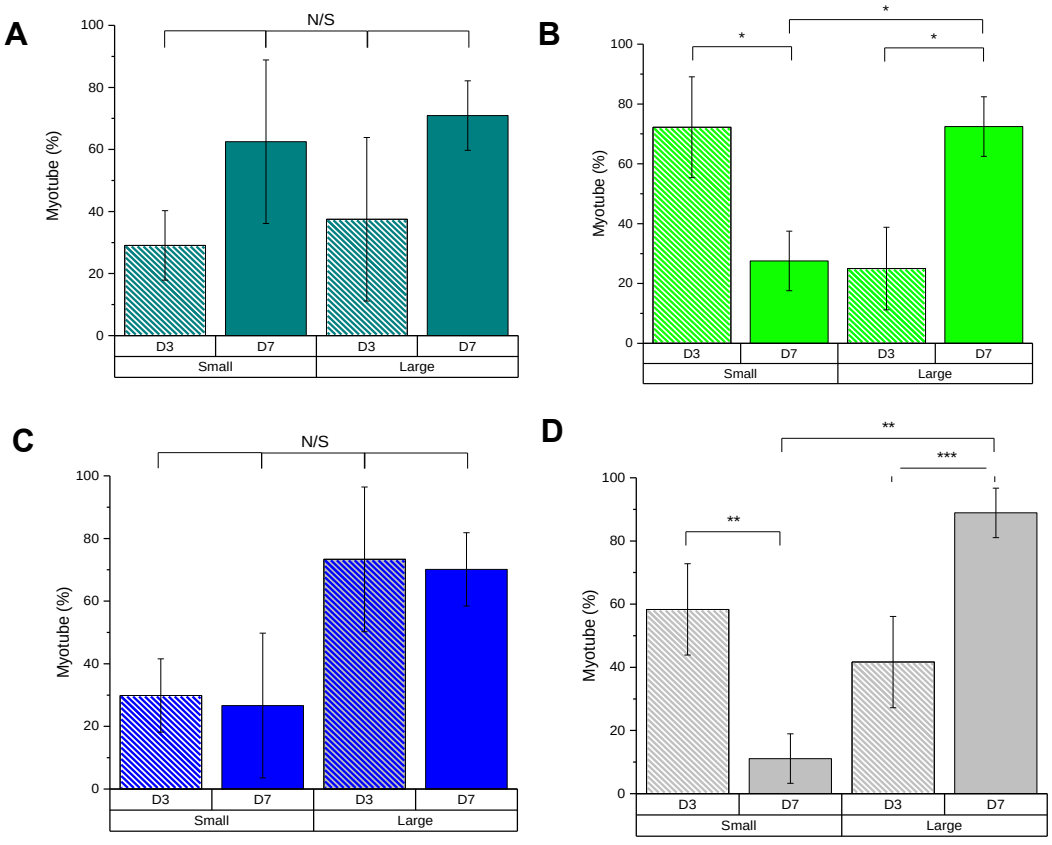

Figure 4.3-14 The effect of different hydrogels on C2C12 myotube formation at day (D) 3 and 7. Small myotubes, 2-4 nuclei and large myotubes, ≥ 5 nuclei. CollPEG3.5 (A), collPEG (B), collPEG4.5 (C) and control (D). Data represented myotube ratio (%) as means ± SEM (n= 3). *p ≤ 0.05, **p ≤ 0.01, ***P ≤ 0.005 and N/S, no significant difference.

A statistical significance is shown between the number of large myotubes (%) on day 7 compared to day 3 for collPEG4 (72.4 ± 10.0% to 22.2 ± 12.0% respectively) and the control (88.9 ± 7.9% to 41.7 ± 14.4% respectively). At day 7, these samples were also shown to have significantly higher percentage of myotubes with five or more nuclei (large myotubes) compared to smaller myotubes ($p \leq 0.05$). To provide a direct comparison of the three hydrogels with varied stiffness' and the tissue plastic control, the data for the large myotubes (%) on day 7 was compared. However no sample was shown to have a significantly higher number of large myotubes on day 7, again implying that the increased substrate stiffness of the hydrogel had no effect of myotube formation.

In comparison, the same representation of myotube (%) was performed by Ding *et al*, which reported a significantly higher difference in the percentage of large myotubes for the hydrogel (12 kPa) compared to the tissue culture plastic control group at day 5 of differentiation, 79.6 ± 4.9% to 49.4 ± 5.7% respectively [239]. Whereas in this work, when the hydrogel of similar stiffness, collPEG4.5 (13 kPa) was compared to the tissue culture plastic control group at day 7, there was no statistical significance in the percentage of large myotubes, 70.1 ± 11.7 to 88.9 ± 7.9% respectively.

The work by Ding *et al* used cells cultured on the hydrogel substrate rather than encapsulated, similar to this work, however, their hydrogel outperformed the tissue culture plastic control despite similar stiffness' ~ 7, 10 and 13 kPa compared to 12 kPa [239]. It is noted that a necessary condition for the different cellular reactions in response to matrices with different stiffness is that the cells feel the matrix stiffness, and on the cellular scale, the cells probe elasticity as they anchor and pull on their surroundings [239]. This could be easier for the cells to do on an alginate gel (Ding *et al*) rather than a collagen-PEG hybrid hydrogel. Additionally, it was also noted that the experiment by Ding *et al* used SCs rather than C2C12 cells which could account for the tissue-appropriate hydrogel statistically outperforming the tissue culture plastic for their work.

The MF20 monoclonal antibody recognises the heavy chain of myosin. This can be used as a late stage marker for myogenic differentiation, so whereas f-actin (phalloidin) staining was chosen to analyse cell morphology, MF-20 Alexa Fluor 488 was chosen to examine the phenotype [265].

Figure 4.3-15 shows the myosin expression after 3 and 7 days of maturation/ differentiation as thick green filaments.

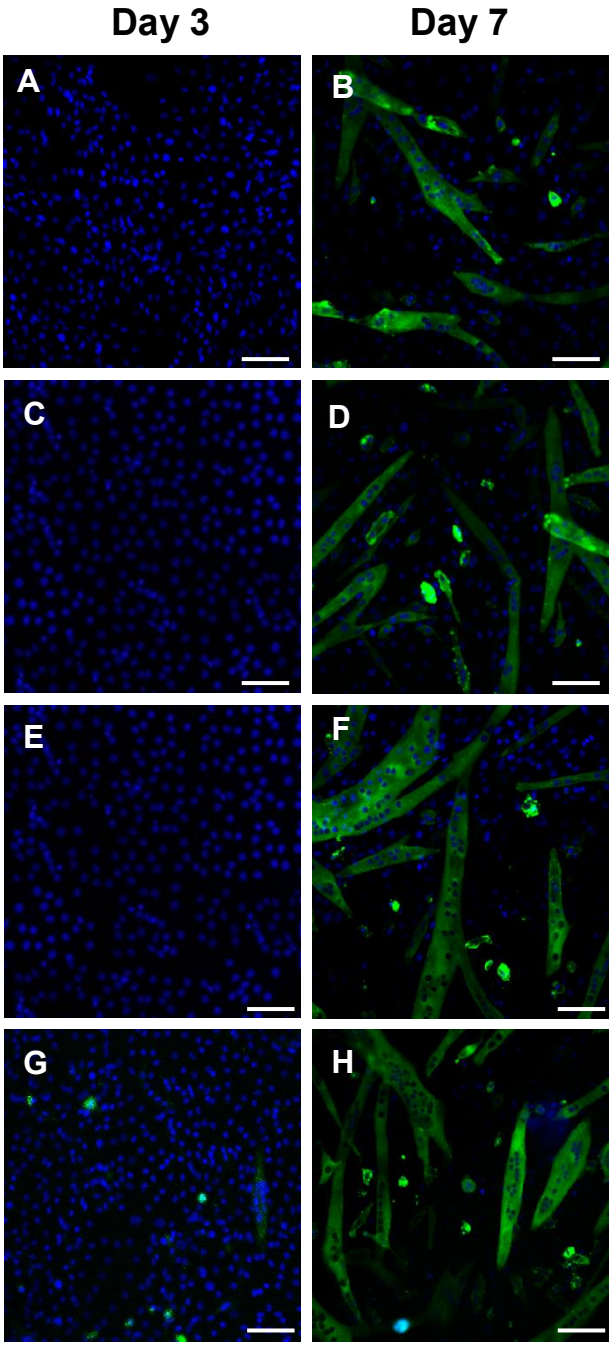

Figure 4.3-15 Myosin heavy chain (green) nuclear counterstain (blue). Images taken at day 3 and 7 of differentiation. CollPEG3.5 (A) and (B), collPEG4 (C) and (D), collPEG4.5 (E) and (F) and control (G) and (H). Scale bars represent 100 µm.

Interestingly, even though there were myotubes observed using f-actin staining on day 3, there was little/ no myosin expression on day 3 compared to day 7 for all three hydrogels and the control. This is because the first phase of myogenic

maturation/ differentiation is characterised by actin filament remodelling and myosin is used as a late stage marker.

Similar results were reported by Chen *et al* with negative staining of myosin (conjugated with AF 488) at day 2 and positive staining and the appearance of thick myosin filaments reported on day 6 of maturation/ differentiation [265]. Day 0 was also taken at 70% confluency similar to this work.

The maturation (%) was calculated for the three hydrogels and the tissue culture plastic control at day 3 and 7 (Figure 4.3-16).

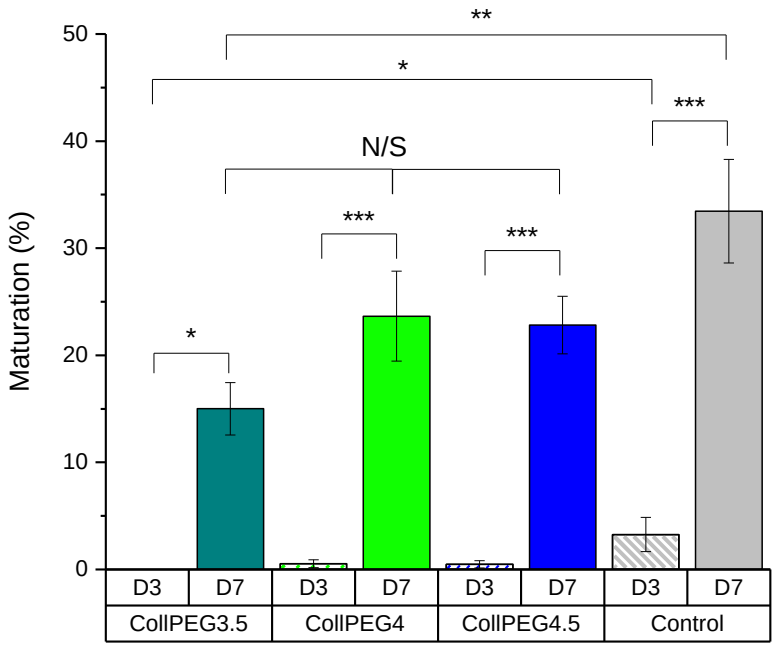

Figure 4.3-16 Myosin expression and maturation (%) at day 3 and 7. Data represented as means SEM (n= 3). *p ≤ 0.05, **p ≤ 0.01, ***P ≤ 0.005 and N/S, no significant difference.

At day 3, the control was shown to express significantly more myosin than collPEG3.5 ($p \leq 0.05$) and whilst collPEG4 and collPEG4.5 were shown to express more myosin than collPEG3.5, there was no statistical significance between the three hydrogels.

By day 7, all the groups had significantly promoted C2C12 cell maturation compared to the same substrate on day 3 ($p \leq 0.05$). The control group was shown to express significantly more myosin than collPEG3.5 ($p \leq 0.05$)

suggesting that it outperforms this hydrogel in terms of a substrate for C2C12 maturation at both time points.

Due to the three varied stiffness' of the hydrogels, it was expected that that the C2C12 cells would form myotubes preferentially on the stiffness closest to that of natural muscle, however, similar to day 3, there was no significant difference between the three hydrogels, although it was noted that collPEG3.5, the weakest hydrogel, expressed less myosin than the other two stiffer hydrogels.

The tissue culture plastic control showed a higher mean % of myosin expression and thereby a higher degree of maturation compared to the three hydrogels on both days of the study, which suggests that the hydrogels have comparatively inhibited the C2C12 maturation (Table 4.3-1).

Table 4.3-1 Percentage of myosin positive stained cells on different substrates. Data represented as means ± SEM (n= 3).

Sample ID	Myosin positive stained cells (%)	
	Day 3	Day 7
CollPEG3.5	0 ± 0	15.0 ± 2.4
CollPEG4	0.53 ± 0.38	23.6 ± 4.2
CollPEG4.5	0.47 ± 0.34	22.8 ± 2.7
Control	3.3 ± 1.9	33.4 ± 4.8

Romanazzo *et al* used f-actin (phalloidin) staining to analyse morphology and antibody staining with MF-20 Alexa Fluor 488 to examine the phenotype of C2C12 cells grown on PCL films and tissue culture plastic similar to this work. Tissue culture plastic control was shown to express myosin (%) 8 ± 2% at day 3 and 51 ± 5% at day 5 similar to the results reported in this work [266]. However, the difference was that Romanazzo *et a*l took d0 as 50% confluence to minimise the impact of cell-to-cell contact on the results.

Many papers report that confluency needs to be near 100% at d0 because the differentiation of skeletal muscle cells is stimulated by a contact-dependent process [267]. The fact that a critical step in skeletal muscle differentiation is cell fusion which requires cells to be confluent enough to contact each other cannot be overlooked. Cells do have to reach a critical confluence necessary for muscle differentiation, however, Romanazzo *et al* reported that the differentiation media

still allowed the cells to proliferate until they were confluent enough to contact each other and undergo cell fusion. In comparison, a paper by Liu *et al*, which used C2C12 cells and d0 ~ 100% confluency reported that 20% of nuclei were in myosin heavy chain positive cells at day 3 and 50% at day 7, so despite initial d0 confluency, the amount of cells expressing positive for myosin heavy chain was similar to the final time point reported by Romanazzo *et al* [266].

Myogenic differentiation was found to occur earlier on tissue culture plastic compared to collPEG3.5 due to a significantly higher amount of myosin expression on day 3. If the maturation/ differentiation of muscle cells is stimulated by a contact-dependent process to a higher extent than from the cells experiencing their environment (similar elastic modulus to the natural tissue), then one way to explain the results would be due to cell proliferation on the different substrates. Tissue culture plastic showed a higher mean cell proliferation than collPEG3.5 which displayed the lowest mean proliferation. Both substrates displayed initial confluency of 70%, however, the cells grown on the tissue culture plastic control might proliferate and reach the critical cell-to-cell-contact faster than the cells grown on collPEG3.5, thus leading to the earlier expression of myosin.

A paper by Yeung *et al* stated that the stiffness-dependence of fibroblasts was no longer evident when they became confluent, and that cell-cell contact may have a similar effect to elasticity when cells are grown at a high density [268]. This was reflected in the results from this work, despite the varied substrate stiffness', statistically similar fusion index and number of large myotubes (%) were reported between the three hydrogels and the tissue culture plastic with the similarity laying in the confluency of the cells and thereby the cell-cell interactions.

However, the work by Engler *et al* showed a very narrow elasticity preference for C2C12 cells cultured on hydrogels with varied stiffness'. Engler stated that after 2 and 4 weeks in culture, striated myotubes doubled in percentage on intermediate stiffness gels (8 kPa and 11 kPa) and gels with elastic moduli of 6.5 and 17 kPa showed a significant but lower percentage of striated cells [56]. However, it was noted that the time points of 2 and 4 weeks are far longer than any C2C12 differentiation protocol which recommends from 24 hours to 7 days, despite the paper stating that myotubes began to form after 2 days. Collinsworth *et al* reported the effect of myotube differentiation on the transverse mechanical properties of mammalian myocytes using atomic force microscopy. The apparent elastic modulus increased from 11.5 ± 1.3 kPa for undifferentiated myoblasts to

45.3 ± 4.0 kPa for myotubes after 8 days of differentiation [227]. With the cells remodelling the hydrogels, it is possible that after the formation of myotubes (45 kPa), the initial elasticity of the hydrogels would no longer be experienced by the cells at 2 and 4 weeks and shorter time points should have been used.

Unlike what was predicted, myogenic differentiation did not occur earlier on the softer hydrogels as a result of the cells sensing their surroundings and finding it more suitable for myoblast differentiation as described previously [56].

Out of the three hydrogels, collPEG3.5 was shown to be least preferential in terms of myosin expression and it was decided that the subcutaneous model would be performed using collPEG4 or collPEG4.5. Out of these, collPEG4.5 was chosen because it was the strongest hydrogel (~13 kPa) and therefore would be easier to handle in surgery.

4.3.2 Subcutaneous Implant Model

All materials when implanted into living tissue initiate a host response that reflects the first steps of tissue repair, including acute or chronic inflammation, foreign body reaction and fibrosis/fibrous capsule development. The performance of a device implanted in the body is dependent on its interaction with the host immune system. However, modern implant design can be directed to make use of this immune response to improve implant integration, whilst avoiding chronic inflammation [143, 269].

The photo-click hydrogels developed during this project are new materials and for this reason, it was important to analyse the host response to them, especially since their development was on a biocompatible basis.

The collPEG4.5 hydrogel was chosen to take forward with the subcutaneous model to analyse the local immune response. Geistlich Mucograft® was chosen as the control, this is already commercially available as a collagen matrix for soft tissue regeneration (muscle).

The pilot study for the subcutaneous model was performed to ensure the collPEG4.5 hydrogel was still present and did not degrade within 2 weeks *in vivo*. The time points for the real subcutaneous study would be adjusted accordingly. This was imperative to do especially with a new material in case it degraded too quickly and no results were gained from the animal model. After 14 days the samples were still present and the diameter of the scaffold was the same size prior to implantation (Figure 4.3-17).

Figure 4.3-17 Gross appearance of collPEG4.5 after 14 days of subcutaneous implantation *in vivo.*

The hydrogel could be identified by its dark purple colour using a H&E stain (Figure 4.3-18 A). It appears to have pulled away from this tissue, likely due to the dehydration and wax embedding process. Chronic inflammation and the foreign body reaction (FBR) occur within the first 2 weeks following implantation and there appeared to be no sign of foreign body giant cells. A Van Gieson stain was also performed on a sample of striated muscle taken from the rat (positive control). This allowed the elongated, parallel myofibrils to be visualised (B).

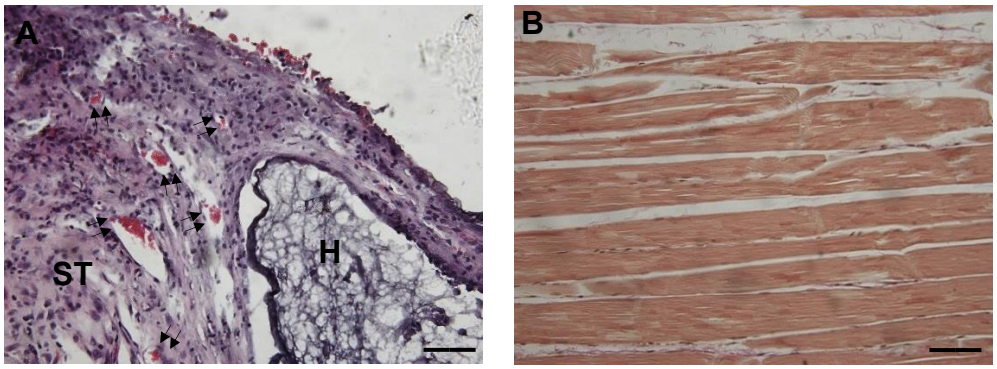

Figure 4.3-18 Histology stains of samples from a pilot study *in vivo* after 14 days of subcutaneous implantation of collPEG4.5 (A) H&E stain of collPEG4.5 (H) with attached surrounding tissue (ST), arrows indicate blood vessels. (B) Van Giesson stain of striated rat muscle sample shows the natural, parallel myofibrils. Scale bars 50 µm.

Innate immunity is the initial response and defence to an antigen by the host pathogens (hours) and does not require prior exposure to the material, whereas adaptive immunity is the later response (several days) as lymphocytes are activated to an antigen, differentiate and expand [17]. Innate immunity takes a matter of hours, whereas adaptive immune response takes at least 4 days. Similarly acute inflammation can develop in minutes and last for days, whereas chronic inflammation takes over this process if the tissue injury in prolonged. It

was decided that the time points to analyse the subcutaneous model would be 1, 4 and 7 days.

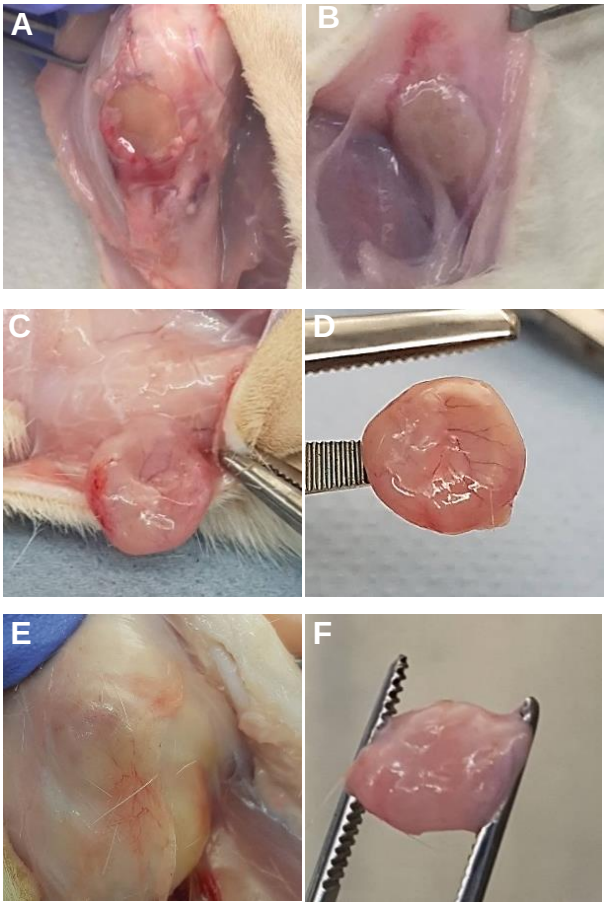

Figure 4.3-19 *In situ* images of implanted collPEG4.5 after 1 day (A) & (B), 4 days (C) & (D) and 7 days (E) & (F) of subcutaneous implantation.

Figure 4.3-19 shows the *in situ* pictures at 1, 4 and 7 days after implantation of collPEG4.5. Angiogenesis (formation of new blood vessels) was visible on some of the hydrogel sample (D). The hydrogel at day 1 was still translucent (as they were before the implantation), compared to day 4 and 7 which appeared a red/ pink colour synonymous with healing and integration. Although, the production of a provisional matrix around the scaffold has resulted in an inflamed appearance in the tissue surrounding the scaffold in response to the foreign material.

A commercially available product - Mucograft® was used as the positive control for this study. It is composed of two structures, the compact macro and the spongey micro structure. This immediately was more difficult to handle in surgery compared to the hydrogel, - because of this dual structure, the collagen matrix

almost wanted to slide apart from each other. In comparison, the fact that the hydrogel was stiff and had good shape memory (after sterilisation, the hydrogel would rehydrate back to its original volume and shape) made it easy to handle. Figure 4.3-20 shows the surgical pictures after 1,4 and 7 days after implantation of the Mucograft®.

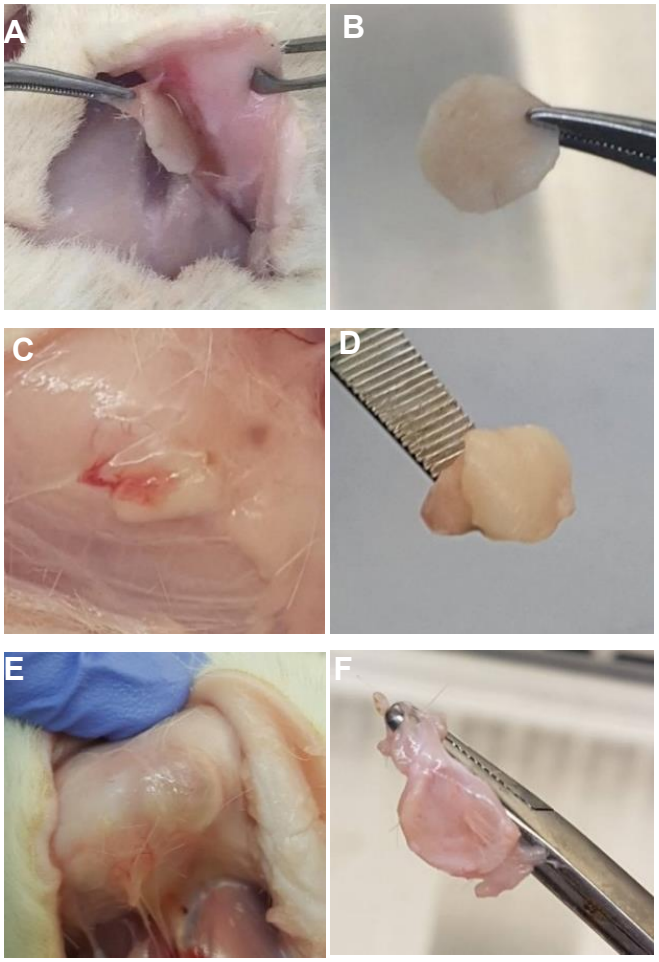

Figure 4.3-20 Images taken after surgery for the Mucograft® after 1 day (A) and (B), 4 days (C) and (D) and 7 days (E) and (F) after subcutaneous implantation.

In comparison to the collPEG4.5 hydrogel, there appeared to be far less integration with the tissue, the white coloured Mucograft® was clearly visible at day 4 and the white outline visible on day 7. This implied that there was poor tissue integration and poor vascularisation, but also had the advantage that it has not been covered by a fibrous capsule. Both materials retained their size and volume – although for the hydrogel sample, this could have been due to the

fibrous capsule and inflammation. There was no premature breakdown for either Mucograft® or collPEG4.5 and both presented with tissue integration by day 7.

During the sample retrieval, the samples had to be cut out from the subcutaneous tissue. However, due to the early initial time point of 1 day, the samples did not have enough time to integrate/ immune response had not caused fibrous capsule development. So rather than being cut out, the material would 'pop' out of the tissue instead. The number of samples of collPEG4.5 hydrogel or Mucograft® which 'popped' out was recorded and has been visualised as a graph (Figure 4.3-21). The production of a provisional matrix around the scaffold, as a result of the foreign material as well as a response to the surgical procedure, was a slow process with Mucograft® and even at day 4 all the samples 'popped' out thus indicating no tissue surrounding it, despite it being a foreign material. This was a sign of lack of cell ingrowth or good cell-material interface.

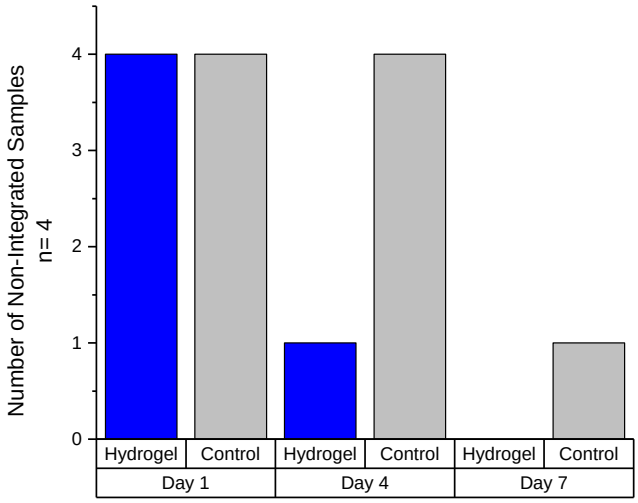

Figure 4.3-21 The number of samples of hydrogel or the Mucograft® control 'popped' out when dissected at different time points (n =4).

The first cells present during the innate immune response are the platelets and neutrophils which mediate the earliest phases of inflammatory reactions. Neutrophils are identifiable by their spherical shape (~15 μm) and multilobed nucleus (different from eosinophils which have a dual segmented nucleus) [17].

Figure 4.3-22 shows a clear differentiation of the Mucograft® and the collPEG4.5 hydrogel under H&E stain. The hydrogel appears dark purple and the Mucograft® appears light purple with a fibrous structure. The Mucograft® scaffold appears to have a layer of cells attached to the outside with no infiltration and unlike the cells attached to the outside of the hydrogel, they appear just as a hemotoxylin stained nucleus and appear to have no surrounding cytoplasm.

This instantly raised a question of cytotoxicity of the material and a H&E stain was performed on wax embedded sections taken from the tissue surrounding the Mucograft® (Figure 4.3-23).

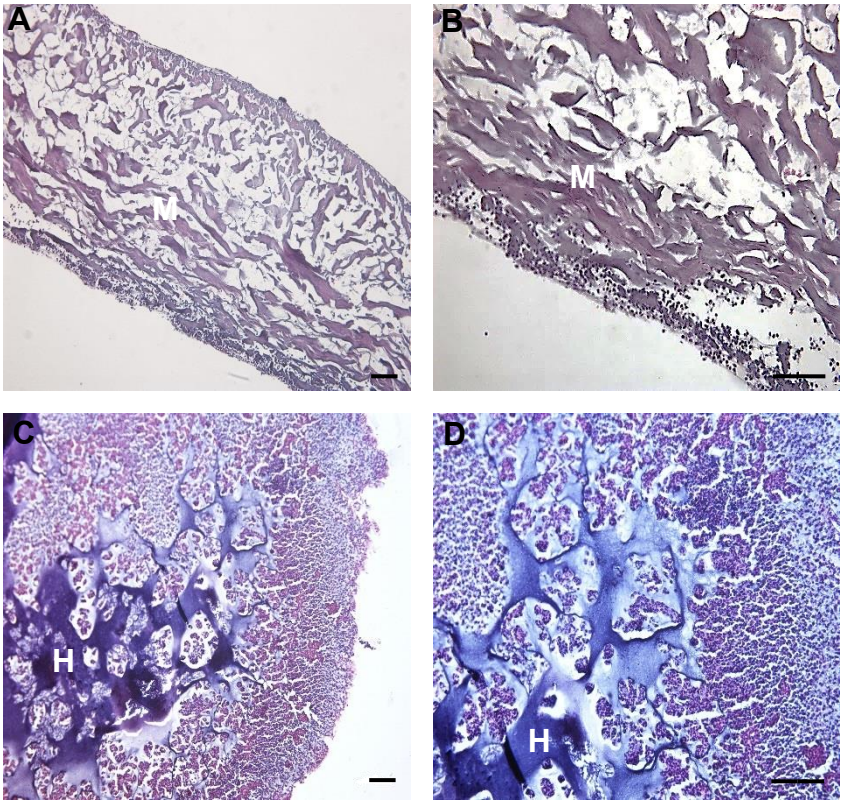

Figure 4.3-22 H&E stain of samples after 1 day of subcutaneous implantation. Mucograft® (A) & (B). CollPEG4.5 (C) & (D). Magnifications (A) & (C) 10x; (B) & (D) 20x. Hydrogel (H) and Mucograft® (M). Scale bars 50 µm.

From this image, nuclei of the same morphology as the ones surrounding the Mucograft® can be observed, however they have a supporting matrix. Alternatively, the cells could be in possession of a large nucleus with little surrounding cytoplasm similar to lymphocytes. However these cells are part of the adaptive immune response which take days to manifest. The rats would not have encountered the Mucograft®, or collPEG4.5 hydrogel antigen so the lymphocytes are said to be naïve.

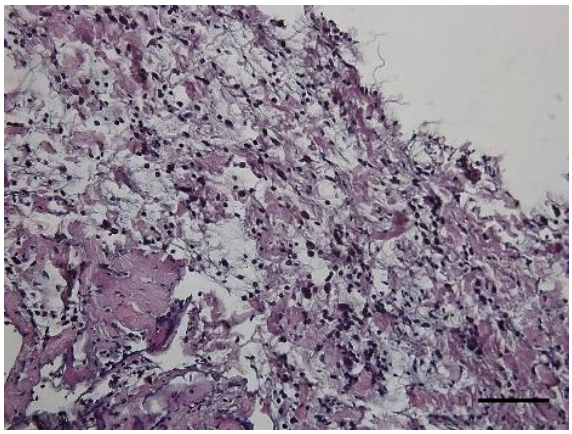

Figure 4.3-23 Tissue surrounding Mucograft® sample day 1. Scale bar 50 µm.

Although the collPEG4.5 hydrogel showed no visible signs of the polynuclear neutrophils or eosinophils, the surrounding protective matrix which has been secreted around the material is an early sign of the innate immune response - which is expected after any implantation of a foreign material.

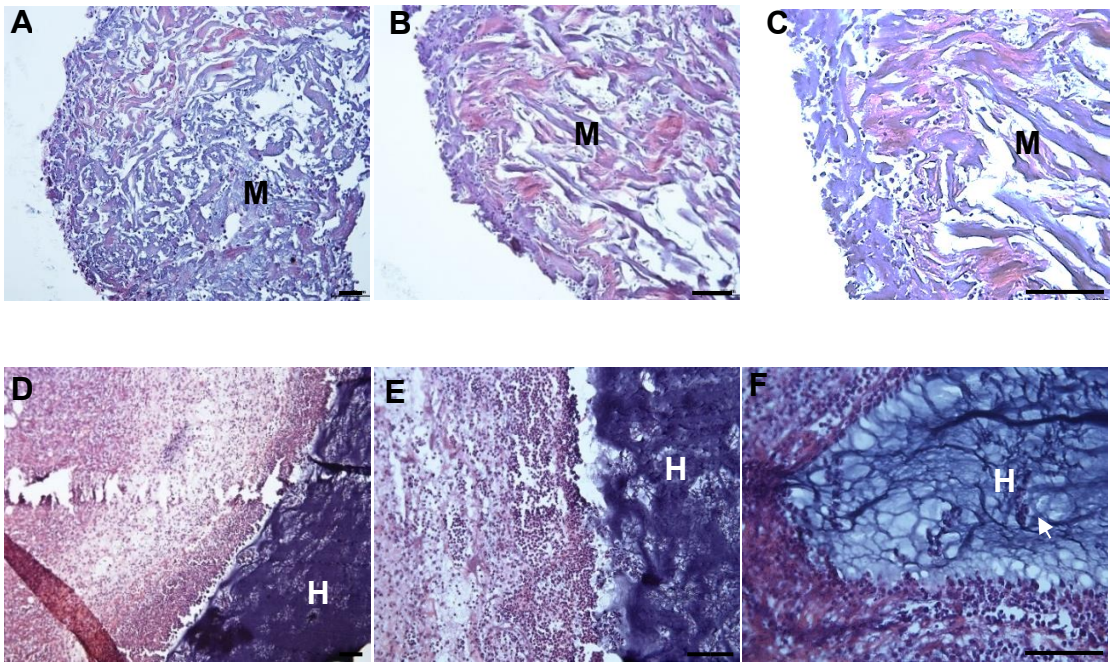

Figure 4.3-24 H&E stain of samples after 4 days of subcutaneous implantation. Mucograft® (A), (B) & (C). CollPEG4.5 (D), (E) & (F). Magnifications (A) & (D) 10x; (B) & (E) 20x; (C) & (F) 40x. Hydrogel (H) and Mucograft (M) and white arrow indicates macrophage debridement. Scale bars 50 µm.

Day 4 after implantation and the immune response for the hydrogel was apparent from the thick layer of surrounding cells (Figure 4.3-24). Cell infiltration and hydrogel debridement was also apparent from the presence of fried egg shaped macrophages (white arrow).

There was still no tissue attachment on the outside of the Mucograft® and whilst a small amount of cell infiltration was apparent, they appeared as rounded nuclei again rather than with a surrounding cytoplasm. Ghanaati *et al* evaluated the tissue response to this bilayer collagen material in CD-1 mice over 3, 10 15, 30 and 60 days [270]. At day 3 post implantation, which will be compared to the above day 4 results, they also reported that there was no evidence of capsule formation around the material. They also stated that tissue ingrowth was already observed, indicated by evidence of several infiltrating cells, although these cells appeared identical to the results above, just as nuclei [270].

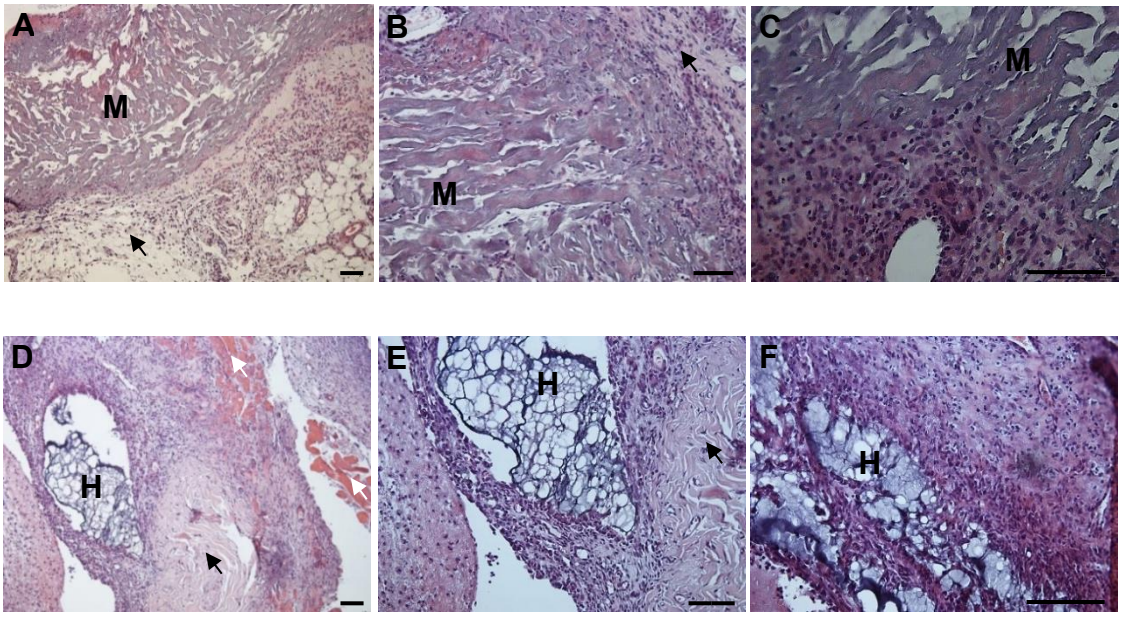

Figure 4.3-25 H&E stain of samples after 7 days of subcutaneous implantation. Mucograft® (A), (B) & (C). CollPEG4.5 (D), (E) & (F). Magnifications (A) & (D) 10x; (B) & (E) 20x; (C) & (F) 40x. Hydrogel (H), Mucograft® (M), black arrows indicate connective tissue and white arrows indicate muscle. Scale bars 50 µm.

Day 7 after implantation (Figure 4.3-25) and there was still a thick layer of cells surrounding the collPEG4.5 hydrogel, although less prominent than day 4 and cells also appear to have infiltrated through the material (C). Connective tissue can be observed from the spindle-shaped fibroblasts in addition to muscle formation near the collPEG4.5 hydrogel. Fibroblasts proliferate at the injury site

and remodel the local ECM to repair the wound. Whether this period results in tissue regeneration or scar formation is partially dependent on the duration of the chronic response that contributes to cytokine production and formation of granulation tissue [271].

Mucograft® has integrated with the surrounding tissue by day 7, with no dense surrounding population of cells indicative of the immune response. There are blood vessels near the base of the scaffold, although this could either be a regenerative response or an immune response to deliver more cells to fight the antigen. More cells have infiltrated into the scaffold, but again they appear just as nuclei with no surrounding stained cytoplasm. Ghanaati *et al* reported that at the 10 day time point, there was more tissue ingrowth with more cells reaching deeper within the scaffold compared to day 3 [270]. The health of the infiltrated cells was an issue in this work, however, Ghanaati *et al* showed that at 60 days the infiltrated cells were well integrated and a matrix had been secreted throughout the Mucograft® with the material completely invaded by cells and an appearance more like connective tissue [270]. These results subsided the issues about Mucograft®-induced cell cytotoxicity.

CD68 recognises the rat ED1 antigen which is expressed on most macrophage populations. The immunohistochemical stain to identify CD68+ was based on work by Keeler *et al* [272]. This antibody stain was attempted at 3 different concentrations. However, either this antibody did not work or the auto fluorescence from the collagen in the collPEG4.5 hydrogel or Mucograft® was too strong, so no information about immune response could be taken from the antibody-stained images (Figure 4.3-26).

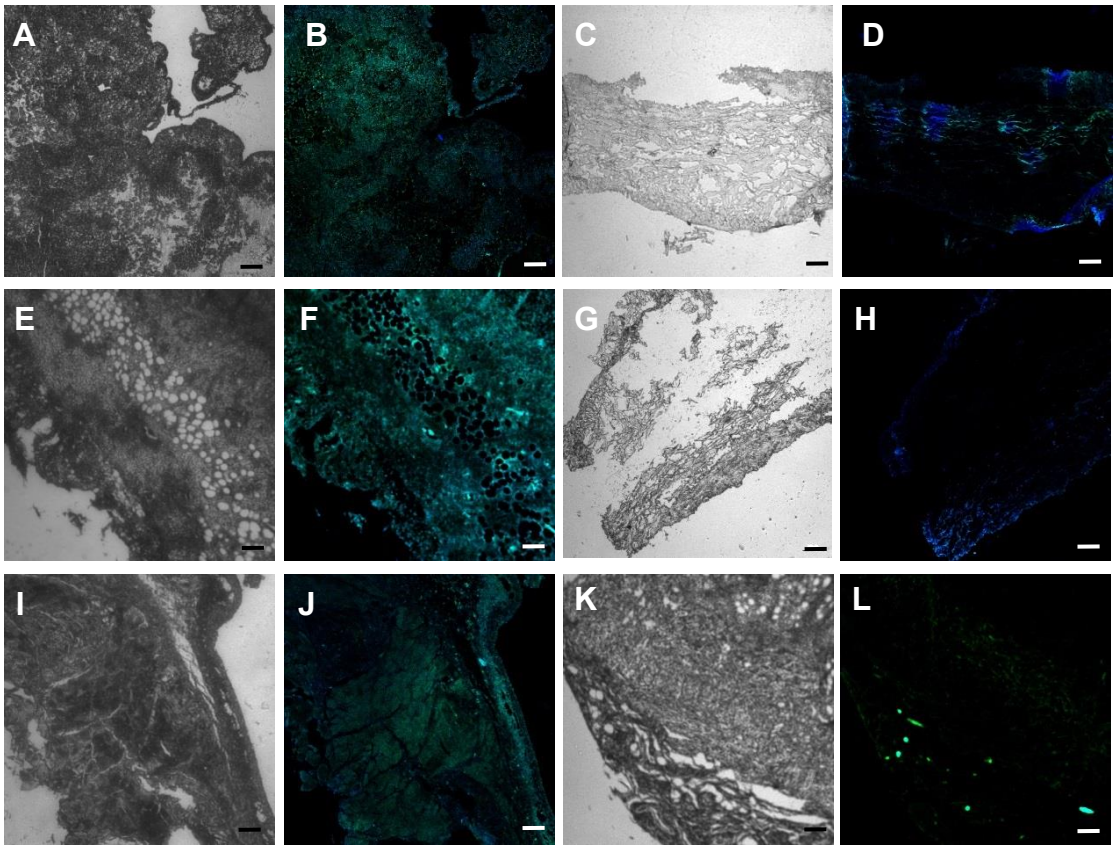

Figure 4.3-26 IHC results to image CD68-AF 488 rat macrophage marker. Hydrogel at day 1 (A) and (B) Mucograft® at day 1 (C) and (D), hydrogels at day 4 (E) and (F) and Mucograft® at day 4 (G) and (H), hydrogel at day 7 (I) and (J) and Mucograft® at day 7 (K) and (L). Magnification x10, scale bar 50 µm.

The host reaction to Mucograft® was favourable, with minimal inflammation, no strong immune response and no degradation or change in shape throughout the study, although the health of the infiltrated cells was an initial concern.

After correspondence with Geistlich, it was discovered the lyophilisation of the material can make Mucograft® very hydrophobic, even though it is reported to have excellent hydrophilicity. So the material's surface could modulate protein adsorption from the interstitial fluids after the first contact with the tissue. Cell adhesion and activation could occur later due to the interaction of adhesion receptors with these adsorbed proteins which provide the recognition of the foreign biomaterial [143]. Although there are other receptor-ligand interactions that activate the immunocompetent cells. The hydrophobicity could also explain the reduced immune response and poor health of the infiltrated cells. After 7 days, the collPEG4.5 hydrogel displayed attached connective tissue as well as a dense layer of cells which could be seen infiltrating into the scaffold. These

observations were consistent with an expected acute foreign body reaction that follows implantation [273].

An important aspect of biomaterial design is the tailoring of the device to meet the needs of the body's immune system. The photo-click hydrogels were designed to mimic muscle tissue in terms of matrix elasticity, and ultimately to repair tissue and encourage biomaterial integration [274]. Both materials held their own benefits in this study, Mucograft® presented a lower immune response and reduced inflammation, whereas the hydrogel, with its immune response promoted angiogenesis, which is beneficial later for muscle regeneration. This leaves the paradigm of whether to evade or evoke the host immune system and to what extent. It is noted that there is no point designing a new system if it is ultimately destroyed by the influx of inflammatory cells (chronic inflammation) and foreign body giant cells (FBGCs), however, the collPEG4.5 did not show signs of chronic inflammation or the macrophage-fused FBGCs (easily identified with H&E due to their fused-cell appearance) after 2 weeks of subcutaneous implantation (Figure 4.3-27).

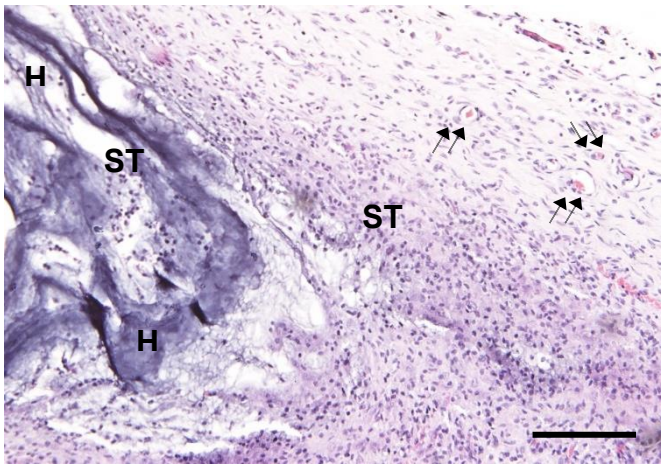

Figure 4.3-27 H&E stain of collPEG4.5 after 2 weeks of subcutaneous implantation. Hydrogel (H), subcutaneous tissue (ST), black arrows indicate blood vessel. Scale bars 50 µm.

4.3.3 Critical Sized Calvarial Defect Model

Injury to either tissue, whether muscle, tendon or bone compromises the physical function of the trauma-exposed extremity and interest lay in recreating the muscle-tendon-bone bridge, conceivably with a gradient hydrogel. CollPEG4.5 was created to mimic the mechanical properties of natural muscle, whereas

collagen-4VBC was a stiff, stable hydrogel which benefited from π-π stacking and possessed mechanical properties similar to that of pre-calcified bone.

A critical size bone-defect model (4 mm) was created on SD rats, which was repaired with collagen-4VBC hydrogel as the test material (stiffness similar to that of pre-calcified bone ~60 kPa and hereafter referred to as 4VBC) and Bio-Gide® as the control. No subject experienced complications such as infection during this study.

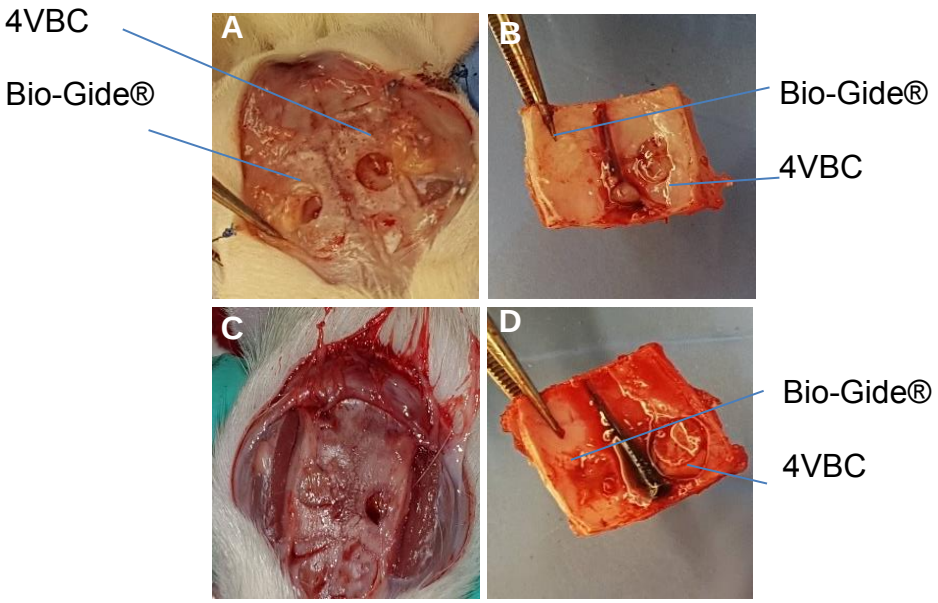

Figure 4.3-28 Photographs of the Bio-Gide® and 4VBC after the fibrous tissues were removed to expose the bone defect area (A&B) after 2 weeks and (C&D) after 6 weeks. Bio-Gide® is in the LHS defect and 4VBC in the RHS defect. The cut-out bone sample after (B) 2 weeks and (D) 6 weeks.

The bone defect areas were visualised by photography after schedule 1 (Figure 4.3-28). Bio-Gide® is pictured on the left hand side (LHS) of the cranium and 4VBC on the right hand side (RHS). After 2 weeks, the defects could be easily detected from either sample (Figure 4.3-28 A), although, the 4VBC appears to experience gel shrinkage/ degradation which would impede its use as a template for bone formation. The visual representation of Bio-Gide®'s superior bone formation is obvious at 6 weeks, where the defect was almost filled in.

New bone formation was confirmed in all groups and microCT allowed a 3D reconstruction of mineralised tissue within the defect and a visualisation of the

volumetric and spatial density of bone regeneration of the tissue at 2 and 6 weeks (Figure 4.3-29) [249].

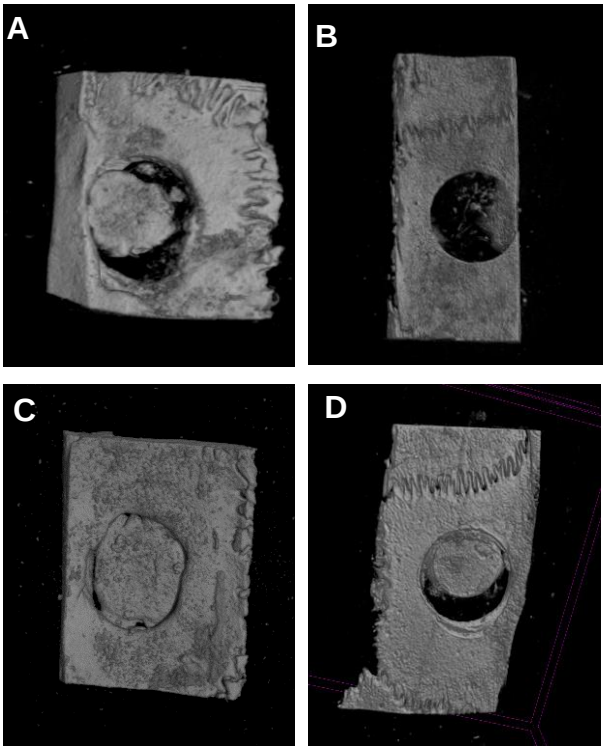

Figure 4.3-29 Micro-CT 3D scans of the bone samples. (A) Bio-Gide® after 2 weeks (B) Bio-Gide® after 6 weeks (C) 4VBC after 2 weeks and (D) 4VBC after 6 weeks.

Lohmann *et al* visualised the bone defect using *in vivo* microCT analysis at 1 d, 3 d, 3 w, 6 w, 12 w post implantation [251]. This advanced technique was not available during this research but would be used preferentially to reduce sample variance, although the calculation of bone volume from this advanced technique was impeded by the addition of hydroxyapatite in the samples by Lohmann which could not be distinguished from newly formed bone.

The bone samples were scanned for structural analysis by SkyScan-1072 high-resolution desk-top micro-CT system. Image J analysis provided quantitative information about new bone volume (Figure 4.3-30).

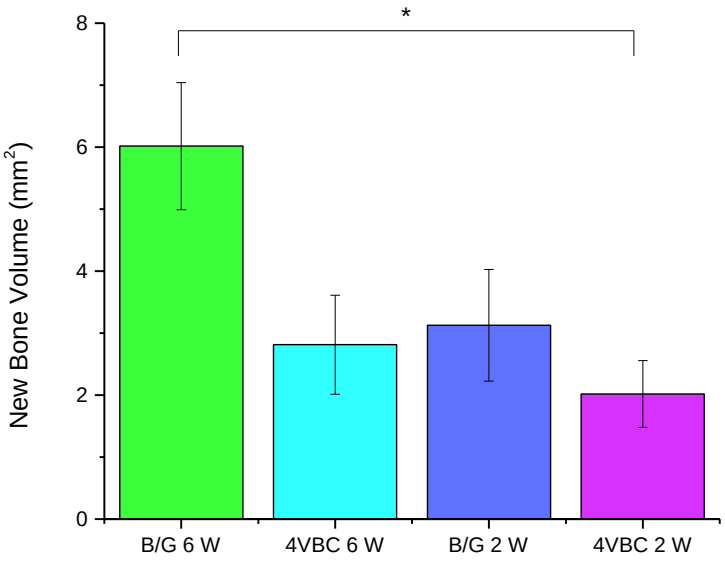

Figure 4.3-30 New bone volume determined by microCT analysis. Data represented as means ± SEM (n=3). *p < 0.05.

The thickness of the calvarial defect was calculated to be 1.243 ± 0.04 mm which was used to calculate the total volume of the empty defect (15.7 mm^3) and the new bone (%) (Table 4.3-2).

Spicer *et al* reported a calvarial thickness of 1 mm in rats, similar to the 1.243 mm from the microCT results [249].

Table 4.3-2 MicroCT analysis of new bone formation after 2 and 6 weeks (2/ 6 W) of implantation in rat calvaria defect model. Data represented as means ± SEM (n = 3).

Sample ID	New Bone Volume (mm^3)	New Bone (%)
4VBC 2 W	2.0 ± 0.5	13.0
4VBC 6 W	2.8 ± 0.8	17.8
B/G 2 W	3.1± 0.9	20.1
B/G 6 W	6.0 ± 1.0	38.2

Bio-Gide® formed twice the amount of new bone compared to the 4VBC hydrogel at 6 weeks, 6 mm^3 to 2.8 mm^3, although the small sample size (n= 3) meant that the bone volume of Bio-Gide® 6 W was only significantly higher when

compared to 4VBC 2 W. Although both materials supported bone regeneration, Bio-Gide displayed a higher mean new bone volume compared to 4VBC for both 2 W and 6 W and appeared to support bone formation more than the 4VBC hydrogel.

Gielkens *et al* used Bio-Gide® to repair a 5 mm mandible defect with estimated bone volume of the defect of 16.81 mm^3. MicroCT results showed that new bone formation (%) of Bio-Gide® at 2, 4 and 8 weeks was 8.9, 56.8 and 84.1% respectively. These results for new bone (%) are higher at 4 and 8 weeks and lower for the result at 2 weeks, (20% to 8.9% respectively) compared to the current study. However, it was noted that the blank control used by Gielkens *et al* presented new bone (%) at 2, 4 and 8 weeks of 20.2, 21.3, 27.3% [275]. This implied that the bone healing capacity of the animals used in the study was higher, potentially because only one defect was used per animal, compared to this study where there were two defects per animal [249].

Huebsch *et al* used an alginate hydrogel (60 kPa) for their bone defect model (Charles River Nude Rats) with the notion that this elasticity would be able to support cell migration and proliferation based on *in vitro* assays [276]. After 12 weeks, the alginate hydrogel presented a calculated new bone (%) 19.9% comparable to the results at 6 weeks for the 4VBC hydrogel (17.8%). Additionally, the work showed a statistically significant difference in the new bone volume of hydrogels 5 and 60 kPa after 12 weeks model, 7 to 12 mm^3 respectively [276]. This suggests that mechanotransduction pathways that regulate stem cell gene and protein expression *in vitro* might be directly transferred to complex *in vivo* processes such as bone formation. Although whilst acknowledging this, the Bio-Gide® has outperformed the 4VBC hydrogel (~60 kPa) in this work despite the mechanotransduction pathways.

As discussed in the methods, this bone formation model was performed rather than a guided bone regeneration (GBR) model. The principle of GBR uses a barrier membrane to prevent soft tissue cells (fibroblastic cells) from colonising the defect during healing since osteoprogenitor cells grow relatively slowly. Thus serving as a space-maintaining device to allow osteoblast cells to migrate and fill the defect/ bone graft material, thus resulting in direct bone regeneration [277, 278]. For a calvarial model, this would require the barrier to be between the periosteum and the defect. There have been several papers showing the success of GBR [279, 280]. However, an observation when retrieving the samples was that more bone was present on the ‘top’ of the bone where the

periosteum was covering it compared to the ‘bottom’ of the bone that had been in contact with the dura mater (Figure 4.3-31).

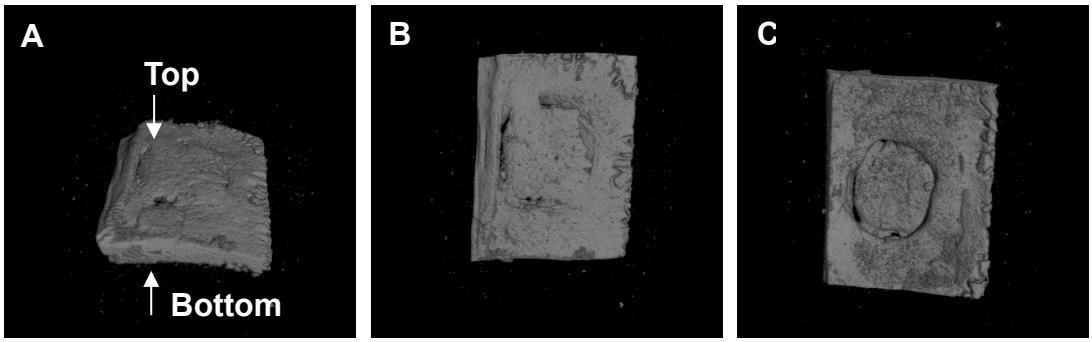

Figure 4.3-31 MicroCT images of Bio-Gide® 6 weeks. (A) Top represents the side of the bone the periosteum is covering and bottom represents the side of the bone in contact with the dura mater. (B) Visualisation of the top of the defect and (C) the bottom of the defect,

The microCT image from the top of the bone where it has been in contact with the periosteum, visually looks as though it has greater bone healing. Work by Stevens *et al* involved the design of a bioreactor between the surface of a long bone (tibia) and the periosteum, to induce the body’s natural healing mechanism and to generate new tissue and provide all the necessary cells and factors in the correct temporal and biochemical sequence [281]. This was performed to successfully reconstitute living bone. This insight is purely written in argument to GBR. As mentioned in the introduction, muscle, tendon and blood vessels influence the healing of bone, although the relative contributions of the cells and the exact cellular mechanism during the healing of bone has remained an active area of ongoing research [247]. Whilst the visualisation of these standalone microCT images have no quantitative backing; it is to emphasise that the biology of the cells is as of yet, still not thoroughly understood in the complex bone healing process.

The bone samples used for microCT were then embedded in a plastic resin using an Osteobed kit and the bone samples that were not used for microCT (n=3) were demineralised using formic acid (10%) before paraffin embedding and histological analysis.

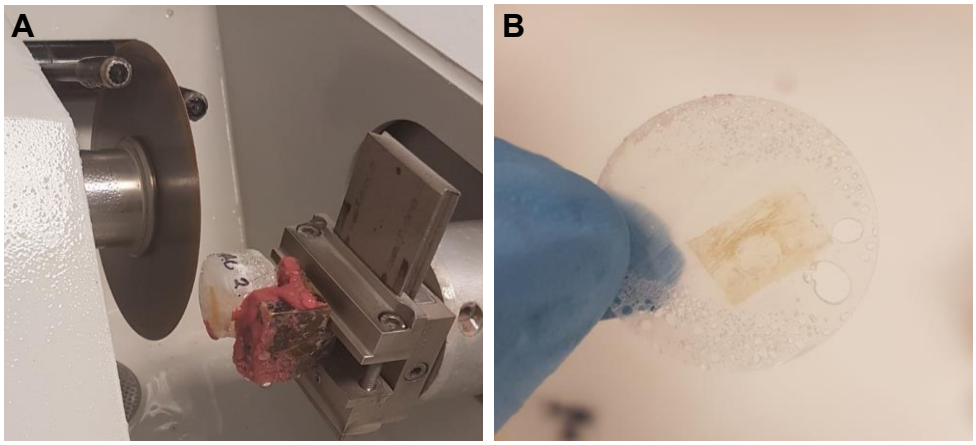

Figure 4.3-32 (A) Struers Accutom-5 and 9 cm blade (B) plastic-embedded bone section (100- 200 µm).

The accutom could not cut thin sections and would grind away the top of the plastic if the settings were set too small (Figure 4.3-32). However, after de-plasticising, a Von Kossa stain was attempted where calcium deposits are stained black, cytoplasm pink and nuclei red (Figure 4.3-33).

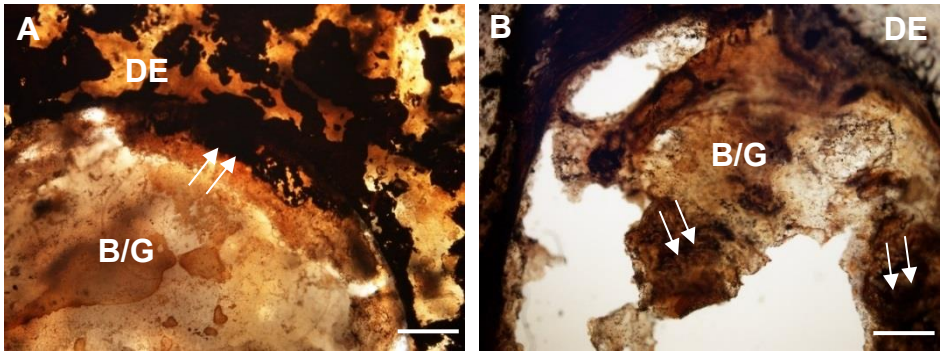

Figure 4.3-33 Von Kossa stain of Bio-Gide® at 2 weeks (A) and 6 weeks (B). B/G indicates Bio-Gide®, where the sample is apparent, DE indicates defect edge and white arrows indicates calcium deposition (black mark. Scale bars 50 µm.

Due to the thick sample (as a result of the accutom) and due to the poor Osteo-bed method of plasticising, the Von Kossa images are not well detailed. Although, from the images of Bio-Gide® and 2 and 6 weeks, the increase in calcium deposition (black marks) is apparent and hence degree of mineralisation.

Figure 4.3-34 shows that formic acid (10%) can be successfully used to demineralise calvarial bone. The x-ray images show the removal of the mineral before and after incubation with formic acid. These samples were then dehydrated, fixed and mounted onto slides.

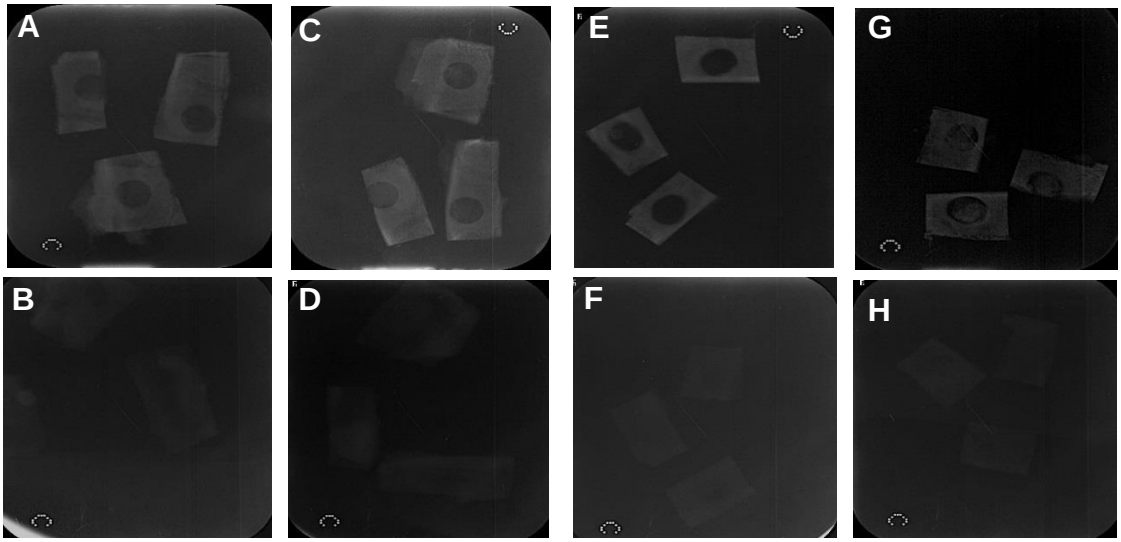

Figure 4.3-34 X-ray images to examine mineral content of bone samples. A – 4VBC 2 W, B – 4VBC 2 W demineralised, C – 4VBC 6 W, D – 4VBC 6 W demineralised, E – B/G 2 W, F B/G 2 W demineralised and E – B/G 6 W demineralised.

Figure 4.3-35 shows H&E, Goldner's Masson trichrome and Sanderson's rapid bone stains for 4VBC at 2 and 6 weeks. The defect edge where the trephine drill was used to cut the 4 mm defect is obvious for (A) and (F). As shown in the Masson trichrome staining images presented the newly formed bone, and mineralised bone, can be easily recognised at different stages (2 weeks vs 6 weeks) with the white arrows directing towards the immature new bone osteoid.

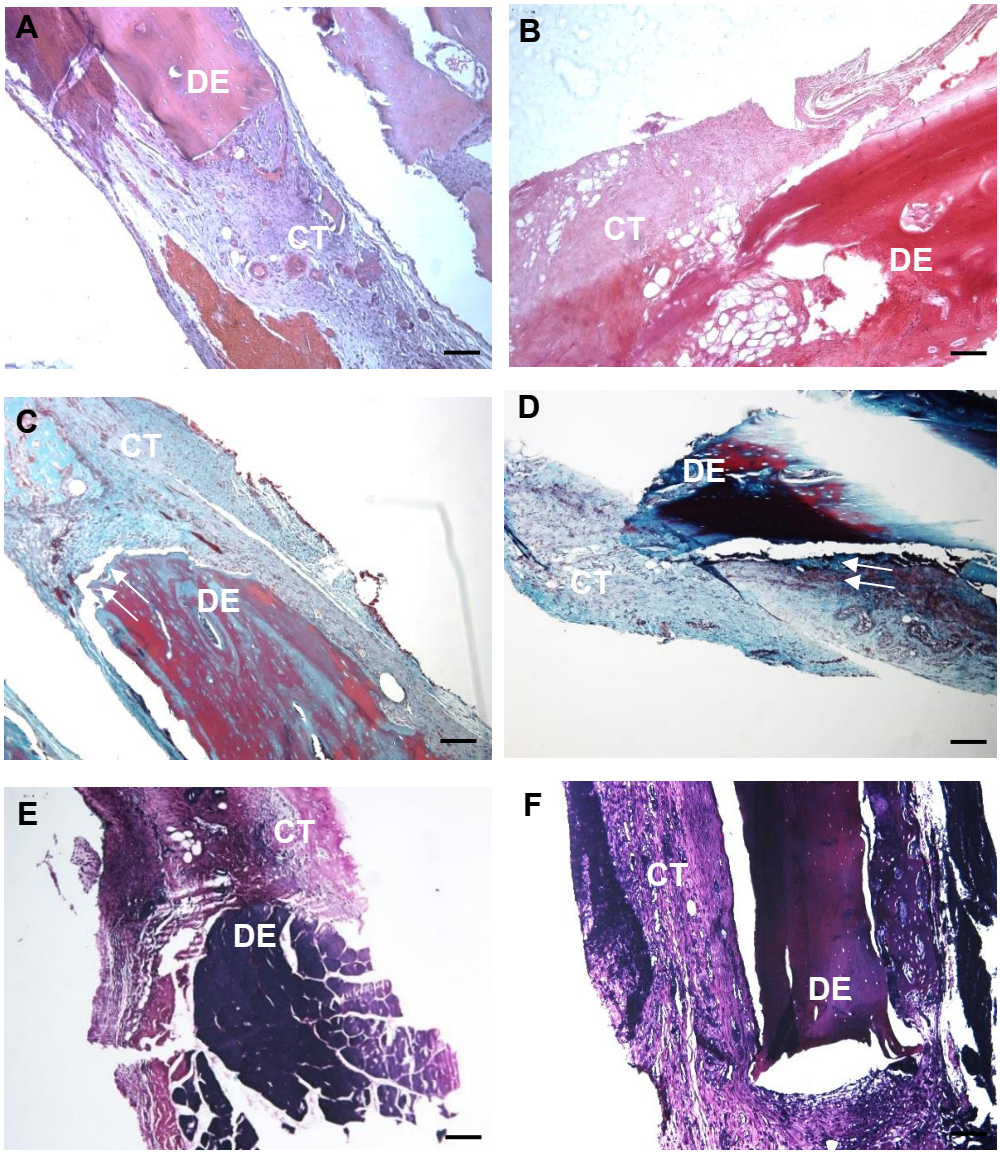

Figure 4.3-35 Representative histological stained images of demineralised samples from the cranial defects of the rats using 4VBC hydrogels two weeks after surgery (A), (C) and (E) and six weeks after surgery (B), (D), (F) with examination using H&E, Goldner's Trichrome and Sanderson's rapid bone stain respectively. In (A-F) CT, indicates connective tissue, DE indicates defect edge and white arrows indicate the presence of new bone formation. (A-F) Scale bars 100 µm and magnification x10.

Figure 4.3-36 shows the de-mineralised histology stains for Bio-Gide at 2 and 6 weeks. The biggest difference between the stains for the 4VBV hydrogel and Bio-Gide is the appearance of a clear, cut defect edge. No defect edge is obvious for Bio-Gide 6 weeks and the new bone appears in lumps attached around the old bone.

From the histological evaluation alone, Bio-Gide appears to have better bone formation compared to 4VBC and no definitive edges are visualised for Bio-Gide and the bone appears surrounded by connective tissue.

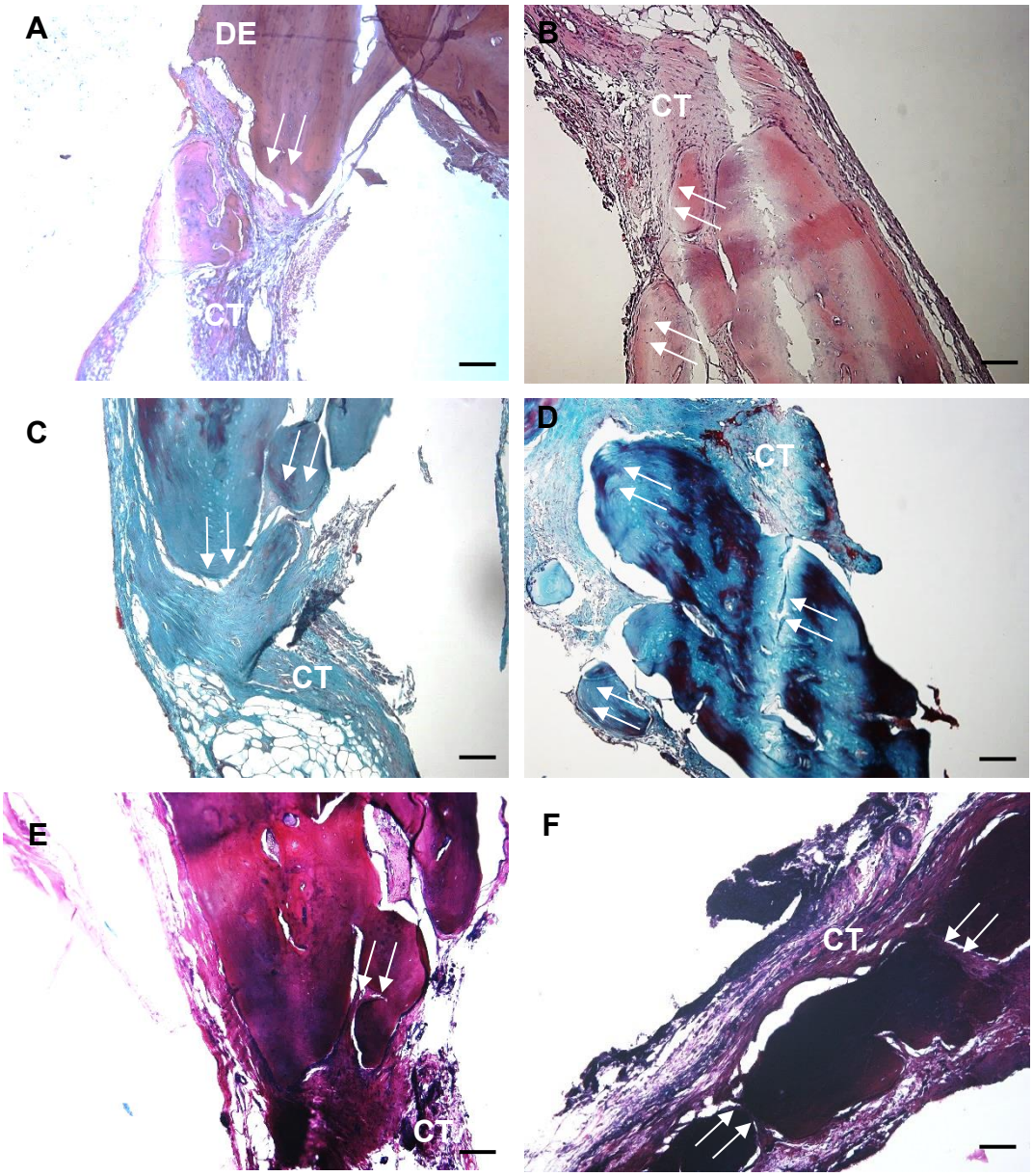

Figure 4.3-36 Representative histological stained images of demineralised samples from the cranial defects of the rats using Bio-Gide® two weeks after surgery (A), (C) and (E) and six weeks after surgery (B), (D), (F) with examination using H&E, Goldner's Trichrome and Sanderson's rapid bone stain respectively. In (A-F) CT, indicates connective tissue, DE indicates defect edge and white arrows indicate the presence of new bone formation. (A-F) Scale bars 100 µm and magnification x10.

Cells can either grow on top or be encapsulated inside hydrogels due to their water-swollen nature. They also possess the ability to incorporate composites such as hydroxyapatite or silk [282, 283]. One disadvantage is that they tend to be very soft materials, although the 4VBC hydrogels have been shown to have good mechanical competence (~ 60 kPa) similar to that of natural pre-calcified bone [57]. The properties of the 4VBC hydrogel which might have contributed to the reduced bone formation include poor cell penetration, poor mechanical properties of hydrogels at both macroscopic and microscopic levels compared to the Bio-Gide®, hydrogel shrinkage and a lack of complex microvasculature [88]. Additionally, Bio-Gide® contains a unique bilayer structure and been optimally developed to allow for the cascade of biologic events leading to regeneration. As mentioned in chapter 3, collagen-4VBC hydrogels have poor shape memory, so when they are rehydrated they are film-like. This impeded their handleability in surgery and they were difficult to place in the defect. Additionally, due to their transparent appearance they could often be misplaced or lost entirely. The Bio-Gide® was far easier to handle and was white in colour so it was always obvious that the scaffold was in the correct position in the defect.

Bio-Gide® has been shown to achieve new bone formation of 38% after 6 weeks as a purely biomaterial-based approach with no additional growth factors or cells.

4.4 Conclusion

The three photo-click hydrogels collPEG3.5, collPEG4 and collPEG4.5 were shown to be non-toxic as a result of a direct and indirect cytotoxicity test using C2C12 cells. The three hydrogels were shown to support cell attachment, spreading, proliferation and maturation/ differentiation of C2C12 mouse myoblast cells. Although despite their varied stiffness' (7, 10 and 13 kPa), there was no significant difference between the results for each hydrogel.

The tissue culture plastic control showed a higher mean % of myosin expression compared to collPEG4 and collPEG4.5 and a statistically higher expression compared to collPEG3.5 on both day 3 and 7 of the study, which suggested that the hydrogels have comparatively inhibited the C2C12 maturation. On the cellular scale, the cells probe elasticity as they anchor and pull on their surroundings. This could be difficult for the cells to do on the collagen-PEG hybrid hydrogel due to the high fibrillar arrangement of the hydrogel – collagen, 1 wt.% and PEG8NB 3.5-4.5% (w/v) and because the cells were cultured on top of the hydrogel rather than encapsulated inside it. It was possible that rather than

migrating inside the hydrogel, the cells remained and grew on top due to the high concentration of material. This would mean the cells would ‘feel’ more from their cell-cell interactions rather than the cell-substrate interactions.

The immune response of the new material, collPEG4.5 was analysed at 1, 4 and 7 days after subcutaneous implantation using Mucograft® as the commercial control and presented with a biocompatibility paradigm. From the literature, it was discovered that modern implants are designed to create a small immune response (steering clear of chronic inflammation) in order to encourage integration with the tissue, rather than remain ‘invisible’ to the host. The Mucograft® showed reduced inflammation and immune response compared to the collPEG4.5 hydrogel which was concluded to be due to the hydrophobic nature of the material. The collPEG4.5 hydrogel appeared to induce a greater host response with angiogenesis observed on day 4 of the study. The degree to which a modern implant should invoke an immune response is not clear, however, the pilot study at 2 weeks implantation showed no signs of FBGCs (fused macrophages) indicative of no unresolved inflammation chronic inflammation which would holds implications in terms of the material’s longevity.

Collagen-4VBC and BioGide® were compared as a purely biomaterial-based approach for bone formation in a critical sized bone defect model. Interface tissue engineering (ITE) is an emerging field that aims to regenerate functional tissues in order to repair or to regenerate diseased or damaged tissue zones. Due to the similarity in elasticity of the collPEG4.5 to muscle and collagen-4VBC to pre-calcified bone, a gradient hydrogel could have been created to mimic the hard-soft gradient of natural tissue such as bone, cartilage, muscle, skin, and vessels, - this could be formed from a concentration gradient, diffusive mixing of two hydrogels or by regulating cross-linking density [282-285]. However, BioGide® was shown to support bone formation more than collagen-4VBC, so the application of gradient hydrogels for ITE was abandoned.

Chapter 5 - Telopeptides and Polymeric Collagen

5.1 Introduction

The aim of this chapter was to assess the influence of telopeptide removal on the structural and physical properties of mature 'polymeric' and acid-soluble (normal) 'monomeric' collagen type I, before the material could be used as a means to provide an immunological benefit to the material. It was also of interest to prepare collagen-4VBC (coll4VBC30) hydrogels from atelo collagen in order to compare whether similar chemical, physical and mechanical properties were achievable compared to previous data using RT collagen.

The biocompatibility and versatility of collagen derived products for medical applications has long been recognised and reflected in its wide scale research [286]. As a scaffold material, collagen benefits from good biodegradability, affinity for biomolecules and exhibits organisational and macromolecular properties similar to the natural extracellular matrix (ECM) [73, 74]. Collagen has a unique triple helix structure made of three left-handed polypeptide (α-chains) chains held together by hydrogen bonds between the peptide bond of a glycine residue with the peptide carbonyl (C=O) of the adjacent polypeptide [287]. Each chain follows the amino acid motif, -Gly-X-Y-, where X and Y are often proline and hydroxyproline [287]. Glycine (Gly) is the smallest essential amino acid, and provides the H atom which is able to fit inside the crowded centre of the triple helix to form the hydrogen bonds. The fixed angle of the C-N bond is due to the high content of peptidyl-proline or peptidyl-hydroxyproline bonds which allow the rotational freedom needed to form the tight packaging of the three chains, thus organising the triple helix [287, 288]. The short segments of the C- and N- termini of the polypeptides (the telopeptides), do not possess the repeating Gly-X-Y motif and are therefore non-helical [289, 290]. In human type I collagen, there are 38 lysine residues in an α1 chain (36 in the helical domain, one in the C-telopeptide domain and one in the N-telopeptide domain) and 31 in an α2 chain (30 in the helical domain, one in the N-telopeptide domain, and none in the C-telopeptide domain) [149]. The fibrils are stabilised by covalent aldol cross-links between lysine-lysine or lysine-hydroxylysine from the C- terminus to the N-terminus of adjacent molecules, thus stabilising the side packing [63, 287]. These

self-assemble into cross-striated fibrils (periodic D spacing ~ 67 nm) with high tensile strength [85, 287].

The use of biological material for medical applications requires a distinction between immunogenicity and antigenicity. Immunogenicity is about triggering an immune response, whilst antigenicity can be determined by macromolecular features of an antigen molecule such as three-dimensional (3D) conformation and amino acid sequence [77].

Collagen, as an animal-derived biomaterial has always raised concerns regarding its potential to evoke immune responses [289, 291]. However, the interpretation of immunochemical reactions to collagen-containing implants is often complicated by the presence of cell remnants, or chemicals from extraction or cross-linking treatments [292-294].

5.1.1 Atelo Collagen

The collagen molecule can be divided into three domains: the terminal amino (N-) telopeptide, the triple helix, and the terminal carboxy (C-) telopeptide [295]. Treatment of collagen with proteolytic enzymes (e.g. pepsin or ficin) can cleave the terminal telopeptides to produce atelo collagen with an intact triple helical conformation [287].

The antigen determinants of collagen can be classified in three categories: helical recognition by antibodies dependent on 3D conformation located within the triple helical portion of native collagen, central recognition dependent on the amino acid sequence and terminal recognition dependent on the non- helical telopeptides of the molecule.

It has been claimed that the majority of collagen's antigenicity is attributed to the terminal telopeptides and that collagen devoid of terminal telopeptides can eliminate its immunogenicity, whereas realistically, the biological effects of atelo collagen are not yet fully understood [77, 296]. The removal of telopeptides results in an amorphous arrangement of collagen molecules and a loss of the collagen fibril pattern in the reconstituted product. This is due to the roles of the C- and N-terminus telopeptides in cross-linking and fibril formation [77, 297]. The induced positively charged surface of the atelo collagen can significantly increase its solubility and therefore the ability to process the collagen as a biomaterial.

5.1.2 Polymeric Collagen

All collagenous tissues contain a fraction of soluble ‘monomeric’ collagen which is extractable in weak acidic solutions such as acetic acid (17.4 mM) and is the material commonly used in research. However, in mature tissues, such as tendons, the bulk of the collagen consists of insoluble, highly cross-linked polymerised fibres of type I collagen (‘polymeric’ collagen) with a smaller amount as acid-soluble monomeric collagen (<10 %) [123, 298]. The natural fibrillar cross-links are chemically rearranged with age to form acid-stable aldminine cross-links, which provide increased mechanical strength of the tissue and forms ‘polymeric’ collagen [123, 299].

5.2 Methods

Hereafter, acid-soluble collagen will be referred to as monomeric collagen and mature, acid-stable collagen will be referred to as polymeric collagen as distinction between the two types. Atelo collagen has been pepsin treated to remove the end telopeptides.

5.2.1 Materials

The materials were provided as part of an industrial collaboration with Collagen Solutions, UK and Southern Lights Biomaterials, New Zealand. Monomeric atelo collagen (Collagen Solutions, UK), Polymeric collagen (Southern Lights Biomaterials, New Zealand), Polymeric atelo collagen (Southern Lights Biomaterials, New Zealand). 4-vinylbenzyl chloride (4VBC) was purchased from Sigma, Tween20 and triethylamine (TEA) were purchased from Sigma-Aldrich.

5.2.2 Preparation of Monomeric Collagen Type I

Type I collagen was isolated in-house via acidic treatment of rat-tail tendons. Briefly, rat-tails (RT) were defrosted in ethanol before the skin was removed using a scalpel. The tails were allowed to dry before the exposed tendons (approx. four per tail) were removed, sliced and placed in acetic acid (17.4 mM) and stirred for 48 hours. The solution was centrifuged and the pellet removed to leave the soluble collagen type I dissolved in the acetic acid, which was freeze-dried to remove the solvent to leave the white, acid-soluble collagen type I.

5.2.3 Chemical and Structural Characterisation

Chemical and structural characterisation was used to analyse the influence of telopeptides on monomeric and polymeric collagen

5.2.3.1 Circular Dichroism (CD)

Circular dichroism (CD) spectra of collagen samples (0.2 mg.ml^{-1}) were acquired (ChirascanCD spectrometer, Applied Photophysics Ltd) using solutions in HCl (10 mM). A homogeniser was used to dissolve polymeric and atelo polymeric collagen. Sample solutions were collected in quartz cells of 1.0 mm path length, whereby CD spectra were obtained with 4.3 nm band width and 20 nm.min^{-1} scanning speed. A spectrum of the HCl (10 mM) solution was subtracted from each sample spectrum.

Equation 5.2-1

$$\theta_{mrw,\lambda} = \frac{MRW\ x\ \theta_{\lambda}}{10\ x\ d\ x\ c}$$

Where θ_{λ} is observed molar ellipticity (degrees) at wavelength λ, d is path length (1 cm) and c is the concentration (0.2 mg.ml^{-1}) [163].

A temperature ramp was conducted from 20 to 60 °C with 20 °C/hour heating rate with ellipticity measurements at 221 nm fixed wavelength. The 221 nm coincides with the positive band associated with the collagen triple helix and its destruction will be related to a lower value of ellipticity. The denaturation temperature (T_d) was determined as the mid-point of thermal transition.

5.2.3.2 Differential Scanning Calorimetry (DSC)

Differential Scanning Calorimetry (DSC) was used in order to investigate the thermal denaturation (T_m) of collagen samples (TA Instruments Thermal Analysis 2000 System and 910 Differential Scanning Calorimeter cell base). DSC temperature scans were conducted with 10-200 °C temperature range and 10 °C.min^{-1} heating rate. 5-10 mg sample weight was applied in each measurement and three scans were used for each sample formulation. The DSC cell was calibrated using indium with 10 °C.min^{-1} heating rate under nitrogen atmosphere.

5.2.3.3 High Pressure Liquid Chromatography (HPLC)

High pressure liquid chromatography (HPLC) was used to investigate the amino acid occurrence in collagen samples (Dionex Ultimate 3000 HPLC, Dionex Softron GmbH, Germany). This service was paid for by Southern Lights Biomaterials and provided by Massey University's Institute of Fundamental Sciences. For acid stable amino acids, hydrolysis was performed in HCl (6 M) for 24 hours at 110 ^{o}C in an evacuated sealed tube followed by fluorescence detection. Results were calculated as residues per 1000 residues.

5.2.4 Physical Characterisation

5.2.4.1 Scanning Electron Microscopy (SEM)

Scanning electron microscopy (SEM) was used for microscopic analysis of collagen by gold-coating the samples in order to examine the fibrillary meshwork and banding pattern. Samples were mounted onto 10 mm stubs and electron micrographs captured (FEI Quanta 600) via backscattered electron detection at 10 kV and 12 - 13 mm working distance.

5.2.5 Telopeptides and Hydrogel Properties

To analyse whether medical grade atelo collagen could be used as a replacement for monomeric collagen i.e. display similar chemical, physical and mechanical properties, collagen hydrogels were prepared by base mediated nucleophilic substitution reaction using 4-vinylbenzoyl chloride (4VBC). The nomenclature coll4VBC30 was given to collagen hydrogels functionalised with 30 x excess 4VBC. RTColl and AColl were used to refer to rat tail (RT) and atelo type I collagen respectively.

5.2.5.1 Functionalisation of Collagen Type I

Medical grade atelo collagen type I and in-house isolated monomeric collagen were dissolved in HCl (10 mM, 0.25 wt.%). The pH was adjusted to 7.4 and Tween20 (1% (v/v)) added to the solution followed by 4VBC (30 molar excess) and triethylamine (1:1 to 4VBC). The solution was stirred for 24 hours followed by precipitation in ethanol (20 x excess) which was stirred for a further 24 hours. The solution was centrifuged to remove the pellet and air dried.

5.2.5.1.1 2,4,6-trinitrobenzenesulfonic acid (TNBS) assay

Functionalised collagen (0.011 g) including a reference sample (0.011 g) were placed in a vial. Sodium hydrogen carbonate ($NaHCO_3$) (4%, 1 mL) and TNBS (0.5%, 1 mL) were added. Hydrochloric acid (HCl) (6 N, 3 mL) was added to the reference sample. This was stirred at 40 ^oC for 3 hours. HCl (6 N, 3 mL) was added to non-reference sample and stirred at 60 ^oC for 1 hour to complete the reaction. This was diluted in water (5 mL), followed by extraction in diethyl ether (3 x 15 mL). An aliquot (5 mL) was removed and diluted in water (15 mL). Absorbance was measured at 346 nm.

The degree of collagen functionalisation, F, was determined by TNBS colorimetric assay, according to the following equations:

Equation 5.2-2

$$\frac{mol\ (Lys)}{g\ (collagen)} = \frac{2.Abs\ (346\ nm).0.02\ L}{1.46\ x\ 10^4 (M^{-1}cm^{-1}).b.x}$$

Where: *Abs (346 nm)* is the absorbance value at 346 nm, *0.02* is the volume of sample solution (in litres), 1.46 x 10^4 $M^{-1}.cm^{-1}$ is the molar absorption coefficient for 2,4,6-trinitrophenyl lysine, *b* is the cell path length (1 cm) and *x* is the sample weight.

Equation 5.2-3

$$F = 100 - \frac{mol(Lys)_{functionalised\ collagen}}{mol(Lys)_{native\ collagen}}\ x\ 100$$

Where: $mol(Lys)_{native\ collagen}$ and $mol(Lys)_{functionalised\ collagen}$ represent the total molar content of free amino groups in native and functionalised collagen, respectively. The nomenclature (Lys) is hereby used to recognise the free amine groups from (hydroxy) lysine.

5.2.5.2 Preparation of Collagen Hydrogels

Hydrogels were prepared by dissolving coll4VBC30 in HCl (0.8 wt.%, 10 mM) solution containing I2959 (1% (w/v)). After dissolution, the solution was dispensed into 12 cell well plates and irradiated with UV light (365 nm) for 30 minutes on each side.

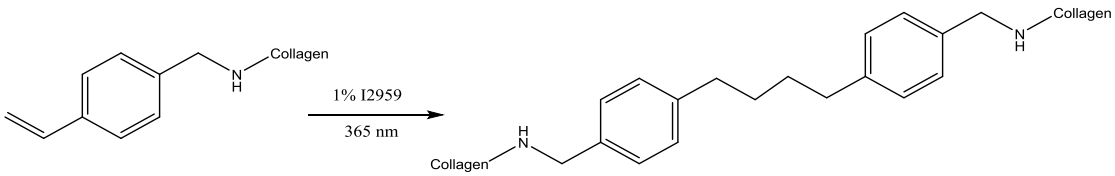

Figure 5.2-1 Reaction of coll-4VBC30 using I2959 and UV light (365 nm)

5.2.5.2.1 Physical Characterisation

Swelling ratio was determined by placing a dehydrated sample (2 – 5 mg) in distilled water overnight. The *SR* was calculated according to the following equation:

Equation 5.2-4

$$SR = \frac{M_s - M_d}{M_d} \, x \, 100$$

Where M_s is swollen weight and M_d is dried weight. Swollen samples were paper blotted prior to measurement of M_s, in order to take into account, the contribution from bound water only.

In addition to the swelling ratio, the gel content was determined to investigate the overall portion of the covalent hydrogel network insoluble in HCl (10 Mm) solution. Dried hydrogel networks of known mass (M_d) were equilibrated in HCl (10 Mm) solution for 24 hours. Resulting hydrogels were air dried and weighed (M_{d1}). The gel content (*G*) was calculated according to:

Equation 5.2-5

$$G = \frac{M_{d1}}{M_d} \, x \, 100$$

5.2.5.2.2 Mechanical Characterisation

Compression testing was used for mechanical characterisation. water-equilibrated hydrogel discs (Ø: 12 mm) were compressed at room temperature with a compression rate of 3 mm·min^{-1} (Instron ElectroPuls E3000). A 250 N load cell was operated up to complete sample compression. Stress-strain lines were recorded and the compression modulus was calculated:

Equation 5.2-6

$$\sigma = \frac{F}{A}$$

Where σ is stress (Nm^{-2} or Pa), F is force (N), and A is the cross sectional area of the sample (m^2).

Equation 5.2-7

$$\epsilon = \frac{\Delta l}{l_0}$$

Where ϵ is strain, l_0 is the original length (m) and Δl is the difference between l and l_0 (m).

Equation 5.2-8

$$E = \frac{\sigma}{\epsilon}$$

Where E is Young's modulus (Nm^{-2} or Pa).

5.3 Results and Discussion

Sample nomenclature used in this work is as follows: acid-soluble collagen will be referred to as monomeric collagen and mature, acid-stable collagen will be referred to as polymeric collagen.

5.3.1 Chemical and Structural Characterisation

CD is defined as the unequal absorption of left-handed and right-handed circularly polarised light. When the chromophores of the amides on the polypeptide backbone of proteins are aligned in arrays, their optical transitions are shifted or split into multiple transitions [300]. The spectra of proteins are dependent on their conformation, so CD is a useful tool to estimate the structure of unknown proteins and monitor conformational changes due to denaturation [300]. Far-UV CD spectra of monomeric type I collagen displayed a positive band

at 221 nm and a negative band at 198 nm, characteristic of the triple helical conformation (Figure 5.3-1) [301].

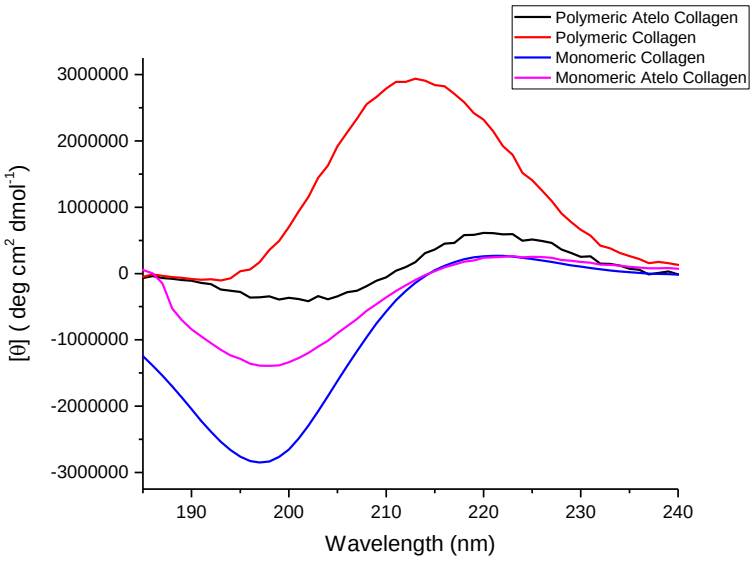

Figure 5.3-1 CD spectra of polymeric atelo, polymeric, monomeric atelo and monomeric type I collagen

The magnitude ratio of the positive to negative band (RPN) for the monomeric type I collagen spectrum was found to be 0.094, comparable to the literature value of native collagen, RPN: 0.117 [79].

Monomeric atelo collagen displayed a RPN value of 0.189. The positive band at 221 nm had similar molar ellipticity to monomeric collagen. This represents an intact triple helical conformation, despite the removal of the telopetides and the covalent inter-strand cross-links they provided. This was beneficial for atelo collagen and showed that the structure was not disrupted during pepsin treatment.

Polymeric type I collagen displayed a wide positive band centred at 214 nm, characteristic of random coils and no negative band. The change in the absorption wavelengths was evidence for alterations in the secondary structure, in terms of electronic transitions in the chain backbone or in the helically arranged side groups of collagen [302]. The spectra could imply that the natural cross-links found in the mechanically stronger polymeric collagen, hinder the coiled supramolecular assembly characteristic of monomeric collagen.

The CD spectrum of polymeric atelo collagen bore no resemblance to the broad positive band displayed for polymeric collagen, and instead showed a positive band (221 nm) similar to monomeric atelo collagen which displayed a RPN: 1.21

(native monomeric collagen, RPN: 0.117). This could suggest that the enzyme-catalysed procedure to cleave the telopeptides, also resulted in the destruction of the natural cross-links that differentiate polymeric collagen from monomeric collagen. Additionally, the difference between the molar ellipticity of the positive and negative peak for polymeric atelo collagen suggest some denaturation of the triple helical structure.

A temperature ramp between 20 and 60 ^{o}C was used to follow the denaturation of collagen triple helices to randomly coiled form. This could not be performed on polymeric collagen due to the lack of the characteristic 221 nm band maximum. Instead, it was used as a tool to examine the influence of telopeptides on the denaturation temperature of monomeric collagen (Figure 5.3-2).

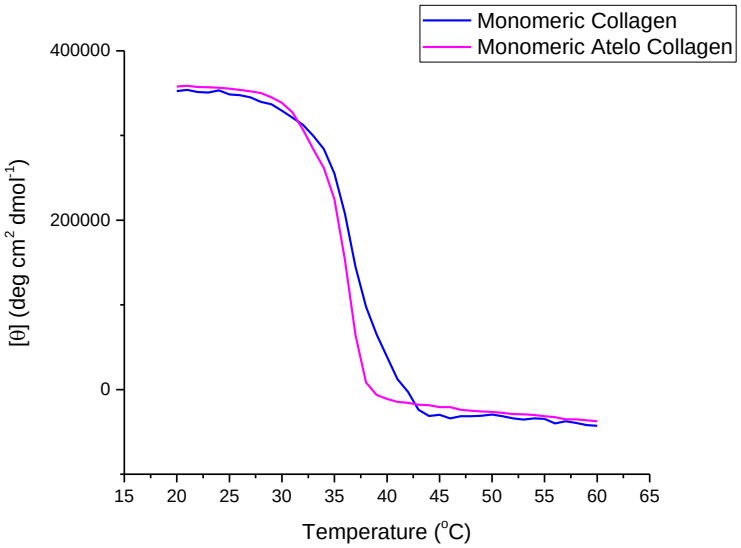

Figure 5.3-2 Temperature ramp CD of monomeric collagen and monomeric atelo collagen.

Denaturation temperature (T_d) was measured at half the initial molar ellipticity of the characteristic positive band (221 nm). For monomeric collagen, T_d was 36.5 ^{o}C and monomeric atelo collagen, T_d was 35.5 ^{o}C. These differing values could be due to the subdomain of collagen, and the roles that the C- and N-telopeptides provide for intermolecular covalent cross-links which help to stabilise the collagen triple helix; without these additional interactions, the atelo collagen triple helices denature at a lower temperature.

DSC was used to determine shrinkage, indicated by T_s, related to the thermal transitions of the collagens on heating and was employed in this study to investigate the effect telopeptide cleavage has on the thermal properties [303] (Figure 5.3-3).

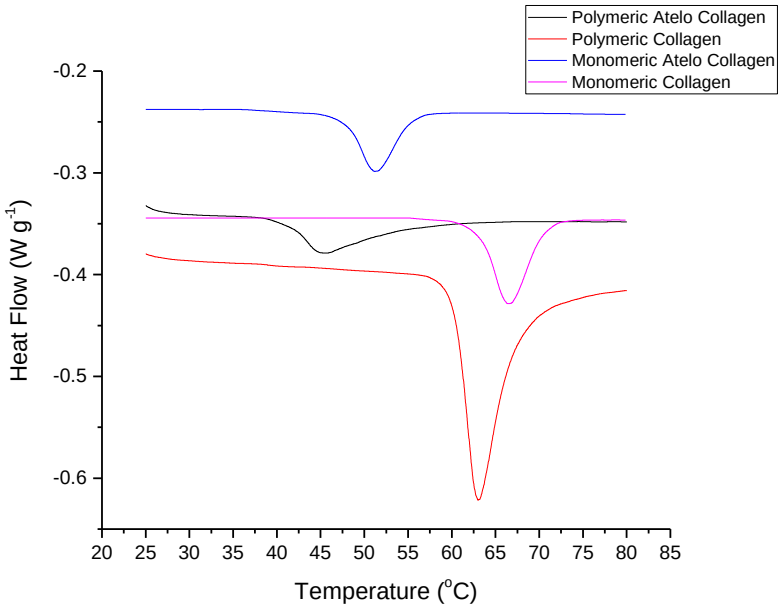

Figure 5.3-3 DSC data for polymeric atelo, polymeric, monomeric atelo and monomeric type I collagen.

Higher shrinkage temperatures (peak maximum) typically indicate a higher degree of intramolecular interactions between the collagen molecules. Telopeptide cleavage results in a smaller shrinkage temperature for both polymeric and monomeric collagen (Table 5.3-1). This can be contributed to the covalent aldol cross-links provided by the C- and N- terminus to the adjacent molecule. Monomeric atelo collagen possesses a higher peak maximum compared to polymeric atelo collagen, despite the additional natural cross-links specific to polymeric collagen. This pattern is again portrayed with polymeric and monomeric collagen. The reason for this could be due to the loss of the triple helical conformation of polymeric collagen which was shown by the CD spectrum.

Table 5.3-1 DSC data from polymeric atelo, polymeric, monomeric atelo and monomeric type I collagen.

Collagen Type I	Average Enthalpy ($W.g^{-1}$)	Average Peak Maximum (^oC)
Polymeric Atelo	-0.378	44.8
Polymeric	-0.621	62.7
Monomeric Atelo	-0.320	51.4
Monomeric	-0.432	66.5

High pressure liquid chromatography (HPLC) was used to determine the amino acid content (residues per 1000 residues) in polymeric atelo and polymeric type I collagen (Table 5.3-2). Monomeric collagen was not tested due to the polymeric-specific interest of Southern Lights Biomaterials.

Table 5.3-2 HPLC data from polymeric atelo and polymeric collagen displayed as residues per 1000 residues.

Amino Acid	Atelo Polymeric Collagen	Polymeric Collagen
Aspartic Acid	46.2	47.3
Threonine	16.2	16.4
Serine	34.1	33.2
Glutamic Acid	73.7	72.3
Proline	123	122.5
Glycine	337	334
Alanine	108	108.8
Valine	22.9	23.5
Methionine	6.3	6.6
Isoleucine	12.9	13.7
Leucine	25.2	26.3
Tyrosine	3.9	5.3
Phenylalanine	13.6	13.8
Histidine	5.7	5.9
Lysine	22.2	21.4
Arginine	52.0	52.6
Hydroxyproline	96.6	96.6

Hydroxyproline is formed intracellularly from the post-translational hydroxylation of proline and constitutes 10–14% of the total amino acid content of mature collagen [304]. The hydroxyproline content for both collagenous proteins was

9.66% of the total amino acid content (96.6 residues per 1000 residues) for polymeric collagen confirming to the literature value for mature (polymeric) collagen. Tyrosine is only present in the telopeptides of the collagen molecule and can be used as a measure of telopeptide cleavage [302]. Existing normally as 0.5% of the total amino acid content, a total content below 0.2% (2 residues per 1000 residues) is representative of atelo collagen [305, 306]. The amino acid sequence of the α(1) telopeptides are shown below for bovine type I collagen [307].

The free α (1) N-terminal telopeptide conformation:

GLU-LE-SER-TYR-GLY-TYR-ASP-GLU-LYS-SER-THR-GLY-ILE-SER-VAL-PRO

The free α (1) C-terminal telopeptide conformation:

SER-GLY-GLY-TYR-ASP-LEW-SER-PHE-LEU-PRO-GLN-PR-PRO-GLN-GLX-LYS-ALA-HIS-ASP-GLY-GLY-ARG-TYR-TYR-ARG-ALA

Polymeric collagen had a tyrosine total content of 0.53% and polymeric atelo collagen had a total content of 0.39%. A common misconception is that pepsin treatment leads to the complete cleavage of both the N and C-telopeptides, this is not true and is why the mark of atelo collagen is 0.2% tyrosine rather than 0%. The 3.9/1000 residues for polymeric atelo collagen is higher than the literature value, however, the previous data from CD and DSC showed a definitive difference between polymeric atelo and polymeric collagen which indicates that some telopeptide cleavage has occurred and the terminal cross-links have been disrupted. The higher tyrosine occurrence could be explained by means of telopeptide docking, whereby the free terminal structure docks onto the triple-helix chain as a staggered structure, so the tyrosine would still be accounted for in HPLC [308].

5.3.2 Physical Characterisation

SEM images were taken at varying magnifications to examine the internal material architecture (Figure 5.3-4)Figure 5.3-4 Fig. 3. SEM images: polymeric atelo collagen (A 30 magnification, B 2000 magnification, C 8000 magnification) and polymeric collagen ((D 30 magnification, E 2000 magnification, F 8000 magnification) Different morphologies are observed which shows the amorphous arrangement of collagen molecules and a loss of the collagen fibril structure after telopeptide cleavage.

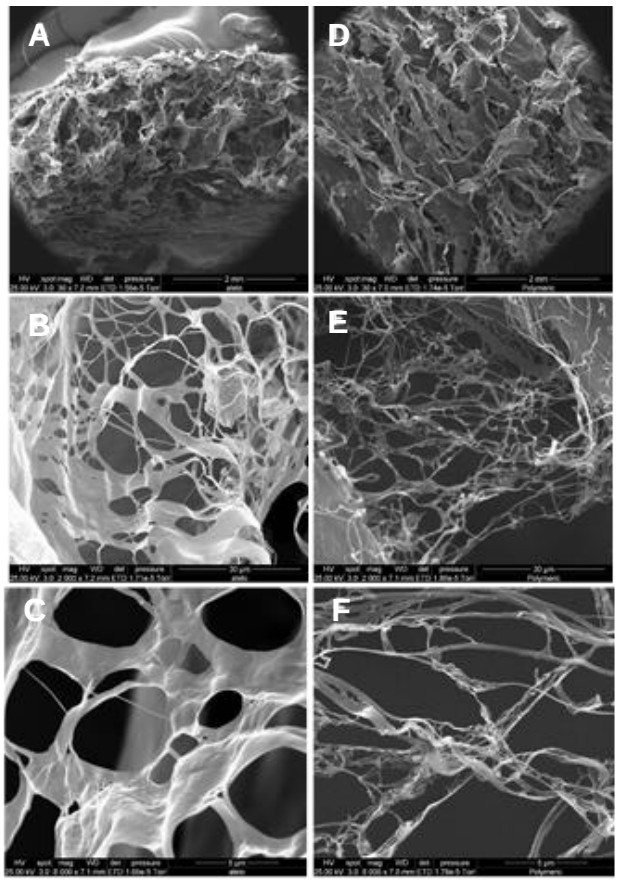

Figure 5.3-4 Fig. 3. SEM images: polymeric atelo collagen (A 30 magnification, B 2000 magnification, C 8000 magnification) and polymeric collagen ((D 30 magnification, E 2000 magnification, F 8000 magnification)

5.3.3 Telopeptides and Hydrogel Properties

Both RT and atelo monomeric collagen were functionalised with 4VBC (30 x excess) to form RTColl4VBC30 and AColl4VBC30. These were analysed chemically by TNBS assay and CD to determine degree of functionalisatoin (F) and triple helical preservation (RPN) before photopolymerisation to form hydrogels using UV light (365 nm) and I2959 (1% (w/v)). The physical parameters of the two collagen types were compared using gel content (G) and swelling ratio (SR) and the mechanical properties were compared using compression tests (E_c). (Table 5.3-3) [84].

Table 5.3-3 Chemical, physical and mechanical properties of 4VBC (30 x excess) networks using either RT or atelo type I collagen. Data presented as mean ± SEM.

Sample ID	F (mol.%)	RPN	G (wt.%)	SR (wt.%)	E_c (kPa)
RTColl-4VBC30	45 ± 4	0.14	97 ± 4	2065 ± 191	84 ± 17
AColl-4VBC30	44 ± 1	0.12	100 ± 0	1900 ± 200	81 ± 9

A molar content of primary amino groups of 3 x 10^{-4} mol·g^{-1} was measured via TNBS on atelo collagen in agreement with previously reported values despite the telopeptide cleavage. The amine content is primarily from the lysine group which is more prevalent in the helical domain of collagen. In the α1 polypeptide chain for human type I collagen, there are 38 lysine residues, 36 in the helical domain and 2 in the telopeptides [149]. Additionally, pepsin-treated atelo collagen does not result in full cleavage of the terminal telopeptides and is classified by a reduce tyrosine content from 0.5% to 0.2%, so similar TNBS results for the quantification of primary amino groups was to be expected [305, 306]. Functionalisation with 4VBC (30x) resulted in similar degrees of amino group conversion for both the RT and atelo collagen ~44%, therefore the nucleophilic substitution reaction was unaffected by telopeptide cleavage.

Far-UV CD analysis indicated typical dichroic spectral patterns of type I collagen for AColl4VBC30 in terms of a positive triple helix-related absorption band at 221 nm, and a negative absorption band around 198 nm, associated with the presence of polyproline chains. The ratio of positive and negative peak intensities (RPN) for AColl4VBC30 and RTColl4VBC30 were recorded as 0.12 and 0.14 similar to previous results [75].

The functionalised atelo collagen displayed improved solubility compared to the functionalised RT collagen as a result of the induced positive charge on the surface from telopeptide cleavage. This was beneficial because the high concentration of I2959 (1% (w/v) required to initiate the reaction can be detrimental to collagen solutions.

The high G value for both collagen types (97 and 100%) showed that the all the material was held together in a strong covalent network. Swollen hydrogels exhibited a swelling ratio of ~2000 wt.% and E_c ~80 kPa, confirming comparable

macroscopic properties for RT and atelo collagen despite the telopeptide cleavage [84].

5.3.4 Immune Response

Various biomaterial companies and numerous publications claim that telopeptide removal results in collagen that is non-immunogenic, or with low levels of immunogenicity due to little inter-species variation in the amino acid sequence of the central, helical segment collagen [309].

A statement from the Koken website reads: *"Since the telopeptides are not present in atelocollagen, the antigenicity of atelocollagen is even lower than that of collagen"*

This is very misleading.

The location of the major antigenic sites on the collagen molecule varies depending on the donor/ recipient species pairing and can be from the terminal telopeptides, central (amino acid sequence) or helical (3D conformation). When calf collagen was transferred to a rabbit, the major antigenic site was from the terminal telopeptides and in comparison, when calf collagen was transferred to a rat, the major antigenic site was helical [77, 87]. No study has been made on the major antigenic sites when bovine collagen is transferred to humans, and as of yet there is no proof that the antigenicity of atelo collagen is lower than that of collagen.

It is also a misconception that pepsin-treatment completely removes the telopeptides. In fact, Herman *et al*, documented that atelo collagen can be characterised by a tyrosine count of 2/1000 residues which is the figure still used today [305]. This questions whether the antigenic activity of the atelo collagen would even be distinguishable compared to non-treated collagen if it was shown that the major antigenic site from bovine/ human pairing is the terminal telopeptides.

5.4 Conclusions

The influence of telopeptides on the structural and physical properties of polymeric and monomeric collagen was investigated. Monomeric atelo collagen displayed the characteristic positive band at 221 nm on the CD spectrum associated with the triple helical conformation of collagen. This implies that

despite the covalent aldol cross-links provided by the telopeptides, their cleavage does not disrupt the natural collagen structure. It was found that polymeric collagen did not display the characteristic positive peak at 221 nm, thereby implying that the natural cross-links associated with mature collagen disrupt the native triple helical structure. The presence of the negative peak in atelo polymeric collagen could imply that the harsh pepsin treatment to cleave the telopeptides, could be disrupting the mature cross-links and would therefore no longer be termed polymeric. The shrinkage temperature was shown to decrease after telopeptide cleavage for both monomeric and polymeric collagen, likely due to the reduced intramolecular aldol covalent cross-links attributed to the telopeptides.

Whilst atelo collagen is beneficial in terms of increased solubility, it was decided that its prevalence in the literature and in collagen-based biomaterial companies was far overstated. Macromolecular features of a protein not common to the host species is more likely to encourage an immune response than shared features, so atelo collagen *could* provide a mildly lower level of immunogenicity. This is because there is little inter-species variation in the amino acid sequence of the central, helical segment, although this is unknown and could be grossly overstated [77, 87].

Chapter 6 – Discussion and Future Work

6.1 General Discussion

The aim of this project was to design defined collagen-based hydrogel networks to investigate stiffness-induced cell differentiation for skeletal muscle tissue engineering.

The field of tissue engineering and regenerative medicine has evolved rapidly in the last two decades. The core aim of the field is to enhance the body's innate healing capacity using a combination of bioactive scaffolds, cells and chemical and physical cues to achieve improved clinical outcomes for the patients.

The general approach requires the development of a material that can support cells by providing a surface for adherence, a template for new tissue growth and a mechanical environment that can withstand the forces at a given site in the body. The influence of the microenvironment in which a cell is situated was discussed in chapter 1, whereby cells adhering to the ECM can sense the mechanical properties through specific interactions of cell surface integrins and from 'pulling' on the surface, these interactions influence cytoskeletal tension and lead to changes in cell shape, cell proliferation and can be used to direct cell fate.

Hydrogels represent a rapidly growing niche in tissue engineering because their 3D water-swollen environment mimics *in vivo* conditions more than traditional cellular monolayers. Collagen-based hydrogels are gaining widespread popularity due to the abundance of collagen in the ECM and their natural cell-recognition sites and biocompatibility. A disadvantage of self-assembled collagen hydrogels is that there is a degree of variability depending on the tissue source and gelation pH and temperature. They also lack the mechanical properties of native tissues (E_{muscle} ~ 8-16 kPa). One method to address this challenge is to chemically cross-link collagen or to incorporate varied natural/ synthetic polymers to create a hybrid hydrogel.

There are many techniques currently being investigated to permit collagen hydrogels to be used for cell encapsulation or for injectable devices. Fundamentally this would require the use of a non-toxic catalyst or photoinitiator,

low temperatures (>37 ^{o}C), cell-friendly light source and fast gelation times (clinically acceptable time-scale) for an injectable device.

Click chemistry is a technique that invokes fast reaction times, high yields, is insensitive to ambient oxygen or water and typically requires a lower concentration of photoinitiator or catalyst than traditional reactions. There have been studies that have incorporated click chemistry with natural hydrogels as means to create tissue engineered constructs which benefit from the combined fast, high yielding reactions with added biocompatibility and natural cell attachment sites of the natural polymers [98-100, 111, 183]. Far fewer have incorporated collagen, likely due to the retrosynthetic restrictions, and to date, no papers could be found which used a thiol-ene reaction to prepare collagen hydrogels [93].

6.1.1 Development of Functionalised Collagen Precursor Materials for Click Chemistry

The objective of chapter 2 was to develop a facile, non-toxic means to functionalise collagen abiding by retrosynthetic considerations represented in terms of solubility, non-harmful reagents/ solvents, low reaction temperatures, occurrence and availability of functional groups and most importantly, the preservation of the triple helical conformation.

The rationale for using collagen and the need to modify/ cross-link it prior to its use as a biomaterial for skeletal muscle tissue engineering (SMTE) has been discussed. Thiol click chemistry appeared to be an appealing and novel route to cross-link collagen to form hydrogels with fast gelation times and low catalyst concentrations.

This was an achievable approach and it was easy to access thiol and ene reagents that could react with the available amine group on collagen by nucleophilic substitution or addition.

Collagen-2IT and collagen-NAC were two thiol-precursors that were prepared in this chapter and it was shown that the degree of functionalisation could be controlled by the ratio of [Lys]:[2IT] with good preservation of the triple helix conformation. To date, no literature of collagen functionalised with NAC to produce collagen-NAC was found and whilst collagen-2IT had been reported, the method required the immersion of pre-formed collagen scaffolds with resulting low conversions (1%) [179-181]. In comparison, the systematicaly developed method from this work reported thiol-conversions of up to 80%. This

method of thiol-functionalisation meant the collagen-2IT could be dissolved in PBS (0.01 M) and therefore opened the door to the possibility of using it for cell encapsulation.

Collagen-norbornene was synthesised as a non-homopolymerisable thiol-ene precursor reagent. This method however, was not facile and due to the poor solubility of the norbornene reagent, DMSO had to be used as the solvent. It was not desirable to use collagen-norbornene due to the retrosynthetic implications. Instead collagen-GMA and collagen-4VBC were considered as potential Michael-acceptors in the thiol Michael-addition reaction and multi-arm PEG norbornene terminated was selected as a water-soluble precursor material for the thiol-ene reaction. PEG benefits from adjustable mechanical properties, the ability to maintain high volumes of water, easy to modify end groups and it has been approved by the Food and Drug Administration (FDA) for various clinical applications.

An analysis of three water-soluble photoinitiators in terms of relative cell survival, light absorbance and collagen suitability was performed as a prerequisite before the development of a novel cross-linking strategy. The results showed that LAP and I2959 were more suited to the reaction that eosin Y/ TEOA.

6.1.2 Systematic Development of Collagen Click Chemistry Hydrogels

The objective of chapter 3 was to examine novel synthetic strategies for cross-linking collagen to prepare defined covalent networks with reliable, varied molecular architecture and substrate stiffness.

Five requirements were set up during the systematic development process to allow application as an *in situ* injectable device or for *in vitro* encapsulation:

- All the reagents should be cell-friendly/ bioinert.
- The precursor materials should be water- soluble for dissolution in PBS or basal media.
- A low concentration of photoinitiator/ catalyst should be used to ensure good cell viability and cytocompatible hydrogel formation.
- Fast gelation times to ensure minimal cell-damage particularly if a UV light source is required.
- Facile, accurate means to provide tunable mechanical/ physical properties to represent ECM of muscle tissue.

The Michael-addition reaction was attempted with both collagen-NAC and hexa(ethylene glycol) dithiol as the Michael-donors, and collagen-GMA and PEG diacrylate as the Michael-acceptors. These reactions were attempted using varied pH with and without a base catalyst, however, no reaction occurred. This could be due to the nature of the thiol group (pK_a) and the corresponding thiolate species, base catalyst strength, steric bulk of the thiol and how susceptible the carbon double bond was for nucleophilic attack (nature of the EWG). Another explanation could be due to the slow reaction times for Michael-addition which have been reported in other papers (~ hours) [80, 104].

At the time, the electron deficient double bond and the structure and pK_a of the thiol group were considered the most important factors impacting the reaction rate. Concern was had over the high pK_a of the collagen-NAC and it was thought that the additional alkyl group gained from functionalisation of NAC with collagen, may have further increased the pK_a of the thiol hydrogen. Additionally, there could be issues due to the viscosity of the collagen solution which could impede the Michael-addition reaction. It was also noted that the considerations set out for cell-hydrogel *in situ* encapsulation were not being followed. The base catalyst was not cell-friendly and neither was the pH of the solution and the collagen-NAC was only soluble in weak acetic acid solutions rather than PBS. The cross-linking method was supposed to be simple, robust, and highly effective under mild reaction conditions, so Michael-addition was abandoned.

Thiol-ene reactions require a double bond incapable of homopolymerisation for a true step-growth mechanism. There are many cases in the literature where it has been claimed that a thiol-ene reaction, or a mixed step-and-chain growth reaction was taking place between PEGdA and a dithiol, when actually the most dominant reaction was more likely from chain-growth polymerisation [310].

As mentioned, collagen-norbornene had been synthesised although this was not used due to its harsh reaction conditions and poor solubility. Instead, 4-arm (PEG4NB) and 8-arm PEG norbornene (PEG8NB) terminated water-soluble macromers were selected.

The hydrogel properties were compared using both PEG4NB or PEG8NB with collagen-2IT (1 wt.%). Lower gel content and lower compressive moduli were recorded when used with PEG4NB compared to PEG8NB. It was thought this was due to the ratio of SH:NB, and the proceeding experiments used PEG8NB in addition to collagen-2IT (due to its solubility in PBS) and either LAP or I2959 at 365 nm.

Photoinitiators had been discussed in chapter 1 and chapter 2 and I2959 and LAP were both recognised as water-soluble materials capable of releasing radicals when exposed to UV light at 365 nm. The maximum absorption wavelength of LAP is 380 nm, with a high absorbance still recorded at 365 nm (molar extinction coefficient (ε): 218 $M^{-1} \cdot cm^{-1}$) [132]. In comparison, I2959 had a peak maximum at 285 nm, where it also displayed competing absorbance with the aromatic amino acids in collagen, whilst displaying minimal absorbance at 365 nm (ε: 4 $M^{-1} \cdot cm^{-1}$) [132]. The competing absorbance and low molar extinction coefficient (365 nm) meant a higher concentration of this photoinitiator can be required to generate a sufficient number of radicals to initiate a reaction, although this again is inhibited due to the poor solubility of I2959 in aqueous solutions. This was demonstrated with the work by Tronci *et al.* Two vinyl containing moieties, collagen-GMA and collagen-4VBC were reported to require I2959 (1% (w/v) and UV light exposure ~30 minutes for gelation to occur, whereas synthetic molecules with no competing absorbance from aromatic amino groups require I2959 (≤ 0.1% (w/v)) with complete curing times less than 5 minutes [75, 79, 130, 189].

These two photoinitiators were compared using a UV photo-rheometer with collagen-2IT and PEG8NB. The time to complete gelation was taken at G'_{max}. LAP-initiated reactions were significantly faster the I2959-iniated reactions. The gelation time for LAP (0.5% (w/v)) was 187 seconds and LAP (0.1% (w/v)) was 279 seconds. In comparison I2959 (0.5% (w/v)) was 1683 seconds and I2959 (0.1% (w/v)) was 1496 seconds. There was an average 7-fold decrease in gelation time when using LAP rather than I2959. The competing absorbance when used in conjunction with collagen due to the aromatic amino acids absorbing at ~265 nm and the light source at 365 nm (I2959, A_{max} ~ 280 nm) made I2959 a poor photoinitiator for this application.

Interestingly, the success of the step-growth reaction compared to the chain-grown reaction can be observed in the halved concentration of I2959 required to complete the reaction 0.5% (w/v) compared to 1% (w/v) previously reported by Tronci *et al*, likely due to its insensitivity to ambient oxygen or water and therefore lower radical concentration required to start the reaction [79].

In chapter 2, the cell survival results for LAP, 0.1 and 0.5 % (w/v) made it clear that for cell-encapsulation to be viable, less than 0.1% (w/v) should be used to prevent photoinitiator induced cytotoxicity. However, the results from the previous experiment showed a 15-fold decrease in the storage modulus when the concentration of photoinitiator was reduced, LAP (0.5% (w/v)) was 3360 Pa

and LAP (0.1% (w/v)) 232 Pa. This was likely due to an insufficient release of enough radicals to complete the click chemistry reaction, thus resulting in fewer thiol-norbornene cross-links and a hydrogel with reduced storage modulus. Unfortunately, due to these results, the application of cell-hydrogel encapsulation or *in situ* injectable devices had to be abandoned using LAP and I2959.

It was still in the interest of this work to develop hydrogels with varied mechanical properties to investigate stiffness induced differentiation of myoblasts to myotubes. In the literature, it was shown that the mechanical properties of thiol-click hydrogels could be controlled by the thiol/ene ratio, PEG molecular weight and architecture or polymer concentration [110, 184]. Tronci *et al* also stated that mechanical properties could be tuned by cross-linker type and density.

Previous work in chapter 2 showed that the degree of functionalisation of the collagen backbone could be controlled by the ratio of [Lys]:[2IT], thus providing a means for the cross-link density to be controlled. The cross-link type had been changed by comparing PEG8NB to PEG4NB with E_c recorded as 4.3 and 2.8 kPa respectively. This could have been used as a way to control the mechanical properties but the low gel content of the PEG4NB hydrogels made their use undesirable. For the same experiment gel content was 85 and 58 wt.% respectively, so all the material for PEG4NB was not held together in a covalent network.

The mechanical properties were shown to be easily tailored by controlling the thiol/ene ratio with the PEG8NB concentration. CollPEG2 to CollPEG4.5 were shown to have varied mechanical and physical properties G' 0.5 to 6.4 kPa, E_c 1.5 to 13 kPa and SR 1530 to 3010 wt.%.

Of these photo-click hydrogels, collPEG3.5, collPEG4 and collPEG4.5 were taken forward in the cell culture experiments due to their similarity to the elasticity of muscle (E_c ~ 7,10 and 13 kPa) in order to examine how matrix elasticity effects the myoblast cells in terms of spreading, proliferation and maturation/ differentiation. The small difference in elasticity ~ 6 kPa was assumed to be sufficient to provide statistically significant results due to work by Engler at al which reported a narrowness in the optimum substrate compliance for C2C12 differentiation in culture [56].

6.1.3 Cell Attachment, Spreading, Proliferation and Differentiation on Hydrogels with Varied Elastic Moduli

The objective of chapter 4 was to perform *in vitro* tests with a myoblast cell line to examine cell attachment, spreading, proliferation and differentiation when

cultured on three photo-click hydrogels with elastic moduli similar to that of natural muscle.

These hydrogels are new materials and the first crucial step was to examine their cytocompatibility with cells. This was done using both an extract and a direct cytotoxicity test.

The extract test is often used to provide an initial first impression of the cytotoxicity which is said to be consistent with the results of animal toxicity tests, there was no significant difference between the three hydrogels and the control for this test which was beneficial.

The direct cytotoxicity test is more reflective of the *in vitro* success of the device. Results showed that the number of cells on the hydrogel at each timepoint was generally lower than the tissue culture plastic control, however, this was predicted to be due to initial cell attachment. From the results, a significantly higher number of cells were observed on day 5 compared to day 1 for all three hydrogels which confirmed that there was no direct cytotoxic effects as a result of the material.

Cell adhesion 3 hours after seeding was examined. The tissue culture plastic control showed a statistically higher number of cells attached to it compared to the three hydrogels. However, tissue culture plastic is plasma treated prior to distribution to improve cell attachment by incorporating more oxygen onto the surface, rendering it more hydrophilic. The flat tissue culture plastic also provides more contact surface. In comparison, the hydrogels have not been plasma treated and are more porous than the tissue culture plastic (less contact surface) so it is expected that tissue culture plastic outperforms the hydrogels in terms of attachment. Despite the varied stiffness' of the three hydrogels, there was no significant difference between the cell attachment after 3 hours with C2C12 cells.

Cell spreading was examined after 24 hours and unlike the cell seeding experiment where the tissue culture plastic outperformed the hydrogels, all results showed that no material promoted a statistically higher degree of cell spreading after 24 hours. It was assumed that differing elastic moduli would effect cell spreading, however, these results were mirrored in work by Engler *et al*. After 24 hours, this work showed that spreading on the stiffest hydrogels and the glass control were statistically similar in terms of cell area [56]. This indicated that with time, spreading was less dependent on substrate elasticity. Another similarity between the results from this work and the results by Engler *et al* was that the highest mean cell area was reported on the control. The control had a

stiffness of ~3 MPa rendering it supraphysiological and does not agree with previous reports that dictate that substrate stiffness effects cell spreading on tissue-like elasticities.

Cell proliferation was examined and there was no statistical difference between the three hydrogels despite the varied stiffness' of the substrates. The proliferation on the tissue culture plastic control was shown to have the highest mean result although not statistically higher when compared with the three hydrogels.

Cells were stained with f-actin and the cell morphology was visualised on day 0, 3 and 7 as the nuclei began to fuse together. It was noted that the myoblast cells appeared more 'clumpy' on the hydrogels at day 0 compared to the tissue culture plastic control likely due to the surface topography. However, once the cells began to fuse together this observation was no longer true and myotube formation was observed from day 3 in a random alignment.

Fusion index was calculated, however, no statistical significance was observed between the three hydrogels or the tissue culture plastic control at day 3 or 7 of maturation/ differentiation. Although at day 7, these samples were shown to have significantly higher percentage of myotubes with five or more nuclei (large myotubes) compared to smaller myotubes.

The myosin expression and degree of maturation/ differentiation was statistically higher at day 7 compared to day 3 for all of the samples. The tissue culture plastic control showed a higher level of myosin expression and a higher degree of maturation/ differentiation compared to the hydrogels with a statistically higher expression compared to collPEG3.5 on both days of the study. Due to the three varied stiffness' of the hydrogels, it was expected that that the C2C12 cells would mature/ differentiate preferentially on the stiffness closest to that of natural muscle. However, it would appear that in terms of myosin expression, there was no statistical difference between the three hydrogels.

It has been reported that substrate elasticity plays an important role in cell fate and by recapitulating the elasticity of muscle tissues, you can create an appropriate microenvironment for *in vitro* cell culture [56, 57]. The elasticity of the hydrogels used during this work were ~ 7, 10 and 13 kPa similar to muscle. On the cellular scale, the cells probe elasticity as they anchor and pull on their surroundings. This could be difficult for the cells to do on the collagen-PEG hybrid hydrogel due to the high fibrillar arrangement of the hydrogel – collagen, 1 wt.% and PEG8NB 3.5- 4.5% (w/v) and because the cells were cultured on top of the

hydrogel rather than encapsulated inside it. It is possible that rather than migrating inside the hydrogel, the cells remained and grew on top due to the high concentration of material. This would mean the cells would ‘feel’ more from their cell-cell interactions rather than the cell-substrate interactions.

6.1.4 Immune Response to the New Photo-Click Material

The objective of chapter 4 was to study the body’s immune response to the new material using an *in vivo* subcutaneous model. This work lead into chapter 5 which examined atelo collagen as a potential non-immunogenic material.

The photo-click hydrogels developed during this project are new materials and for this reason, it was important to analyse the host response to them. Once implanted, the innate immunity takes a matter of hours to respond to the material, whereas adaptive immune response takes at least 4 days. Similarly acute inflammation can develop in minutes and last for days, whereas chronic inflammation takes over this process if the injury is prolonged. From this knowledge, it was decided that the time points to analyse the subcutaneous model would be 1, 4 and 7 days.

Geistlich Mucograft® was chosen as the commercial control for this study. It is composed of a collagen matrix with a dual, macro and spongey microstructure and is used for soft tissue (muscle) regeneration. However, the dual structure proved difficult to handle in surgery compared to the hydrogel, and the material almost wanted to slide apart from each other when handling which made it difficult to place. In comparison, the fact that the hydrogel was stiff and had good shape memory (after sterilisation, the hydrogel would rehydrate back to its original volume and shape) made it easy to handle. The hydrogel was a better construct material in this sense. Although if the hydrogel was cell-laden it would be more difficult to handle.

The response to the Mucograft® after 4 days appeared to very minimal in comparison the hydrogel (Figure 6.1-1).

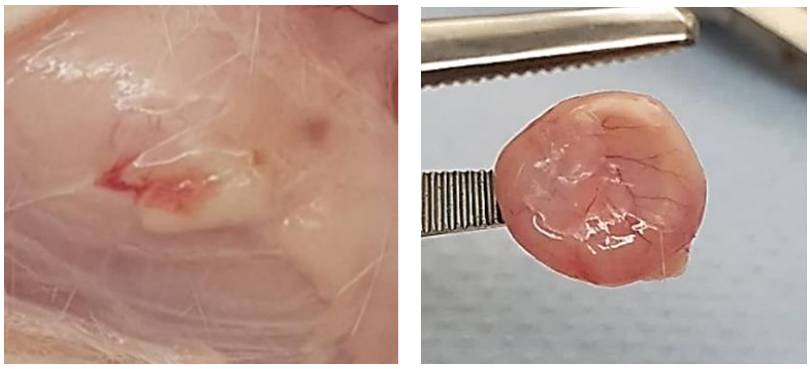

Figure 6.1-1 Day 4 after implantation. Left, Mucograft® and right, hydrogel.

The hydrogel showed signs of inflammation compared to the surrounding tissue and blood vessels have formed to cover the surface (angiogenesis) both indicative of the body's immune response to the material. Inflammatory microenvironments can drastically limit the integration of biomaterials with surrounding native tissue. In comparison, the Mucograft® sample does not appear to have any inflammation in the surrounding tissue and the sample has very poor integration, so rather than being cut out, like the hydrogel, the material 'popped' out of the tissue instead.

At day 4, all four of the Mucograft® samples 'popped' out, whereas only one of the hydrogel samples did, the rest had to be cut out, thus indicating no tissue integration of the Mucograft®, despite it being a foreign material.

It would be expected that by day 4 the adaptive immunity would have kicked in, with a provisional matrix already deposited and blood vessels formed to deliver various immune cells to the site. By day 7, the Mucograft® had integrated more with the tissue with only one sample 'popping' out during sample retrieval. There was no dense surrounding population of cells indicative of the immune response and blood vessels had appeared near the base of the scaffold. The immune reaction to Mucograft® was favourable, with minimal inflammation, no strong immune response and no degradation or change in shape throughout the study. However, at each time point, the cells which had infiltrated into the scaffold, appeared just as nuclei with no surrounding stained cytoplasm which raised questions about cytotoxicity. After correspondence with Geistlich, it was discovered the lyophilisation of the material can make Mucograft® very hydrophobic, even though it is reported to have excellent hydrophilicity. The hydrophobicity could explain the reduced immune response and poor health of the infiltrated cells because methods of immunomodulating biomaterials include

altering hydrophilic/ hydrophobic and thereby the protein affinity from the interstitial fluids.

The photo-click hydrogels were designed to mimic muscle tissue in terms of matrix elasticity, and ultimately to repair tissue and encourage biomaterial integration. However, the intended application is heavily affected by the body's response to the material composition, structure and surface properties and there is no point in designing a new system if it is ultimately destroyed by the influx of inflammatory cells.

The outcome of biomaterial implantation varies depending on the extent of the foreign-body response and subsequent processes of inflammation and wound healing. Both materials held their own benefits in this study, Mucograft® presented a lower immune response and reduced inflammation, whereas the hydrogel, with its immune response promoted angiogenesis, which is beneficial later for muscle regeneration and leaves the paradigm of whether to evade or evoke the host immune system and to what extent.

Chapter 5 investigated the use of atelo collagen as a potential non-immunogenic form of the material. It was decided that whilst atelo collagen was beneficial in terms of increased solubility, its prevalence in the literature and in collagen-based biomaterial companies is overstated. It was also deduced that it was a misconception that pepsin-treatment completely removes all collagen telopeptides and some remain behind. Herman *et al* documented that atelo collagen can be characterised by a tyrosine count (amino acid present only in the telopeptides) of 2/1000 residues which is the figure still used today [305]. The leftover telopeptides questioned whether the antigenic activity of the atelo collagen would even be distinguishable compared to non-treated collagen if it was shown that the major antigenic site bovine/ human is from the terminal telopeptides.

Hydrogels prepared from atelo collagen and RT collagen displayed similar chemical, physical and mechanical properties which suggested that collagen functionalisation with 4VBC occurs primarily in the helical segment of collagen and was not affected by telopeptide cleavage.

6.1.5 Biomaterial-Based Approach for Bone Formation

Injury to either tissue, whether muscle, tendon or bone compromises the physical function of the trauma-exposed extremity and interest lay in recreating the muscle-tendon-bone bridge. Due to the similarity in elasticity of the collPEG4.5 to muscle and collagen-4VBC to pre-calcified bone, a gradient hydrogel could have been created to mimic the hard-soft gradient of natural tissue such as bone, tendon, muscle and skin. Collagen-4VBC hydrogels were tested in a preliminary study using a calvarial defect model as a purely biomaterial-based approach for bone formation. Time points of 2 and 6 weeks were used with commercially available Bio-Gide® as the positive control. Bio-Gide® was shown to encourage bone formation to a greater extent than collagen-4VBC with 38.2% new bone formation after 6 weeks *in vivo* compared to collagen-4VBC which displayed 20% new bone formation and the application of gradient hydrogels using collagen-4VBC was abandoned.

6.2 Future Work

Presented within this thesis is the design of a new cross-linking method to prepare collagen hybrid hydrogels using thiolated collagen and multi-arm PEG norbornene by a step-growth thiol-ene reaction.

Future work should employ strategies to allow this cross-linking method to be incorporated with *in vitro* cell encapsulation to provide cells with a 3D environment. The main issue with cell encapsulation was with the UV-photoinitiator required, and whilst this new reaction mechanism meant half the previous amount of photoinitiator was required to form collagen hydrogels due to the rapid, ambient reaction conditions of the step-growth mechanism, the concentration was still too high for practical cell viability. Instead, future work should explore using eosin Y as the only visible-light photoinitiator.

Eosin Y was shown to be non-toxic and uses a cytocompatible visible-light source. This was used with a co-initiator, TEOA in chapter 2 to sufficiently cleave the hydrogen from a PEGdA group. However, the TEOA was shown to be an inappropriate material to use with collagen. Alternatively, it has been shown that eosin Y can be used as the sole photoinitiator with the thiol-norbornene reactions with appropriate design considerations [131]. Shih *et al* reported that the gelation and cross-linking efficiency of visible light initiated thiol-norbornene hydrogels was significantly improved by incorporating soluble tyrosine to mediate the

deprotonation of the bisycysteine peptide [186]. It would be beneficial to research reagents (e.g. tyrosine) that could increase the efficiency of the eosin Y mediated deprotonation of collagen-2IT, so that photo-click hydrogels could be prepared in a cytocompatible manner using visible light, thus enabling cell encapsulation.

As a construct material for SMTE, the photo-click hydrogels need to be improved to encourage the parallel arrangement of myotubes. This could be done by micro-patterning the surface by moulding or printing to create nanoscale channels or micro tunnels. This should firstly encourage the alignment of myotubes and promote cell fusion, and secondly, it should enable the recreation of the vasculature system needed for the construct material to be viable.

Further work could also focus on improvements to the cell attachment, spreading and immune response of the material to encourage their appeal as novel biomaterials. It would be more preferable to have a material that significantly increased cell attachment and cell spreading. Anseth *et al*, reported a synthetic method to modify PEGdA with the adhesive Arg-GlyAsp (RGD) peptide sequence which significantly increased the adhesion and spreading of rat osteoblast cells [311]. This was also shown in work by Chadhuri *et al* which used carbodiimide chemistry to incorporate a peptide sequence into an alginate gel. Spreading was shown to increase significantly with increased RGD concentration for both gels (150 µM compared to 1,500 µM RGD in a 2% wt/vol alginate gel) [312]. It has been shown that PEG hydrogels can be used to load growth factors such as basic fibroblast growth factor and vascular endothelial growth factor during hydrogel formation [313, 314]. These transmit signals to modulate cellular activities and it would be very beneficial to incorporate them into the hydrogel. In terms of immunomodulation, nitric-oxide releasing hydrogels have been shown to reduce thrombogenesis and inflammation following the surgical implantation, with sustained release reported with PEG hydrogels [143, 144, 315].

Collagen-2IT provides a source of type I collagen with an available thiol group for facile, high yielding thiol click reactions. It benefited from improved solubility and preservation of the natural triple helical conformation. The main applications of collagen are for sutures, burn/ wound dressings and bone composites. By replacing the collagen for collagen-2IT in these applications, it could provide a

facile route for incorporation of drugs, antimicrobial agents or growth factors by either click reaction or by coatings due its improved hydrophilicity [194].

6.3 Conclusion

The five main objectives for this project were outlined in the introduction (i) to functionalise collagen with either thiols or vinyl groups using facile, non-toxic method whilst keeping the triple helical conformation intact; (ii) examine novel synthetic strategies for cross-linking and the formation of defined covalent networks with reliable, varied molecular architecture and substrate stiffness; (iii) chemical, physical and mechanical characterisation of hydrogels; (iv) *in vitro* tests with a myoblast cell line to examine differentiation and proliferation; and (v) *in vivo* subcutaneous model on best performing hydrogel to analyse the immune response, with the aim to design defined collagen-based hydrogel networks to investigate stiffness-induced cell differentiation.

Collagen was functionalised with several different reactive moieties. Of these, the successful new products were collagen-NAC and collagen-2IT which were both deemed thiolated collagen and were prepared using novel methods that were systematically constructed.

Thiol click chemistry such as Michael-addition or the thiol-ene reaction was examined as the novel synthetic strategy for cross-linking. A thiol-ene reaction was successfully incorporated with collagen to form novel photo-click collagen-PEG hybrid hydrogels. These were easy to perform and highly reproducible. Good control was had over the mechanical properties by altering the thiol/ ene ratio and six hydrogels with varied mechanical and physical properties were prepared with fast gelation kinetics. The downfall was that the concentration of photoinitiator required was still too high for cell-encapsulation. As discussed in the future work, there could be improvement made with these hydrogels as visible-light initiated devices with eosin Y as the photoinitiator.

In vitro tests were performed with a myoblast cell line to examine cell attachment, spreading, proliferation and differentiation of three of these hydrogels. They were shown to support cell spreading and were cytocompatible with cells. The surface topography of the hydrogels made the cells grow in a more ‘clumpy’ manner than on tissue culture plastic, however, when differentiation media was added, they fused into myotubes with no issue. The downfall of these experiments was that there was no statistical significance between the three hydrogels even though

they possessed different elastic moduli (~ 7, 10, 13 kPa). It was concluded that the myoblasts were responding to cell-cell interactions more than cell-matrix interactions and were growing on top of the hydrogels rather than migrating inside of them. This could mean the cells experienced the tissue-mimetic elasticity less than if they had been encapsulated inside prior to gel formation.

An *in vivo* subcutaneous model was performed which showed a higher degree of host immune response to the hydrogel than to the commercial control, Mucograft®. However, it was proposed that the focus of modern biomaterial design should shift from evasion of the host immune system to an orchestrated interaction with it in order to encourage the natural healing process.

References

[1] J. Vacanti, C. Vacanti, The History and Scope of Tissue Engineering, in: R. Lanza, R. Langer, J. Vacanti (Eds.), Principles of Tissue Engineering, Elsevier2013.
[2] R. Langer, J. Vacant, Tissue Engineering, Science 260 (1993) 920-926.
[3] M. Tate, Top down and bottom up engineering of bone, Journal of biomechanics 44(2) (2011) 304-12.
[4] Y. Liu, S. Mai, N. Li, C. Yiu, J. Mao, D. Pashley, F. Tay, Differences between top-down and bottom-up approaches in mineralizing thick, partially demineralized collagen scaffolds, Acta biomaterialia 7(4) (2011) 1742-51.
[5] J.W. Nichol, A. Khademhosseini, Modular Tissue Engineering: Engineering Biological Tissues from the Bottom Up, Soft Matter 5(7) (2010) 1312-1319.
[6] D.L. Elbert, Bottom-up tissue engineering, Curr Opin Biotechnol 22(5) (2011) 674-680.
[7] J. Huard, Y. Li, F. Fu, Muscle injuries and repair: current trends in research, J Bone Joint Surg Am 84 (2002) 822-832.
[8] A.R. Gillies, R.L. Lieber, Structure and Function of the Skeletal Muscle Extracellular Matrix, Muscle Nerve 44(3) (2011) 318-331.
[9] T.A.H. Järvinen, T.L.N. Järvinen, M. Kääriäinen, H. Kalimo, M. Järvinen, Muscle Injuries: Biology and Treatment, The American Journal of Sports Medicine 33(5) (2005).
[10] M. Sandri, Autophagy in skeletal muscle, FEBS Letters 584(7) (2010) 1411-1416.
[11] N.J. Turner, S.F. Badylak, Regeneration of skeletal muscle, Cell and Tissue Research 347 (2012) 759-774.
[12] B. Crow, J. Haltom, W. Carson, W. Greene, J. Cook, Evaluation of a novel biomaterial for intrasubstance muscle laceration repair, J Orthop Res 25(3) (2007) 396-403.
[13] J.M. Grasman, M.J. Zayas, R.L. Page, G.D. Pins, Biomimetic scaffolds for regeneration of volumetric muscle loss in skeletal muscle injuries, Acta Biomaterialia 25 (2015) 2-15.
[14] C. Barakat-Haddada, S. Shin, H. Candundo, P.V. Lieshout, R. Martino, A systematic review of risk factors associated with muscular dystrophies, Neuro Toxicology 61 (2017) 55-62.
[15] F.S. Tedesco, A. Dellavalle, J. Diaz-Manera, G. Messina, G. Cossu, Repairing skeletal muscle: regenerative potential of skeletal muscle stem cells, J Clin Invest 120(1) (2010) 11-19.
[16] A. Emery, The muscular dystrophies, Lancet 23 (2002) 687-695.
[17] A.K. Abbas, A.H. Lichtman, S. Pillai, Cellular and Molecular Immunology, Eighth ed., Elsevier Saunders Philadelphia, 2015.
[18] S. Barrientos, O. Stojadinovic, M. Golinko, H. Brem, M. Tomic-Canic, Growth factors and cytokines in wound healing, Wound Repair Regen 16(5) (2008) 585-601.
[19] G. Brounghton, J. Janis, C. Attinger, The basic science of wound healing, Plast Reconstr Surg 117 (2006) 12S- 34S.

[20] S. Werner, R. Grose, Regulation of wound healing by growth factors and cytokines, Physiol Rev 83(3) (2003) 835-870.
[21] M. Sweetwyne, J. Murphy-Ullrich, Thrombospondin1 in tissue repar and fibrosis: TGF-beta-dependent and independent mecahnisms, Matrix biology 31(3) (2012) 178-86.
[22] K. D, A review of research examining the regulatory role of lymphocytes in normal wound healing, J Wound Care 17(5) (2008) 218-20.
[23] R. Diegelmann, M. Evans, Wound healing: an overview of actute, fibrotic and dealyed healing, Front Biosci 9 (2004) 283-289.
[24] J. Liu, D.J. Burkin, S.J. Kaufman, Increasing α7β1-integrin promotes muscle cell proliferation, adhesion, and resistance to apoptosis without changing gene expression, American Jounal of Physiology 294(2) (2008) 627-640.
[25] T. Qazi, D. Mooney, M. Pumberger, S. GeiBler, G. Duda, Biomaterials based strategies for skeletal muscle tissue engineering: Existing technologies and future trends, Biomaterials 53 (2015) 502-521.
[26] J.P. Mertens, K.B. Sugg, J.D. Lee, L.M. Larkin, Engineering muscle constructs for the creation of functional engineered musculoskeletal tissue, Regen Med 9(1) (2014) 89-100.
[27] Y. Shandalov, D. Egozi, A. Freiman, D. Rosenfeld, S. Levenberg, A method for constructing vascularized muscle flap, Methods 84 (2015) 70-75.
[28] B.J. Kwee, D.J. Mooney, Biomaterials for skeletal muscle tissue engineering, Curr Opin Biotechnol 47 (2017) 16-22.
[29] G.C. Vigodarzere, S. Mantero, Skeletal muscle tissue engineering: strategies for volumetric constructs, Frontiers in Physiology 5(362) (2014).
[30] M. Juhas, N. Bursac, Engineering skeletal muscle repair, Curr Opin Biotechnol 24(5) (2013) 880-886.
[31] A. Bach, J. Stem-Straeter, J. beier, H. Bannasch, G. Stark, Engineering of Muscle Tissue, Journal of clinical plastic surgery 30 (2003).
[32] X. Jiang, W. Zheng, S. Takayama, R.G. Chapman, R.S. Kane, G.M. Whitesides, Micro-Scale Patterning of Cells and their Environment, in: R. Lanza, R. Langer, J. Vacanti (Eds.), Principles of Tissue Engineering, Elsevier2013.
[33] K.J. Aviss, J.E. Gough, S. Downes, Aligned electrospin polymer fibres for skeletal muscle regeneration, European Cells and Materials 19 (2010) 193-204.
[34] D. Pedrotty, J. Koh, B. Davis, Engineering skeletalmyoblasts: roles of three-dimensional culture and electricalstimulation., Am J Phyiol Heart Circ Physiol 288(1620-1626) (2005).
[35] M. Koning, M.C. Harmsen, MarjaJ.A.vanLuyn, P.M.N. Werker, Current opportunities and challenges in skeletalmuscle tissue engineering, Journal of Tissue Engineering and Regenerative Medicine 3 (2009) 407-415.
[36] R.M. Nerem, S.C. Schutte, The Challenge of Imitatiting Nature, in: R. Lanza, R. Langer, J. Vacanti (Eds.), Principles of Tissue Engineering, Elsevier2013.
[37] H. Schmalbruch, D. Lewis, Dynamics of nuclei of muscle fibers and connective tissue cells in normal and denervated rat muscles Muscle Nerve 23 (2000) 617-626.
[38] B.D. Cosgove, H.M. Blau, Skeletal Muscle Stem Cells, in: A. Atala (Ed.), Principles of Regenerative Medicine, Academic Press2010.
[39] F.E. Stockdale, Gene Expression, Cell Determination and Differentiation, in: R. Lanza, R. Langer, J. Vacanti (Eds.), Principles of Tissue Engineering, Elsevier2013.

[40] Y.X. Wang, M. A. Rudnicki, Satellite cells, the engines of muscle repair, Nature Reviews (2011).
[41] M. Post, C.v.d. Weele, Principles of Tissue Engineering Food, in: R. Lanza, R. Langer, J. Vacanti (Eds.), Principles of Tissue Engineering, Elsevier2013.
[42] P. Gilbert, K. Havenstrite, K. Magnusson, A. Sacco, N. Leonardi, P. Kraft, N. Nguyen, S. Thrun, M. Lutolf, H. Blau, Substrate elasticity regulates skeletal muscle stem cell self-renewal in culture, Science 329 (2010) 1078-1081.
[43] J.M. Fishman, A. Tyraskis, P. Maghsoudlou, L. Urbani, G. Totonelli, M.A. Birchall, P.D. Coppi, Skeletal Muscle Tissue Engineering: Which Cell to Use?, Tissu Engineering. Part B 19(6) (2013).
[44] D. Montarras, J. Morgan, C. Collins, F. Relaix, S. Zaffran, A. Cumano, T. Partridge, M. Buckingham, Direct Isolation of Satellite Cells for Skeletal Muscle Regeneration, Science 309(5743) (2005) 2064-2067.
[45] K. Takahashi, K. Tanabe, M. Ohnuki, M. Narita, T. Ichisaka, K. Tomodo, Induction of pluripotent stem cells from adult human fibroblasts by defined factors, Cell 131 (2007) 861-872.
[46] M. Pittenger, A. Mackay, S. Beck, R. Jaiswal, R. Douglas, J. Mosca, Multilineage potential of adult human mesenchymal stem cells, Science 284 (1999) 333-344.
[47] A. Dellavalle, M. Sampaolesi, R. Tonlorenzi, Pericytes of human skeletal muscle are myogenic precursors distinct from satellite cells, Nat Cell Biol 9 (2007) 255-67.
[48] M. Meregalli, A. Farini, M. Belicchi, Y. Torrente, CD133(+) Cells for the Treatmnet of Degenerative Diseases: Update and Perspectives, Adv Exp Med Biol 777(229-243) (2013).
[49] G. Cossu, P. Bianco, Mesoangioblasts vasculat progenitors for extravascular mesodermal tissues, Curr Opin Genet Dev 13 (2003) 537-42.
[50] J.-H. Lee, H. Tachibana, Y. Morinaga, Y. Fujimura, K. Yamada, Modulation of proliferation and differentiation of C2C12 skeletal muscle cells by fatty acids, Life Sciences 84 (2009) 415-40.
[51] L.B. Hazeltine, J.a. Selekman, S.P. Palecek, Engineering the human pluripotent stem cell microenvironment to direct cell fate, Biotechnology advances 31(7) (2013) 1002-19.
[52] M. Guvendiren, J. Burdick, Engineering synthetic hydrogel microenvironments to instruct stem cells, Biotechnology 24(5) (2013) 841-846.
[53] R.G. Wells, The role of matrix stiffness in regulating cell behavior, Hepatology (Baltimore, Md.) 47(4) (2008) 1394-400.
[54] F.-M. Chen, S. Shi, Principles of Tissue Engineering, Fourth ed., Academic Press2014.
[55] F. Gattazzo, A. Urciuolo, Extracellular matrix: A dynamic microenvironment for stem cell niche, Biochimica et Biophysica Acta (2014) 2506-2519.
[56] A.J. Engler, M.A. Griffin, S. Sen, C.G. Bönnemann, H.L. Sweeney, D.E. Discher, Myotubes differentiate optimally on substrates with tissue-like stiffness, Journal of Cell Biology 6 (2004) 877-888.
[57] A. Engler, S. Sen, H.L. Sweeney, D. Discher, Matrix Elasticity Directs Stem Cell Lineage Specification, Cell (2006) 677-689.
[58] M. Komura, J. Kim, A. Atala, J.J. Yoo, S.J. Lee, The Digit: Engineering of Phalanges and Small Joints, in: A. Atala (Ed.), Principles of Regenerative Medicine, Academic Press2010.

[59] M.R. Ladd, S.J. Lee, J.D. Stitzel, A. Atala, J.J. Yoo, Co-electrospun dual scaffolding system with potential for muscle–tendon junction tissue engineering, Biomaterials 32(6) (2011) 1549-1559.
[60] H. Hofmann, P.P. Fietzek, K. Kuhn, The role of polar and hydrophobic interactions for the molecular packing of type I collagen: a three-dimensional evaluation of the amino acid sequence, Jounral of Molecular Biology 125 (1978) 127-165.
[61] K. Gelse, E. Poschl, T. Aigner, Collagens- structure, function and biosynthesis, Advanced Drug Delivery Reviews 55 (2003) 1531-1546.
[62] R. Rennie, A Dictionary of Chemistry, Oxford University Press, 2016.
[63] M. Shoulders, R. Raines, Collagen Structure and Stability, Annual Review of Biochemistry 78 (2009) 929-958.
[64] K.A. Piez, Collagen, Encylopedia off Polymer Science and Technology 3 (1985) 699-727.
[65] W. Friess, Collagen- biomaterial for drug delivery, Eur J Pharm Biopharm 45(2) 113-136.
[66] M.E. Nimini, R.D. Harkness, Molecular structures and functions of collagen, Biochemistry, CRC Press, Florida, 1988.
[67] S. Caliari, J. Burdick, A practical guide to hydrogels for cell culture, Nature Methods 13(5) (2016) 405-414.
[68] E.N.d.C. Calvi, F.X. Nahas, M.V. Barbosa, J.A. Calil, S.S.M. Ihara, M.d.S. Silva, M.F.d. Franco, L.M. Ferreira, An experimental model for the study of collagen fibers in skeletal muscle, Acta Cirurgica Brasileira 27(10) (2012).
[69] S. Grimal, S. Puech, R. Wagener, A.F.-. Carroll, Collagen XXVIII is a distinctive component of the peripheral nervous system nodes of ranvier and surrounds nonmylelinating glial cells, Glia 58(16) (2010) 1977-1987.
[70] J. Gebauer, B. Kobbe, R. Wagener, Structure, evolutioon and expression of collagen XXVIII: Lessons from zebrafish, Matrix biology 49 (2016) 106-119.
[71] C. Soderhall, I. Marenholz, T. Kerscher, M. Worm, C. Gruber, Variants in a novel epidermal collagen gene (COL29A1) are associated with atopic dermatitis, PLoS Biology 5(9) (2007).
[72] S. Ricard-Blum, The Collagen Family, Cold Spring Harbor Perspectives in Biology 3(1) (2011).
[73] J.L. Drury, D.J. Mooney, Hydrogels for tissue engineering: scaffold design variables and applications, Biomaterials 24 (2003) 4337-4351.
[74] A.M. Ferreira, P. Gentile, V. Chiono, G. Ciardelli, Collagen for bone tissue regeneration, Acta biomaterialia 8(9) (2012) 3191-200.
[75] G. Tronci, S. Russel, D. Wood, Photo-active collagen systems with controlled triple helix architecture, Journal of Materials Chemistry B 1 (2013) 20720-20720.
[76] C. Niyibizi, D.R. Eyre, Bone type V collagen: chain composition and location of a trypsin cleavage site, Connective Tissue Research 20 (1989) 247-250.
[77] A.K. Lynn, I.V. Yannas, W. Bonfield, Antigenicity and immunogenicity of collagen, Journal of Biomedical Materials Research 71B(2) (2004) 343-354.
[78] G. Tronci, A. Doyle, S.J. Russell, D.J. Wood, Structure-property-function relationships in triple-helical collagen hydrogels, MRS Proceedings 1498 (2012) mrsf12-1498-l12-34.
[79] G. Tronci, C.A. Grant, N.H. Thomson, S.J. Russell, D.J. Wood, B. Bd, G. Tronci, Multi-scale mechanical characterization of highly swollen photo-activated collagen hydrogels, (2015).

[80] R. Ravichandran, M.M. Islam, E.I. Alarcon, A. Samanta, S. Wang, P. Lundstro, J. Hilborn, M. Griffith, J. Phopase, Functionalised type-I collagen as a hydrogel building block for bio-orthogonal tissue engineering applications, Journal of Materials Chemistry B 4(318) (2016).
[81] S. Ryglová, M. Braun, T. Suchy, Collagen and Its Modifications—Crucial Aspects with Concern to Its Processing and Analysis, Macromolecular Materials Engineering 302(6) (2017).
[82] Z. Tian, W. Liu, G. Li, The microstructure and stability of collagen hydrogel cross-linked by glutaraldehyde, Polymer Degradation and Stability 130 (2016) 264-270.
[83] G. Tronci, A.T. Neffe, B.F. Pierce, A. Lendlein, An entropy–elastic gelatin-based hydrogel system, Journal of Materials Chemistry 20 (2010) 8875-8884
[84] G. Tronci, J. Yin, R.A. Holmes, H. Liang, S.J. Russel, D.J. Wood, Protease-sensitive atelocollagen hydrogels promote healing in a diabetic wound model, Journal of Materials Chemistry B 4 (2016) 7249-7258.
[85] J. Li, N. Ren, J. Qiu, H. Jiang, H. Zhao, G. Wang, R.I. Boughton, Y. Wang, H. Liu, Carbodiimide crosslinked collagen from porcine dermal matrix for high-strength tissue engineering scaffold, International journal of biological macromolecules 61 (2013) 69-74.
[86] K.E. Kadler, D.F. Holmes, J.A. Trotter, J.A. Chapman, Collagen fibril formation, Journal of Biochemistry 316 (1996) 1-11.
[87] B. Pontz, W. Migel, J. Rauterberg, K. Kuhn, Localization of two species specific antigenic determinants on the peptide chains of calf skin collagen, Eur J Biochem 16 (1970) 50-54.
[88] I.M. El-Sherbiny, M.H. Yacoub, Hydrogel scaffolds for tissue engineering: Progress and challenges, Glob Cardiol Sci Pract 3 (2013) 316-342.
[89] J. Zhu, R.E. Marchant, Design properties of hydrogel tissue-engineering scaffolds, Expert Rev Med Devices (2011).
[90] E.E. Antoine, P.P. Vlachos, M.N. Rylander, Review of Collagen I Hydrogels for Bioengineered Tissue Microenvironments: Characterization of Mechanics, Structure, and Transport, Tissu Engineering Part B Rev 20(6) (2014) 683-696.
[91] V.L. Cross, Y. Zheng, N.W. Choi, S.S. Verbridge, B.A. Sutermaster, L.J. Bonassar, C. Fischbach, A.D. Stroock, Dense type I collagen matrices that support cellular remodeling and microfabrication for studies of tumor angiogenesis and vasculogenesis in vitro., Biomaterials 31 (2010) 8596-8607.
[92] B. Marelli, C.E. Ghezzi, D. Mohn, W.J. Stark, J.E. Barralet, A.R. Boccaccini, S.N. Nazhat, Accelerated mineralization of dense collagen-nano bioactive glass hybrid gels increases scaffold stiffness and regulates osteoblastic function, Biomaterials 32(34) (2011) 8915-26.
[93] R. Holmes, X. Yang, A. Dunne, L. Florea, D. Wood, G. Tronci, Thiol-Ene Photo-Click Collagen-PEG Hydrogels: Impact of Water-Soluble Photoinitiators on Cell Viability, Gelation Kinetics and Rheological Properties, Polymers 9(6) (2017) 226.
[94] H. Geckil, X. Feng, Engineering hydrogels as extracellular matrix mimics, Nanomedicine 5(3) (2011) 469-484.
[95] C. Hartmuth, M.G. Finn, B. Sharpless, Click Chemistry: Diverse Chemical Function from a Few Good Reactions, Angewandte Chemie International Edition 40 (2001) 2004-2021.
[96] J.E. Moses, A.D. Moorhouse, The growing applications of click chemistry, Chemical society reviews (2007).

[97] K.S. Anseth, H.-A. Klok, Click Chemistry in Biomaterials, Nanomedicine, and Drug Delivery, Biomacromolecules 17 (2016) 1-3.
[98] O. Guaresti, C. García–Astraina, T. Palomares, A. Alonso–Varona, A. Eceizaa, N. Gabilondo, Synthesis and characterization of a biocompatible chitosan–based hydrogel cross–linked via 'click' chemistry for controlled drug release, International journal of biological macromolecules 102 (2017) 1-9.
[99] S. Fu, H. Dong, X. Deng, R. Zhuo, Z. Zhong, Injectable hyaluronic acid/poly(ethylene glycol) hydrogels crosslinked via strain-promoted azide-alkyne cycloaddition click reaction, Carbohydrate Polymers 169 (2017) 332-340.
[100] R.M. Desai, S.T. Koshy, S.A. Hilderbrand, D.J. Mooney, N.S. Joshi, Versatile click alginate hydrogels crosslinked via tetrazineenorbornene chemistry, Biomaterials 50 (2015) 30-37.
[101] Y. Jiang, J. Chen, C. Deng, E.J. Suuronen, Z. Zhong, Click hydrogels, microgels and nanogels: emerging platforms for drug delivery and tissue engineering, Biomaterials 35(18) (2014) 4969-85.
[102] M.A. Azagarsamy, K.S. Anseth, Bioorthogonal Click Chemistry: An Indispensable Tool to Create Multifaceted Cell Culture Scaffolds, ACS Macro Lett 2(1) (2013) 5-9.
[103] C.E. Hoyle, C.N. Bowman, Thiol-Ene Click Chemistry, 49 (2010) 1540-1573.
[104] R. Li, Z. Cai, Z. Li, Q. Zhang, S. Zhang, L. Deng, L. Lu, L. Li, C. Zhou, Synthesis of in-situ formable hydrogels with collagen and hyaluronan through facile Michael addition, Mater Sci Eng Mater Biol Appl 77 (2017) 1035-1043.
[105] J.W. Chan, C.E. Hoyle, A.B. Lowe, M. Bowman, Nucleophile-initiated thiol-michael reactions: Effect of organocatalyst, thiol, and Ene, Macromolecules 43(15) (2010) 6381-6388.
[106] J. Kim, Y.P. Kong, S.M. Niedzielski, R.K. Singh, A.J. Putnam, A. Shikanov, Characterization of the crosslinking kinetics of multi-arm poly(ethylene glycol) hydrogels formed via Michael-type addition, Soft Matter (7) (2016).
[107] N.J. Darling, Y.-S. Hung, S. Sharma, T. Segura, Controlling the kinetics of thiol-maleimide Michael-type addition gelation kinetics for the generation of homogenous poly(ethylene glycol) hydrogels, Biomaterials 101 (2016) 199-206.
[108] A. Gress, A. Volkel, H. Schlaad, Thio-Click Modification of Poly[2-(3-butenyl)-2-oxazoline], Macromolecules 40 (2007) 7927-7933.
[109] T.O. Machado, C. Sayer, P.H.H. Araujo, Thiol-ene polymerisation: A promising technique to obtain novel biomaterials, European Polymer Journal 86 (2017) 200-215.
[110] C.-C. Lin, A. Raza, H. Shih, PEG hydrogels formed by thiol-ene photo-click chemistry and their effect on the formation and recovery of insulin-secreting cell spheroids, Biomaterials 32 (2012) 9685-9695.
[111] Z. Munoz, H. Shih, C.-C. Lin, Gelatin hydrogels formed by orthogonal thiol-norbornene photochemistry for cell encapsulation, (2014).
[112] L. Russo, C. Battocchio, V. Secchi, E. Magnano, S. Nappini, F. Taraballi, L. Gabrielli, F. Comelli, A. Papagni, B. Costa, G. Polzonetti, F. Nicotra, A. Natalello, S.M. Doglia, L. Cipolla, Thiol−ene Mediated Neoglycosylation of Collagen Patches: A Preliminary Study, Langmuir 4(30) (2014).
[113] D. Campbell, Biomimetic Biomaterials: Injectable Biomimetic Hydrogels for Soft Tissue Repair, Woodhead Publishing Ltd, Aston, 2013.
[114] G. Xu, X. Wang, C. Deng, Injectable biodegradable hybrid hydrogels based on thilated collagen and oligo(acryloyl carbonate-poly(ethylene glycol)-

olgo(acryloyl carbonate) copolymer for functional cardiac regeneration, Acta biomaterialia (2015).
[115] J.L. Drury, D.J. Mooney, Hydrogels for tissue engineering: scaffold design variables and applications, Biomaterials 24(24) (2003) 4337-4351.
[116] Y. Takemoto, H. Ajiro, T. Asoh, Fabrication of Surface Modified Hydrogels with Polyion Complex for Contolled Release, Chemistry of Materials 22 (2010) 2923-2929.
[117] V.L. Cross, Y. Zheng, N.W. Choi, S.S. Verbridge, B.A. Sutermaster, L.J. Bonassar, C. Fischbach, A.D. Stroock, Dense type I collagen matrices that support cellular remodeling and microfabrication for studies of tumor angiogenesis and vasculogenesis in vitro, Biomaterials 31 (2010) 8596-8607.
[118] C. Helary, I. Bataille, A. Abed, C. Illoul, A. Anglo, L. Louedec, D. Letourneur, A. Meddahi-Pell, M.M. Giraud-Guille, Concentrated collagen hydrogels as dermal substitutes, Biomaterials 31 (2010) 481-490.
[119] B.D. Fairbanks, M.P. Schwartz, A.E. Halevi, C.R. Nuttelman, C.N. Bowman, K.S.A. author, A Versatile Synthetic Extracellular Matrix Mimic via Thiol-Norbornene Photopolymerization, Adv Mater 21(48) (2009) 5005-5010.
[120] J. Liu, H. Zheng, P.S.P. Poh, H.-G. Machens, A.F. Schilling, Hydrogels for Engineering of Perfusable Vascular Networks, Int J Mol Sci 16(7) (2015).
[121] M. Lovett, D. Ph, K. Lee, A. Edwards, D.L. Kaplan, Vascularization Strategies for Tissue Engineering, 15(3) (2009).
[122] B.R. Coyac, F. Chicatun, B. Hoac, V. Nelea, C. Chaussain, S.N. Nazhat, M.D. McKee, Mineralization of dense collagen hydrogel scaffolds by human pulp cells, Journal of dental research 92(7) (2013) 648-54.
[123] J.P.F. Wong, D. Baptista, R.a. Brown, Pre-crosslinked polymeric collagen in 3-D models of mechanically stiff tissues: Blended collagen polymer hydrogels for rapid layer fabrication, Acta biomaterialia (2014).
[124] X. Jia, K.L. Kiick, Hybrid Multicomponent Hydrogels for Tissue Engineering, Macromol Biosci 9(2) (2009) 140-156.
[125] S. Zhong, L.Y.L. Yung, Enhanced biological stability of collagen with incorporation of PAMAM dendrimer, Journal of Biomedical Materials Research 91(1) (2008).
[126] X. Maa, Z. He, F. Han, Z. Zhonga, L. Chen, B. Li, Preparation of collagen/hydroxyapatite/alendronate hybrid hydrogels as potential scaffolds for bone regeneration, Colloids and Surfaces B: Biointerfaces 143 (2016) 81-87.
[127] F. Edalat, I. Sheu, S. Manoucheri, A. Khademhosseini, Material strategies for creating artificial cell-instructive niches, Curr Opin Biotechnol 23 (2012) 820-825.
[128] C. Hutson, J. Nichol, H. Aubin, H. Bae, S. Yamanlar, S. Al-Haque, S. Koshy, A. Khademhosseini, Synthesis and characterization of tunable poly(ethylene glycol): gelatin methacrylatecomposite hydrogels, Tissue Eng 17 (2011) 1713-23.
[129] C. Williams, Variable Cytocompatibility of Six Cell Lines with Photoinitiators Used for Polymerizing Hydrogels and Cell Encapsulation, Biomaterials 26 (2005) 1211-1218.
[130] C.S. Bahney, T.J. Lujan, C.W. Hsu, M. Bottlang, J.L. West, B. Johnstone, Visible light photoinitiation of mesenchymal stem cell-laden bioresponsive hydrogels, European Cells and Materials 22 (2011) 43-55.

[131] H. Shih, C.-C. Li, Visible-Light-Mediated Thiol-Ene Hydrogelation Using Eosin-Y as the Only Photoinitiator Macromolecular Rapid Communications 34 (2013) 269-273.
[132] D. Fairbanks, Photoinitiated Polymerization of PEG-diacrylate with lithium phenyl-2,4,6-trimethylbenzoylphosphinate: polymerization rate and cytocompatibility,, Biomaterials 30(35) (2009) 6702-6707.
[133] D. Hari, B. Konig, Synthetic applications of eosin Y in photoredox catalysis, Chem. Commun. 50 (2014) 6688-6689.
[134] A. Talla, B. Driessen, N.J.W. Straathof, L.-G. Milroy, L. Brunsveld, V. Hessel, T. Noël, Metal-Free Photocatalytic Aerobic Oxidation of Thiols to Disulfides in Batch and Continuous-Flow, Advanced Synthesis & Catalysis (2015).
[135] X.-J. Yang, B. Chen, L.-Q. Zheng, L.-Z. Wu, C.-H. Tung, Highly efficient and selective photocatalytic hydrogenation of functionalized nitrobenzenes, Green Chemistry (2014) 1082-1086.
[136] J.S. Lewis, K. Roy, B.G. Keselowsky, Materials that harness and modulate the immune system, Materials for Biological Modulation, Sensing and Imagine 30(1) (2014).
[137] A.B. Gardner, S.K.C. Lee, E.C. Woods, A.P. Acharya, Biomaterials-Based Modulation of the Immune System, BioMed Research International (2013).
[138] J. Anderson, A. Rodriguez, D. Chang, Foreign body reaction to biomaterials, Semin Immunol 20(2) (2008) 86-100.
[139] M. Dadestan, J. Jones, A. Hiltner, J. Anderson, Surface chemistry mediates adhesive structure, cytoskeletal organization, and fusion of macrophages, J Biomed Mater Res A 71(3) (2004) 439-48.
[140] B. Brown, S. Badylak, The Role of the Host Immune Response in Tissue Engineering and Regenerative Medicine, in: R. Lanza, R. Langer, J. Vacanti (Eds.), Principles of Tissue Engineering, Elsevier2013.
[141] D. Williams, On the mechanisms of biocompatibility, Biomaterials (2008) 1-13.
[142] H. TA, The role of adsorbed proteins in tissue responsee to biomaterials, Biomaterials science: an introduction to biomaterials in medicine, Elsevier, San Diego, CA, 2004, pp. 237-46.
[143] S. Franz, S. Rammelt, D. Scharnweber, J.C. Simon, Immune responses to implants - A review of the implications for the design of immunomodulatory biomaterials, Biomaterials 32 (2011) 6692-6709.
[144] S. Chen, J.A. Jones, Y. Xu, H.-Y. Low, J.M. Anderson, K.W. Leong1, Characterization of Topographical Effects on Macrophage Behavior in a Foreign Body Response Model, Biomaterials 31 (2010) 3479-3491.
[145] Y.K. Kim, R. Que, S.-W. Wang, W.F. Liu, Modification of Biomaterials with a Self Protein Inhibits the Macrophage Response, Adv Healthc Mater 3(7) (2014) 989-994.
[146] S. Chang, Y. Popowich, R.S. Greco, B. Haimovich, Neutrophil survival on biomaterials is determined by surface topography, J. Vasc. Surg 37 (2003) 1082-1090.
[147] D.F. Williams, There is no such thing as a biocompatible material, Biomaterials 35 (2014) 10009-10014.
[148] X. Liu, N. Dan, W. Dan, J. Gong, Feasability study of the natural derived chitosan dialdehyde for chemical modification of collagen, International journal of biological macromolecules 82 (2016) 989-997.

[149] M. Yamauchi, M. Sricholpech, Lysine post-translational modifications of collagen, Essays Biochem 52 (2012) 113-133.
[150] C. Dong, Y. Lv, Application of Collagen Scaffold in Tissue Engineering: Recent Advances and New Perspectives, Polymers 8(2) (2016).
[151] J. Glowacki, S. Mizuno, Collagen Scaffolds for Tissue Engineering, Biopolymers 89(5) (2008).
[152] L. Cen, W. Liu, L. Cui, W. Zhang, Y. Cao, Collagen Tissue Engineering: Development of Novel Biomaterials and Applications, Pediatric Research 63 (2008) 492-496.
[153] J. Ward, J. Kelly, W. Wang, D.I. Zeugolis, A. Pandit, Amine Functionalization of Collagen Matrices with Multifunctional Polyethylene Glycol Systems, Biomacromolecules 11 3093-3101.
[154] R. Parenteau-Bareil, R. Gauvin, F. Berthod, Collagen-based biomaterials for tissue engineering applications, Materials 3 (2010).
[155] J.E. Gough, C.A. Scotchford, S. Downes, Cytotoxicity of glutaraldehyde crosslinked collagen/poly(vinyl alcohol) films is by the mechanism of apoptosis, Journal of Biomedical Materials Research 61(1) (2002).
[156] L.H.O. Damink, P.J. Dijkstra, M.J.v. Lyun, P.B.v. Wachem, P. Nieuwenhuis, J. Feijen, Cross-linking of dermal sheep collagen using a water soluble carbodiimide, Biomaterials 17(8) (1996) 765-773.
[157] L.H.O. Damink, P.J. Dijkstra, M.J.v. Luyn, J. Feijen, Glutaraldehyde as a cross-linking agent for collagen based biomaterials, Journal of Materials Science 6(8) (1995).
[158] M.E. Nimni, D. Cheung, B. Strates, M. Kodama, K. Sheikh, Chemically modified collagen: A natural biomaterial for tisseue replacement, Journal of Biomedical Materials Research 21(6) (1987).
[159] R. Zeeman, Cross-linking of collagen-based materials, 1998.
[160] S.Z. F. Taraballi, C. Lupo, C. Cunha, L. Cipolla, Amino and carboxyl plasma functionalization of collagen films for tissue engineering applications, Journal of Colloid and Interface Science 394 (2013) 590-597.
[161] K. Nguyen, Photopolymerizable Hydrogels for Tissue Engineering, Biomaterials 23 (2002) 4307-4314.
[162] D.P. Hari, B. König, Synthetic applications of eosin Y in photoredox catalysis, Chemical communications (Cambridge, England) 50(51) (2014) 6688-99.
[163] S.M. Kelly, T.J. Jess, N.C. Price, How to study proteins by circular dichroism, Biochimica et Biophysica Acta - Proteins and Proteomics 1751(2) (2005) 119-139.
[164] N.J. Greenfield, Using circular dichroism spectra to estimate protein secondary structure, Nat Protoc. 1(6) (2006) 2876-2890.
[165] K.E. Drzewiecki, D.R. Grisham, A.S. Parmar, V. Nanda, D.I. Shreiber, Circular Dichroism Spectroscopy of Collagen Fibrillogenesis: A New Use for an Old Technique, Biophysical Journal 11 (2016) 2377-2386.
[166] B.Madhan, V.Subramanian, J.R. Raoa, B.U. Nair, T.Ramasami, Stabilization of collagen using plant polyphenol: Role of catechin, International journal of biological macromolecules 37(1) (2005) 47-53.
[167] E. Leikina, M. Mertts, N. Kuxnetsova, S. Leikin, Type I collagen is thermally unstable at body temperature, Proc Natl Acad Sci U.S.A 3 (2002) 1314-1318.

[168] H. Saito, M. Yokoi, A 13C NMR Study on Collagens in the Solid State: Hydration/ Dehydration-Induced Conformational Change of Collagen and Detection of Internal Motions J. Biochem 111 (1992) 376-382.
[169] P.D.S. Peixoto, G. Laurent, T. Azaïs, G. Mosser, Solid-state NMR Study Reveals Collagen I Structural Modifications of Amino Acid Side Chains upon Fibrillogenesis, J Biol Chem 288(11) (2013) 7528-7535.
[170] A.E. Aliev, Solid-State NMR Studies of Collagen-Based Parchments and Gelatin, Biopolymers 77(4).
[171] B.d.C. Vidal, M.L.S. Mello, Collagen type I amide I band infrared spectroscopy, Micron 42 (2011) 283-289.
[172] M.-T. Nistor, A.P. Chiriac, C. Vasile, L. Verestiuc, L.E. Nita, Synthesis of hydrogels based on poly(NIPAM) inserted into collagen sponge, Biointerfaces 87 (2011) 382-390.
[173] A.L. Barnes, P.G. Genever, S. Rimmer, M.C. Coles, Collagen–Poly(N-isopropylacrylamide) Hydrogels with Tunable Properties, Biomacromolecules 17(3) (2016) 723-734.
[174] S.D. Fitzpatrick, M.A.J. Mazumder, F. Lasowski, L.E. Fitzpatrick, H. Sheardown, PNIPAAm-Grafted-Collagen as an Injectable, In Situ Gelling, Bioactive Cell Delivery Scaffold, Biomacromolecules 11(9) (2010) 2261-2267.
[175] Y. Yan, L. Huang, Q. Zhang, H. Zhou, Concentration effect on aggregation and dissolution behavior of poly(N-isopropylacrylamide) in water, Journal of Applied Polymer Science 132(12) (2015).
[176] S. Ohyaa, S. Kidoakib, T. Matsuda, Poly(N-isopropylacrylamide) (PNIPAM)-grafted gelatinhydrogel surfaces: interrelationship between microscopic structure and mechanical property of surface regions and cell adhesiveness, Biomaterials 26 (2005) 3105-3111.
[177] Y. Samuni, S. Goldstein, O.M. Dean, M. Berk, The chemistry and biological activities of N-acetylcysteine, Biochimica et biophysica acta 1830(8) (2013) 4117-29.
[178] G.B. Fields, The Collagen Triple-Helix: Correlation of the Conformation with Biological Activities, Connective Tissue Research 31(3) (1995).
[179] Q. Zhang, Q.-F. He, T.-H. Zhang, X.-L. Yu, Q. Liu, F.-l. Deng, Improvement in the delivery system of bone morphogenetic protein-2: a new approach to promote bone formation, Biomedical materials 7(4) (2012).
[180] Y. Li, Q. He, X. Hu, Y. Liu, X. Cheng, X. Li, F. Deng, Improved performance of collagen scaffolds crosslinked by Traut's reagent and Sulfo-SMCC, Journal of Biomaterials Science 28(7) (2017).
[181] C. Shi, Q. Li, Y. Zhao, W. Chen, B. Chen, Z. Xiao, H. Lin, L. Nie, D. Wang, J. Dai, Stem-cell-capturing collagen scaffold promotes cardiac tissue regeneration, Biomaterials 32(2508-2515) (2011).
[182] S. Kommareddy, M. Amiji, Preparation and Evaluation of Thiol-Modified Gelatin Nanoparticles for Intracellular DNA Delivery in Response to Glutathione, Bioconjugate Chem 16 (2005) 1423-1432.
[183] G. Xu, X. Wang, C. Deng, X. Teng, E.J. Suuronen, Z. Shen, Z. Zhong, Injectable biodegradable hybrid hydrogels based on thiolated collagen and oligo(acrylolyl carbonate)-poly(ethylene glycol)-oligo(acryloyl carbonate) copolymer for functional cardiac regeneratoin, Acta Biomaterialia 15 (2015) 55-64.

[184] Z. Mũnoz, H. Shih, C.-C. Lin, Gelatin hydrogels formed by orthogonal thiol–norbornene photochemistry for cell encapsulation, Biomaterials Science 2 (2014).
[185] Y. Hao, H. Shih, Z. Munoz, A. Kemp, C.-C. Lin, Visible light cured thiol-vinyl hydrogels with tunable degradation for 3D cell culture, Acta Biomaterialia 10 (2014) 104-114.
[186] H. Shih, H.-Y. Liu, C.-C. Lin, Improving gelation efficiency and cytocompatibility of visible light polymerized thiol-norbornene hydrogels via addition of soluble tyrosine, Biomaterials Science (2017).
[187] H. Shih, Step-growth thiol-ene photopolymerisation to form degradable cytocompatible and multi-structural hydrogels, Biomedical Engineering, Purdue University, Indianapolis, 2013.
[188] J.P. Fouassier, Photoinitiation, Photopolymerization and Photocuring: Fundamentals and Applications, Carl hanser Verlag GmbH & Co, Munich, Germany, 1995.
[189] I. Mironi-Harpaz, D.Y. Wang, S. Venkatraman, D. Seliktar, Photopolymerization of cell-encapsulating hydrogels: Crosslinking efficiency versus cytotoxicity, Acta Biomaterialia 8(5) (2012) 1838-1848.
[190] L. Lecamp, B. Youssef, C. Bunel, p. Lebaudy, Photoinitiated polymerization of a dimethacrylate oliomer: 1 influence of photoiniator conncentration, termperature and light intensity, Polymer 38(25) (1997).
[191] F.M. Chen, S. Shi, Principles of Tissue Engineering, Elsevier, New York, USA, 2014.
[192] C.M. Kirschner, K.S. Anseth, Hydrogels in healthcare from static to dynamic material microenvironments, Acta Mater 61 (2013) 931-944.
[193] B.V. Slaughter, S.S. Khurshid, O.Z. Fischer, A. Khademhosseini, N. Peppas, Hydrogels in regenerative medicine, Adv. Mater. 21 (2009) 3307-3329.
[194] R. Khan, M.H. Khan, Use of collagen as a biomaterial: An update, J Indian Soc Periodontal 17(4) (2013) 539-542.
[195] R.L. Lundblad, Chemical Reagents for Protein Modifications, Taylor & Francis Group, Chapel Hill, North Carolina, 2014.
[196] K.M. Galler, L. Aulisa, K.R. Regan, J.D. Hartgerink, Self-assembling multidomain peptide hydrogels: designed susceptibly to enzymatic cleavage allows enhanced cell migration and spreading, Journal americal chemical society 132 (2010) 3217-3223.
[197] H.C. Kolb, K.B. Sharpless, The growing impact of click chemistry on drug discovery, Drug Discovery Today 8 (2003).
[198] R. Censi, P.J. Fieten, P. di Martino, W.E. Hennink, T. Vermonden, In Situ Forming Hydrogels by Tandem Thermal Gelling and Michael Addition Reaction between Thermosensitive Triblock Copolymers and Thiolated Hyaluronan, Macromolecules 43(13) (2010) 5771-5778.
[199] W. Xi, T. Scott, C. Kloxin, C. Bowman, Click Chemistry in Materials Science, Advanced Functional Materials 24 (2014) 2572-2590.
[200] A. Hingham, L. Garber, D. Latshaw, C. Hall, J. Pojman, S. Khan, Gelation and Cross-Linking in Multifunctional Thiol and Multifunctional Acrylate Systems Involving an in Situ Comonomer Catalyst, Macromolecules 47 (2014) 821-829.
[201] C. Lin, C. Ki, H. Shih, Thiol-norbornene photo-click hydrogels for tissue engineering applications, Journal applied polymer science 132(8) (2015).

[202] S. Stichler, T. Jungst, M. Schamel, I. Zilkowski, J. Groll, Thiol-ene Clickable Poly(glycidol) Hydrogels for Biofrabication, Additive Manufactruing of Biomaterials, Tissues and Organs (2016).
[203] R. Pereira, P. Bartolo, Photopolymerizable hydrogels in regerative medicine and drug delivery, Topics in Biomaterials2014, pp. 6-28.
[204] C. Lin, K. Anseth, Glucagon-like peptide-1-functionalized PEG hydrogels promote survival and function of encapsulated pancreatic beta-cells, Biomacromolecules 10 (2009) 2460-2467.
[205] A. Hilderbrand, E. Ovadia, M. Rehmann, A. Kloxin, Biomaterials for 4D stem cell culture, Current Opinion in Solid State and Materials Science 20 (2016) 212-224.
[206] B. Mann, A. Gobin, A. Tsai, R. Schemdlen, J. West, Smooth muscle cell growth in photopolymerised hydrogels with cell adhesive and proteolytically degradable domains: synthetic ECM analogs for tissue engineering, Biomaterials 22 (2001) 3045-3051.
[207] J.D. McCall, K.S. Anseth, Thiol–Ene Photopolymerizations Provide a Facile Method To Encapsulate Proteins and Maintain Their Bioactivity, Biomacromolecules 13 (2012) 2410–2417.
[208] G. Nicodemus, S. Bryant, Cell Encapsulation in Biodegradable Hydrogels for Tissue Engineering Applications, Tissue Engineering: Part B 14(2) (2008).
[209] G.-Z. Li, R.K. Randev, A.H. Soeriyadi, G. Rees, C. Boyer, Z. Tong, T.P. Davis, C.R. Becera, D.M. Haddleton, Investigation into thiol-(meth)acrylate Michael addition reactions using amine and phosphine catalysts, Polymer Chemistry 1 (2010) 1196-1204.
[210] N.B. Cramer, S.K. Reddy, M. Cole, C. Hoyle, C.N. Bowman, Initiation and kinetics of thiol-ene photopolymerizations without photoinitiators, Journal of Polymer Science Part A: Polymer Chemistry 42(22) (2004) 5817-5826.
[211] K. Xu, Y. Fu, W. Chung, X. Zheng, Y. Cui, I.C. Hsu, W.J. Kao, Thiol–ene-based biological/synthetic hybrid biomatrix for 3-D living cell culture, Acta Biomaterialia 8 (2012) 2504-2516.
[212] U. Burner, C. Obinger, Transient-state and steady-state kinetics of the oxidation of aliphatic and aromatic thiols by horseradish peroxidase, FEBS Letters 411 (1997) 269-274.
[213] R.E. Hansen, H. Ostergaard, P. Norgaard, J.R. Winther, Quantificationo of protein thiols and dithiols in the picomolar range using sodium borohydride ad 4,4'-dithiodipyridine, Analytical Biochemistry 363 (2007) 77-82.
[214] D. Dingova, J. Leroy, A. Check, V. Garaj, E. Krejci, A. Harbovska, Optimal detection of chlorinesterase activity in biological samples: Modifications to the standard ellman's assay, Analytical Biochemistry 462 (2014) 67-75.
[215] J.R. Winther, C. Thorpe, Quanitification of Thiols and Disulfides, Biochim Biophys Acta (2) (2014).
[216] D.P. Nair, M. Podgorski, S. Chatani, T. Gong, W. Xi, C.R. Fenoli, C.N. Bowman, The Thiol-Michael Addition Click Reaction: A Powerful and Widely Used Tool in Materials Chemistry, Chemistry of Materials 26 (2014) 724-744.
[217] P.K. Working, M.S. Newman, J. Johnson, J.B. Cornacoff, Safety of Poly(ethylene glycol) and Poly(ethylene glycol) Derivatives, American Chemical Society1997, pp. 45-57.
[218] N.B. Cramer, C.L. Couch, K.M. Schreck, J.A. Carioscia, E. Boulden, J.W. Stansbury, C.N. Bowman, as dental restorative materials, 26(1) (2011) 21-28.

[219] S. Singh, M. Schwartz, E. Tokuda, Y. Luo, R.E. Rogers, M. Fujita, N. Ahn, K. Anseth, A synthetic modular approach for modeling the role of the 3D microenvironment in tumor progression, Scientific Reports 5 (2015).
[220] J. Goodwin, R. Hughes, Rheology for Chemists: An Introduction, in: RSC (Ed.)2008, p. 203.
[221] G. Song, Z. Zhao, X. Peng, C. He, R.A. Weiss, H. Wang, Rheological Behaviour of Tough PVP-in Situ-PAAm Hydrogels Physically Cross-Linked by Cooperative Hydrogels Bonding, Macromolecules 49 (2016) 8265-8273.
[222] A. Dunne, C. Delaney, L. Florea, D. Diamond, Solvato-morphologically controlled, reversible NIPAAm hydrogel photoactuators, RSC Adv 6 (2016).
[223] G. Tronci, A. Doyle, S.J. Russel, D.J. Wood, Triple-helical collagen hydrogels via covalent aromatic functionalisation with 1,3- phenylenediacetic acid, Journal of Materials Chemistry B 1 (2013) 5478-5488.
[224] S. Byrant, K. Anseth, Hydrogel properties influence ECM production by chondrocytes photoencapsulated in poly(ethylene glycol) hydrogels, Biomedical Materials Research Part A (2002).
[225] H.-W. Kang, Y. Tabata, Y. Ikada, Fabrication of porous gelatin scaffolds for tissue engineering, Biomaterials 20 (1999) 1339-1344.
[226] Y.-C. Chiu, M.-H. Cheng, H. Engel, S.-W. Kao, J.C. Larson, S. Gupta, E.M. Brey, The role of pore size on vascularization and tissue remodeling in PEG hydrogels, Biomaterials 32 (2011) 6045-6051.
[227] A. Collinsworth, S. Zhang, W. Kraus, G. Truskey, Apparent elastic modulus and hysteresis of skeletal muscle cells throughout differentiation, Am J Physiol 283 (2002).
[228] A. Castro, P. Laity, M. Shariatzadeh, C. Wittkowske, C. Holland, D. Lacroix, Combined numerical and experimental biomechanical characterization of soft collagen hydrogel substrate, J Mater Sci: Mater Med 27 (2016).
[229] D. Knapp, V. Barocas, A. Moon, J. Yoo, L. Petzold, R. Tranquillo, Rheology of reconstituted type I collagen gel in confined compression, J Rheol 41 (1997) 971-993.
[230] P. Parmar, L. Chow, J.-P. St-Pierre, C.-M. Horejs, Y. Peng, J. Werkmeister, J. Ramshaw, M. Stevens, Collagen-mimetic peptide-modifiable hydrogels for articular cartilage regeneration, Biomaterials 54 (2015) 213-225.
[231] R. Kocen, M. Gasik, A. Gantar, S. Novak, Viscoelastic behaviour of hydrogel-based composites for tissue engineering under mechanical load, Biomedical materials 12 (2017).
[232] K. Alberti, Q. Xu, Biocompatibility and degradation of tendon-derived scaffolds, Regen Biomater 3(1) (2016) 1-11.
[233] A. Helling, E. Tsekoura, M. Biggs, Y. Bayon, A. Pandit, D. Zeugolis, In Vitro Enzymatic Degradation of Tissue Grafts and Collagen Biolmaterials by Matrix Metalloproteniases: Improving the Collagenase Assay, ACS Biomater. Sci. Eng (2016).
[234] S. Duan, S. Ma, Z. Huang, X. Zhang, X. yang, P. Gao, M. Yin, Q. Cai, Visualization of in vivo degradtion of aliphatic polyesters by a fluorescent dendritic star macromolecule, Biomedical Materials 10 (2015).
[235] J. Tse, A. Engler, Stiffness Gradients Mimicking In Vivo Tissue Variation Regulate Mesenchymal Stem Cell Fate, PLoS ONE 6 (2011).
[236] K. Ren, T. Crouzier, C. Roy, C. Picart, Polyelectrolyte Multilayer Films of Crontrolled Stiffness Modulate Myoblast Cell Differentiation, Advanced Functional Materials 18 (2008) 1378-1389.

[237] E.V. Alakpa, V. Jayawarna, A. Lampel, K.V. Burgess, C.C. West, S.C.J. Bakker, S. Roy, N. Javid, S. Fleming, D.A. Lamprou, J. Yang, A. Miller, A.J. Urquhart, P.W.J.M. Frederix, N.T. Hunt, B. Péault, R.V. Ulijin, M.J. Dalby, Tunable Supramolecular Hydrogels for Selection of Lineage-Guiding Metabolites in Stem Cell Cultures, Chem 1 (2016) 298-319.
[238] J.R. Tse, A.J. Engler, Preparation of hydrogel substrates with tunable mechanical properties, Current protocols in cell biology / editorial board, Juan S. Bonifacino ... [et al.] Chapter 10(June) (2010) Unit 10.16-Unit 10.16.
[239] K. Ding, Z. Yang, J.-z. Xu, W.-y. Liu, Q. Zeng, F. Hou, S. Lin, Elastic hydrogel substrate supports robust expansion of murine myoblasts and enhances their engraftment, Experimental Cell Research 227 (2015) 111-119.
[240] D. Yaffe, O. Saxel, Serial passaging and differentiation of myogenic cells isolated from mouse muscle, Nature 270 (1977).
[241] C.A. Collins, I. Olsen, P.S. Zammit, L. Heslop, A. Petrie, T.A. Partridge, J.E. Morgan, Stem cell function, self renewal, and behavioral heterogeneity of cells from the adult muscle satellite cell niche, Cell 122(289) (2005).
[242] A. Sacco, R. Doyonnas, P. Kraft, S. Vitorovic, H.M. Blau, Self-renewal and expansion of single transplanted muscle stem cells, Nature 456(502) (2008).
[243] N.F. Huang, S. Patel, R.G. Thakar, J. Wu, B.S. Hsiao, B. Chu, R.J. Lee, S. Li, Myotube Assembly on Nanofibrous and Micropatterned Polymers, Nano Letters 6(2) (2006) 537-542.
[244] M. Madaghiele, A. Sannino, I.V. Yannas, M. Spector, Collagen-based matrices with axially oriented pores, Journal of Biomedical Materials Research Part A 85(3) (2007).
[245] D. Klumpp, R.E. Horch, U. Kneser, J.P. Beier, Engineering skeletal muscle tissue – new perspectives in vitro and in vivo, J Cell Mol Med 14(11) (2010) 2622-2629.
[246] S. Ciciliot, S. Schiaffino, Regeneration of mammalian skeletal muscle. Basic mechanisms and clinical implications., Curr Phar Des 16(8) (2010).
[247] K. Shah, Z. Majeed, J. Jonason, R.J. O'Keefe, The Role of Muscle in Bone Repair: the Cells, Signals, and Tissue Responses to Injury, Curr Osteoporos Rep 11(2) (2013) 130-135.
[248] R. Liu, A. Schindeler, D. Little, The potential role of muscle in bone repair, J Musculoskelet Neuronal Interact. 10 (2010) 71-76.
[249] P.P. Spicer, J.D. Kretlow, S. Young, J.A. Jansen, F.K. Kasper, A.G. Mikos, Evaluation of Bone Regeneration Using the Rat Critical Size Calvarial Defect, Nat Protoc. 7(10) (2012) 1918-1929.
[250] J. Mulliken, J. Glowacki. Induced osteogenesis for repair and construction in the craniofacial region., Plast Reconstr Surg 65(5) (1980) 553-560.
[251] P. Lohmann, A. Willuweit, A.T. Neffe, S. Geisler, T.P. Gebauer, S. Beer, H.H. Coenen, H. Fischer, B. Hermanns-Sachweh, A. Lendlein, N.J. Shah, F. Kiessling, K.-J. Langen, Bone regeneration induced by a 3D architectured hydrogel in a rat critical-size calvarial defect, Biomaterials 113 (2017) 158-169.
[252] M. Stevens, Biomaterials for bone tissue engineering, Materials Today 11(5) (2008) 18-25.
[253] W. Li, J. Zhou, Y. Xu, Study of the in vitro cytotoxcity testing of medical devices, biomedical Reports 5 (2015) 617-620.
[254] K. Ren, T. Crouzier, C. Roy, C. Picart, Polyelectrolyte Multilayer Films of Controlled Stiffness Modulate Myoblast Cells Differentiation, Adv Funct Mater 18(9) (2008) 1378-1389.

[255] L. Ricotti, S. Taccola, I. Bernardeschi, V. Pensabene, P. Dario, A. Menciassi, Quantification of growth and differentiation of C2C12 skeletal muscle cells of PSS-PAH-based polyelectrolyte layer-by-layer nanofilms, Biomed. Mater 6 (2011).
[256] V. Horsley, B.B. Friday, S. Matteson, K.M. Kegley, J. Gephart, G.K. Pavlatha, Regulation of the Growth of Multinucleated Muscle Cells by an Nfatc2-Dependent Pathway, J Cell Biol 16 (2001) 329-338.
[257] A. Salimath, Biofunctional Hydrogels for Skeletal Muscle Constructs, Mechanical Engineering, Georgia Institute for Technology, Georgia, USA, 2015.
[258] K.J.M. Boonen, K.Y. Rosaria-Chak, F.P.T. Baaijens, D.W.J.v.d. Schaft, M.J. Post, Essential environmental cues from the satellite cell niche: optimizing proliferation and differentiation, Am J Physiol C Physiol 296 (2009) 1338-1345.
[259] T.L. Riss, R.A. Moravec, A.L. Niles, S. Duellman, H.A. Benink, T.J. Worzella, L. Minor, Cell Viability Assays, Assay Guidance Manual (2015).
[260] W. Hassan, Y. Dong, W. Wang, Encapsulation and 3D culture of human adipose-derived stem cells in an in-situ crosslinked hybrid hydrogel composed of PEG-based hyperbranched copolymer and hyaluronic acid, Stem Cell Research & Therapy 4(32) (2013).
[261] K. Webb, V. Hlady, P.A. Tresco, Relationships among cell attachment, spreading, cytoskeletal organization, and migration rate for anchorage-dependent cells on model surfaces, J Biomed Mater Res 49(3) (2000) 362-368.
[262] D. Missirlis, J.P. Spatz, Combined Effects of PEG Hydrogel Elasticity and Cell-Adhesive Coating on Fibroblast Adhesion and Persistent Migration, Biomacromolecules 15 (2014) 195−205.
[263] A. Skardal, D. Mack, A. Atala, S. Soker, Substrate elasticity controls cell proliferation, surface marker expression and motile phenotype in amniotic fluid-derived stem cells, J Mech Behav Biomed Mater 17 (2013) 307-316.
[264] P. Velica, C. Bunce, A quick and simple unbiased method to quantify C2C12 myogenic differentiation, Muscle & Nerve 44(3) (2011).
[265] Y. Chen, V. Stegaev, V.P. Kouri, T. Sillat, P.L. Chazot, H. Stark, J.G. Wen, Y.T. Konttinen, Identification of histamine receptor subtypes in skeletal myogenesis, Molecular Medicine Reports 11 (2015) 2624-2630.
[266] S. Romanazzo, G. Forte, M. Ebara, K. Uto, S. Pagliari, T. Aoyagi, E. Traversa, A. Taniguchi, Substrate stiffness affects skeletal myoblast differentiation in vitro, Sci. Technol. Adv. Mater 13 (2012).
[267] S.R. Chowdhury, Y. Muneyuki, Y. Takezawa, M. Kino-oka, A. Saito, Y. Sawa, M. Taya, Growth and differentiation potentials in confluent state of culture of human skeletal muscle myoblasts, Journal of Bioscience and Bioengineering 109(3) (2010).
[268] T. Yeung, P.C. Georges, L.A. Flanagan, B. Marg, M. Ortiz, M. Funaki, N. Zahir, W. Ming, V. Weaver, P.A. Janmey, Effects of Substrate Stiffness on CellMorphology, Cytoskeletal Structure,and Adhesion, Cell Motility and the Cytoskeleton 60 (2005) 24-34.
[269] O. Veiseh, J.C. Doloff, M. Ma, A.J. Vegas, H.H. Tam, J.L. Andrew R. Bader, E. Langan, J. Wyckoff, W.S. Lo, S. Jhunjhunwala, A. Chiu, S. Siebert, K. Tang, J. Hollister-Lock, S. Aresta-Dasilva, M. Bochenek, J. Mendoza-Elias, Y. Wang, M. Qi, D.M. Lavin, M. Chen, N. Dholakia, R. Thakrar, I. Lacík, Size- and shape-dependent foreign body immune response to materials implanted in rodents and non-human primates, Nature Materials 14 (2015) 643-651.

[270] S. Ghanaati, M. Schlee, R. Sader, C.J. Kirkpatrick, Evaluation of the tissue reaction to a new bilayered collagen matrix in vivo and its translation to the clinic, Biomedical materials 6 (2011).
[271] R.M. Boehler, J.G. Graham, L.D. Shea, Tissue engineering tools for modulation of the immune response, Biotechniques 51(4) (2011).
[272] G. Keeler, J. Durdik, J. Stenken, Effects of delayed delivery of dexamethasone-21-phosphate via subcutaneous microdialysis implants on acrophage activation in rats, Acta Biomaterialia 23 (2015) 27-37.
[273] D.J. Modulevsky, C.M. Cuerrier, A.E. Pelling, Biocompatibility of Subcutaneously Implanted Plant-Derived Cellulose Biomaterials, PLOS One (2016).
[274] G.S. Selders, A.E. Fetz, M.Z. Radic, G.L. Bowlin, An overview of the role of neutrophils in innate immunity, inflammation and host-biomaterial integration, Regen Biomater 4(1) (2017) 55-68.
[275] P. Geilkens, J. Schortinghuis, J.d. Jong, G. Raghoebar, B. Stegenga, R. Bos, Vivosorbs, Bio-Gides, and Gore-Texsasbarrier membranes in rat mandibulardefects: an evaluation by microradiography and micro-CT, Clin. Oral Impl. Res 19 (2008) 516-521.
[276] N. Huebsch, E. Lippens, K. Lee, M. Mehta, S.T. Koshy, M.C. Darnell, R. Desai, C.M. Madl, M. Xu, X. Zhao, O. Chaudhuri1, C. Verbeke, W.S. Kim, K. Alim, A. Mammoto, D.E. Ingber, G.N. Duda, D.J. Mooney, Matrix Elasticity of Void-Forming Hydrogels Controls Transplanted Stem Cell-Mediated Bone Formation, Nature Materials 14(12) (2015) 1269-1277.
[277] R. Smeets, C. Knabe, A. Kolk, M. Rheinnecker, A. Grobe, M. Heiland, R. Zehbe, M. Sachse, C. Große-Siestrup, M. Woltje, H. Hanken, Novel silk protein barrier membranes for guided bone regeneration, Journal of Biomedical Materials Research Part B: Applied Biomaterials (2016).
[278] Z. Sheikh, J. Qureshi, A.M. Alshahrani, H. Nassar, Y. Ikeda, M. Glogauer, B. Ganss, Collagen based barrier membranes for periodontal guided bone regeneration applications, Odontoology 105 (2017) 1-12.
[279] M. Simion, M. Baldoni, P. Rossi, D. Zaffe, A comparative study of the effectiveness of e-PTFE membranes with and without early exposure during the healing period., Int J Periodontics Restorative Dent 14 (1994) 166-180.
[280] I. Elgali, O. Omar, C. Dahlin, P. Thomsen, Guided bone regeneration: materialsand biological mechanisms revisited, Eur J Oral Sci (2017) 1-23.
[281] M.M. Stevens, R.P. Marini, D. Schaefer, J. Aronson, R. Langer, V.P. Shastri, In vivo engineering of organs: The bone bioreactor, PNAS 102(32) (2005).
[282] M. Ribeiro, M.A. de Moraes, M.M. Beppu, M.P. Garcia, M.H. Fernandes, F.J. Monteiro, M.P. Ferraz, Development of silk fibroin/nanohydroxyapatite composite hydrogels for bone tissue engineering., Eur. Polym. J 67 (2015) 66-77.
[283] G. Tozzi, A.D. Mori, A. Oliveira, M. Roldo, Composite Hydrogels for Bone Regeneration, Materials 9(267) (2016).
[284] S. Sant, M.J. Hancock, J.P. Donnelly, D. Iyer, A. Khademhosseini, Biomimetic gradient hydrogels for tissue engineering, Can J Chem Eng 88(6) (2010) 899-911.
[285] T.H. Kim, D.B. An, S.H. Oh, M.K. Kang, H.H. Song, J.H.L. a, Creating stiffness gradient polyvinyl alcohol hydrogel using a simple gradual freezing-

thawing method to investigate stem cell differentiation behaviors, Biomaterials 40 (2015) 51-60.
[286] H. Cao, S. Xu, Purification and characterization of type II collagen from chick sternal cartilage, Food Chemistry 108 (2008) 439-445.
[287] B.Z. Lodish, Molecular Cell Biology, 4th editio ed., W. H. Freeman, New York, 2000.
[288] B.D. Walters, J.P. Stegemann, Strategies for directing the structure and function of three-dimensional collagen biomaterials across length scales, Acta biomaterialia 10 (2014) 1488-1501.
[289] R. Parenteau-Bareil, R. Gauvin, F. Berthod, Collagen-Based Biomaterials for Tissue Engineering Applications, Materials 3(3) (2010) 1863-1887.
[290] K. Hanai, N. Sawada, Effects of Atelocollagen Formulation Containing Oligonucleotide on Endothelial Permeability, Journal of Drug Delivery (2012).
[291] F. Furthmayr, R. Timpl, Immunochemistry of collagens and procollagens, Int Rev Connect Tissue Rev 7 (1976) 61-99.
[292] F. DeLustro, F. Condell, A comparative study of the biolofical and immunological response to medical devices derived from dental collagen, J Biomed Mater Res 20 (1986) 109-120.
[293] E. Allaire, C. Guettier, Morphological characteristics of aortic isografts, allografts and xenografts in rats, J Vasc Surg 19 (1994) 446-456.
[294] D. M, W. Lyman, Immunogenicity of glutaraldehyde-tanned bovine pericardium, J Thorac Cardiovasc Surg (1990) 1082-1090.
[295] K. Morimoto, S. Kunii, K. Hamano, B. Tonomura, Preparation and Structural Analysis of Actinidain-processed Atelocollagen of Yellowfin Tuna, Bioscience, Biotechnology and Biochemistry 68 (2014) 861-867.
[296] T. Miyata, T. Taira, Collagen Engineering for Biomaterial Use, Clinical Materials 9 (1992) 139-148.
[297] S. Amani, A. Shamsi, G. Rabbani, A. Naim, An Insight into the Biophysical Characterization of Insoluble Collagen Aggregates: Implication for Arthritis, J Fluoresc (2014) 1423-1431.
[298] F.S. Steven, A. Torrre-Blanco, A neutral protease in rheumatoid synovial fluid capapble of attacking the telopeptide regions of polymeric collagen fibrils, Biochimica et Biophysica Acta 405 (1975) 188-200.
[299] J.P.R.O. Orgel, J.D. San Antonio, O. Antipova, Molecular and structural mapping of collagen fibril interactions, Connective Tissue Research 52(1) (2011) 2-17.
[300] N. Greenfield, Using circular dichroism spectra to estimate protein secondary structure, Nat Protoc. 1(6) (2006) 2876-2890.
[301] R. Holmes, S. Kirk, G. Tronci, X. Yang, D. Wood, Influence of telopeptides on the structural and physical properties of polymeric and monomeric acid-soluble type I collagen, Materials Science and Engineering C 77 (2017) 823-827.
[302] O. Menders, Fundamental Aspects of the Chrome Tanning Reaction, University of Northampton, 2002.
[303] V. Samouillan, F. Delaunay, J.-P. Gardou, C. Lacabanne, The Use of Thermal Techniques for the Characterization and Selection of Natural Biomaterialas, Journal of Functional Biomaterials 2 (2011) 230-248.
[304] M. Seibel, Biochemical Markers of Bone Turnover Part I: Biochemistry and Variability, Clin Biochem Rev 26 (2005) 97-122.
[305] H. Herrmann, v.d. Mark, Isolation and characterization of type III collagen from chick skin, Physiol. Chem 356 (1975) 1605-1612.

[306] S. Cliche, J. Amiot, C. Avezard, C. Gariépy, Extraction and characterization of collagen with or without telopeptides from chicken skin, Poultry science 82(3) (2003) 503-509.
[307] E.Y. Jones, M. Biophysics, Structural Models for the N- and C-Terminal Telopeptide Regions of Interstitial Collagens, 26 (1987) 463-480.
[308] J. Malone, A. George, A. Veis, Type I collagen N Telopeptides adopt an ordered structure when docked to their helix receptor during fibrillogenesis, Proteins: Structure, Function 54(2) (2004) 206-15.
[309] J. Iwasa, M. Ochi, Y. Uchio, K. Katsube, N. Adachi, K. Kawasaki, Effect of cell density on proliferation and matrix synthesis of condrocytes embedded in atelocollagen gel., Artif Organs 27 (2003) 249-255.
[310] A.M. Emmakah, H.E. Arman, J.C. Bragg, T. Greene, M. Alvarez, P. Childress, W. Goebel, M. Kacena, C. Lin, T. Chu, A fast-degrading thiol–acrylate based hydrogel for cranial regeneration, Biomedical materials 12 (2016).
[311] J.A. Burdicka, K.S. Anseth, Photoencapsulation of osteoblasts in injectable RGD-modified PEG hydrogels for bone tissue engineering, Biomaterials 23 (2002) 4315-4323.
[312] O. Chaudhuri, L. Gu, D. Klumpers, M. Darnell, S.A. Bencherif, J.C. Weaver, N. Huebsch, H.-p. Lee, E. Lippens, G.N. Duda, D.J. Mooney, Hydrogels with tunable stress relaxation regulate stem cell fate and activity, Nature Materials 15 (2015) 326-336.
[313] F. Andreopoulos, I. Persaud, Delivery of basic fibroblast growth factor (bFGF) from photoresponsive hydrogel scaffolds, Biomaterials 27(22) (2006) 2468-76.
[314] D. Seliktar, A. H. Zisch, M. P. Lutolf, J. L. Wrana, J.A. Hubbell, MMP-2 sensitive, VEGF-bearing bioactive hydrogels for promotion of vascular healing, Journal of Biomedical Materials Research 68A(4) (2004) 704-716.
[315] K. Bohl, J. West, Nitric oxide-generating polymers reduce platelet adhesion and smooth muscle cell proliferation., Biomaterials 21(22) (2000) 2273-8.

Research Publications

Róisín Holmes, Xuebin B Yang, Aishling Dunne, Larisa Florea, David Wood and Giuseppe Tronci (2017) Thiol-ene photo-click collagen-PEG hydrogels: impact of water-soluble photoinitiators on cell viability, gelation kinetics and rheological properties. *Polymers*, 226 (9)

Róisín Holmes, Steve Kirk, Giuseppe Tronci, Xuebin Yang, David Wood (2017) Influence of telopeptides on the structural and physical properties of polymeric and monomeric acid-soluble type I collagen. *Materials Science and Engineering: C*, 77 (1) 823-827.

Giuseppe Tronci, Jie Yin, Roisin A. Holmes, He Liang, Stephen J. Russell, David J. Wood (2016) Protease-sensitive atelocollagen hydrogels promote healing in a diabetic wound model. *Journal of Materials Chemistry B*, 4 (45) 7249-7258.